Platinum Picoline Anticancer Complexes

A Thesis Submitted for the Degree of

Doctor of Philosophy

by

Geraldine McGowan, *BSc.*

Department of Chemistry
Faculty of Science and Engineering
University of Edinburgh

August 2005

Abstract

The 2-picoline (2-methylpyridine) complex, *cis*-[$PtCl_2(NH_3)$(2-pic)] (AMD473), is a promising new generation platinum antitumour agent currently in clinical trials and highly active against cisplatin resistant cell-lines. The antitumour activity of *trans* platinum complexes has attracted renewed interest since it has been shown that some *trans* compounds, in particular those possessing planar amine ligands, are anticancer-active. Therefore, three *trans* isomers, *trans*-[$PtCl_2(NH_3)$(2-pic)] (**1**), *trans*-[$PtCl_2(NH_3)$(3-pic)] (**2**) and *trans*-[$PtCl_2(NH_3)$(4-pic)] (**3**), were synthesised and characterised. The crystal structure of **1** shows steric hindrance induced by the 2-methyl group towards an axial approach to Pt, while its 3-pic (**2**) and 4-pic (**3**) analogues are less sterically hindered. Notable however, is that in the solid state complex **1** is less sterically-hindered than its *cis* isomer. ^{15}N-labelling of complexes **1**–**3** allowed both the hydrolysis rates and pK_a values of the complexes to be determined using 2D [^1H,^{15}N] NMR spectroscopy.

Adducts of *cis*- and *trans*-[$PtCl_2(NH_3)$(2-pic)] with neutral 9-ethylguanine (9-EtGH) and anionic (N1-deprotonated) 9-ethylguanine (9-EtG) were prepared and their structures determined by X-ray crystallography. Platinum is coordinated at the guanine N7 position with a head-to-tail arrangement of the bases in all cases. Two of the complexes exhibited intermolecular triple hydrogen bonding between neutral and deprotonated guanine ligands. In addition, adducts of *cis*- and *trans*-[$PtCl_2(NH_3)$(2-pic)] with guanosine and 2'-deoxyguanosine were prepared and characterised in solution by NMR spectroscopy and ESI mass spectrometry. The complexes *cis*-[$Pt(NH_3)$(2-pic)$(Guo)_2]^{2+}$, and *cis*- and *trans*-[$Pt(NH_3)$(2-pic)$(2'\text{-}dGuo)_2]^{2+}$ were assigned as head-to-tail conformations, on the basis of their NOE cross-peaks.

The reaction of *cis*-$[Pt(^{15}NH_3)(2\text{-pic})(OH_2)_2]^{2+}$ and guanosine (Guo) was followed by 2D [^{1}H,^{15}N] NMR spectroscopy and was found to proceed through two mono(guanosine) intermediate species to yield the dominant product *cis*-$[Pt(^{15}NH_3)(2\text{-pic})(Guo)_2]^{2+}$. Initial guanosine substitution *trans* to 2-picoline was faster than substitution *cis* to 2-picoline due to steric hindrance, but the rates of the second guanosine substitution were similar.

The binding of ^{15}N-labelled-**1** to a self-complementary DNA duplex, $d(TATGGTACCATA)_2$, was investigated using 1D ^{1}H and 2D [^{1}H,^{15}N] NMR spectroscopy. The first aquation step appeared to be the rate-limiting step in the formation of the monofunctional adducts. Several DNA products were observed but could not be identified unambiguously.

The rate constants for reactions between ^{15}N-labelled **1** and guanosine 5'-monophosphate (5'-GMP) were determined via 2D NMR studies, and compared to those previously reported for *cis*-$[PtCl_2(NH_3)(2\text{-pic})]$. Complex **1** was very reactive towards the thiol glutathione (GSH). Competitive reactions of **1** with GSH and 5'-GMP showed a clear preference for GSH adduct formation.

Also, using [^{1}H,^{15}N] 2D NMR spectroscopy together with ^{15}N-labelled amines, the reactions of *cis*- and *trans*-$[PtCl_2(NH_3)(2\text{-pic})]$ with L-methionine (L-MetH) (1:1, 298 K) were investigated. The reactivity of *cis*-$[PtCl_2(NH_3)(2\text{-pic})]$ with L-methionine was greatly reduced compared to cisplatin, with the hydrolysis reaction predominating. *Trans*-$[PtCl_2(NH_3)(2\text{-pic})]$, on the other hand, appeared to react without prior aquation and was entirely consumed within 8 h of reaction.

Dedicated to Etienne

Acknowledgements

I would like to thank Professor Peter J. Sadler for his supervision and enthusiasm. I am very grateful to him for everything I have learned and achieved throughout my project.

Special thanks go to several members of the PJS group for their help and support. Among them, thanks are especially due to Dr. Vivienne Munk for all her help and teaching and assistance with molecular modelling, Dr. Abraha Habtemariam as a constant source of expertise and advice, and Dr. Ana Pizarro for advice in the lab and stimulating discussion. I would also like to express my thanks to Dr. Tina Hunter for her invaluable support and friendship over the years.

I would like to thank Dr. Simon Parsons and his group members for their efficient X-ray crystal structure determination service. Also, particular thanks are due to Juraj Bella for assistance with NMR experiments.

I am very grateful to Dr. Junyong Zhang of the University of Western Australia for her expertise and assistance with kinetic fits.

I am indebted to AnorMED for their support (including financial) of my project and also to the EC COST programme for giving me the opportunity to attend and present at the workshop meetings.

Finally, my sincere thanks go to my fiancé Etienne and my parents for their constant support and encouragement along the way.

Contents

Abbreviations

ATP	adenosine triphosphate
5'-AMP	adenosine 5'-monophosphate
5'-CMP	cytosine 5'-monophosphate
DNA	deoxyribonucleic acid
ESI-MS	electrospray ionisation mass spectrometry
9-EtGH	9-ethylguanine
5'-GMP	guanosine 5'-monophosphate
GSH	glutathione
HH	head-to-head
HMG	high mobility group protein
HPLC	high performance liquid chromatography
HSQC	heteronuclear single-quantum coherence
HT	head-to-tail
L-HMet	L-methionine, L-MetH
MT	metallothionein
NOE	nuclear Overhauser effect
NOESY	nuclear Overhauser effect spectroscopy
Pic	picoline, methyl pyridine
RNA	ribonucleic acid
SAR	structure activity relationship
ROESY	rotating frame nuclear Overhauser effect spectroscopy
TFA	trifluoroacetate
5'-TMP	thymidine 5'-monophosphate

Chapter 1

Introduction

1.1 Platinum

Platinum (Pt, atomic number 78, mass number 195.08) is found in Group 10 of the periodic table. Platinum-containing objects date back as early as 700 BC, although Pt was not formally discovered until 1735 by the Spanish astronomer A. de Ulloa, in deposits from the Pinto River in Columbia and brought to Europe. A systematic study of the chemistry of platinum began soon after its arrival in Europe, and by 1830 not only had many of the inorganic compounds been made, but the first organometallic derivative $K[Pt(C_2H_4)Cl_3].H_2O$ had actually been prepared.[1] The chemistry was further developed during the rest of the 19th century and, with increasing acceleration in the 20th century. There were three factors which attracted interest to and sustained research on platinum.

Firstly, in the divalent oxidation state platinum readily forms complexes with ligands containing donor atoms from most groups of the periodic table.

Secondly, there came the recognition of the square-planar geometry of the 2+ oxidation state, which opened up the possibility of *cis-, trans-* isomerisation in such complexes. From this followed the discovery of the *trans*-effect in Pt(II) complexes in the 1920s.[2] Its elucidation enabled the systematic synthesis of any desired platinum(II) complex to be accomplished. These investigations led to the synthesis of all three possible geometric isomers of $[Pt(pyr)(NH_3)BrCl]$.[3]

Thirdly, there followed a tremendous growth in interest in platinum triggered off by the burgeoning of its organometallic chemistry. This is a vast subject of great intrinsic interest. It has applications in the field of homogenous catalysis in the reactions of organic compounds, and also provides a basis for a discussion of the

mechanisms of organic reactions that are heterogeneously catalysed by the metals themselves and by their oxides.

The abundance of platinum in the earth's crust is approximately 10^{-6} % by weight. Almost all platinum comes from nickel or copper sulfide ores and must be selectively extracted from other Platinum Group metals (ruthenium, rhodium, palladium, osmium, and iridium). The world's major deposits are found in South Africa, Canada and Russia.

There are six naturally occurring isotopes of platinum, ^{190}Pt (0.01 %), ^{192}Pt (0.78 %), ^{194}Pt (32.9 %), ^{195}Pt (33.8 %), ^{196}Pt (25.3 %), ^{198}Pt (7.21 %), of which ^{195}Pt is NMR-active, with a nuclear spin quantum number ½. The principal oxidation states of platinum are II and IV, but there is extensive chemistry in the I and III states where Pt – Pt bonds are involved, and in the 0 state where PR_3, CO, or other π-acid ligands are present and metal clusters are also found. The higher states V and VI occur only in a few fluoro compounds.

1.1.1 Coordination Chemistry of Platinum

Platinum(II) complexes are d^8 and diamagnetic. They are principally square-planar as the splitting of the d-orbitals in this geometry provides the opportunity to place all 8 d-electrons in four lower-energy orbitals leaving the uppermost ($d_{x^2-y^2}$) orbital empty. As a third row transition metal, the d-orbital splitting is sufficient to offset the energy required to pair-up two electrons, leading these complexes to favour a square-planar geometry (Figure 1.1).

Platinum(II) shows soft or class-b characteristics, preferring CN^- and ligands with nitrogen or heavy donor atoms like I^- and π-bonding ligands rather than O-donor or F^- ligands. Pt^{II} complexes have played an important role in the development of

various aspects of coordination chemistry, such as geometric isomerism and reaction mechanisms due to their conveniently slow rates of reaction.

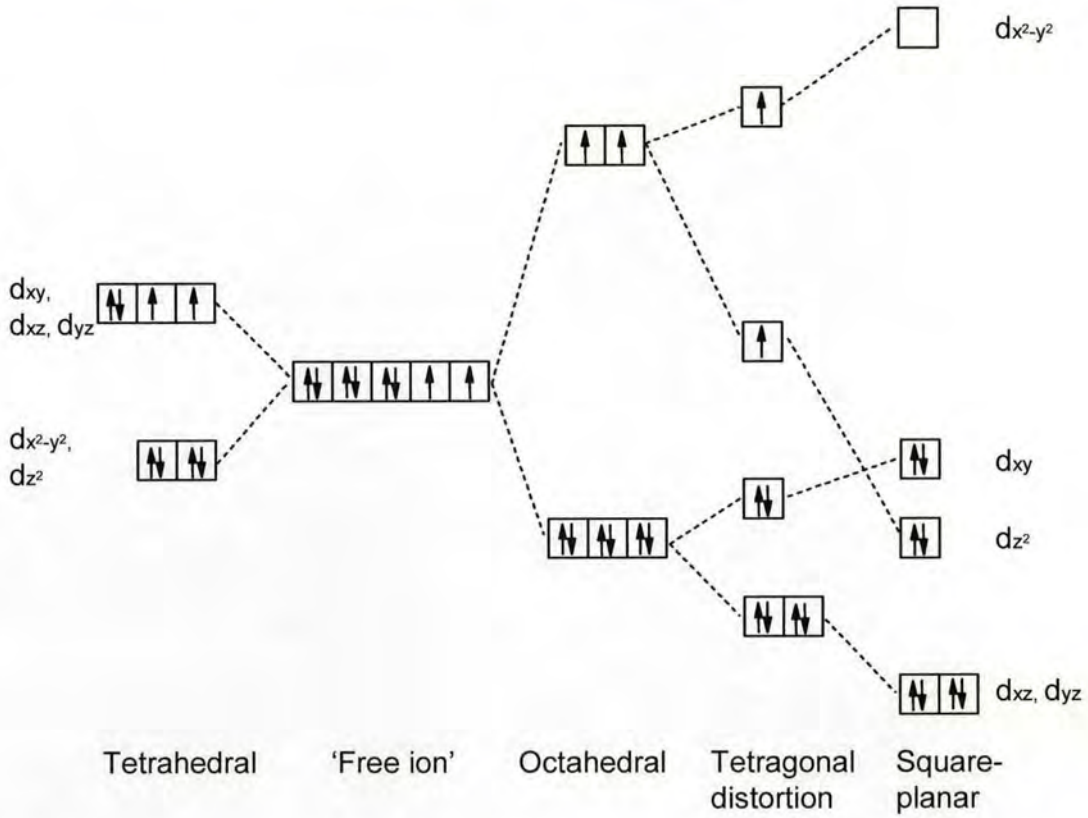

Figure 1.1 The splitting of d-orbitals in fields of different symmetries, and the resulting electronic configurations of the Pt^{II} d^8 ion.

An important phenomenon of reactions of square-planar complexes is the *trans* effect – the effect of the ligand on the rate of substitution of the group *trans* to it. Ligand displacement on Pt^{II} occurs almost entirely by an associative pathway, via a 5-coordinate intermediate (Figure 1.2). Such substitution reactions follow a two-term rate law, assuming an excess of solvent, i.e. rate = $k_1[L_3PtY] + k_2[L_3PtX][Y^-]$, where k_1 and k_2 are first-order and second-order rate constants, respectively. Generally, the stereochemistry of the complex is retained but if the intermediate is sufficiently long-lived it can undergo pseudorotation leading to the opposite isomer.

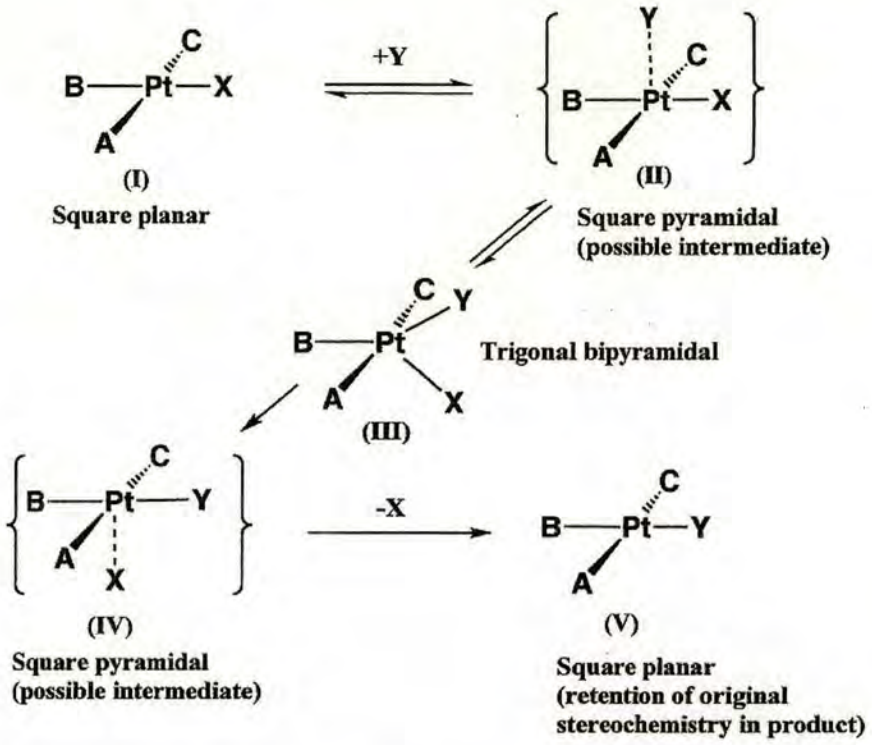

Figure 1.2 Associative mechanism of ligand substitution in Pt^{II} square-planar complexes.

By comparison with a large number of reactions, it is possible to set up a *trans*-directing series. The ordering of ligands in this series is as follows:[4]

$$CO, CN^-, C_2H_4 > PR_3, H^- > CH_3^- > C_6H_5^-, NO_2^-, I^-, SCN^- > Br^-, Cl^- > py, NH_3, OH^-, H_2O$$

The ligands exerting the strongest *trans* effect are those for which the bonding to Pt^{II} is thought to have the most π-acceptor character. This removes electron density from the metal and the reduced density on the opposite side means that nucleophilic attack is more likely to take place. The *trans* effect is a kinetic phenomenon affecting the rates of reaction and isomer formation. This series is useful in rationalising known synthetic procedures and devising new ones.

A related property of ligands in square-planar complexes is the *trans* influence. This is a thermodynamic effect of one ligand on the strength of the bond *trans* to it. The ordering of ligands in this series is as follows:[4]

$$H^- > PR_3 > SCN^- > I^-, CH_3^-, CO, CN^- > Br^- > Cl^- > NH_3 > OH^-$$

This effect is greatest for ligands which are strong σ-donors.

Platinum(IV) complexes are octahedral and diamagnetic with the low-spin t_{2g}^6 configuration. In contrast to Pt^{II}, Pt^{IV} shows nearly hard or class-a characteristics. Pt^{IV} complexes are thermodynamically stable and kinetically inert. Complexes with halide, pseudo-halide and N-donor ligands are especially numerous. $K_2[PtCl_6]$ is the most common commercially available form, and it is a useful route into Pt^{II} chemistry, by reduction with sulfur dioxide to $K_2[PtCl_4]$.[5]

1.2 Cisplatin

Although most heavy metals are considered to be very toxic, some may also have beneficiary effects in the treatment of diseases.[6, 7] Platinum drugs against cancer are one of the most successful applications of metals in medicine. Platinum complexes are now among the most widely used drugs for the treatment of cancer and one of the world's best selling anticancer drugs is cisplatin, *cis*-diamminedichloroplatinum(II), Figure 1.3.

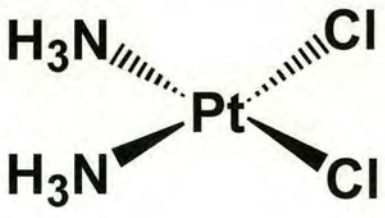

Figure 1.3 The anticancer drug cisplatin.

Cisplatin was chemically described in 1844 but its anticancer properties went unnoticed until the mid-1960s when Dr. Barnett Rosenberg set out to investigate the effects of electric fields on the growth of *E. coli*.[8] Cell division was found to be inhibited in these experiments. Rosenberg and co-workers found that the electric field was not responsible for the cell division arrest, but that this could be attributed to traces of platinum compounds, and in particular *cis*-$[Pt(NH_3)_2Cl_4]$. Such compounds were formed by electrochemical reactions of the platinum electrodes used in the experiment.[9] Clinical trials demonstrating the efficacy of cisplatin, *cis*-$[Pt(NH_3)_2Cl_2]$, soon followed. Both *cis*-diamminedichloroplatinum(II) and *cis*-diamminetetrachloroplatinum(IV) were shown to have potent antitumour activity against sarcoma 180 and leukaemia L1210,[10, 11] whereas the *trans* geometric isomers of these compounds were ineffective.[12, 13] After the clear demonstration of activity against a broad range of animal tumours, clinical trials were initiated by the National Cancer Institute in 1972. These early reports indicated promising anticancer activity, particularly against nonseminomatous testicular tumours, but stressed the limitations imposed by severe toxicity to the kidneys and bone marrow.[14] Nausea and vomiting and sometimes audiotoxicity were also severe. However, subsequent studies showed that high doses could be tolerated by means of forced diuresis.[15]

The development of cisplatin marked a watershed in the treatment of cancer. The three major classes of anticancer drugs then available – antimetabolites, alkylating agents, and anthracyclines – shared a common origin in the treatment of leukaemias. The exception, 5-fluorouracil, was developed as a thymidine analogue, but surprisingly was relatively inactive in the more rapidly replicating acute leukaemias. Cisplatin was remarkable for its lack of myelosuppression and so its

investigation was targeted to solid tumours. Now, almost 40 years after the description of its anticancer activity, the continuing central role of cisplatin in the management of several major solid tumours attests to its therapeutic importance.

Despite the successful therapeutic use of cisplatin, there are still serious drawbacks associated with this drug including severe toxicity (e.g. nausea, ear damage, vomiting, diarrhoea, loss of sensation in hands and kidney toxicity), poor solubility in saline and resistance to the drug, either intrinsic or acquired. Also, cisplatin is only effective in a relatively narrow range of tumour types. These drawbacks have provided the impetus for the development of new generations of platinum drugs which can overcome these limitations.

1.2.1 Mechanism of Action

It is widely accepted that the cytotoxic effects of cisplatin are due to the formation of a variety of stable adducts on DNA which then block replication or inhibit transcription. Some of the important events relating to the mechanism of action of cisplatin and cellular resistance are summarised in Figure 1.4.

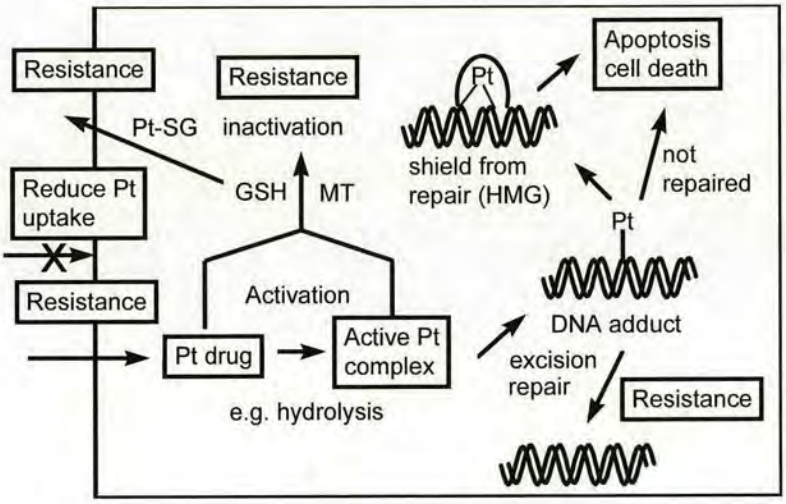

Figure 1.4 Schematic representation of reactions of cisplatin in the cell.[16]

After administration, either by injection or infusion, cisplatin is transported through the body. Due to the relatively high chloride ion concentration in blood (~100 mM), the hydrolysis of cisplatin is inhibited and the complex remains almost unchanged before entering both normal and tumour cells. The precise mechanism of cellular uptake of cisplatin still remains unclear. There are some data to suggest that cisplatin enters the cell via passive diffusion,[17] although there is also evidence for an additional pathway involving active transport, and an altered expression of some membrane proteins is reported for cisplatin-resistant cells.[18, 19]

Once inside the cell, cisplatin hydrolyses to give active forms such as *cis*-$[PtCl(NH_3)_2(H_2O)]^+$ and *cis*-$[Pt(NH_3)_2(H_2O)_2]^{2+}$ because of the much lower chloride ion concentration (4-25 mM).[20] Hydrolysis is known to be the rate-limiting step in the binding of cisplatin to DNA.[21] A summary of the hydrolysis reactions, including half lives of aquation[22] and pK_a values,[23] is given in Figure 1.5.

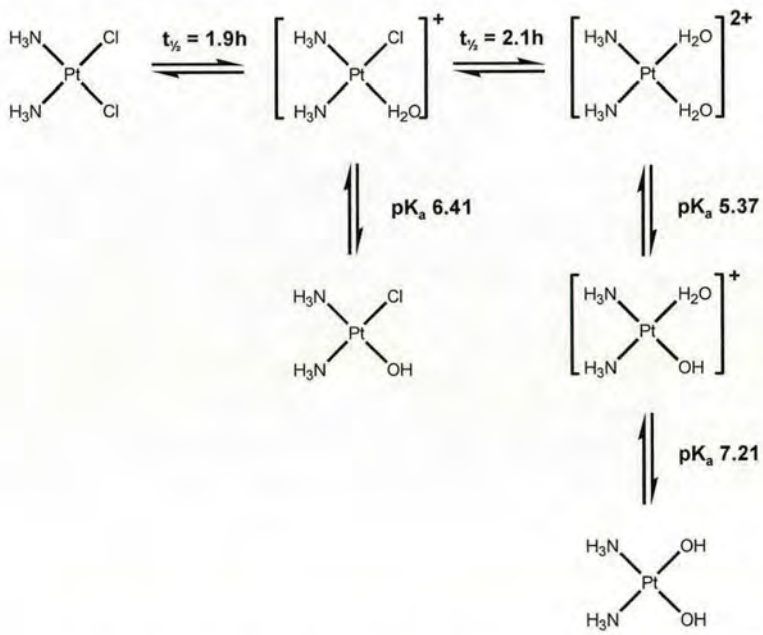

Figure 1.5 Hydrolysis scheme of cisplatin in aqueous solution with half-lives for hydrolysis (310 K)[22] and pK_a values (300 K) of its aqua adducts.[23]

In theory, a large variety of biological molecules could be potential targets for platinum compounds, including DNA, RNA and proteins. From the Hard-Soft Acid-Base theory, sulfur-donor ligands in proteins would bind strongly and generate the most stable bonds. Binding to lone pairs of nitrogen atoms can also be very strong. These types of binding would involve amino acid side chains of proteins from cysteine, methionine, histidine and the solvent-exposed N7 atoms of adenine and guanine in the major groove of double-stranded DNA. Usually, interactions of platinum antitumour complexes with S-containing biomolecules are thought to have an overall negative effect on antitumour activity. Such interactions can be responsible for the inactivation of Pt^{II} species, development of resistance and toxic side effects such as nephrotoxicity. Nevertheless, studies have shown that sulfur ligands, especially the thioether of methionine and perhaps thiol of glutathione, could also play a key role in the transfer of platinum to the nucleic acids.[24, 25]

1.2.1.1 DNA Platination

The antitumour activity of cisplatin depends on its ability to modify the structure of the DNA of cancer cells. Approximately 1% of the intracellular cisplatin reacts with genomic DNA and yields a variety of mono-adducts and intra- and inter-strand cross-links. The most nucleophilic sites in duplex DNA are known to be guanine residues located adjacent to a second guanine residue.[26] For platinum coordination, the guanine-N7 position appears to be the preferred binding site. Therefore, it is not surprising that the major DNA lesions both *in vitro* and *in vivo* are intrastrand d(GpG) cross-links. Besides GG intrastrand cross-links (~65%), the other major DNA adducts of cisplatin are intrastrand AG (but not GA) cross-links (~25%) with the remainder being minor 1,3-intrastrand cross-links, interstrand cross-links

and monofunctional adducts,[27] Figure 1.6. DNA-protein cross-links have also been reported.[28, 29] Platination of DNA by transplatin was found to give the following adducts after digestion: dG-Pt-dC (50%), dG-Pt-dG (40%), dG-Pt-dA (10%).[30] As expected, transplatin does not form intrastrand chelates between adjacent nucleotides.

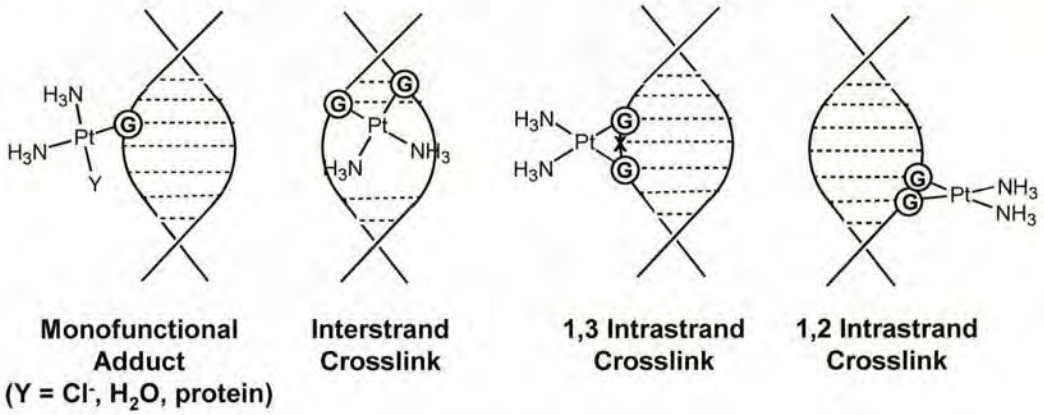

Figure 1.6 Cisplatin-DNA binding modes.

Since the most prevalent adduct formed on treatment of DNA with cisplatin is the 1,2-intrastrand cross-link, it was suggested that these may be important for anticancer activity. The assumption is supported by the finding that nucleotide excision repair (NER), an important DNA-repair system, repairs 1,3-intrastrand adducts more efficiently than 1,2-adducts, while the 1,2-d(GpG) adducts are repaired the least effectively.[31] However, the possible importance of other adducts should not be neglected. Many structural studies have been carried out to determine the nature of this 1,2-intrastrand cisplatin adduct on double and single-stranded DNA fragments.[32]

The first X-ray crystal structures determined of *cis*-GG cross-links were for the dinucleotide d(pGpG)[33] and the trinucleotide d(CpGpG).[34] These structures are shown in Figure 1.7. The dinucleotide structure has the guanine bases in a head-to-

head configuration, with the two O6 atoms on the same side of the coordination plane. The bases are forced to destack with an average dihedral angle of 81.2°. There is intramolecular hydrogen bonding between the coordinated ammine and the oxygen atom of the 5'-phosphate group. Similarly, the trinucleotide structure has a head-to-head orientation of the guanine bases, with an average dihedral angle of 82°. Also, there is a weak intramolecular hydrogen bond between the NH_3 ligand and O6 of the central guanine.

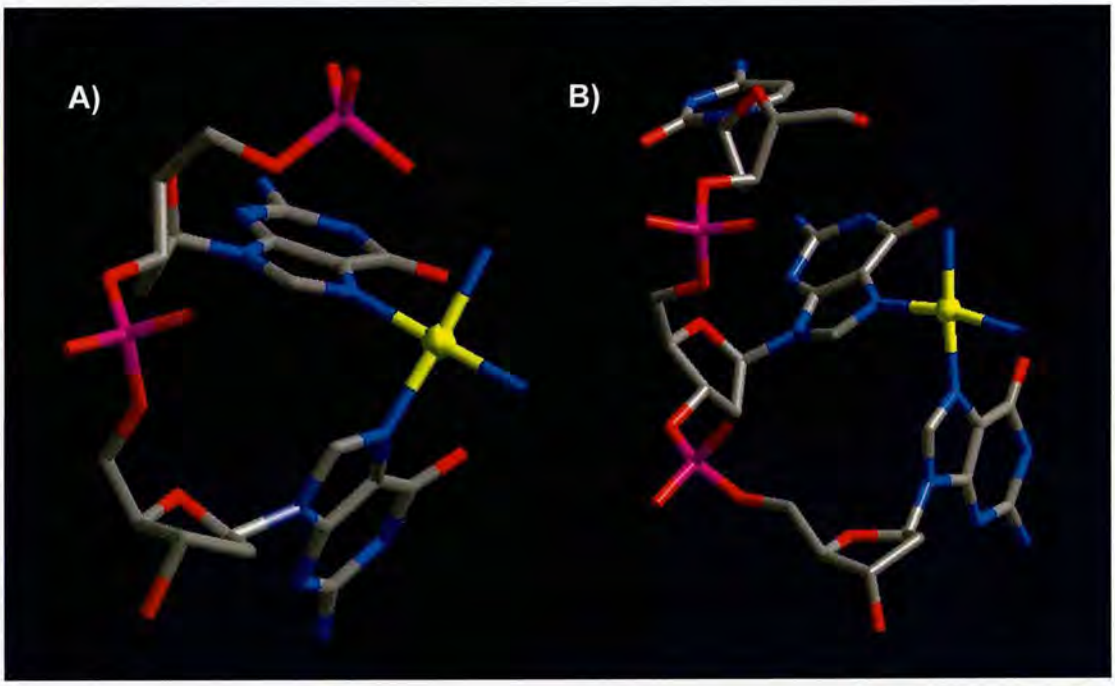

Figure 1.7 X-ray crystal structures of A) d(pGpG) containing a *cis*-GG Pt adduct[33] and B) d(CpGpG) containing a *cis*-GG Pt adduct.[34]

More recently, several structures of 1,2-dGG adducts have been determined in longer oligonucleotides (8-12 base pairs) by X-ray crystallography[35, 36] and NMR spectroscopy.[37-39] These indicated a bending and unwinding of the DNA duplex structure. Takahara et al.[35, 36] determined an important X-ray structure of a DNA dodecamer duplex containing a 1,2-intrastrand cross-link, Figure 1.8. The structure contained two molecules in the asymmetric unit with very similar structures. The two

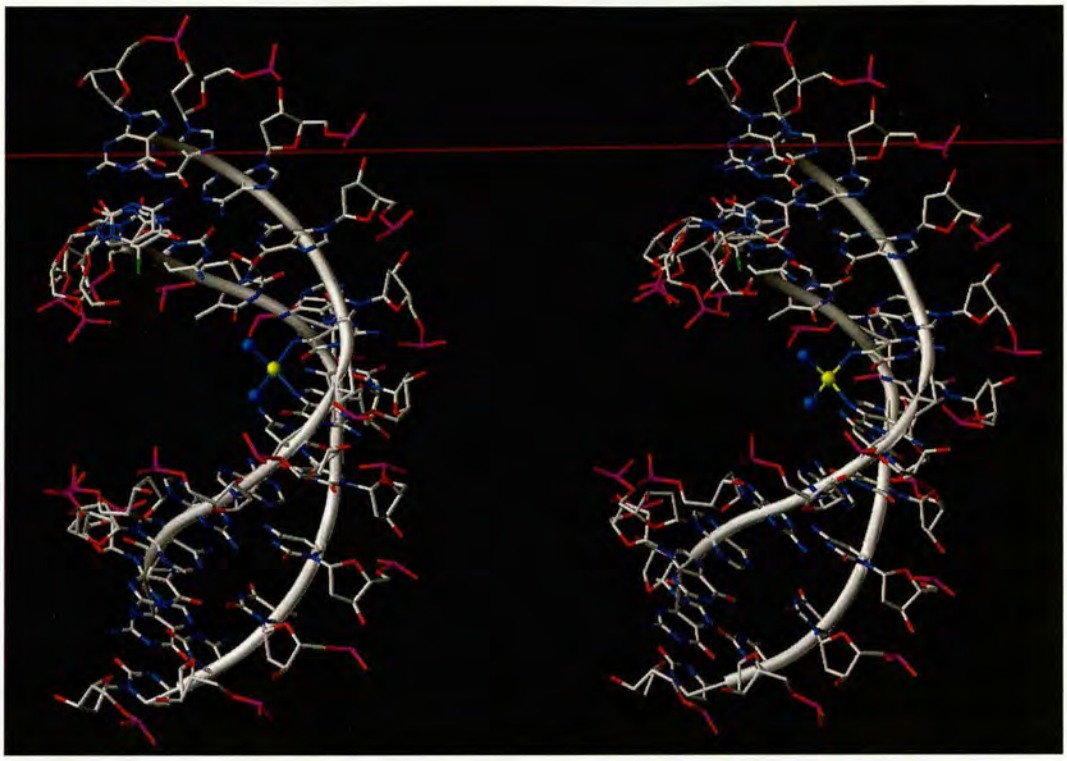

Figure 1.8 X-ray crystal structure of d(CCTCTG*G*TCTCC)·d(GGAGACCAGAGG), where G*G* represents the platination site of *cis*-$\{Pt(NH_3)_2\}^{2+}$.[35, 36]

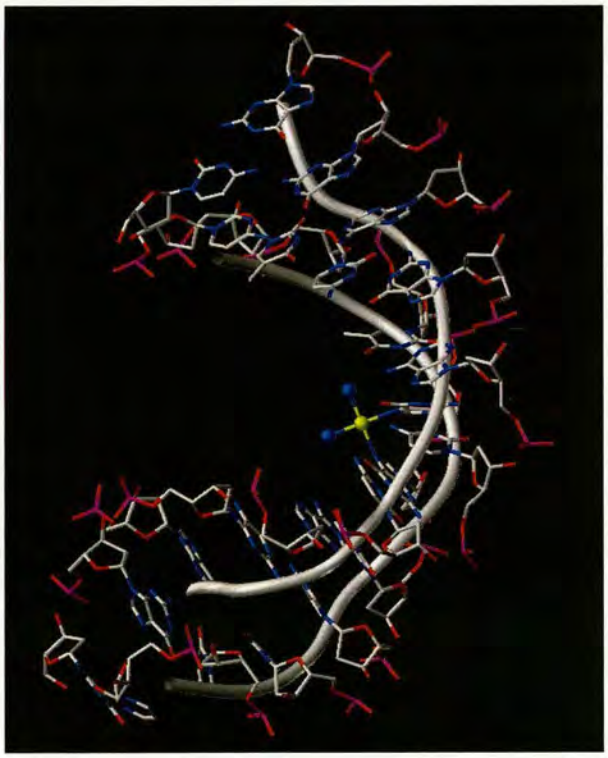

Figure 1.9 NMR solution structure of d(CCTCTG*G*TCTCC)·d(GGAGACCAGAGG), where G*G* represents the platination site of *cis*-$\{Pt(NH_3)_2\}^{2+}$.[39]

duplexes show a significant bend towards the major groove (39° and 55°). The dihedral angle between the guanine bases is 30°, considerably less than that of the d(pGpG) and d(CpGpG) structures. A consequence of the platinum binding is a widened shallow minor groove, a feature that may be important for protein recognition and anticancer activity.

An NMR structure of the same platinated dodecamer duplex has been determined,[39] allowing comparison of solid and solution phase structures. This structure (Figure 1.9) shows an overall helix bend of 78° and a dihedral angle between adjacent guanines of 47°. These values are larger than those observed for the crystal structure reflecting the influence of crystal packing. The base pairing is also more distorted in the solution structure but overall, the helix structure is similar with a wide flat minor groove.

1.2.1.2 Protein Recognition of Cisplatin-DNA Adducts

Since the discovery of a protein that preferentially binds to cisplatin-damaged DNA,[40] the HMG protein, many such proteins have been identified with similar binding affinities toward cisplatin-modified DNA. These proteins may participate in the DNA-repair process, but their *in vivo* function is largely unknown. Damage recognition proteins reported to bind to the kink in DNA induced by cisplatin adducts have been reviewed,[28] and include the XPA-RPA complex, the TATA-box binding protein TBP, hMSH2, and nonhistone HMG1 and HMG2.[28, 29, 41-43] Although it is evident that multiple factors are involved, the recognition of adducts by these proteins may be the first step towards the triggering of apoptosis.

The HMG (high mobility group) proteins have been studied the most extensively.[28, 44] HMG domains are DNA-binding motifs of approximately 80

amino acids that bind specifically to kinks in DNA. The crystal structure of a cisplatin-1,2 GpG adduct in an oligonucleotide complexed with a HMG protein has been reported[29] (Figure 1.10). The HMG domain specifically recognises the kinks formed by 1,2 adducts of cisplatin with GpG and ApG, but not the less kinked 1,3-d(G-X-G) adducts.[43, 45]

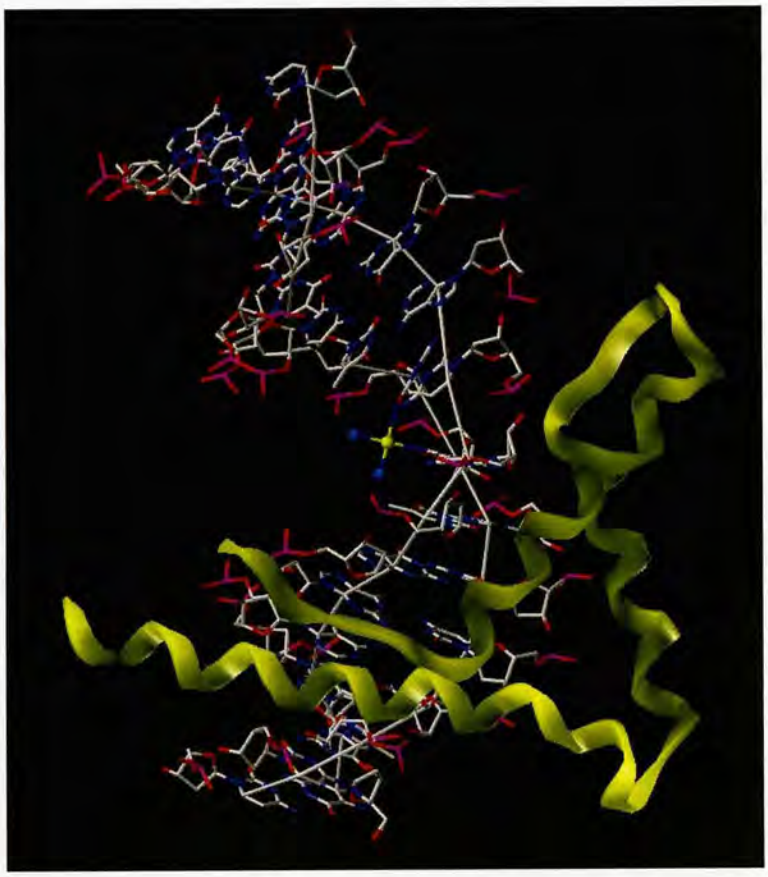

Figure 1.10 X-ray crystal structure of a HMG1 protein bound to a cisplatin 1,2-GG intrastrand adduct.[29]

1.2.1.3 Pt – Sulfur Interactions

Although the major target for cisplatin in cells appears to be DNA, many other molecules can react with the platinum compound. Pt(II) being a 'soft' metal ion is known to have a very high affinity for 'soft' ligand atoms such as sulfur. Sulfur-containing ligands, e.g. glutathione, N-acetyl-L-cysteine, have been investigated as

rescue agents for the removal of platinum from the body. The amino acid and thioether L-methionine (L-HMet) is thought to play an important role in the metabolism of cisplatin. One of the few characterised metabolites of cisplatin is Pt(L-Met)$_2$ which has been isolated from urine.[46] [Pt(L-Met)$_2$] exists as a mixture of *cis* and *trans* isomers in aqueous solution,[47, 48] Figure 1.11. At neutral pH the isomers interconvert extremely slowly (half-lives of 22.4 h and 3.2 h for the *cis* and *trans* isomers respectively, at 310K) with the *cis* isomer predominating at equilibrium (10:1, K = 7.0).[48]

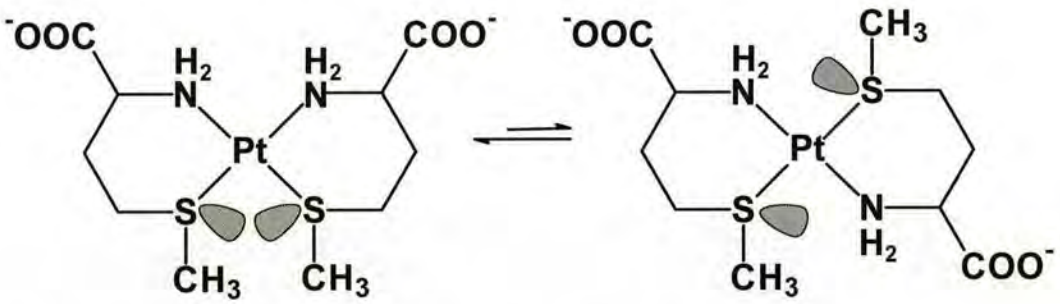

Figure 1.11 *Cis* and *trans* isomers of [Pt(L-Met)$_2$] in aqueous solution.

The sulfur-containing tripeptide glutathione (γ-Glu-Cys-Gly)(Figure 1.12) is present in cells at millimolar concentrations. The formation of Pt:GSH complexes may play an important role in the biological activity of platinum complexes. GS-Pt complexes can be pumped out of cells through an ATP-dependent process.[49, 50]

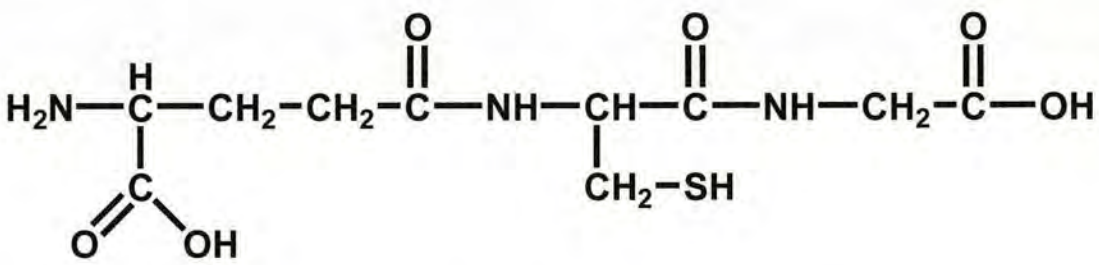

Figure 1.12 The sulfur-containing tripeptide glutathione (GSH).

During the reaction of *cis*-[$PtCl_2(^{15}NH_3)_2$] with GSH, the monosubstituted complex *cis*-[$PtCl(SG)(^{15}NH_3)_2$] is formed first, but several other species containing a $^{15}NH_3$-Pt-S linkage are present within a few minutes.[51] Release of $^{15}NH_3$ ligands has been observed and no coordinated $^{15}NH_3$ is contained in the final product, which is consistent with a high molecular mass polymer with a 1:2 Pt:GSH stoichiometry. A product containing a dinuclear Pt_2S_2 four-membered ring has been observed from reactions of *cis*-$[Pt(NH_3)_2(H_2O)_2]^{2+}$ with GSH.[52] Glutathione can also affect the macrochelate ring closure of cis- and trans-platin monofunctional adducts on DNA.[53] Compared with cisplatin, the reaction between GSH and transplatin monofunctional adduct more rapidly leads to the formation of sulfur-bound, glutathione-trapped monofunctional adducts. GSH does not appear to react with cis- or trans-platin bifunctional adducts. These results are consistent with proposals that the biological inactivity of transplatin may arise from selective trapping of monofunctional adducts before they ring-close to form bifunctional lesions.

Metallothionein (MT) is a low-molecular-weight protein rich in cysteine (~30%) and thought to be responsible for cisplatin detoxification. The tetrapeptide Boc-Cys(SMe)-Ser-Ala-Cys(SMe)-$CONH_2$(CSAC) has been used as a model for MT for reactions of cis- and trans-platin.[54] The reaction with cisplatin forms a mixture of different stereoisomers and polymeric species, with NH_3 liberation due to the strong *trans*-effect of sulfur. Transplatin, on the other hand, forms a 2:1 complex coordinated to the –S-CH_3 groups and no amine release is observed.

Therapeutic nucleophilic agents for cisplatin, such as Na(ddtc) (sodium diethyldithiocarbamate) and thiourea, can help to remove platinum from certain proteins so as to relieve toxicity.[55] The mechanism may be based on the relatively

easy reversal of platinum binding to methionine side chains. In contrast, nephrotoxicity, thought to be caused by formation of Pt-cysteine adducts (Pt(II) thiolate bonds), cannot be reversed by Na(ddtc) and thiourea.

Although the kinetic reactivity of sulfur is high, the Pt-thioether bond is labile in the presence of other nucleophiles.[25] This could provide a novel pathway for DNA platination. The competitive binding of Met, His, 5'-GMP, 5'-AMP, 5'-TMP and 5'-CMP to $\{Pt(dien)Cl\}^+$ in aqueous solution shows that 5'-GMP selectively displaces S-bound Met. Initially only L-Met coordinates to platinum with little GMP coordination, but in the later stages of the reaction coordinated L-Met is displaced by N7 of GMP.[25, 56] It is notable that thioethers such as L-Met react with Pt(II) amines faster than thiols such as GSH, and reactions of thiols tend to be irreversible.[57]

1.2.1.4 Resistance Mechanisms

The occurrence of resistance in cancer chemotherapy is a common problem, and cisplatin is no exception. Some types of cancer are intrinsically insensitive to cisplatin treatment, whereas other cancers develop resistance during the chemotherapy. The mechanisms of resistance against cisplatin can be divided into two groups: 1) mechanisms that prevent cisplatin reaching its therapeutic target, DNA, and 2) mechanisms that block the induction of apoptosis after the formation of the cisPt-DNA adduct. In resistant cancer cells, several resistance mechanisms often act simultaneously.

Decreased uptake/increased efflux leads to lower intracellular drug concentrations.[58] As a result, higher drug doses are needed to induce the same amount of cell damage. A more established mechanism of resistance is the scavenging of platinum drugs by intracellular thiol-containing molecules, especially

glutathione (GSH) which is available in cells at high concentrations (0.5-10 mM).[59] Glutathione reacts with platinum drugs to form deactivated conjugates that are readily excreted by a glutathione S-conjugate export pump.[49] Raised intracellular concentrations of GSH often correlate with cisplatin resistance, but other platinum complexes may be less sensitive towards GSH deactivation.[60]

An important resistance mechanism that occurs after platinum binding is the repair of DNA damage. For 1,2-intrastrand adducts of cisplatin, the nucleotide excision repair (NER) system is of particular importance.[61] The mechanism recognises the kink induced by cisplatin, and subsequently excises the part of the DNA strand that includes the kink. The gap that remains is then filled again by DNA polymerase.

The post-binding mechanism described as 'increased tolerance' is probably one of the most general resistance mechanisms encountered in cancer chemotherapy.[62, 63] In this case, the cellular damage inflicted by the drug fails to kill the cancer cell. This phenomenon is generally associated with the failure of apoptotic pathways. In order to trigger apoptosis, it is believed the cellular damage has to pass a certain threshold level. However, damaged genes are common in cancer cells, and proteins involved in the apoptotic pathways often malfunction, thus making certain cancer types rather insensitive to damage. In particular cancer apoptosis is very hard to trigger, although all cells may eventually be killed when cellular damage rises to levels where essential processes are simply not functioning anymore.[63]

1.3 Development of New Platinum Anticancer Drugs

Although cisplatin is currently one of the best-selling anticancer drugs in the world there are still many drawbacks associated with it. Patients treated with the drug experience many toxic side effects including nausea, vomiting, loss of high frequency hearing and kidney toxicity. Drug resistance is also a problem as some cell lines are not affected by the drug. So far, cisplatin is used only against testicular and ovarian cancers and increasingly against cervical, bladder and head/neck tumours. More recently trials have shown acquired drug resistance developing in certain tumours after repeated treatment with the drug. In an attempt to overcome these problems over 3000 platinum compounds have been synthesised and tested for antitumour activity.[28] In order to design new drugs in a logical manner, a set of structure-activity relationships (SARs) was established for platinum compounds with the general formula *cis*-$[PtX_2(Am)_2]$ (in which X is an anionic leaving group and Am is ammonia, primary or secondary amine), and include the following:[64]

1) the complexes exchange only some of their ligands quickly in reactions with biomolecules,
2) the complexes should be neutral, although the active form may be charged after undergoing ligand exchanges,
3) the leaving groups (e.g. Cl in cisplatin) should be in the *cis* configuration and their lability should be neither too high nor too low,
4) relatively inert amine type systems are required and there must be at least one N-H group on the amine.

These restrictions led to a second generation of platinum drugs, all of which were analogues of cisplatin containing two *cis* primary or secondary amine groups and two

anionic leaving groups.

1.3.1 Cisplatin Derivatives

The structures of some interesting new platinum compounds are shown in Figure 1.13. The most successful of these second generation platinum compounds is carboplatin (**1**). Since its introduction in 1986 it has largely replaced cisplatin in the treatment of many platinum-sensitive malignancies. Carboplatin has less severe side effects and nephrotoxicity and vomiting are reduced but it is cross-resistant with cisplatin. Its activity is equivalent to cisplatin in the treatment of ovarian cancers, but in the treatment of testicular and head and neck cancer cisplatin is still superior.[65]

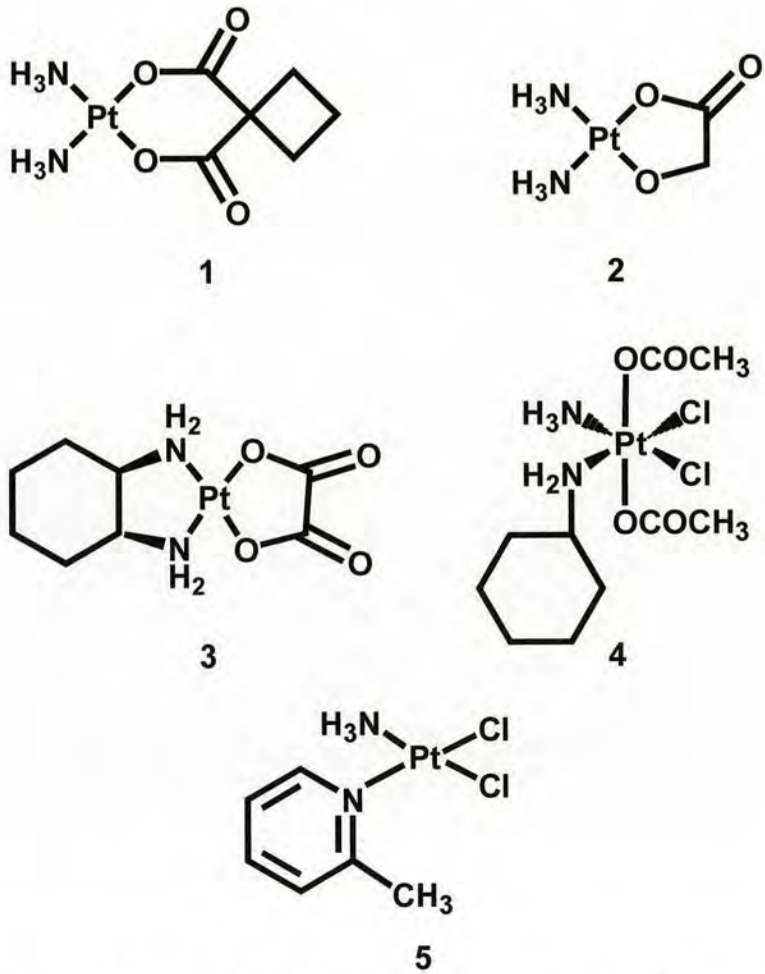

Figure 1.13 Second generation Pt anticancer agents, clinically approved or in human trials.

Two other second generation compounds have been approved for clinical use. Nedaplatin (**2**) has been approved for use in Japan,[66] and oxaliplatin (**3**) has been approved in France, Asia and Latin America.[66, 67] Both are effective in the treatment of lung, colorectal and ovarian cancers. However, like carboplatin, nedaplatin is cross-resistant with cisplatin, meaning that these drugs are affected by the same resistance mechanisms.[68] This may be related to the fact that the drugs form the same type of DNA damage. Thus, although useful for patients suffering from toxic side effects, these cisplatin derivatives are not expected to circumvent the resistance problem.

On the other hand, oxaliplatin can circumvent cisplatin resistance and is being increasingly used in chemotherapy.[67] Oxaliplatin features a dicarboxylate leaving group and a chelating 1,2-diaminocyclohexane carrier ligand which increases the lipophilicity, which helps the drug to permeate cell membranes. The DNA adducts of oxaliplatin are more effective than those of cisplatin in inhibiting DNA chain elongation.[69] Better cellular uptake and different DNA adducts are believed to help oxaliplatin in circumventing cisplatin resistance mechanisms. In clinical trials, oxaliplatin displayed activity against a wide range of tumours, but neurotoxicity is a dose-limiting factor in its clinical use.[66] Most recently, oxaliplatin has been approved in the USA for the treatment of colorectal cancer.[70]

The complex JM216 (**4**), also known as satraplatin, was shown to have superior activity against cervical, small cell lung, and ovarian cancer cell lines.[71] This Pt(IV) complex has a big advantage over most Pt(II) drugs as it can be administered orally. This is much more convenient for patients and also reduces costs of therapy. Moreover, JM216 circumvents cisplatin/carboplatin resistance and

showed low nephrotoxicity and neurotoxicity in phase I clinical trials.[72] Phase II trials are ongoing and some results have been reported.[71] The decreased toxicity is thought to be due to the fact that Pt(IV) complexes are kinetically more inert than Pt(II) complexes. It is known that the Pt(IV) complex undergoes a biotransformation into its Pt(II) analogue in patients, and thus acts as a prodrug.[73]

Another promising complex currently in clinical trials is *cis*-[$PtCl_2(NH_3)$(2-picoline)] (AMD473) (**5**)[74] which will be further discussed in Section 1.4. The steric hindrance exerted by the methyl group of the 2-picoline ligand makes this compound less reactive, especially with respect to deactivating scavengers such as glutathione.[75, 76] AMD473 was found to be active against cisplatin-resistant tumours, and has been shown to be orally active in preclinical tumour models.[71] It has the added advantage that it lacks nephrotoxicity. Also, this complex appears to form a highly stereoselective G*G* adduct with duplex DNA which may be recognised differently to that of cisplatin by the excision repair system.[77]

1.3.2 New Concepts in Platinum Anticancer Chemistry

Although the second generation of platinum drugs is less toxic than cisplatin, many appear to be cross-resistant with cisplatin. In the last decade, nearly all the previously accepted structure activity relationships (SARs) have been disproved and now new generations of drugs are being designed with much more widely ranging structures. Requirements which are influencing the search for new generations of active complexes include (1) lower toxicity to normal cells than cisplatin, (2) activity against tumours with acquired cisplatin resistance, (3) activity against a wider spectrum of types of cancer and (4) oral activity.

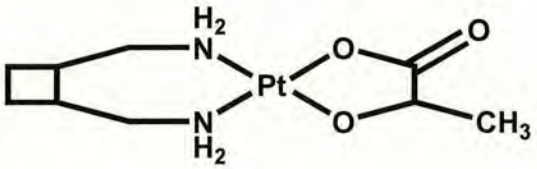

6

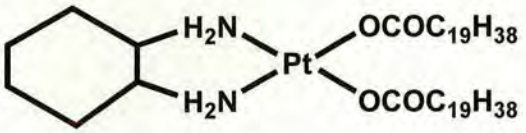

7

Figure 1.14 Lobaplatin (**6**) and *cis*-bis(neodecanoato)(*trans*-R,R-1,2 diaminocyclohexane)Pt^{II} (**7**).

There are currently various platinum complexes at different stages of clinical trials. Laboplatin, **6**, (Figure 1.14) which has a cyclobutane-derived carrier group, and lactate as a leaving group, was introduced into clinical trials in 1992. Lobaplatin has been approved in China for the treatment of chronic myelogenous leukaemia (CML) and inoperable, metastatic breast and small cell lung cancer.[78] It has also completed phase II trials in the US, Australia, Europe, Brazil and South Africa for the treatment of several cancers including oesophageal, lung and ovarian cancers as well as CML.[78] Complex **7** (Figure 1.14), *cis*-bis(neodecanoato)(*trans*-R, R-1,2 diaminocyclohexane) platinum(II), is a liposome-incorporated lipophilic cisplatin analogue with *in vivo* activity against liver metastases and tumours resistant to cisplatin[79] and is currently under clinical evaluation. This drug may be activated by forming intermediates in lipid bilayers, and the activity is highly dependent on the presence of liposomes.[80] The only active intermediate identified so far is *cis*-dichloro-*trans*-R, R-1,2-diaminocyclohexane platinum(II).[81]

1.3.2.1 Multinuclear Platinum Complexes

Dinuclear and trinuclear compounds present a new class of platinum anticancer complexes (Figure 1.15). BBR3005 (**8**) is a dinuclear complex that exhibits antitumour activity especially in cisplatin-resistant cell lines. Binding studies

showed that DNA binding for this compound is different to that of cisplatin, as illustrated by the increased interstrand cross-linking.[82, 83] In June 1998 the trinuclear complex BBR3464 (**9**) entered phase I clinical trials and is currently in phase II clinical trials in the UK.

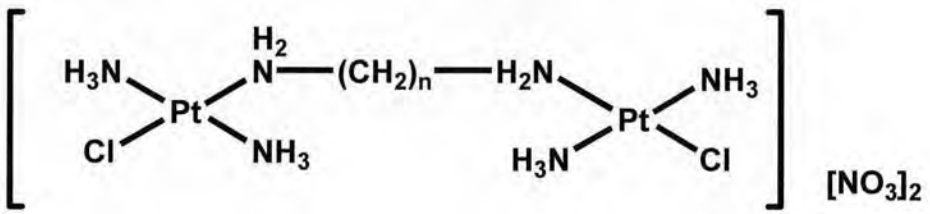

8

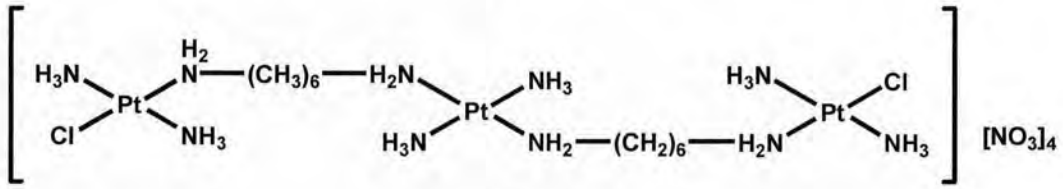

9

Figure 1.15 Multinuclear Pt complexes BBR3005 (**8**) and BBR3464 (**9**).

The central platinum unit is capable only of H-bonding interactions with DNA.[84] The overall charge (+4) greatly enhances DNA affinity, which is characterised by long-range inter- and intra-strand cross-linking and irreversible conversion of B- to Z- DNA.[84, 85] In contrast to cisplatin, DNA intrastrand adducts induced by BBR3464 do not lead to DNA bending and are not recognised by high mobility group (HMG) proteins, which recognise cisplatin-damaged DNA. These features could be a critical reason for the ability of BBR3464 to overcome cisplatin resistance. BBR3464 is approximately 40-fold more potent than cisplatin on a molar basis and is active in both cisplatin-sensitive and cisplatin-resistant tumour models.[85]

1.3.2.2 *Trans* Platinum Complexes

Trans platinum complexes are another class of compounds where reduction of activity has lead to improved anticancer drugs. The *trans* isomer of cisplatin, *trans*-$[PtCl_2(NH_3)_2]$ (**10**) is clinically inactive.[86] Reasons that have been invoked to explain the lack of antitumour activity of transplatin include its inability to form the 1,2-intrastrand cross-link and structural differences between interstrand cross-links.[86]

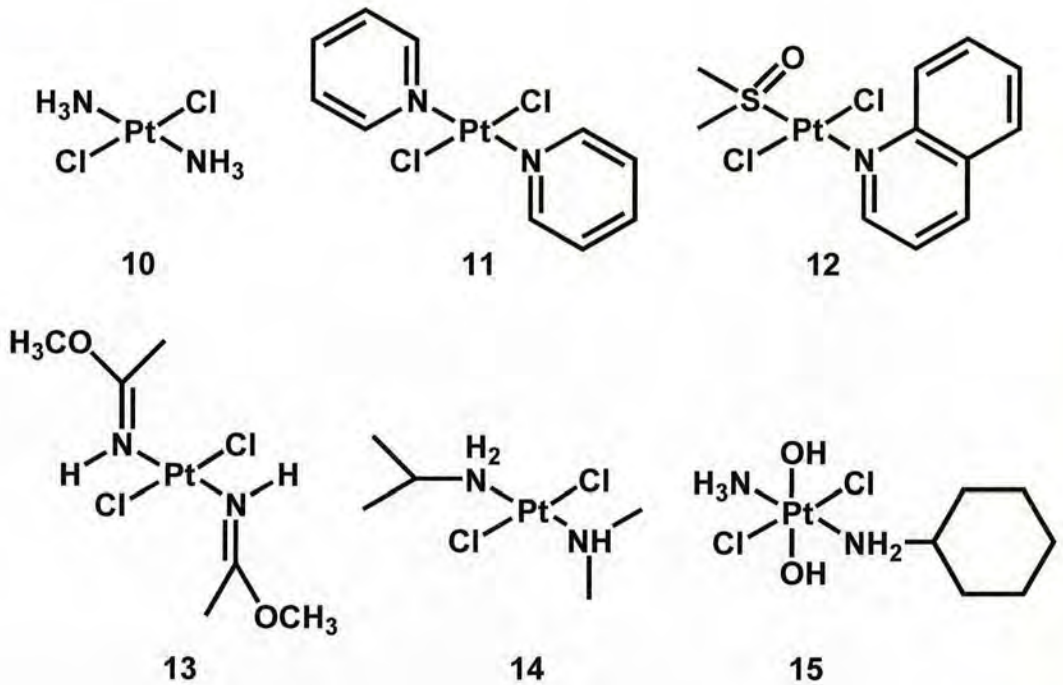

Figure 1.16 *Trans* Pt complexes.

Whereas cisplatin forms a 1,2-intrastrand cross-link between guanines of adjacent base pairs, definitive evidence shows that monofunctional adducts of transplatin slowly transform into interstrand adducts involving guanine-N7 and complementary cytosine-N3 of the same base pair.[87, 88] However, substitution of the ammonia ligands has lead to an increasing number of antitumour-active *trans* complexes.[86] Apart from the fact that *trans* complexes form DNA adducts different from cisplatin, there are also indications that preliminary deactivation by binding to proteins and

other non-DNA components is an explanation for the lack of anticancer activity of transplatin.[89, 90] Sterically more demanding ligands, as in *cis*-[$PtCl_2(NH_3)$(2-pic)], may reduce the detoxification reactions, thus evading preliminary detoxification before binding to DNA.

The four known types of antitumour active mononuclear *trans* compounds are:[90] 1) *trans*-Pt(II)Cl_2 complexes with planar aromatic ligands (**11**, **12**), 2) *trans*-iminoether compounds (**13**), 3) *trans*-Pt(II)Cl_2 compounds with asymmetric aliphatic amines (**14**), and 4) *trans*-Pt(IV) mixed amine complexes(**15**), Figure 1.16.

For the first class, *trans*-Pt(II)Cl_2 complexes with planar aromatic ligands, three distinct series of *trans*-[$PtCl_2$(L)(L')][91] complexes were examined: a) L = L' = pyridine, N-methylimidizole, or thiazole b) L = quinoline and L' = RR'SO (R = Me, R' = Me, Bz or Ph) and c) L = quinoline or thiazole and L' = NH_3. In general, the cytotoxicity of all *trans* complexes examined was approximately one order of magnitude greater than that of transplatin and furthermore, the *trans* complexes were at least as cytotoxic as their direct *cis*-analogues.[92] As a general feature, *trans* complexes with bulky planar ligands were not cross-resistant to cisplatin (the resistance factor defined as IC_{50} (acquired resistance cells)/IC_{50} (sensitive cells), was $\leq$ 1) in both murine L1210 leukaemia and human ovarian tumour cells resistant to cisplatin.[92] Importantly, the thiazole complex, *trans*-[$PtCl_2(NH_3)$(tz)], also shows *in vivo* antileukaemic activity, thus overcoming the main caveat of *trans* bispyridine complexes, i.e. the lack of *in vivo* efficacy.[90]

The enhanced cytotoxic potency of *trans*-platinum complexes with pyridine-like ligands along with their ability to overcome cisplatin resistance disclosed novel

mechanistic implications, suggesting that complexes structurally different from cisplatin may be characterised by distinct cellular pharmacological properties.

Coluccia and Natile[93] have reported another class of active *trans*-platinum complexes having the general formula *trans*-[$PtCl_2$(iminoether)$_2$] or *trans*-[$PtCl_2(NH_3)$(iminoether)], where iminoether = HN=C(OR)R'. Iminoether ligands are unsymmetrical with the possibility of isomerism within the ligand moiety. The *in vitro* cell growth inhibitory activity was evaluated in comparison to those of cisplatin in a panel of human tumour cell lines containing examples of ovarian, colon, lung and breast cancers, as well as a subline of ovarian cancer cells with acquired resistance to cisplatin (A2780/cp8).[94] The *trans*-iminoether compounds showed a growth inhibitory potency similar to that of cisplatin (mean IC_{50} = 8 μM). Moreover, *trans*-iminoether compounds were able to circumvent the cisplatin resistance of A2780/cp8 cells which are characterised by having a reduced cisplatin accumulation and greater intracellular glutathione content with respect to the parental cell line. The *trans*-[$PtCl_2(NH_3)$(iminoether)] compounds also showed cytotoxic potency higher than that of transplatin in a panel of human tumour cell lines.

Compounds with asymmetric aliphatic amines, such as the *trans*-[$PtCl_2$(amine)(isopropylamine)] complexes, exhibit activity comparable to that of cisplatin.[95, 96] These compounds have IC_{50} values lower than that of cisplatin in HL-60 leukaemic cells (tumour cells overexpressing *c-myc* and *N-ras* oncogenes).[95] The same complexes exhibit IC_{50} values significantly lower than those of cisplatin against cisplatin resistant murine keratinocytes transformed by *H-ras* oncogene (Pam 212-ras cells). Contrary to cisplatin, these complexes display a much lower cytotoxicity in normal Pam 212 murine keratinocytes than in Pam 212-ras transformed murine

keratinocytes.[96] *Trans*-[$PtCl_2$(dimethylamine)(isopropylamine)] is also able to circumvent resistance to cisplatin in A2780 cells.[97]

The fourth class of active *trans*-platinum compounds are the *trans*-[$Pt^{IV}Cl_2X_2(L)(L')$] complexes where X = hydroxide, carbamate or carboxylate, L = amine and L' = ammine. Many of these *trans* complexes studied *in vitro* against a panel of human cell lines exhibited comparable potency to cisplatin and also overcame acquired cisplatin resistance (mainly due to either reduced uptake or enhanced platinum-DNA removal).[98] Fourteen of these *trans* complexes showed significant *in vivo* antitumour activity against the subcutaneous murine ADJ/PC6 plasmacytoma model. All were Pt^{IV} complexes possessing axial hydroxide ligands, except one which had axial ethylcarbamate ligands. When tested, all of their dichloroplatinum(II) or tetrachloroplatinum(IV) counterparts were inactive.

1.4 AMD473

Cis-[$PtCl_2(NH_3)$(2-picoline)] (AMD473), is a recently reported anticancer complex for which phase I and phase II clinical trials are currently underway in a range of tumour types, including lung, colorectal and small cell lung cancers.[99] AMD473 has demonstrated promising activity against several tumours including ovarian, lung and breast. It was developed at the Institute of Cancer Research, in collaboration with Johnson Matthey Technology Centre/AnorMED, and has recently been licensed to NeoRx Corporation, Seattle. AMD473 is reported to possess activity against cisplatin-resistant cell lines, and against an acquired cisplatin-resistant subline of a human ovarian carcinoma xenograph, by injection and oral administration.[100] It showed significantly reduced cross-resistance to cisplatin in a panel of three cell lines with known acquired platinum drug resistance mechanisms:

reduced accumulation, increased cytoplasmic detoxification by cellular thiols and increased DNA repair/tolerance of Pt-DNA adducts.[101] The toxicity of AMD473 is also greatly reduced, with no renal toxicity observed.[100]

AMD473 was designed specifically to circumvent thiol mediated drug resistance by sterically hindering its reaction with glutathione (GSH), but still having the ability to form cytotoxic lesions with DNA. Interestingly, AMD473 also circumvents cisplatin resistance in tumour cell lines where cisplatin resistance is known to include some non-glutathione based mechanisms.[102]

The crystal structure of AMD473[75] showed that the complex has a typical square-planar configuration. The most notable feature is the orientation of the picoline ring which is almost perpendicular (103°) to the platinum square-plane, so that the 2-methyl group lies directly over the Pt centre. This introduces steric hindrance to an axial approach to platinum from above, leading to a destabilisation of the expected bipyramidal transition state.

Hydrolysis may be an important step in the intracellular activation and interaction with DNA. Hydrolysis rates and pK_a values of AMD473 have been determined using [^{1}H,^{15}N] NMR spectroscopy.[75] The Cl^- ligand *cis* to 2-picoline (*trans* to NH_3) hydrolyses about 4 times more slowly than that in cisplatin[22] ($t_{1/2}$ = 8.7 h at 310 K, compared with 1.9 h for cisplatin), whilst the Cl^- ligand *trans* to 2-picoline (*cis* to NH_3) hydrolyses about three times more slowly than that in cisplatin ($t_{1/2}$ = 6.0 h at 310 K). The pK_a values for the monoaqua adduct are 6.13 and 6.49, and values of 5.22 and 7.16 are reported for the diaqua adduct, all of which are > 0.3 units lower than for cisplatin.[23] The slowness of the hydrolysis, combined with the

dominance of (inert) hydroxo species, is expected to contribute to a greatly reduced reactivity of AMD473 under intracellular conditions.

1.5 Aims of this Thesis

The overall aim of this thesis is to generate a greater understanding of the chemical and biochemical properties of sterically hindered Pt^{II} compounds, including the anticancer drug AMD473, to aid the development of more novel platinum chemotherapeutic agents, capable of further improving antitumour activity in resistant tumours.

In order to investigate the influence of steric hindrance on *trans* Pt^{II} complexes, the initial challenge is to synthesise and perform a full structural characterisation of a series of *trans* picoline complexes. As hydrolysis may be an important step in the mechanism of action of such compounds with DNA, the determination of hydrolysis rates and pK_a values will be investigated also.

To gain further insight into stereochemical effects on the structure and dynamics of nucleobase adducts in solution and in the solid state, a study will be undertaken of AMD473 and its *trans* isomer, *trans*-$[PtCl_2(NH_3)(2\text{-pic})]$(AMD443), with the model nucleobase 9-ethylguanine (9-EtGH). This work will also be extended to include the investigation of nucleosides. The kinetics of the reaction of aquated AMD473 with guanosine will be studied and nucleoside adducts of both AMD473 and AMD443 will be characterised.

Since DNA is the major target for Pt^{II} drugs in the body, it is of much interest to study the interaction of *trans*-$[PtCl_2(NH_3)(2\text{-pic})]$ with duplex DNA, which is likely to form distinct adducts with both its *cis* isomer and cisplatin.

Finally, the nature of interactions with small sulphur-containing biomolecules is of particular significance for such sterically hindered Pt complexes, as a reduced susceptibility to deactivating molecules such as glutathione could lead to enhanced anticancer activity. Studies will be performed using the dominant intracellular thiol, glutathione, and the thioether methionine.

1.6 References

[1] F. R. Hartley, *The Chemistry of Platinum and Palladium*, Applied Science Publishers Ltd., London, **1973**.

[2] I. I. Chernyaev, *Chem. Abs.* **1927**, *21*, 2620.

[3] A. D. Gel'man, E. F. Karandashova, L. N. Essen, *Chem. Abs.* **1949**, *43*, 1678.

[4] F. A. Cotton, G. Wilkinson, *Advanced Inorganic Chemistry*, 5th ed., John Wiley and Son, New York, **1988**.

[5] R. N. Keller, *Inorg. Synth., Vol. 2*, McGraw-Hill Book Company Inc., New York, **1946**.

[6] Z. Guo, P. J. Sadler, *Angew. Chem. Int. Ed.* **1999**, *38*, 1512.

[7] J. Reedijk, *Curr. Opin. Chem. Biol.* **1999**, *3*, 236.

[8] B. Rosenberg, L. V. Camp, T. Krigas, *Nature* **1965**, *205*, 698.

[9] B. Rosenberg, L. V. Camp, E. B. Grimley, A. J. Thomson, *J. Biol. Chem.* **1967**, *242*, 1347.

[10] B. Rosenberg, L. V. Camp, J. E. Trosko, V. H. Mansour, *Nature* **1969**, *222*, 385.

[11] B. Rosenberg, L. V. Camp, *Cancer Res.* **1970**, *30*, 1799.

[12] M. J. Cleare, J. D. Hoeschele, *Bioinorg. Chem.* **1973**, *2*, 187.

[13] B. Rosenberg, in *Cisplatin*, Verlag Helvetica Chimica Acta, Zürich, **1999**, pp. 3.

[14] M. Rozencweig, D. D. v. Hoff, M. Slavik, F. M. Muggia, *Annals of Internal Medicine* **1977**, *86*, 803.

[15] D. M. Hayes, E. Cvitkovic, R. B. Golbey, E. Scheiner, L. Helson, I. H. Krakoff, *Cancer* **1977**, *39*, 1372.

[16] Z. Guo, P. J. Sadler, *Adv. Inorg. Chem.* **2000**, *49*, 183.

[17] P. A. Andrews, K. D. Albright, in *Platinum and Coordination Compounds in Chemotherapy*, Plenum Press, New York, **1991**, pp. 151.

[18] K. Kawai, N. Kamatani, E. Georges, V. Ling, *J. Biol. Chem.* **1990**, *265*, 13137.

[19] D. P. Gately, S. S. B. Howell, *Br. J. Cancer* **1993**, *67*, 1171.

[20] M. Jennerwein, P. A. Andrews, *Drug Metab. Dispos.* **1995**, *23*, 178.

[21] N. P. Johnson, J. D. Hoeschele, R. O. Rahn, *Chem. Biol. Interact.* **1980**, *30*, 151.

[22] D. P. Bancroft, C. A. Lepre, S. J. Lippard, *J. Am. Chem. Soc.* **1990**, *112*, 6860.

[23] S. J. Berners-Price, T. A. Frenkiel, U. Frey, J. D. Ranford, P. J. Sadler, *J. Chem. Soc. Chem. Commun.* **1992**, 789.

[24] S. S. G. E. v. Boom, J. Reedijk, *J. Chem. Soc. Chem. Commun.* **1993**, 1397.

[25] K. J. Barnham, M. I. Djuran, P. d. S. Murdoch, P. J. Sadler, *J. Chem. Soc. Chem. Commun.* **1994**, 721.

[26] I. Saito, M. Takayama, H. Sugiyama, K. Nakatani, *J. Am. Chem. Soc.* **1995**, *117*, 6406.

[27] A. M. J. Fichtinger-Schepman, J. L. v. d. Veer, J. H. J. d. Hartog, P. H. M. Lohman, J. Reedijk, *Biochemistry* **1985**, *24*, 707.

[28] E. R. Jamieson, S. J. Lippard, *Chem. Rev.* **1999**, *99*, 2467.

[29] U. M. Ohndorf, M. A. Rould, Q. He, C. O. Pabo, S. J. Lippard, *Nature* **1999**, *399*, 708.

[30] A. Eastman, M. M. Jennerwein, D. L. Nagel, *Chem.-Biol. Interactions* **1988**, *67*, 71.

[31] J. P. Whitehead, S. J. Lippard, *Met. Ions Biol. Syst.* **1996**, *32*, 687.

[32] A. Gelasco, S. J. Lippard, in *Metallopharmaceuticals: DNA Interactions*, Springer-Verlag, Berlin, **1999**, pp. 2.

[33] S. E. Sherman, D. Gibson, A. H.-J. Wang, S. J. Lippard, *Science* **1985**, *230*, 412.

[34] G. Admiraal, J. L. v. d. Veer, R. A. G. d. Graaff, J. H. J. d. Hartog, J. Reedijk, *J. Am. Chem. Soc.* **1987**, *109*, 592.

[35] P. M. Takahara, A. C. Rosenzweig, C. A. Frederick, S. J. Lippard, *Nature* **1995**, *377*, 649.

[36] P. M. Takahara, C. A. Frederick, S. J. Lippard, *J. Am. Chem. Soc.* **1996**, *118*, 12309.

[37] F. Herman, J. Kozelka, V. Stoven, E. Guittet, J.-P. Girault, T. Huynh-Dinh, J. Igolen, J.-Y. Lallemand, J.-C. Chottard, *Eur. J. Biochem.* **1990**, *194*, 119.

[38] D. Yang, S. S. G. E. v. Boom, J. Reedijk, J. H. v. Boom, A. H.-J. Wang, *Biochemistry* **1995**, *34*, 12912.

[39] A. Gelasco, S. J. Lippard, *Biochemistry* **1998**, *37*, 9230.

[40] J. H. Toney, B. A. Donahue, P. J. Kellett, S. L. Bruhn, J. M. Essigmann, S. J. Lippard, *Proc. Natl. Acad. Sci. USA* **1989**, *86*, 8328.

[41] B. A. Donahue, M. Augot, S. F. Bellon, D. K. Treiber, J. H. Toney, S. J. Lippard, J. M. Essigman, *Biochemistry* **1990**, *29*, 5872.

[42] P. M. Pil, S. J. Lippard, *Science* **1992**, *256*, 234.

[43] J.-C. Huang, D. B. Zamble, J. T. Reardon, S. J. Lippard, A. Sancar, *Proc. Natl. Acad. Sci. USA* **1994**, *91*, 10394.

[44] Y. Jung, S. J. Lippard, *Biochemistry* **2003**, *42*, 2664.

[45] J.-M. Teuben, C. Bauer, A. H.-J. Wang, J. Reedijk, *Biochemistry* **1999**, *38*, 12305.

[46] C. M. Riley, L. A. Sternson, A. J. Repta, S. A. Slyter, *Anal. Biochem.* **1983**, *130*, 203.

[47] R. E. Norman, J. D. Ranford, P. J. Sadler, *Inorg. Chem.* **1992**, *31*, 877.

[48] P. d. S. Murdoch, J. D. Ranford, P. J. Sadler, S. J. Berners-Price, *Inorg. Chem.* **1993**, *32*, 2249.

[49] T. Ishikawa, F. Ali-Osman, *J. Biol. Chem.* **1993**, *268*, 20116.

[50] T. Ishikawa, C. D. Wright, H. Ishizuka, *J. Biol. Chem.* **1994**, *269*, 29085.

[51] S. J. Berners-Price, P. W. Kuchel, *J. Inorg. Biochem.* **1990**, *38*, 305.

[52] T. G. Appleton, J. W. Connor, J. R. Hall, P. D. Prenzler, *Inorg. Chem.* **1989**, *28*, 2030.

[53] Y. Chen, Z. Guo, P. J. Sadler, in *Cisplatin*, Verlag Helvetica Chimica Acta, Zürich, **1999**, pp. 293.

[54] N. Hadjiliadis, N. Ferderigos, J.-L. Butour, H. Marzarguil, G. Gasmi, J.-P. Laussac, *Inorg. Chem.* **1994**, *33*, 5057.

[55] E. L. M. Lempers, J. Reedijk, *Inorg. Chem.* **1990**, *29*, 217.

[56] S. S. G. E. v. Boom, B. W. Chen, J. M. Teuben, J. Reedijk, *Inorg. Chem.* **1999**, *38*, 1450.

[57] M. I. Djuran, E. L. M. Lempers, J. Reedijk, *Inorg. Chem.* **1991**, *30*, 2648.

[58] K. Wang, J. Lu, R. Li, *Coord. Chem. Rev.* **1996**, *151*, 53.

[59] J. Reedijk, J. M. Teuben, in *Cisplatin*, Verlag Helvetica Chimica Acta, Zürich, **1999**, pp. 339.

[60] P. Goddard, M. Valenti, L. R. Kelland, *Anticancer Res.* **1994**, *14*, 1065.

[61] S. G. Chaney, A. Sancar, *J. Nat. Cancer Inst.* **1996**, *88*, 1346.

[62] R. P. Perez, *Eur. J. Cancer* **1998**, *34*, 1535.

[63] V. M. Gonzalez, M. A. Fuertes, C. Alonso, J. M. Perez, *Mol. Pharmacol.* **2001**, *59*, 657.

[64] T. W. Hambley, *Coord. Chem. Rev.* **1997**, *166*, 181.

[65] D. S. Alberts, S. Green, E. V. Hannigan, R. O'Toole, D. Stock-Novack, P. Anderson, E. A. Surwit, V. K. Malvlya, W. A. Nahhas, C. J. Jolles, *J. Clin. Oncol.* **1992**, *10*, 706.

[66] D. Lebwohl, R. Canetta, *Eur. J. Cancer* **1998**, *34*, 1522.

[67] M. A. Graham, G. F. Lockwood, D. Greenslide, S. Brienza, M. Bayssas, E. Gamelin, *Clin. Cancer Res.* **2000**, *6*, 1205.

[68] B. J. Monk, D. S. Alberts, R. A. Burger, P. T. Fanta, A. V. Hallum, K. D. Hatch, S. E. Salmon, *Gynecologic Oncol.* **1998**, *71*, 308.

[69] J. M. Woynarowski, S. Faivre, M. C. S. Herzig, B. Arnett, W. G. Chapman, A. V. Trevino, E. Raymond, S. G. Chaney, A. Vaisman, M. Varchenko, P. E. Juniewicz, *Mol. Pharmacol.* **2000**, *58*, 920.

[70] A. Ibrahim, S. Hirschfeld, M. H. Cohen, D. J. Griebel, G. A. Williams, R. Pazdur, *The Oncologist* **2004**, *9*, 8.

[71] L. R. Kelland, in *Cisplatin*, Verlag Helvetica Chimica Acta, Zürich, **1999**, pp. 497.

[72] M. J. McKeage, F. E. Boxall, M. Jones, K. R. Harrap, *Cancer Res.* **1994**, *54*, 629.

[73] E. G. Talman, Y. Kidani, L. Mohrmann, J. Reedijk, *Inorg. Chim. Acta* **1998**, *283*, 251.

[74] L. R. Kelland, S. Y. Sharp, C. F. O'Neill, F. I. Raynaud, P. J. Beale, I. R. Judson, *J. Inorg. Biochem.* **1999**, *77*, 111.

[75] Y. Chen, Z. Guo, S. Parsons, P. J. Sadler, *Chem. Eur. J.* **1998**, *4*, 672.

[76] Y. Chen, Z. Guo, J. A. Parkinson, P. J. Sadler, *J. Chem. Soc. Dalton Trans.* **1998**, 3577.

[77] Y. Chen, J. A. Parkinson, Z. Guo, T. Brown, P. J. Sadler, *Angew. Chem. Int. Ed.* **1999**, *38*, 2060.

[78] *Drugs in R & D* **2003**, *4*, 369.

[79] A. R. Khokhar, S. Al-Baker, T. Brown, R. Perez-Soler, *J. Med. Chem.* **1991**, *34*, 325.

[80] R. Perez-Soler, A. R. Khokhar, *Cancer Res.* **1992**, *52*, 6341.

[81] I. Han, A. R. Khokhar, R. Perez-Soler, *Cancer Chemother. Pharmacol.* **1996**, *39*, 17.

[82] Y. Zou, B. V. Houten, N. Farrell, *Biochemistry* **1994**, *33*, 5404.

[83] N. Farrell, Y. Qu, U. Bierbach, M. Valsecchi, E. Menta, in *Cisplatin*, Verlag Helvetica Chimica Acta, Zürich, **1999**, pp. 479.

[84] P. D. Blasi, A. Bernareggi, G. Beggiolin, L. Piazzoni, E. Menta, M. L. Formento, *Anticancer Res.* **1998**, *18*, 3113.

[85] D. I. Jodrell, T. R. J. Evans, W. Steward, D. Cameron, J. Prendiville, C. Aschele, C. Noberasco, M. Lind, J. Carmichael, N. Dobbs, G. Camboni, B. Gatti, F. D. Braud, *Eur. J. Cancer* **2004**, *2004*, 1872.

[86] N. Farrell, *Met. Ions Biol. Syst.* **1996**, *32*, 603.

[87] V. Brabec, M. Leng, *Proc. Natl. Acad. Sci. USA* **1993**, *90*, 5345.

[88] R. Dalbiès, D. Payet, M. Leng, *Proc. Natl. Acad. Sci. USA* **1994**, *91*, 8147.

[89] B. Lippert, *Met. Ions Biol. Syst.* **1996**, *33*, 105.

[90] G. Natile, M. Coluccia, *Met. Ions Biol. Syst.* **2004**, *42*, 209.

[91] M. V. Beusichem, N. Farrell, *Inorg. Chem.* **1992**, *31*, 634.

[92] N. Farrell, L. R. Kelland, J. D. Roberts, M. V. Beusichem, *Cancer Res.* **1992**, *52*, 5065.

[93] M. Coluccia, A. Nassi, F. Loseto, A. Boccarelli, M. A. Mariggio, D. Giordano, F. P. Intini, P. A. Caputo, G. Natile, *J. Med. Chem.* **1993**, *36*, 510.

[94] M. Coluccia, A. Nassi, A. Boccarelli, D. Giordano, N. Cardellicchio, D. Locker, M. Leng, M. Sivo, F. P. Intini, G. Natile, *J. Inorg. Biochem.* **1999**, *77*, 31.

[95] E. I. Montero, S. Diaz, A. M. González-Vadillo, J. M. Pérez, C. Alonso, C. Navarro-Ranninger, *J. Med. Chem.* **1999**, *42*, 4264.

[96] J. M. Pérez, E. I. Montero, A. M. González, A. Alvarez-Valdés, C. Alonso, C. Navarro-Ranninger, *J. Inorg. Biochem.* **1999**, *77*, 37.

[97] E. I. Montero, J. M. Pérez, A. Schwartz, M. A. Fuertes, J. M. Malinge, C. Alonso, M. Leng, C. Navarro-Ranninger, *ChemBioChem* **2002**, *3*, 61.

[98] L. R. Kelland, C. F. J. Barnard, I. G. Evans, B. A. Murrer, B. R. C. Theobald, S. B. Wyer, P. M. Goddard, M. Jones, M. Valenti, A. Bryant, P. M. Rogers, K. R. Harrap, *J. Med. Chem.* **1995**, *38*, 3016.

[99] *www.neorx.com.*

[100] F. I. Raynaud, F. E. Boxall, P. M. Goddard, M. Valenti, M. Jones, B. A. Murrer, M. Abrams, L. R. Kelland, *Clin. Cancer Res.* **1997**, *3*, 2063.

[101] J. Holford, S. Y. Sharp, B. A. Murrer, M. Abrams, L. R. Kelland, *Br. J. Cancer* **1998**, *77*, 366.

[102] J. Holford, F. Raynaud, B. A. Murrer, K. Grimaldi, J. A. Hartley, M. Abrams, L. R. Kelland, *Anti-Cancer Drug Design* **1998**, *13*, 1.

Chapter 2

Experimental Methods

2.1 NMR Spectroscopy

NMR signals were first recorded in 1946 and can now routinely be detected for almost any magnetic nucleus. Many textbooks have been published describing the theory and applications of NMR.[1-8]

Nuclear magnetic moments are exquisitely sensitive to their surroundings and yet interact very weakly with them. When a magnetic nucleus is placed in a magnetic field, it adopts one of a number of allowed orientations of different energy. For example, the nucleus of the hydrogen atom (a proton) has just two permitted orientations. The magnetic moment can point in the same direction as the field or in the opposite direction. These two states are separated by an energy ΔE, which depends on the strength of interaction between the nucleus and the field, i.e. on the size of the nuclear magnetic moment and the strength of the magnetic field. ΔE may be measured by applying electromagnetic radiation of frequency ν, which causes nuclei to flip from the lower energy level to the upper one, provided the resonance condition $\Delta E = h\nu$ (h is Planck's constant) is satisfied. This is nuclear magnetic resonance spectroscopy.

The magnetic properties of some useful nuclei are listed in Table 2.1.[8, 9] The most important aspects of ^{15}N and ^{195}Pt NMR spectroscopy are reviewed here. A selection of 2D correlation NMR techniques, relevant to this thesis, will also be mentioned.

Table 2.1 NMR properties of common nuclei (in an 11.74 T magnetic field).[8, 9]

Nucleus	% Natural Abundance	Spin Quantum Number (I)	Gyromagnetic Ratio (10^7 rad T^{-1} s^{-1})	Resonant Frequency (MHz)	Relative Sensitivity
^{1}H	99.98	½	26.75	500.00	1.00
^{2}H	0.02	1	4.11	76.75	1.5×10^{-6}
^{13}C	1.11	½	6.73	125.72	1.8×10^{-4}
^{14}N	99.63	1	1.93	36.12	1.0×10^{-3}
^{15}N	0.37	½	-2.71	50.66	3.9×10^{-6}
^{195}Pt	33.8	½	5.77	107.50	3.4×10^{-3}

2.1.1 ^{195}Pt NMR Spectroscopy[9]

^{195}Pt is a reasonably sensitive nucleus for NMR detection, with natural abundance of 33.8%, nuclear spin quantum number I = ½, and a receptivity relative to ^{1}H of 3.4×10^{-3}.

The ^{195}Pt chemical shift range is very large, about 15000 ppm (usually in the range from -6000 to 9000 ppm relative to $[PtCl_6]^{2-}$), and often allows easy differentiation between Pt^{II} and Pt^{IV}, which tend to have chemical shifts at the high-field and low-fields ends of the range, respectively. The ^{195}Pt chemical shift in monomeric complexes is sensitive primarily to the set of bound donor atoms. Some caution is required in searching for peaks, because the shifts of Pt^{IV} halides alone span 12000 ppm. Also, usually there are ^{195}Pt chemical shift differences between geometrical isomers and between diastereomers (chiral ligands). For ^{15}N-enriched ligands, the splitting pattern in the ^{195}Pt spectrum indicates the number of non-equivalent ^{15}N atoms coordinated. These characteristics of the ^{195}Pt chemical shift can be utilised in the detection of different intermediates formed during the reactions of Pt complexes with biomolecules. Sometimes even isotopomers are

distinguishable: the ^{195}Pt isotope shift difference for ^{195}Pt-$^{35/37}$Cl is 0.17 ppm and for ^{195}Pt-$^{79/81}$Br is 0.03 ppm.[10] It is therefore in principle possible to count the number of Cl and Br ligands bonded to Pt via the isotope splitting pattern. In practice it is difficult to resolve because of line broadening, which is usually due to either relaxation mechanisms or poor temperature control of the sample. The latter is a problem because of the strong temperature dependence of ^{195}Pt NMR resonances (0.5 to 1.1 ppm/ K). The spin-lattice relaxation time (T_1) for ^{195}Pt is usually in the range of 0.3 to 1.3 s.

The quadrupolar effects of natural abundance ^{14}N (i.e. 99.6% ^{14}N, I = 1) from am(m)ines which coordinate to Pt can broaden the ^{195}Pt resonances. Such quadrupolar effects of ^{14}N have the beneficial effects of shortening the ^{195}Pt relaxation times and allowing rapid pulsing without saturation effects. ^{195}Pt-^{14}N couplings in ^{195}Pt NMR spectra are usually better resolved at higher temperature, because of the decreased quadrupolar relaxation rate of ^{14}N due to the decrease in correlation time. Even in the absence of ^{14}N ligands, ^{195}Pt resonances can still be very broad owing to chemical shift anisotropy (CSA) relaxation, which can be the dominant relaxation mechanism for Pt complexes at high magnetic field stength. The limit of detection (ca. 10 mM) precludes detection of natural abundance ^{195}Pt signals at physiologically relevant concentrations and has therefore not been used in this thesis. The receptivity can be improved by a factor of three by isotopic enrichment of ^{195}Pt (> 95%).

^{195}Pt satellites in ^{15}N and ^{1}H spectra of Pt^{II} complexes are often broadened beyond detection owing to CSA relaxation of ^{195}Pt.[11] The linewidths of ^{195}Pt

satellites of ^{1}H NMR resonances are dependent on the spin-lattice relaxation time of ^{195}Pt:

$$\Delta\nu_{1/2}(H) = [\pi T_2^*(H)]^{-1} + [2\pi T_1(Pt)]^{-1}$$

where $[\pi T_2^*(H)]^{-1}$ is the natural linewidth plus the contribution from magnetic inhomogenity broadening (measurable from the linewidth of the centre peak). The contribution to ^{195}Pt T_1 relaxation from CSA is given by:

$$[\pi T_1(Pt)]^{-1}\ (CSA) = (6/7)\times[\pi T_2(Pt)]^{-1}\ (CSA) = (2/15) \times \gamma_{Pt}^2 \times B_0^2 \times \Delta\sigma^2 \times \tau_c$$

In general, ^{195}Pt satellites (and ^{195}Pt resonances) are sharper in Pt^{IV} complexes which are six coordinate and hence more symmetrical (smaller anisotropy $\Delta\sigma$) and are broader at higher fields of measurement (B_0) and in larger molecules (longer correlation time τ_c).

2.1.2 ^{15}N NMR Spectroscopy

^{14}N NMR spectroscopy can be useful for am(m)ine complexes, but ^{14}N is a quadrupolar nucleus, and quadrupolar relaxation is dominant when the environment of ^{14}N has a low symmetry. This can lead to very broad lines and a consequent reduction in sensitivity. On the other hand, short relaxation times also have the advantage of allowing rapid pulsing so that a large number of transients can be acquired. Thus, it is possible to follow reactions of cisplatin in blood plasma and cell culture media at millimolar drug concentrations and to detect ammine release.[12]

By using ^{15}N enriched am(m)ine complexes, the broadening of ^{195}Pt signals caused by the quadrupolar effects of ^{14}N can be avoided. Both ^{15}N NMR chemical shifts and $^{1}J(^{195}Pt\text{-}^{15}N)$ coupling constants are sensitive to the nature of the *trans* ligand in Pt am(m)ine complexes, which can provide useful information for

identifying the ligands in the coordination spheres of both Pt(II) and Pt(IV) complexes. Typical ^{15}N and ^{1}H shift ranges for Pt(II) are shown in Figure 2.1.

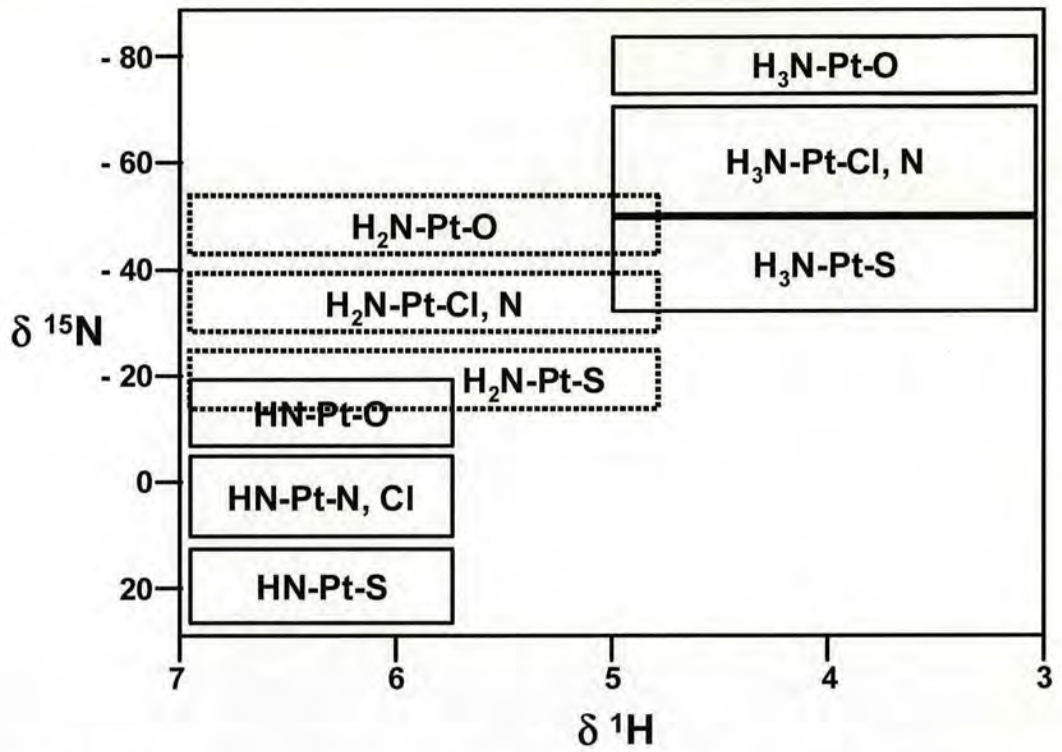

Figure 2.1 Variation of ^{1}H and ^{15}N NMR chemical shifts with the *trans* ligand in Pt(II)-NH, Pt(II)-NH_2 and Pt(II)-NH_3 complexes.

In general, ligands (X) with high *trans* influences give rise to smaller X-^{195}Pt-^{15}N coupling constants (X = S<I<Br<Cl<H_2O) and cause a low-field shift of the ^{15}N resonance. The dominant contribution to one-bond coupling constants between ^{195}Pt and ^{15}N is usually interpreted in terms of the Fermi contact interaction involving Pt 6s and N 2s orbitals.[13] The usefulness of $^{1}J(^{195}Pt\text{-}^{15}N)$ values is limited by the difficulty in determining them for larger molecules especially at high observation frequencies on account of the dominance of relaxation via chemical shift anisotropy (CSA). The $^{1}J(^{195}Pt\text{-}^{15}N)$ values for Pt(IV) are smaller by a factor of about 1.5 to 1.2 and are 1.4 times larger than $^{1}J(^{195}Pt\text{-}^{14}N)$ values.

The low receptivity of ^{15}N (3.9×10^{-6} relative to ^{1}H) limits to some extent its usefulness for directly-detected ^{15}N NMR studies of Pt ammine and amine complexes. However, the sensitivity of detection can be improved by ^{15}N isotopic enrichment combined with enhancement by polarization transfer from ^{1}H (e.g. ^{15}N-$\{^{1}H\}$ DEPT and INEPT pulse sequences). The maximum enhancement in ^{15}N signal intensity achievable via polarization transfer is only 9.8 ($\gamma H/\gamma N$), which means that inverse (^{1}H-detected) ^{15}N methods are usually preferred due to the superior enhancement for ^{15}N-detection (*vide infra*). The repetition time of the pulse sequence is governed by the ^{1}H rather than the longer ^{15}N spin-lattice relaxation time (T_1), which is an additional advantage because it allows more rapid pulsing. For example, ^{15}N-$\{^{1}H\}$ DEPT sequences enable detection of rapidly-changing intermediates in the reaction of ^{15}N-cisplatin with glutathione, and also ammine release following the reaction of ^{15}N-cisplatin with intracellular components in intact red blood cells at concentrations as low as 1 mM.[14]

2.1.3 Water Suppression

NMR spectra for biomolecules are normally obtained from aqueous media, such as D_2O (99.9%) or H_2O/D_2O (90%:10%, v/v). However, for metal anticancer complexes, such as Pt am(m)ine complexes, the Pt – NH ^{1}H NMR resonances cannot be readily detected in D_2O solutions because the half-life for H-D exchange is only a few minutes at ambient temperatures.[15, 16] In H_2O solutions, the intense H_2O peak causes severe dynamic range problems. Therefore, most studies in aqueous media are carried out in H_2O/D_2O (90%:10%, v/v), the D_2O being added to provide a field locking signal. Special techniques are needed to suppress the large HOD (or H_2O) signal. Presaturation and WATERGATE (WATER suppression by GrAdient

Tailored Excitation) were used in this study.[17] The former method is applied by irradiation at the frequency of the HOD (H_2O) resonance during the relaxation delay between pulses, before the observe pulse in an experiment. The disadvantage is that exchangeable NH protons can also be saturated resulting in loss of intensity. The WATERGATE method uses selective 180° pulse field gradients to select different coherence pathways, and yields superior water suppression.

2.1.4 2D Spectra

HSQC (heteronuclear single-quantum correlation) experiments allow identification of the chemical shifts of protons and X-nuclei that are directly coupled. One use of such correlations is to allow assignments already made for one nuclear species to be transferred to the other. A more important use is in overcoming problems caused by overlap in the proton spectrum: in the heteronuclear 2D spectrum the proton resonances are spread out according to the shifts of the heteronuclei to which they are coupled.

The HSQC technique belongs to the family of indirect (or inverse) detection techniques. An important feature of the experiment is that the proton magnetisation which is detected during t_2 originated as proton magnetisation at the start of the sequence. The major advantage of this technique is the sensitivity of detection, which is enhanced by a theoretical maximum of 306 $\{(|\gamma H|/|\gamma N|)^{5/2}\}$ with respect to directly detected ^{15}N, such that signals can be detected from platinum am(m)ine complexes in aqueous solution at concentrations of physiological relevance.[9] These methods are widely applicable to any complex which has a ^{15}N atom with a measurable spin-spin coupling to ^{1}H (i.e. ammine, primary and secondary amines, but not tertiary amines).

In practice the best results are obtained with large one-bond couplings (about 73 Hz for $^{15}NH_3$). The basic HSQC pulse sequence is shown in Figure 2.2.

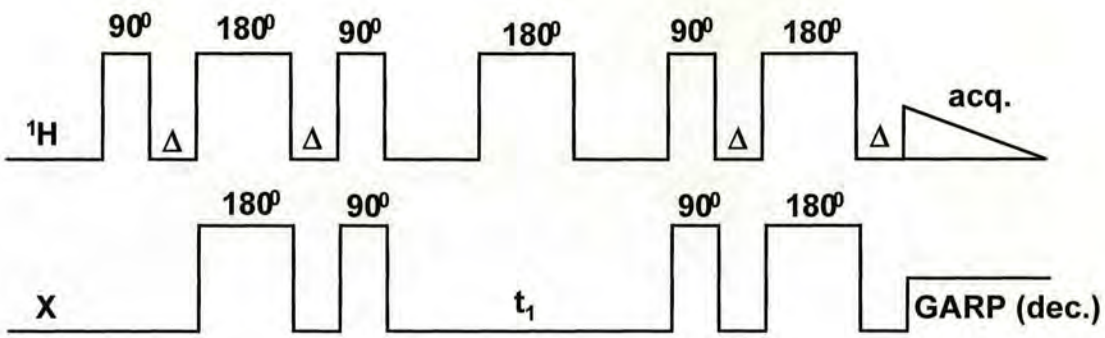

Figure 2.2 Basic HSQC pulse sequence. The delays $\Delta = ½ J(X,H)$, where J is the one-bond HX coupling constant, and one-dimensional ^{15}N-edited spectra are obtained by setting the evolution period t_1 to zero. Spectra may be recorded with or without decoupling of ^{15}N spins (GARP) during the acquisition period.

The Pt – ^{15}NH protons can be detected selectively by the use of [^1H,^{15}N] single quantum coherence (HSQC) pulse sequences. A 1D ^1H spectrum containing only resonances from Pt – ^{15}NH species is obtained by acquiring only the first increment in a 2D experiment; resonances for CH and OH (including water) are eliminated. This is particularly useful in studies of body fluids or cell culture media, where only the signals from the platinum complexes are detected and thousands of other overlapping ^1H resonances are filtered out. If ^{15}N decoupling is employed during acquisition (e.g. the GARP method), then each type of Pt – NH resonance appears as a singlet. In practice, the water resonance is so intense that it is usually necessary to use additional solvent suppression techniques such as presaturation. The addition of an H_2O T_2 relaxation agent (e.g. 0.5 M $(NH_4)_2SO_4$) can also be helpful to detect NH peaks very close to the H_2O peak. A large improvement in water

suppression is achieved by the use of pulsed field gradients for coherence selection, for example, by use of the HSQC sequences of Stonehouse et al.[18]

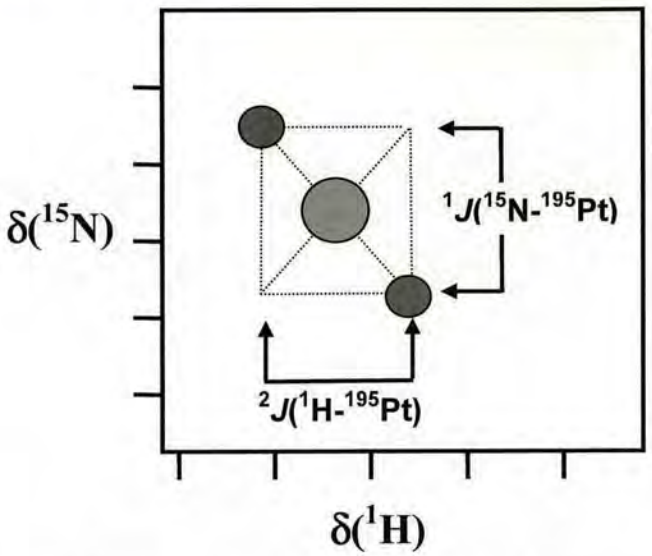

Figure 2.3 General appearance of a 2D [^{1}H,^{15}N] HSQC spectrum. The ^{195}Pt satellites are usually more intense for symmetrical Pt species (Pt^{IV} rather than Pt^{II}).

The combined detection of ^{1}H and ^{15}N in a 2D inverse NMR experiment is especially powerful, since both the ^{15}N NMR chemical shift and the one-bond coupling constant $^{1}J(^{1}H\text{-}^{15}N)$ are diagnostic of the *trans* ligand. As shown in Figure 2.3, the ^{195}Pt satellites (when not broadened beyond detection by the effects of CSA relaxation) in a 2D [^{1}H, ^{15}N] spectrum appear as diagonal peaks which correspond to the $^{2}J(^{195}Pt\text{-}^{1}H)$ coupling constant in the $F_2(^{1}H)$ dimension and to the $^{1}J(^{195}Pt\text{-}^{15}N)$ coupling in the $F_1(^{15}N)$ dimension. Pt^{II} and Pt^{IV} am(m)ine complexes can be distinguished by the combination of ^{1}H and ^{15}N chemical shifts.

COSY (correlated spectroscopy) is a two-dimensional homonuclear (H, H)-correlated NMR experiment which yields NMR spectra in which ^{1}H chemical shifts along both frequency axes are correlated with each other.[19, 20] It is the standard 2D experiment that can be used to identify pairs of protons that have scalar spin-spin

coupling connectivities. There are two inherent drawbacks that limit its usefulness with macromolecules: one is that the fine-structure components that make up each cross-peak appear in anti-phase; the other is that the diagonal peaks and the cross-peaks are 90° out of phase in both dimensions. These give rise to poor sensitivity and extremely harsh weighting functions must be used to give spectra with usable line shapes which in turn gives a further reduction in sensitivity.

TOCSY provides a different mechanism of coherence transfer than COSY for 2D correlation spectroscopy.[6, 21] In TOCSY, cross-peaks are generated between all members of a coupled spin network. An advantage is that the "net" coherence transfer produced can be arranged to create pure absorption mode spectra with positive intensity peaks (rather than "differential" coherence transfer which causes spectra with equal positive and negative intensities). In traditional COSY, cross-peaks have zero integrated intensity and coherence transfer is restricted to directly spin-coupled nuclei. In TOCSY, oscillatory exchange is established which proceeds through the entire coupling network so that there can be net magnetisation transfer from one spin to another even without direct coupling. The isotropic mixing which occurs during the spin-lock period of the TOCSY sequence exchanges all in-phase as well as anti-phase coherences.

The **NOESY** experiment[22, 23] is often used to identify pairs of protons that are undergoing cross-relaxation, i.e. protons that would show an NOE in 1D experiments. The characteristic feature of the NOESY pulse sequence is the mixing time τ. The cross-peaks are generated by magnetisation transfer that takes place during the mixing time so the length of this delay must be chosen according to the rate of the transfer process. In contrast to the COSY experiment, both cross-peaks

and diagonal peaks in NOESY spectra can be obtained with absorption-mode lineshapes. The experiments are therefore very suitable for studying macromolecules. If presaturation is used in a NOESY experiment it is usually also necessary to irradiate the solvent during the mixing time. A complicated factor is that the NOESY pulse sequence cannot distinguish between magnetisation transfer caused by cross-relaxation and magnetisation transfer by chemical exchange. In macromolecules, both give cross-peaks of the same sign as the diagonal.

The **ROESY** experiment[5, 6] is a rotating frame NOESY that provides some advantages for small and medium-sized, as well as large molecules. Whereas the NOE decreases to zero and becomes negative as the mean correlation time, τ_c, for molecular rotation increases (larger molecules move more slowly), in the rotating frame the maximum NOE remains positive and even increases from 50 % to 67.5 %. The pulse sequence for ROESY is similar to TOCSY although the period of spin locking is chosen to optimise magnetisation transfer through the NOE (dipolar interactions) rather than through scalar couplings. In addition to greater signal enhancement, the ROESY experiment also decreases the effects of spin diffusion, so that it offers advantages for larger molecules.

2.2 High Performance Liquid Chromatography (HPLC)[24]

HPLC is one of the fastest developing analytical techniques. It has arisen from the theories of liquid chromatography (LC) and instrumentation that were originally developed for gas chromatography (GC). The mixture to be analysed is dissolved in a suitable solvent, injected at one end of the column, and carried through the column by a continuous flow of the same solvent (mobile phase). The separation

takes place in the column, which contains 'sorptive' particles of large surface area. These particles are referred to as the 'stationary phase'. Injected sample components interact reversibly with the stationary phase in a continuous manner. If a component mixture (a solute) is absorbed weakly onto the surface of the solid stationary phase it will travel down the column faster than another solute that is more strongly absorbed. The mobile phase is pumped through the column bed of tightly packed chromatographic particles using a solvent delivery system (pump). With the selection of proper mobile phase and column packing material, a separation of different components can be achieved. As the sample components emerge from the column, a suitable detector is used to monitor and transmit a signal to a recording device. The chromatogram is a record of the detector response as a function of time and indicates the presence of the components as peaks.

Reverse phase (RP) chromatography is so named because it behaves in the opposite way to normal phase (NP) chromatography. The stationary phase is silica chemically bonded with an alkylsilyl compound to give a non-polar, hydrophobic surface. Solute retention is mainly due to hydrophobic interactions between the solutes and the hydrocarbonaceous stationary phase surface. Polar mobile phases, usually water mixed with methanol, acetonitrile and/or other water-miscible organic solvents, are used for elution. Solutes are eluted in order of decreasing polarity (increasing hydrophobicity), and increasing the polar (aqueous) component of the mobile phase increases the retention of the solutes.

In analytical HPLC, the mobile phase is normally pumped through the column at a flow rate of 1-5 ml/min. If the composition of the mobile phase is constant, the method is called 'isocratic elution'. The composition of the mobile

phase can be a binary, ternary, or quaternary solvent mixture. Alternatively, the composition of the mobile phase can be made to change in a predetermined way during the separation, a technique called 'gradient elution'. Modern solvent delivery systems allow the selection of a wide range of gradient profiles and variation of the time over which the gradient is delivered. Besides the shape of the gradient, other factors including compatibility of the two solvents with the detector, and miscibility with the sample solution, have to be considered.

Some of the important concepts defining the quality of a chromatographic separation are listed below.

Capacity ratio or capacity factor, k'

$$k_1' = \frac{t_1 - t_0}{t_0} \qquad k_2' = \frac{t_2 - t_0}{t_0}$$

- where t_0 is the retention time of an unretained compound, usually a solvent used to dissolve the solutes. It represents the column void volume and the peak is often referred to as the 'solvent front'; t_1 and t_2 are the retention times of compounds 1 and 2 respectively. k' is a measure of solute retention.

Selectivity, α

$$\alpha = \frac{k_1'}{k_2'}$$

- α measures the ability of a column to separate components 1 and 2 due to different affinity and therefore retention.

Efficiency of the column, which can be measured using quantities of plate number (N) and plate height (H).

$$N = 16\left(\frac{t_1}{w_1}\right)^2 \qquad H = \frac{L}{N}$$

- t_1 is the retention time of the component, w_1 is the peak width of solute 1, L and N are the length and plate number of the column, respectively, and H is the height.

Resolution factor, R_s

$$R_s = \frac{t_2 - t_1}{0.5(w_2 - w_1)}$$

- R_s measures the resolution between two components and is dependent on k', α and N.

2.3 Mass Spectrometry

Mass spectrometry is a versatile technique that can provide information on the elemental composition of samples of matter and the structures of inorganic, organic or biological molecules. The general principle of mass spectrometry is the conversion of an analyte sample into gaseous ions which are attracted through the slit of the mass spectrometer and separated according to their mass-to-charge ratios. A spectrum is provided which is like a bar chart depicting the relative intensity of mass peaks according to this ratio. The components of a mass spectrometer are shown in Figure 2.4.

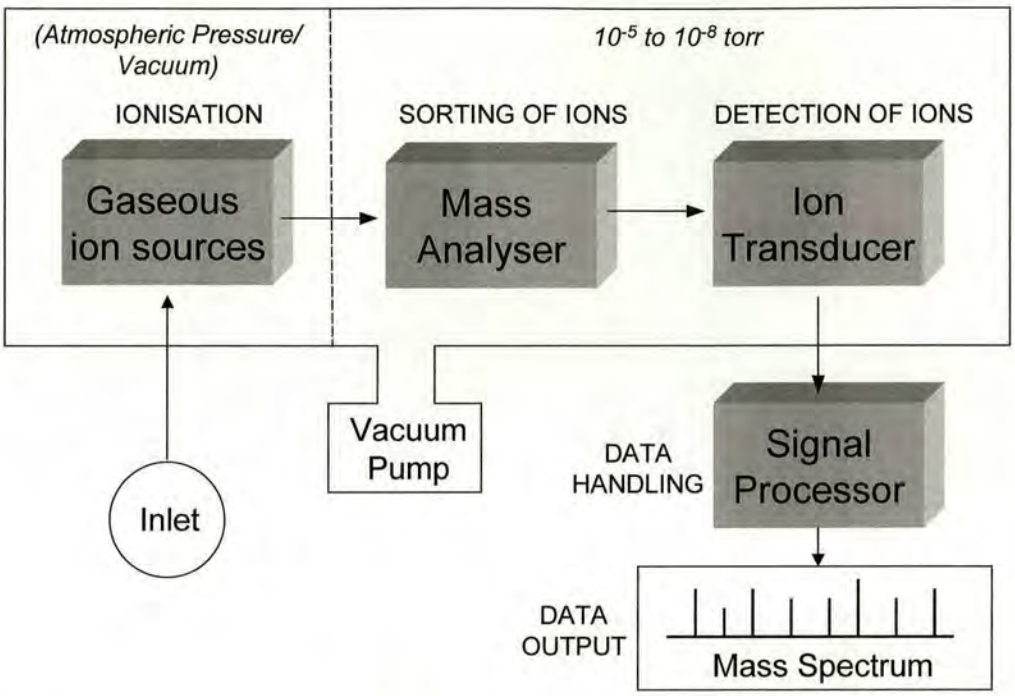

Figure 2.4 Components of a mass spectrometer.

Electrospray Ionisation

Electrospray ionisation (ESI)[25-28] is a desorption ion source where a sample in solution is converted directly into gaseous ions. It is a *soft* ion source in that it does not impart enough energy to the analyte molecules to fragment ions during analysis.

An electrospray is produced by applying a strong electric field, under atmospheric pressure, to a liquid passing through a capillary tube with a weak flux (normally 1-10 μl/min). The electric field is obtained by applying a potential difference of 3-6 kV between this capillary and the counter electrode, separated by 0.3-2 cm. This field induces a charge accumulation at the liquid surface located at the end of the capillary, which will break to form highly charged droplets. Driven by the electric field, the droplets migrate towards the inlet end of the glass capillary at the end wall of the chamber. A drying gas at 320 to 350 K, encourages evaporation of

solvent from each droplet, decreasing its diameter. Consequently, the charge density at its surface increases until the *Rayleigh limit* is reached at which point the Coulomb repulsion becomes of the same order as the surface tension. The resulting instability tears the droplet apart, producing charged daughter droplets that also evaporate. This sequence of events repeats until the radius of curvature of the daughter droplet becomes small enough that the field due to the surface charge density is strong enough to desorb ions from the droplet into the ambient gas.

The ESI mass spectra normally correspond to a statistical distribution of consecutive peaks characteristic of multiply charged molecular ions obtained through protonation $(M + zH)^{z+}$, while avoiding the contributions from dissociations or from fragmentations. ESI can also be used in the case of molecules without any ionizable site through the formation of sodium, potassium, ammonium or other adducts.

Obtaining multiply charged ions is advantageous as it improves the sensitivity and it allows the analysis of high molecular weight molecules using analysers with a weak nominal mass limit.

2.4 References

[1] P. J. Hore, *Nuclear Magnetic Resonance*, Oxford University Press, New York, **1995**.

[2] R. J. Abraham, J. Fisher, P. Loftus, *Introduction to NMR Spectroscopy*, John Wiley and Sons, New York, **1988**.

[3] H. Günther, *NMR Spectroscopy -Basic Principles, Concepts and Applications in Chemistry*, 2nd ed., John Wiley and Sons, Chichester, **1995**.

[4] J. A. Iggo, *NMR Spectroscopy in Inorganic Chemistry*, Oxford University Press, New York, **1999**.

[5] J. K. M. Sanders, B. K. Hunter, *Modern NMR Spectroscopy*, Oxford University Press, New York, **1997**.

[6] J. B. Lambert, H. F. Shurvell, D. A. Lighter, R. G. Cooks, *Organic Structural Spectroscopy*, Prentice Hall, New Jersey, **1998**.

[7] H. Friebolin, *Basic One- and Two- Dimensional NMR Spectroscopy*, VCH, Weinheim, **1991**.

[8] L. M. Harwood, T. D. W. Claridge, *Introduction to Organic Spectroscopy*, Oxford University Press, New York, **1997**.

[9] S. J. Berners-Price, P. J. Sadler, *Coord. Chem. Rev.* **1996**, *151*, 1.

[10] I. M. Ismail, S. J. S. Kerrison, P. J. Sadler, *J. Chem. Soc. Chem. Comm.* **1980**, 1175.

[11] I. S. Ismail, S. J. S. Kerrison, P. J. Sadler, *Polyhedron* **1982**, *1*, 57.

[12] R. E. Norman, P. J. Sadler, *Inorg. Chem.* **1988**, *27*, 3583.

[13] P. S. Pregosin, H. Omura, L. M. Venazi, *J. Am. Chem. Soc.* **1973**, *95*, 2047.

[14] S. J. Berners-Price, P. W. Kuckel, *J. Inorg. Biochem.* **1990**, *38*, 327.

[15] E. Koubek, D. A. House, *Inorg. Chim. Acta.* **1992**, *191*, 103.

[16] S. K. Miller, L. G. Marzilli, *Inorg. Chem.* **1985**, *24*, 2421.

[17] M. Piotto, V. Saudek, V. Sklenar, *J. Biomol. NMR* **1992**, *2*, 661.

[18] J. Stonehouse, G. L. Shaw, J. Keller, E. D. Laue, *J. Magn. Reson. Series A* **1994**, *107*, 178.

[19] W. P. Aue, E. Bartholdi, R. R. Ernst, *J. Chem. Phys.* **1976**, *64*, 2229.

[20] K. Nagayama, A. Kumar, K. Wuethrich, R. R. Ernst, *J. Magn. Reson.* **1980**, *40*, 321.

[21] L. Braunschweiler, R. R. Ernst, *J. Magn. Reson.* **1983**, *53*, 521.

[22] J. Jeener, B. H. Meier, P. Bachmann, R. R. Ernst, *J. Chem. Phys.* **1979**, *71*, 4546.

[23] A. Kumar, R. R. Ernst, K. Wuthrich, *Biochem. Biophys. Res. Commun.* **1980**, *95*, 1.

[24] S. Lindsay, *High Performance Liquid Chromatography*, John Wiley and Sons, London, **1992**.

[25] D. A. Skoog, E. J. Holler, T. A. Nieman, *Principles of Instrumental Analysis*, 5th ed., Saunders College Publishing, Philadelphia, **1998**.

[26] J. B. Fenn, M. Mann, C. K. Meng, S. F. Wong, C. M. Whitehouse, *Science* **1989**, *246*, 64.

[27] R. D. Smith, J. A. Loo, C. G. Edmonds, C. J. Barinaga, H. R. Udseth, *Anal. Chem.* **1990**, *62*, 882.

[28] P. Kebarle, *J. Mass Spectrom.* **2000**, *35*, 804.

Chapter 3

Hydrolysis of *Cis* and *Trans* Picoline Pt^{II} Diamine Anticancer Compounds

3.1 Abstract

Cis-[$PtCl_2(NH_3)$(2-picoline)] (AMD473) is currently on clinical trials as an anticancer drug. The *trans* isomer, AMD443 (**1**), is also cytotoxic in a variety of cancer cell lines. The X-ray crystal structure of the *trans* isomer (**1**) shows that the pyridine ring is tilted by 69° with respect to the platinum square-plane in contrast to the *cis* isomer in which it is almost perpendicular (103°). In the 3-picoline (**2**) and 4-picoline (**3**) *trans* isomers, the ring is tilted by 58°/60° (2 molecules per unit cell) and by 56°, respectively. Hydrolysis may be an important step in the intracellular activation and anticancer mechanism of action of these complexes. The first hydrolysis step is relatively fast even at 277 K, with rate constants (determined by $^{1}H,^{15}N$ NMR) of $k_1 = 2.6 \times 10^{-5}$ s^{-1}, 12.7×10^{-5} s^{-1} and 5.2×10^{-5} s^{-1} (I = 0.1 M) for formation of the monoaqua complexes of **1**, **2** and **3**, respectively. Although the hydrolysis of **3** is slower than **2**, it is hydrolysed to a greater extent. No formation of the diaqua complex was observed for any of the three complexes at 277 K, and it accounts for <3 % of the platinum species at 310 K. In general the extent of hydrolysis of the *trans* complexes is much less than for their *cis* analogues. The pK_a values for the monoaqua adducts of **1**, **2** and **3** were determined to be 5.55, 5.35 and 5.39, respectively, suggesting that they would exist largely as the monohydroxo complex at physiological pH. The pK_a values for the diaqua adducts were determined to be 4.03 and 7.01 for **1**, 3.97 and 6.78 for **2**, and 3.94 and 6.88 for **3**, the first pK_a being > 1 unit lower than for related *cis* complexes.

3.2 Introduction

Cisplatin is now a widely-used clinical drug for the treatment of various neoplastic diseases, including testicular and ovarian cancers, while its congener transplatin is therapeutically inactive.[1] This observation, which is considered a paradigm for the Structure-Activity Relationships (SARs) of platinum-based antitumour compounds, has dominated development in this field for more than two decades. The SARs have aided the design of new drugs and guided attempts to overcome some of the drawbacks associated with cisplatin, such as nausea, neurotoxicity, nephrotoxicity and ototoxicity, as well as drug resistance. These SARs led to a second generation of platinum drugs, all of which are analogues of cisplatin containing two *cis* primary or secondary amine groups and two anionic leaving groups. The most successful of these is carboplatin, which has less severe side-effects than cisplatin.[2, 3] However, many of the second-generation platinum drugs appear to be cross-resistant with cisplatin.[4]

Much recent research work has been aimed at the discovery of platinum complexes which are not cross-resistant with cisplatin, have fewer toxic side-effects, are active against a broader range of types of cancer, and can be administered orally. In 1989, two exceptions to the classic SAR were reported showing that the overall charge on the complex and the *cis* orientation of the N-bound ligands are not a prerequisite for antitumour activity of Pt^{II} complexes. Hollis et al.[5] reported that positively-charged triaminemonochloroplatinum(II) complexes of the general formula $[Pt(NH_3)_2(Am)Cl]^+$ (where Am = planar heterocyclic amine) possess antitumour activity. These complexes were neither neutral nor did they possess two *cis* weakly bound leaving groups. Subsequently, Farrell et al.[6] reported that *trans*

platinum complexes with planar amine ligands have antitumour activity superior to transplatin, especially in cisplatin-resistant cell lines. These were the first examples of platinum-based anticancer agents that defy the classic SARs.

The presence of planar ligands in *trans*-$[PtCl_2(L)_2]$ (L = pyridine, thiazole) and *trans*-$[PtCl_2(NH_3)(L)]$ (L = quinoline) complexes greatly enhances the cytotoxicity of such species, with respect to their corresponding *cis* isomers and also to transplatin.[7] The cytotoxicity is further marked by high activity towards both sensitive and cisplatin-resistant murine leukaemia (L1210) cells (Table 3.1).[7, 8] Thus, the activity is an order of magnitude greater than transplatin. DNA interstrand cross-linking is enhanced relative to transplatin and conformational changes such as unwinding are accentuated in the presence of the planar ligand. The sequence specificity is also altered, with the *trans* complexes exhibiting a higher affinity for alternating purine-pyrimidine (GC) runs.[9]

Table 3.1 Cytotoxicity of Pt^{II} complexes in L1210 and cisplatin-resistant (L1210R) leukaemia cells.[7, 8]

	IC_{50} (μM)	
Complex	L1210	L1210 (R)
cis-$[PtCl_2(py)_2]$	4.4	3.3
trans-$[PtCl_2(py)_2]$	1.2	1.1
cis-$[PtCl_2(tz)_2]$	2.8	7.3
trans-$[PtCl_2(tz)_2]$	1.6	7.4
cis-$[PtCl_2(NH_3)(quin)]$	0.5	2.8
trans-$[PtCl_2(NH_3)(quin)]$	0.5	1.4
cis-$[PtCl_2(NH_3)(tz)]$	3.2	3.1
trans-$[PtCl_2(NH_3)(tz)]$	4.2	15.0
cis-$[PtCl_2(NH_3)_2]$	0.3	9.2
trans-$[PtCl_2(NH_3)_2]$	15.7	22.0

py = pyridine, tz = thiazole, quin = quinoline

Unfortunately, high antitumour activity of such *trans* complexes has not yet been obtained *in vivo*. Nevertheless, the observations on the enhanced cytotoxicity are important mechanistically, because they demonstrate that there is no restriction, *per se*, to development of active antitumour *trans* platinum complexes. The mechanistic importance of these findings is also emphasised by the fact that the vast majority of studies examining the differences between *cis*- and *trans*-platin have been carried out in tissue culture or in cell-free systems. Factors such as water solubility and pharmacokinetic considerations (e.g. partition coefficient, drug metabolism and tissue distribution) may all contribute to *in vivo* deactivation of cytotoxic agents.

Two major chemical differences between NH_3 and a planar amine are evident: steric hindrance by the appropriately positioned H atoms of the ring system reduces chemical reactivity, and surface and stacking interactions become more pronounced over the H-bonding associated with the NH_3 groups. These structural features suggest simple chemical solutions to the design of sequence-specific agents as well as using steric effects to prevent metabolic deactivation.

An understanding of the aqueous chemistry of diamine Pt^{II} complexes is crucial for establishing their mechanism of action. Once dissolved in water, the labile chloride ions of cisplatin are slowly replaced by water molecules in a stepwise manner: first forming monoaqua species, then further hydrolysis to form diaqua species.[10] The relative amounts of all these hydrolysis species vary as a function of pH and chloride concentration. Hydrolysis is likely to be more extensive inside the cells where the Cl^- concentration is much lower (4-23 mM) than outside cells (~100 mM).[11] Hydrolysis is the rate-limiting step in the reaction of cisplatin with DNA.

Since water is a far better leaving group than chloride and hydroxide,[12] it is important to determine the pK_a values of the aqua adducts.

Although both the kinetics and thermodynamics of hydrolysis reactions of cisplatin and related *cis*-Pt^{II} amine complexes are well understood, surprisingly little is known about analogous reactions of *trans* complexes. For transplatin the first aquation step is rapid, whereas the second aquation step is very slow.[13] This is due to the stabilising effect of the entering *trans* oxygen ligand. Moreover, it has been postulated that since transplatin is more reactive than the *cis* isomer, undesired side reactions occurring on its way to the pharmacological target are likely to contribute, at least in part, to the lack of anticancer activity. Sterically-demanding ligands, like iminoethers in *trans*-$[PtCl_2\{(E)\text{-}HN{=}C(OMe)Me\}_2]$ (*trans*-EE) and substituted pyridine ligands in *cis*-$[PtCl_2(NH_3)(2\text{-pic})]$, could in principle reduce the axial accessibility of the platinum centre and slow the hydrolysis reaction and the subsequent substitution of the aqua ligand by biologically relevant substrates.[14]

In this work, three *trans* isomers of *cis*-$[PtCl_2(NH_3)(2\text{-pic})]$ (2-pic = 2-methylpyridine), AMD473, a recently reported anticancer complex currently in phase II clinical trials, have been studied. AMD473 is active against cisplatin-resistant cell lines, and against an acquired cisplatin-resistant subline of a human ovarian carcinoma xenograph, by injection and oral administration.[15, 16] It has shown significantly reduced cross-resistance to cisplatin in a panel of three cell lines with known acquired platinum drug resistance mechanisms: reduced accumulation, increased cytoplasmic detoxification by cellular thiols or increased DNA repair/tolerance of platinum-DNA adducts.[15, 16] The toxicity of AMD473 is also greatly reduced, with no renal toxicity observed. The *trans* isomers $[PtCl_2(NH_3)(2\text{-}$

pic)] (**1**), $[PtCl_2(NH_3)(3\text{-pic})]$ (**2**) and $[PtCl_2(NH_3)(4\text{-pic})]$ (**3**) have been labelled with ^{15}N, and 2D $[^1H,^{15}N]$ HSQC spectroscopy used to compare their hydrolysis behaviour, and to determine the pK_a values for the mono- and di-aqua complexes. The data reveal notable differences between the chemistry of these *trans* complexes (**1** – **3**) and that of *cis*-$[PtCl_2(NH_3)(2\text{-pic})]$ and cisplatin.

3.3 Experimental

Materials: 2-, 3- and 4-Picoline and $^{15}NH_4Cl$ (>98 % ^{15}N) were purchased from Aldrich, and $^{15}NH_4OH$ (>98 % ^{15}N) from Isotec. *Cis*-$[PtCl_2(NH_3)_2]$ and *cis*-$[PtCl_2(^{15}NH_3)_2]$ were prepared according to a reported procedure.[17] Complexes **2** and **3** were prepared by a general procedure described in the literature for natural abundance, mixed-ligand ammine/amine Pt^{II} complexes.[18]

Preparation of *trans*-$[PtCl_2(NH_3)(2\text{-pic})]$ (AMD443) (1): *cis*-$[PtCl_2(2\text{-pic})_2]$ (0.392 g, 0.866 mmol), prepared by literature methods,[19] was dissolved in deionised water (7 mL), heated at reflux and then NH_4OH (2.77 mL, 2.5 M) was added to give a yellow suspension which was heated at reflux and stirred overnight. This produced a clear solution which was filtered and then rotary evaporated. The *cis*-$[Pt(NH_3)_2(2\text{-pic})_2]Cl_2$ intermediate was dissolved in water (2 mL) and heated and stirred under reflux. HCl (289 μL, 11.98 M) was added to the solution and the mixture allowed to stir under reflux for 5 days under nitrogen, during which time it was necessary to add additional aliquots of water. The mixture was then placed on an ice bath to induce precipitation. The yellow product was then filtered off, washed with ice-cold water, and dried *in vacuo* overnight. The product was recrystallised from 0.1 M HCl, giving small yellow crystals. Yield: 258.5 mg, 79%. Anal. Calcd for $C_6H_{10}Cl_2N_2Pt$: C, 19.16%; H, 2.68%; N, 7.45%. Found: C, 18.87%; H, 2.54%; N, 7.11%. ^1H NMR (d_6-

acetone): δ = 8.81 (d, J = 5.7 Hz, 1H, H-6), 7.78 (t, 1H, H-4), 7.43 (d, J = 7.9 Hz, 1H, H-3), 7.27 (t, 1H, H-5), 3.69 (broad, NH_3), 3.14 (s, 3H, CH_3). m/z 399.3 corresponding to $[PtCl_2(NH_3)(2\text{-pic})]Na^+$. *Trans*-$[PtCl_2(^{15}NH_3)(2\text{-pic})]$ (^{15}N-**1**) was prepared by the same method using $^{15}NH_4OH$.

Preparation of *trans*-$[PtCl_2(NH_3)(3\text{-pic})]$ (2): Cisplatin (0.233 g, 0.775 mmol) was suspended in 23 mL water, which had been bubbled with argon, and 2 mol equiv 3-picoline (151 μL, 1.55 mmol) were added. The mixture was stirred at 363 K for 3 h, allowed to cool to room temperature, filtered to remove any traces of precipitate, and then conc. HCl (1.6 mL) was added to the clear solution. The acidic mixture was refluxed under nitrogen overnight. The resulting solution was bright yellow and was placed in ice for several hours to induce precipitation. The yellow precipitate was filtered off, washed with ice-cold water, followed by diethyl ether, and dried *in vacuo* overnight. Yield: 188.3 mg, 64.6%. Anal. Calcd for $C_6H_{10}Cl_2N_2Pt$: C, 19.16%; H, 2.68%; N, 7.45%. Found: C, 19.30%; H, 2.63%; N, 7.39%. ^{1}H NMR (d_6-acetone): δ = 8.66 (s, 1H, H-2), 8.64 (d, J = 5.49 Hz, 1H, H-6), 7.78 (d, J = 7.68 Hz, 1H, H-4), 7.32 (t, 1H, H-5), 3.73 (broad, NH_3), 2.37 (s, 3H, CH_3). m/z = 399.0 corresponding to $[PtCl_2(NH_3)(3\text{-pic})]Na^+$. *Trans*-$[PtCl_2(^{15}NH_3)(3\text{-pic})]$ (^{15}N-**2**) was prepared by the same method using ^{15}N-cisplatin as the starting material.

Preparation of *trans*-$[PtCl_2(NH_3)(4\text{-pic})]$ (3): Cisplatin (0.188 g, 0.627 mmol) was suspended in 19 mL water, which had been bubbled with argon, and 2 mol equiv 4-picoline (122 μL, 1.25 mmol) were added. The mixture was stirred at 363 K for 3 h, allowed to cool to room temperature, filtered to remove any traces of precipitate, and then conc. HCl (1.6 mL) was added to the clear solution. The acidic mixture was refluxed under nitrogen for 6 h. The resulting solution was bright yellow and was

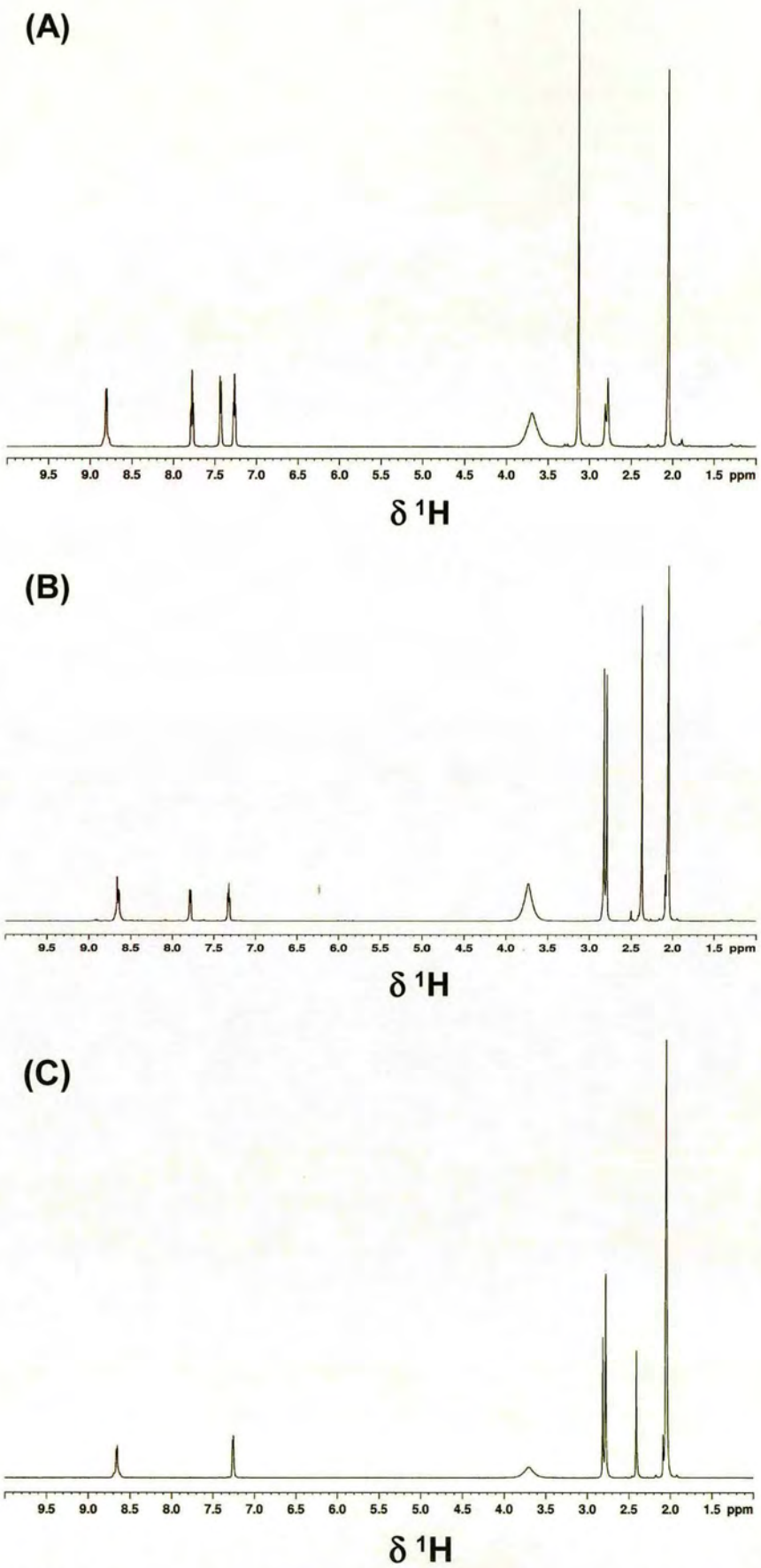

Figure 3.1 ^{1}H NMR spectra of A) complex **1**, B) complex **2** and C) complex **3**.

placed in ice for several hours to induce precipitation. The yellow precipitate was filtered off, washed with ice-cold water, followed by diethyl ether, and dried *in vacuo* overnight. Yield: 80.0 mg, 33.9%. Anal. Calcd for $C_6H_{10}Cl_2N_2Pt$: C, 19.16%; H, 2.68%; N, 7.45%. Found: C, 19.35%; H, 2.66%; N, 8.42%. ^{1}H NMR (d_6-acetone): δ = 8.66 (d, J = 6.3 Hz, 2H, H-2), 7.26 (d, J = 5.65 Hz, 2H, H-3), 3.70 (broad, NH_3), 2.41 (s, 3H, CH_3). m/z = 399.1 corresponding to $[PtCl_2(NH_3)(4\text{-pic})]Na^+$. *Trans*-$[PtCl_2(^{15}NH_3)(4\text{-pic})]$ (^{15}N-**3**) was prepared by the same method using ^{15}N-cisplatin as the starting material.

X-ray Crystallography: Diffraction data were collected with Mo-Kα radiation on a Bruker Smart Apex CCD diffractometer equipped with an Oxford Cryosystems low-temperature device operating at 150 K. Data were corrected for absorption using the SADABS[20] procedure. The structure of **1** was solved by Dr. Simon Parsons using direct methods (SHELXS),[21] while those of **2** and **3** were solved using Patterson methods (DIRDIF[22] and SHELXS, respectively). The structures were refined against F^2 using all data (SHELXL).[23] All non-H atoms were modelled with anisotropic displacement parameters, and H-atoms were placed in calculated positions. CH_3 and NH_3 groups were treated according to the Sheldrick rotating rigid group model.[23]

*Crystal data for **1***: The sample was a pale-yellow needle of dimensions 1.00 x 0.14 x 0.14 mm^3; the crystals tended to split into smaller needles when cut. Orthorhombic, space group *Pccn*, a = 10.5710(12), b = 22.826(3), c = 7.9743(9) Å, V = 1924.1(7) Å^3, Z = 8, D_{calc} = 2.597 Mg m^{-3}. The final conventional R-factor [$R1$, based on $|F|$ and 2018 data with $F > 4\sigma(F)$] was 0.0431, and w$R2$ (based on F^2 and all 2374

unique data to θ_{max} = 28.7°) was 0.0921. The final ΔF synthesis extremes were + 2.32 and -1.82 eÅ^{-3}.

Crystal data for ***2***: The sample was a yellow block of dimensions 0.70 x 0.25 x 0.25 mm^3. Monoclinic, space group $P2_1/c$, a = 8.5867(2), b = 22.8583(3), c = 9.8514(3) Å, V = 1930.00(13) Å^3, Z = 8 (there are two molecules in the asymmetric unit), D_{calc} = 2.589 Mg m^{-3}. The final conventional $R1$-factor (based on 4034 data) was 0.0386, and w$R2$ (based on 4576 unique data to θ_{max} = 28.6°) was 0.0865. The final ΔF synthesis extremes were + 2.31 and -2.22 eÅ^{-3}.

Crystal data for ***3***: The sample was a pale-yellow needle of dimensions 1.06 x 0.08 x 0.04 mm^3. Orthorhombic, space group *Pccn*, a = 11.5185(4), b = 22.3413(7), c = 7.6232(3) Å, V = 1961.74(12) Å^3, Z = 8, D_{calc} = 2.547 Mg m^{-3}. The final conventional $R1$-factor (based on 2193 data) was 0.0307, and w$R2$ (based on 2828 unique data to θ_{max} = 30.5°) was 0.0668. The final ΔF synthesis extremes were +1.70 and -0.81 eÅ^{-3}.

NMR Spectroscopy: NMR spectra were recorded at 298 K, unless otherwise stated, on Bruker DMX500 (^{1}H 500.13 MHz) or Bruker AVA600 (^{1}H 599.81 MHz) spectrometers using 5 mm NMR tubes. ^{1}H NMR chemical shifts were referenced to TSP via dioxane (δ 3.75) and ^{15}N chemical shifts to 1 M $^{15}NH_4Cl$ in 1.5 M HCl (external). Water suppression was achieved by presaturation. Spectra were processed using XWINNMR (Version 3.5, Bruker UK Ltd).

Sample Preparation: NMR samples for hydrolysis reactions were prepared by dissolving the platinum complex in an aliquot of DMF, followed by dilution with H_2O/D_2O to the required concentration. For pK_a determinations, the platinum

complexes were reacted with 1.96 equiv $AgNO_3$ (24 h, RT), and then filtered to remove AgCl. All samples were prepared in 90% H_2O/10% D_2O unless otherwise stated.

Kinetic Analyses: The concentration/time data for each complex were computer-fitted to the first order rate equation [Eq.(1)]:

$$A = C_0 + C_1 e^{-kt} \quad (1)$$

where C_0 and C_1 are computer-fitted constants, and A is the concentration corresponding to time t. All kinetic data were computer-fitted using the program Microcal Origin 7.5 to give the hydrolysis rate constant k_{H2O} (k).

pH Measurements: The pH values of solutions were determined using a Corning 145 pH meter equipped with a micro combination electrode, calibrated with Aldrich buffer solutions at pH 4, 7 and 10. The pH was adjusted with dilute solutions of $HClO_4$ and NaOH. No correction has been made for deuterium isotope effects on the glass electrode.

pK_a Values: These were determined by fitting the NMR pH titration curves for samples in 90% H_2O/10% D_2O to the Henderson-Hasselbalch equation using the program Kaleidagraph (Synergy Software, Reading, PA, USA).

Mass Spectrometry: Ion electrospray mass spectrometry was performed on a Platform II mass spectrometer (Micromass, Manchester, UK). The samples were infused at 8 μL/min and the ions produced in an atmospheric pressure ionization (API)/ESI ion source. The source temperature was 383 K, and the drying gas flow rate was 300 L/h. A potential of 3.5 kV was applied to the probe tip, and cone

voltage gradients of 20 – 40 V over 200 – 1000 Da were used. Data acquisition was performed on a Mass Lynx (V2.5) Windows NT PC data system. All samples were prepared in water.

Table 3.2 X-ray crystal structure data for complexes **1** – **3**.

	1	**2**	**3**
Empirical formula	$C_6H_{10}Cl_2N_2Pt$	$C_6H_{10}Cl_2N_2Pt$	$C_6H_{10}Cl_2N_2Pt$
M_r	376.15	376.15	376.15
Crystal System	Orthorhombic	Monoclinic	Orthorhombic
Space group	Pccn	$P2_1/c$	Pccn
a (Å)	10.5710 (12)	8.5867 (2)	11.5185 (4)
b (Å)	22.826 (3)	22.8583 (7)	22.3413 (7)
c (Å)	7.9743 (9)	9.8514 (3)	7.6232 (3)
α (°)	90	90	90
β (°)	90	93.506 (2)	90
γ (°)	90	90	90
V (Å^3)	1924.1 (4)	1929.99 (9)	1961.74 (12)
Z	8	8	8
λ (Å)	0.71073	0.71073	0.71073
T (K)	150 (2)	150 (2)	150 (2)
ρ_{calcd} (g cm^{-3})	2.597	2.589	2.547
μ_{calcd} (mm^{-1})	15.080	15.034	14.791
F (000)	1376	1376	1376
2θ range (°)	1.78 – 28.70	1.78 – 28.62	1.82 – 30.50
Refls. Collected	14380	13928	11084
Independent refl.	2374	4576	2828
Reflns. (R_{int})	(0.0429)	(0.0428)	(0.0418)
R1 ($F_0 > 4\sigma(F_0)$)	0.0431	0.0386	0.0307
wR2 (all data)	0.0921	0.0865	0.0668

Table 3.3 Selected bond lengths (Å) and angles (°) for complexes **1** – **3**.

	1	**2**	**3**
Pt – N(1)	2.028 (7)	2.014 (6)	2.014 (4)
Pt – N(2)	2.037 (8)	2.047 (6)	2.043(4)
Pt – Cl(1)	2.313 (2)	2.293 (2)	2.2918 (11)
Pt – Cl(2)	2.307 (2)	2.292 (3)	2.3002 (12)
N(1) – Pt – N(2)	178.9 (3)	176.9 (3)	179.22 (15)
N(1) – Pt – Cl(1)	90.1(2)	90.61 (19)	90.95 (11)
N(2) – Pt – Cl(1)	89.6 (2)	88.35 (19)	88.32 (12)
N(1) – Pt – Cl(2)	92.0 (2)	91.26 (19)	90.63 (11)
N(2) – Pt – Cl(2)	88.4 (2)	89.8 (2)	90.08 (12)
Cl(2) – Pt – Cl(1)	177.48 (8)	178.12 (7)	177.40 (5)

N(1) = N of 2-picoline, N(2) = N of NH_3

3.4 Results

X-ray Crystal Structures: X-ray crystallographic data and details of the refinement of the structures of the *trans* ammine/2-picoline, 3-picoline and 4-picoline complexes (**1**, **2** and **3**, respectively) are listed in Table 3.2, and selected bond lengths and angles are given in Table 3.3. All complexes have a square-planar configuration with angles close to the ideal values of 90° and 180°, as shown in Figure 3.2. Pt – Cl bond lengths range from 2.292 – 2.313 Å and are close to the expected values. The Pt – N bond lengths of 2.014 – 2.047 Å are comparable to those of related structures. The most notable feature of the structures is the orientation of the picoline ring with

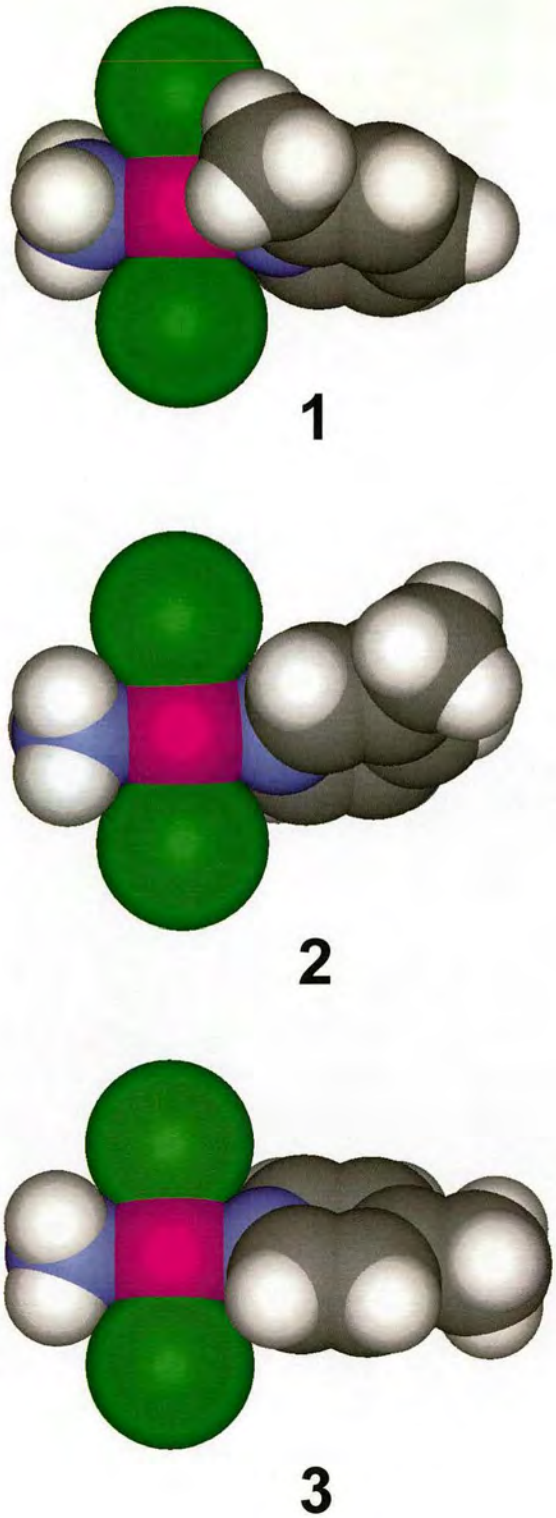

Figure 3.2 Space filling models of the X-ray crystal structures of complexes **1** – **3** showing the steric hindrance caused by the 2-methyl group in complex **1**.

respect to the platinum square plane. In complex **1**, the 2-picoline ligand is tilted by 69.2°, in complex **2** 3-picoline is tilted by 60.0° and 57.8° (2 molecules per unit cell), and for 4-picoline in **3** by only 56.2°. The tilt angle therefore decreases in the order 2-pic > 3-pic, 4-pic. In complex **1**, the 2-methyl group lies over the square plane (H_3C···Pt: 3.207 Å), whereas in complexes **2** and **3** the methyl group is much further away from Pt (H_3C···Pt: 5.452, 5.458 Å for **2** and 6.312 Å for **3**). The space-filling models in Figure 3.2 demonstrate that in complex **1** there is significantly more steric hindrance to an axial approach to Pt from above than in either complexes **2** or **3**.

Strong intermolecular hydrogen bonds are involved in the crystal packing of all complexes (Figure 3.3). For complexes **1** and **3**, the three H-atoms of the NH_3 ligand are H-bonded to three Cl ligands from neighbouring molecules. Similarly for **1** and **3**, chains of complexes are connected by H-bonds and also interact with one another through interleaving π-stacks. Such intermolecular H-bonds are common in chloro Pt^{II} am(m)ine complexes. However, there appears to be an additional H-bonding interaction in complex **1** between the aromatic H5 proton of the 2-picoline ring and a Cl ligand (2.853 Å). For complex **2**, H-bonds of similar strength are formed, but only to two Cl ligands, giving infinite chains composed of channels lined by Cl and NH_3 along the c-direction.

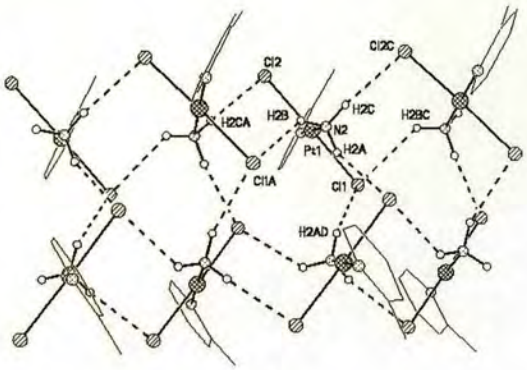

1

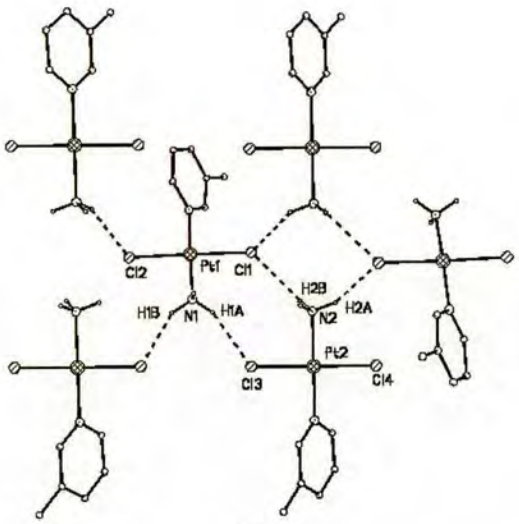

2

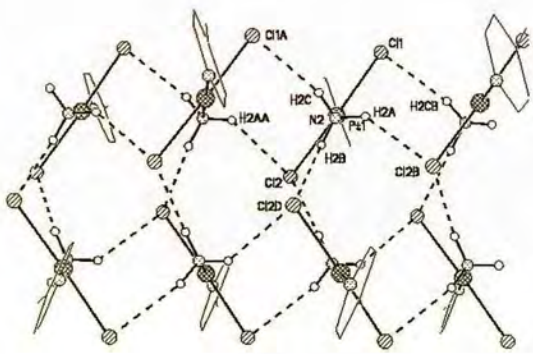

3

Figure 3.3 Intermolecular H-bonding in crystals of complexes **1** – **3**. N – H···Cl distances range from 2.46 – 2.85 Å for complex **1**, 2.49 – 2.55 Å for complex **2** and 2.49 – 2.70 Å for complex **3**.

Hydrolysis of complexes 1 – 3: The hydrolysis of $^{15}NH_3$-labelled **1** – **3** in aqueous solutions containing 0.1 M $NaClO_4$ was monitored by [^{1}H,^{15}N] 2D NMR for over 20 h at 277 K. This low temperature was chosen because the rates were too fast at ambient temperature to allow determination by NMR. Initially for **1**, a single cross-peak was observed at δ = 3.63, -70.11, which was assigned to the dichloro complex **1**. After 2 h, a weak cross-peak was detected at δ = 3.69, -68.30, which was assigned to the monoaqua species. The peak for **1** decreased in intensity as the monoaqua peak increased in intensity over a period of 21 h. No peak assignable to a diaqua species was observed within the time the reaction was followed (48 h). At 310 K (Figure 3.4), two peaks were initially observed. Peak **a**, at δ = 3.78, -69.26, corresponds to **1** and peak **b** at δ = 3.98, -67.87 is the monoaqua species. An additional peak at δ 4.07, -65.99 ppm assignable to the diaqua adduct was observed after 4 h, but its intensity was low, and accounted for <3 % of the Pt present in the solution after 21 h.

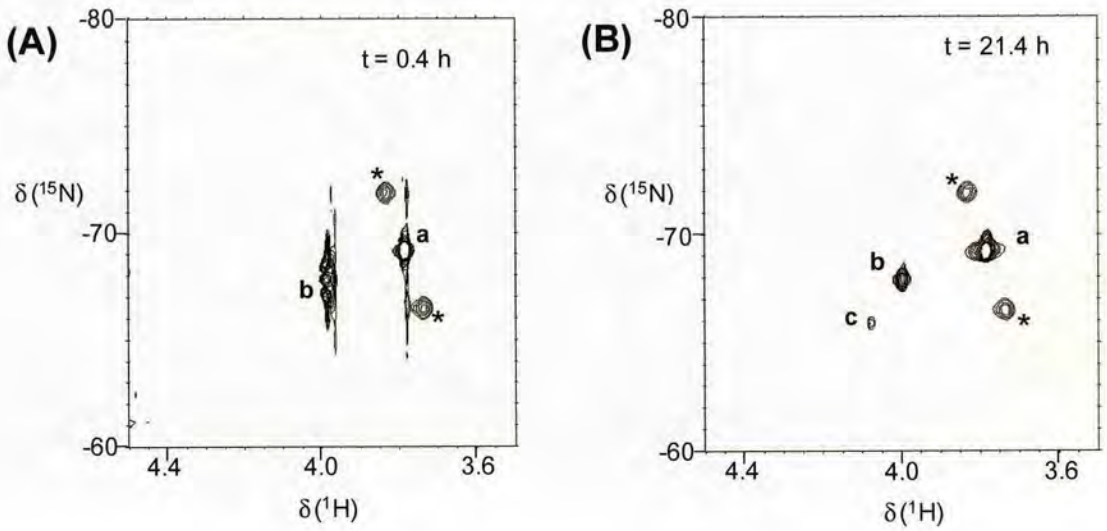

Figure 3.4 2D [^{1}H,^{15}N] HSQC NMR spectra of a 5 mM aqueous solution of *trans*-[$PtCl_2(^{15}NH_3)$(2-pic)] (**1**) at 310 K after A) 0.4 h and B) 21.4 h. Peak a is assigned to **1**, peak b to the monoaqua complex and peak c to the diaqua complex, * = ^{195}Pt satellites.

For the 3-picoline complex **2**, initially, two cross-peaks were observed. The most intense peak at δ = 3.64, -70.60 was assigned to the dichloro complex **2** and the less intense peak at δ = 3.77, -69.21 to the monoaqua species. Again, no diaqua species was observed. The time-dependence of the [^{1}H,^{15}N] 2D NMR spectrum was similar to that of complex **1**, except that equilibrium was reached more quickly (< 7 h at 277 K).

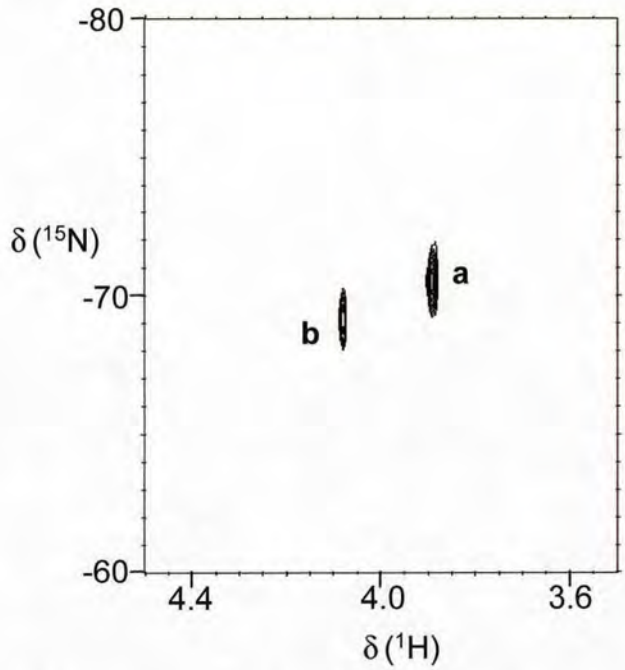

Figure 3.5 2D [^{1}H,^{15}N] HSQC NMR spectrum of 5 mM aqueous solution of *trans*-[$PtCl_2(^{15}NH_3)$(4-pic)] (**3**) at 277 K after 21.3 h. Peak a is assigned to **3**, peak b to the monoaqua complex.

The hydrolysis of the 4-picoline complex **3**, followed a similar time-dependence but, interestingly, reached equilibrium significantly more slowly than for the 3-picoline complex **2**. The chemical shifts for the dichloro complex and monoaqua species are similar to those of **1** and **2**, with the dichloro complex **3** having a cross-peak at δ = 3.63, -70.60, and the monoaqua species at δ = 3.68, -68.89 (Figure 3.5). No diaqua species was observed under these experimental conditions. It

is noteworthy that the ^{1}H NMR peaks, in particular, tended to shift downfield throughout the course of the reaction. This is a consequence of a decrease in pH caused by deprotonation of coordinated water to produce the monohydroxo complex.

The time-dependence of the concentrations of species detected during hydrolysis of complexes **1** – **3** is shown in Figure 3.6. The assignments of the peaks of the aqua complexes were confirmed by pH titrations (Figure 3.7), using aqua adducts of complexes **1** – **3** which had been generated by reactions with Ag^{I} to produce a mixture of monoaqua, diaqua and dichloro species. These allowed the determination of pK_a value for each monoaqua complex as well as two pK_a values for each diaqua complex.

Table 3.4 Rate constants (k) and equilibrium constants (K) for the hydrolysis reactions of complexes **1** – **3** and AMD473.

Complex	T/ K	k ($x10^{-5}$ s^{-1})[a]	K ($x10^{-4}$ M)[a]
1	277	2.6 ± 0.2	3.9 (3.7)[b]
2	277	12.7 ± 0.8	2.0
3	277	5.2 ± 0.3	4.0
AMD473[c]	310	3.2[d], 2.2[e]	12.1[d], 21.4[e]

[a] Based on concentrations derived from integration of 2D [^{1}H,^{15}N] NMR cross-peaks, [b] 310 K, [c] Data from ref. 33, [d] trans to 2-pic, [e] trans to NH_3.

The NMR data allow the determination of the rates for monoaquation of complexes **1** – **3** at 277 K, and these are listed in Table 3.4. It is notable that the rate of monoaquation of the 3-picoline complex **2** is more than twice as fast as that of complex **3**, and ca. five times as fast as complex **1**. However, the extent of hydrolysis of complex **2** was ca. 75 % that of complexes **1** and **3**. An estimate of the half-lives

for hydrolysis of complex **1** at 310 K is included in Table 3.6 and compared with related complexes. Half-lives for hydrolysis (310 K) and pK_a values (298 K) for complex **1** are shown in Scheme 3.1. The enthalpy of reaction ($\Delta H°$) for the monoaquation step was calculated, using the van't Hoff expression,[24] to be -1.0 $KJmol^{-1}$. The negative sign of $\Delta H°$ indicates the equilibrium constant (K) decreases with increasing temperature.

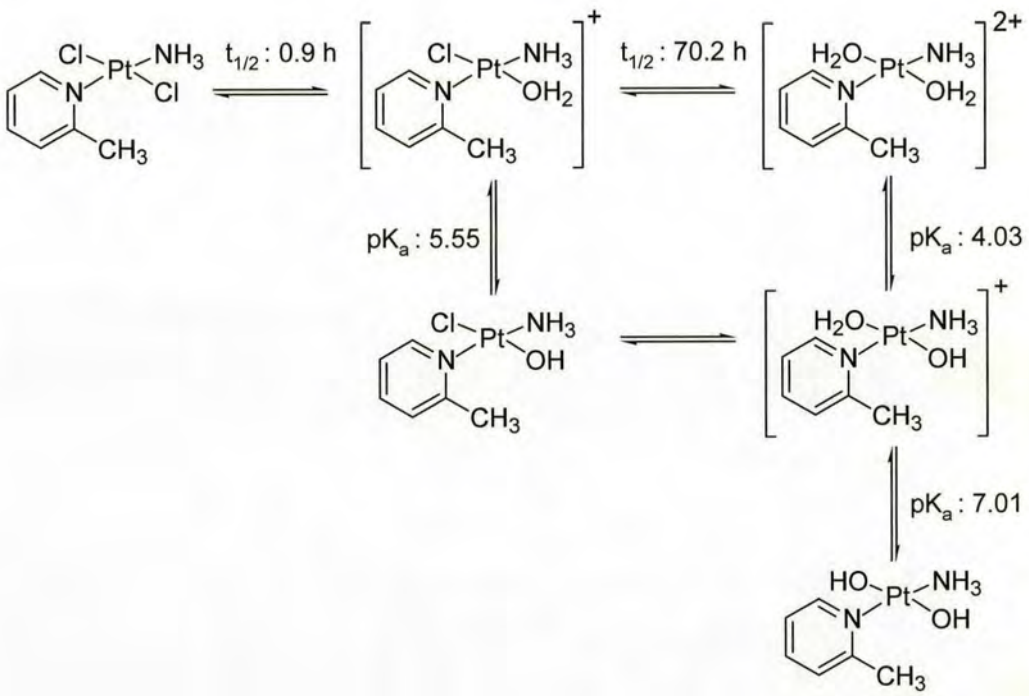

Scheme 3.1 Half-lives for hydrolysis (310 K) of complex **1** and pK_a values (298 K) of its aqua adducts.

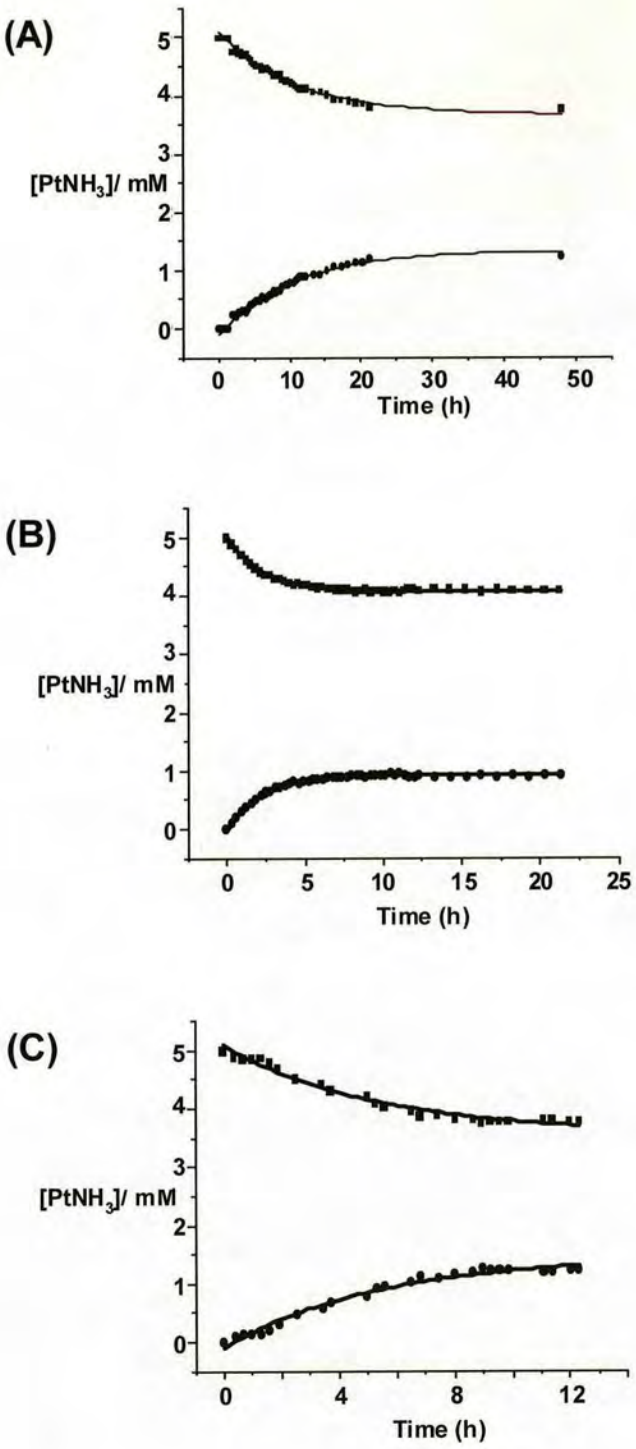

Figure 3.6 Time dependence of the concentrations of the dichloro complexes A) **1**, B) **2** and C) **3** and the aqua adducts during hydrolysis at 277 K. Concentrations are based on integration of 2D NMR cross-peaks. Labels: **1** – **3** (■), monoaqua complexes (●). The full lines represent computer fits giving the first order rate constants listed in Table 3.4.

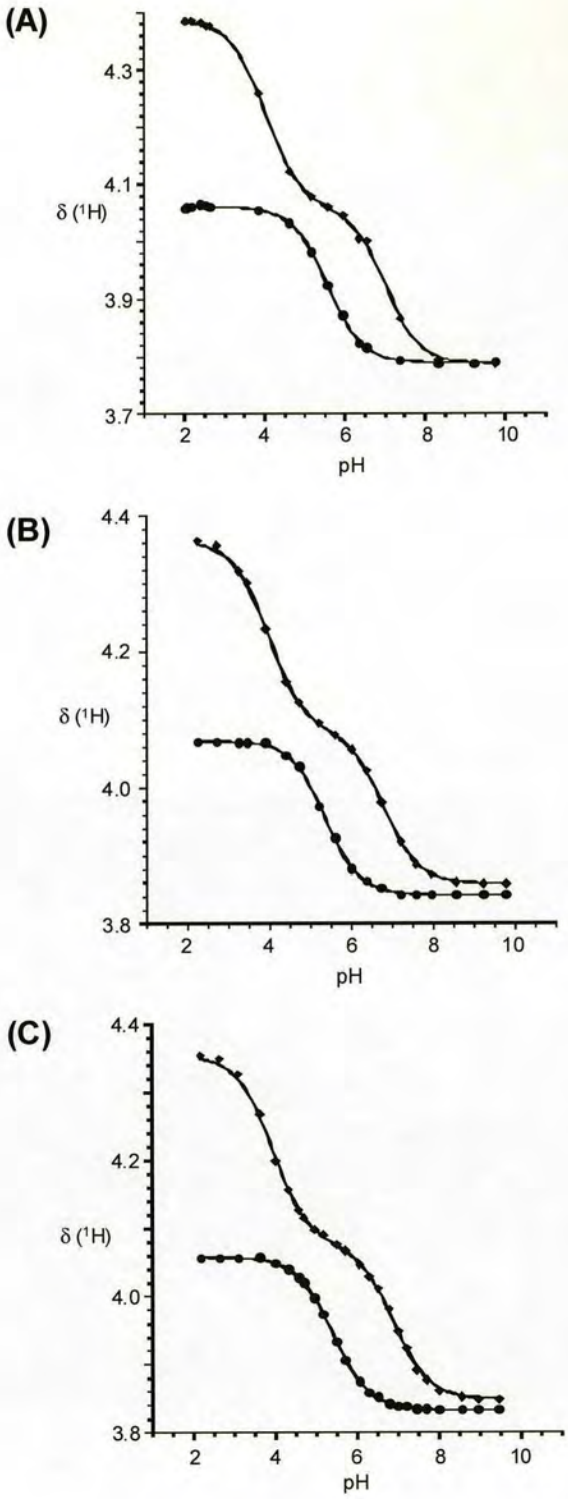

Figure 3.7 pH-dependence of the ^{1}H NMR chemical shifts of NH_3 in the monoaqua and diaqua complexes A) **1**, B) **2** and C) **3**. The curves represent computer fits to the Henderson-Hasselbalch equation giving the pK_a values listed in Table 3.7. Labels: monoaqua complexes (●), diaqua complexes (♦).

3.5 Discussion

cis-[$PtCl_2(NH_3)$(2-picoline)] is currently on clinical trial as an anticancer drug. Its *trans* isomer, complex **1**, shows *in vitro* cytotoxicity[25] even higher than that of cisplatin in a panel of human tumour cell lines (mean IC_{50} = 3.5 and 33.7 μM, respectively), whereas the *trans* 4-picoline complex **3**, tested by Kasparkova et al.,[26] exhibits a lower activity (mean IC_{50} = 80.3 μM), Table 3.5. The 3-picoline complex **2** has not yet been evaluated for its cytotoxic activity. Complex **1** overcomes cisplatin resistance in the resistant cell lines tested, but complex **3** is cross-resistant, implying that complex **1** may have a different mechanism of action to complex **3**. IC_{50} values for these and related compounds are listed in Table 3.5.[25-27] Interestingly, *trans*-[$PtCl_2(NH_3)$(pip)] (where pip = piperidine) and *trans*-$[PtCl_2(NH_3)(pz)]^+$ (where pz = piperazine) are less cytotoxic than both *trans*-[$PtCl_2(NH_3)$(2-pic)] (**1**) or *trans*-$[PtCl_2(py)_2]$ in the cell lines tested. Moreover, *trans*-$[PtCl_2(py)_2]$ overcomes cisplatin resistance whilst *trans*-[$PtCl_2(NH_3)$(2-pic)] has a small average resistance factor of ca. 1.5.

Table 3.5 Mean IC_{50} values for *trans* Pt complexes and cisplatin against various cell lines.[25-27]

Complex[a]	IC_{50} (μM)[b]					
	A2780	A2780(R)	CH1	CH1(R)	41M	41M(R)
cisplatin	2.2	38	6	23	26	107
transplatin	> 200	> 200	> 200	> 200	> 200	> 200
trans-$[PtCl_2(py)_2]$	-	-	1.6	1.7	2.2	2.0
trans-$[PtCl_2(NH_3)(pip)]$	5	20	15	94	27	150
trans-$[PtCl_2(NH_3)(pz)]^+$	5	44	12	34	52	155
trans-[$PtCl_2(NH_3)$(2-pic)] (**1**)	1.6	6	3.8	5.2	2.8	1.7
trans-[$PtCl_2(NH_3)$(4-pic)] (**3**)	7	80	22	154	32	187

[a] py = pyridine, pip = piperidine, pz = piperazine, [b] R = cisplatin-resistant cell line

^{15}N-labelling of **1** – **3** and use of [^{1}H,^{15}N] NMR spectroscopy has allowed study of the speciation of these complexes in aqueous solution. The [^{15}N,^{1}H] NMR method has the advantage that the concentrations of aquated species can usually be measured directly at low (micromolar) concentrations, even when other species are present in the solution. However, due to the extremely fast rate of the monoaquation step, rates were measured at lowered temperature (277 K). At 277 K, only peaks for the monoaqua species were detected, although a peak for the diaqua species was detected after ca. 4 h of hydrolysis of complex **1** at 310 K.

The $t_{1/2}$ values for the first hydrolysis step at 277 K follow the order of **1** (7.43 h) > **3** (3.68 h) > **2** (1.52 h). Even at equilibrium, the monoaqua species of complexes **1** and **3** account for only ca. 24 % of all platinum species present and the monoaqua species of complex **2** only accounts for ca. 18 % of all platinum species. The steric hindrance due to the picoline ligand in complexes **2** and **3** is similar, and it is apparent that the faster hydrolysis of complex **2** relative to complex **3** is due to electronic factors. A methyl substituent at the 2- and 4- positions (complexes **1** and **3**, respectively) increases electron density on the platinum centre, making nucleophilic attack by the incoming water molecule less favorable. However, at the 3-position (complex **2**), the methyl substituent directs less electron density to the platinum centre and thus promotes the hydrolysis reaction. Complex **1** is the slowest to hydrolyse due to both steric and electronic effects. The more sterically demanding 2-picoline ligand hinders axial approach of the incoming water molecule from above. Substitution reactions of square-planar Pt^{II} complexes (i.e. $PtL_2XY + Z \rightarrow PtL_2YZ + X$) usually occur through formation of a five-coordinate intermediate (PtL_2XYZ) in an associative process.[28] The use of a more sterically-hindering non-leaving group

(i.e. Y or L) compared to NH_3 raises the energy of the five-coordinate intermediate (i.e. increases the activation energy associated with entry of Z into the coordination sphere).

Table 3.6 Half-lives ($t_{1/2}$) for hydrolysis of various Pt^{II} complexes.

Complex	Dichloro $t_{1/2}$ (h)	Monoaqua $t_{1/2}$ (h)	Reference
trans-[$PtCl_2(NH_3)$(2-pic)] (**1**)[a]	7.43 (0.9)[b]	- (70.2)[b]	This work
trans-[$PtCl_2(NH_3)$(3-pic)] (**2**)[a]	1.52	-	This work
trans-[$PtCl_2(NH_3)$(4-pic)] (**3**)[a]	3.68	-	This work
transplatin[c]	1.96	3.85	[29]
transplatin[d]	10.13	-	[30]
trans-[$PtCl_2(NH_3)$(4-pic)][c]	0.33	-	[31]
trans-[$PtCl_2$-{E-HN=C(OMe)Me}$_2$][c]	0.92	77.02	[32]
cis-[$PtCl_2(NH_3)$(2-pic)][b]	6.04, 8.71	2.64, 55.01	[33]
cis-[$PtCl_2(NH_3)$(3-pic)][b]	1.86, 4.31	2.47, 5.50	[33]
cisplatin[b]	1.9	2.1	[34]

[a] 277 K, [b] 310 K, [c] 298 K, [d] 298.2 K, calculated from the activation parameters, which were determined from the temperature dependent intercepts of plots of k_{obs} vs. [Cl^-].

When hydrolysis of complex **1** was monitored at 310 K, approximate values of $t_{1/2}$ were determined as 0.9 h for the monoaquation and 70.2 h for the diaquation steps. These values compare well with $t_{1/2}$ = 0.92 h and $t_{1/2}$ = 77.0 h (T = 298 K) for mono- and di-aquation, respectively, of *trans*-[$PtCl_2$-{E-HN=C(OMe)Me}$_2$].[32] Farrell et al.[31] have obtained a $t_{1/2}$ value of 0.33 h for *trans*-[$PtCl_2(NH_3)$(4-pic)] (**3**) at T = 298 K. Table 3.6 lists $t_{1/2}$ values of various related compounds.[29-34] Only a

few studies of transplatin hydrolysis have been reported and there appears to be a large disparity between the reported half-lives. Aprile and Martin[29] reported a $t_{1/2}$ value of 1.96 h (I = 0.318 M, T = 298 K) for monoaquation of transplatin, whereas Miller et al.[30] calculated a $t_{1/2}$ value of 10.13 h (I = 0.1 M, T = 298.2 K) based on the activation parameters, calculated from the temperature dependent intercepts of plots of k_{obs} versus [Cl^-].

The equilibrium constants for mono-aquation determined for complexes **1-3**, 2 – 4 x 10^{-4} M^{-1} (Table 3.4), are an order of magnitude less than reported values (298 K) for cisplatin[29, 30, 35] of 33 – 68 x 10^{-4} M^{-1}. The equilibrium constants reported for transplatin,[29, 30] 3.2 x 10^{-4} M^{-1} and 6.2 x 10^{-4} M^{-1}, are also an order of magnitude smaller than those of cisplatin, and our values for complexes **1-3** fall within this range. Thus the amount of (reactive) mono-aqua species formed by the *trans* complexes at intracellular chloride concentrations (4 - 23 mM) is likely to be < 10 %, much smaller than for the *cis* analogues (Table 3.4). A consequence of the higher stability of the *trans* chloro complexes is that little of the diaqua adduct is formed during the hydrolysis. It has been suggested for cisplatin that the diaqua complex plays a key role in the attack on DNA.[36]

[^1H,^{15}N] NMR allowed also the determination of the pK_a values of the aqua ligands in the monoaqua and diaqua species of complexes **1** – **3**. Movement of the methyl group from the 2- to the 3- to the 4-position has little affect on the pK_a values of the aqua ligands. A comparison of pK_a values for mono-aqua adducts, Table 3.7,[37-42] shows those for complexes **1** – **3** are fairly typical for *trans*-{$Pt(NH_3)$(amine)}-type complexes (5.3 - 5.9), and significantly lower than those of

cis complexes such as cisplatin and AMD473. Also, the first pK_a value for the *trans* diaqua complexes is ca. 1 unit lower than those for related *cis* complexes (Table 3.7).

Table 3.7 Comparison of pK_a values for a selection of *cis* and *trans* diam(m)ine Pt^{II} aqua complexes.

Complex	pK_a	Reference
trans-$[PtCl(OH_2)(^{15}NH_3)(2\text{-pic})]^+$	5.55	This work
trans-$[Pt(OH_2)_2(^{15}NH_3)(2\text{-pic})]^{2+}$	4.03, 7.01	This work
trans-$[PtCl(OH_2)(^{15}NH_3)(3\text{-pic})]^+$	5.35	This work
trans-$[Pt(OH_2)_2(^{15}NH_3)(3\text{-pic})]^{2+}$	3.97, 6.78	This work
trans-$[PtCl(OH_2)(^{15}NH_3)(4\text{-pic})]^+$	5.39	This work
trans-$[Pt(OH_2)_2(^{15}NH_3)(4\text{-pic})]^{2+}$	3.94, 6.88	This work
trans-$[PtCl(OH_2)(^{15}NH_3)_2]^+$	5.63	[37]
trans-$[Pt(OH_2)_2(^{15}NH_3)_2]^{2+}$	4.35, 7.40	[37]
trans-$[PtCl(OH_2)(^{15}NH_3)$(2-Me-(^{15}N)butylamine)$]^+$	5.90	[38]
trans-$[Pt(OH_2)_2(^{15}NH_3)$(2-Me-(^{15}N)butylamine)$]^{2+}$	4.16, 7.17	[38]
trans-$[PtCl(OH_2)$(isopropylamine)((S)-2-methyl(^{15}N) butylamine)$]^+$	5.86	[39]
trans-$[Pt(OH_2)_2$(isopropylamine)((S)-2-methyl(^{15}N) butylamine)$]^{2+}$	4.21, 7.33	[39]
[{*trans*-$PtCl(^{15}NH_3)_2$}{*trans*-$Pt(OH_2)(^{15}NH_3)_2$}(μ-$^{15}NH_2(CH_2)_6{}^{15}NH_2$)]$^{3+}$	3.9	[40]
[{*trans*-$Pt(OH_2)(^{15}NH_3)_2$}$_2$(μ-$^{15}NH_2(CH_2)_6{}^{15}NH_2$)]$^{4+}$	5.62[a]	[40]
trans-$[PtCl(OH_2)(^{15}NH_3)$(c-$C_6H_{11}{}^{15}NH_2$)]$^+$	5.40	[41]
cis-$[PtCl(OH_2)(^{15}NH_3)(2\text{-pic})]^+$	6.13, 6.49	[33]
cis-$[Pt(OH_2)_2(^{15}NH_3)(2\text{-pic})]^{2+}$	5.22, 7.16	[33]
cis-$[PtCl(OH_2)(^{15}NH_3)(3\text{-pic})]^+$	5.98, 6.26	[33]
cis-$[Pt(OH_2)_2(^{15}NH_3)(3\text{-pic})]^{2+}$	5.07, 6.94	[33]
cis-$[PtCl(OH_2)(^{15}NH_3)_2]^+$	6.41	[42]
cis-$[Pt(OH_2)_2(^{15}NH_3)_2]^{2+}$	5.37, 7.21	[42]

[a] Average value

In recent years, there has been an increasing number of investigations of *trans* platinum complexes.[9, 13, 43] One of the most striking differences between *cis* and *trans* isomers apparent from such investigations is the variation in formation and reactivity of the diaqua species. However, Arpalahti[44] reported that for cisplatin and transplatin, the second complexation step in the formation of the bis(inosine) adduct appears to be kinetically similar. In the case of multinuclear platinum am(m)ine complexes, which hydrolyse only to a small extent, and yet have a high DNA affinity (rapid DNA binding), it has been suggested that formation of aqua species may not be a necessary step in DNA adduct formation of such compounds.[40] Moreover, the high cytotoxicity of the *trans*-$[PtCl_2(NH_3)$(planar amine)] class of compounds has been attributed to an alteration of the mode of DNA binding in comparison to cisplatin, resulting in an altered spectrum of antitumour activity and enhanced reactivity in cisplatin-resistant cell lines. For example, an intercalative manner of interaction of the quinoline or thiazole moiety with the duplex has been proposed for all or a significant fraction of the DNA adducts of *trans*-$[PtCl_2(NH_3)$(quin)] and *trans*-$[PtCl_2(NH_3)$(tz)][45] (where quin = quinoline, tz = thiazole). Also, it has been reported that the mechanism of antitumour activity of *trans*-$[PtCl_2(NH_3)$(pip)] does not involve recognition of its DNA adduct by HMG domain proteins as a crucial step,[46] in contrast to the proposals for cisplatin and its analogues. Thus, further studies are warranted to develop the potential of such *trans* platinum anticancer complexes which act by a different mechanism and exhibit activity complementary to agents such as cisplatin.

3.6 Conclusions

$^{1}H,^{15}N$ NMR studies of the aquation of the *trans*-ammine-picoline-dichloro complexes **1** – **3** (2-pic, 3-pic and 4-pic, respectively) showed that the monoaquation step is relatively rapid ($t_{1/2}$ 1.5 - 7.5 h at 277 K). However, aquation occurs only to a limited extent (18-24 % hydrolysis, 5 mM Pt, 277 K), the equilibrium favouring the dichloro species, with little formation of the diaqua complex. Increased steric hindrance to an axial approach to Pt^{II} in the 2-picoline complex **1** was apparent in the X-ray crystal structure. This hindrance has the effect of destabilising the expected trigonal bipyramidal transition state, an effect well-known in substitution reactions of square-planar Pt^{II} complexes. The low pK_a values of the monoaqua complexes **1** – **3** (5.3-5.6) implies that these complexes will be largely in the less reactive hydroxo forms at physiological pH. However, the extent of hydrolysis at intracellular chloride concentrations (4 - 23 mM) is expected to be low (<10%). This, together with the faster rate of hydrolysis, due to the higher *trans* effect of Cl^- compared with NH_3, are likely to have a major influence on the biological activity of *trans* compared to *cis* complexes.

3.7 References

[1] N. Farrell, *Transition Metal Complexes as Drugs and Chemotherapeutic Agents*, Kluwer, Dordrecht, The Netherlands, **1989**.

[2] D. S. Alberts, S. Green, E. V. Hannigan, R. O'Toole, D. Stock-Novack, P. Anderson, E. A. Surwit, V. K. Malvlya, W. A. Nahhas, C. J. Jolles, *J. Clin. Oncol.* **1992**, *10*, 706.

[3] K. R. Harrap, *Cancer Res.* **1995**, *55*, 2761.

[4] B. J. Monk, D. S. Alberts, R. A. Burger, P. T. Fanta, A. V. Hallum, K. D. Hatch, S. E. Salmon, *Gynecologic Oncol.* **1998**, *71*, 308.

[5] L. S. Hollis, A. R. Amundsen, E. W. Stern, *J. Med. Chem.* **1989**, *32*, 128.

[6] N. Farrell, T. T. B. Ha, J.-P. Souchard, F. L. Wimmer, S. Cros, N. P. Johnson, *J. Med. Chem.* **1989**, *32*, 2240.

[7] M. V. Beusichem, N. Farrell, *Inorg. Chem.* **1992**, *31*, 634.

[8] U. Bierbach, Y. Qu, T. W. Hambley, J. Peroutka, H. L. Nguyen, M. Doedee, N. Farell, *Inorg. Chem.* **1999**, *38*, 3535.

[9] N. Farrell, *Met. Ions Biol. Syst.* **1996**, *32*, 603.

[10] M. S. Davies, S. J. Berners-Price, T. W. Hambley, *Inorg. Chem.* **2000**, *39*, 5603.

[11] M. Jennerwein, P. A. Andrews, *Drug Metab. Dispos.* **1995**, *23*, 178.

[12] M. E. Howe-Grant, S. J. Lippard, *Met. Ions Biol. Syst.* **1980**, *11*, 63.

[13] B. Lippert, *Met. Ions Biol. Syst.* **1996**, *33*, 105.

[14] Y. Liu, J. Vinje, C. Pacifico, G. Natile, E. Sletten, *J. Am. Chem. Soc.* **2002**, *124*, 12854.

[15] J. Holford, S. Y. Sharp, B. A. Murrer, M. Abrams, L. R. Kelland, *Br. J. Cancer* **1998**, *77*, 366.

[16] J. Holford, F. Raynaud, B. A. Murrer, K. Grimaldi, J. A. Hartley, M. Abrams, L. R. Kelland, *Anti-Cancer Drug Design* **1998**, *13*, 1.

[17] S. C. Dhara, *Indian J. Chem.* **1970**, *8*, 193.

[18] L. R. Kelland, C. F. J. Barnard, I. G. Evans, B. A. Murrer, B. R. C. Theobald, S. B. Wyer, P. M. Goddard, M. Jones, M. Valenti, A. Bryant, P. M. Rogers, K. R. Harrap, *J. Med. Chem.* **1995**, *38*, 3016.

[19] C. Tessier, F. D. Rochon, *Inorg. Chim. Acta* **1999**, *295*, 25.

[20] G. M. Sheldrick, *SADABS, version 2004/ 1*, Göttingen, Germany, **2004**.

[21] G. M. Sheldrick, *SHELXS*, Göttingen, Germany, **1997**.

[22] P. T. Beurskens, G. Beurskens, R. d. Gelder, S. Garcia-Granda, R. O. Gould, R. Israel, J. M. M. Smits, *Crystallography Laboratory,* University of Nijmegen, The Netherlands, **1999**.

[23] G. M. Sheldrick, *SHELXL*, Göttingen, Germany, **1997**.

[24] P. W. Atkins, *The Elements of Physical Chemistry*, 2nd ed., Oxford University Press, Oxford, **1996**.

[25] K. Harrap, *ICR Report*, AnorMED Inc., **1992**.

[26] J. Kasparkova, V. Marini, Y. Najajreh, D. Gibson, V. Brabec, *Biochemistry* **2003**, *42*, 6321.

[27] N. Farrell, L. R. Kelland, J. D. Roberts, M. V. Beusichem, *Cancer Res.* **1992**, *52*, 5065.

[28] M. L. Tobe, J. Burgess, in *Inorganic Reaction Mechanisms*, Addison Wesley Longman Inc., New York, **1999**, pp. 70.

[29] F. Aprile, D. S. Martin, *Inorg. Chem.* **1962**, *1*, 551.

[30] S. E. Miller, K. J. Gerard, D. A. House, *Inorg. Chim. Acta* **1991**, *190*, 135.

[31] N. Farrell, E. S. Kozma, *Unpublished Results*.

[32] Y. Liu, F. P. Intini, G. Natile, E. Sletten, *J. Chem. Soc. Dalton. Trans.* **2002**, 3489.

[33] Y. Chen, Z. Guo, S. Parsons, P. J. Sadler, *Chem. Eur. J.* **1998**, *4*, 672.

[34] D. P. Bancroft, C. A. Lepre, S. J. Lippard, *J. Am. Chem. Soc.* **1990**, *112*, 6860.

[35] S. E. Miller, D. A. House, *Inorg. Chim. Acta* **1989**, *161*, 131.

[36] F. Legendre, V. Bas, J. Kozelka, J.-C. Chottard, *Chem. Eur. J.* **2000**, *6*, 2002.

[37] T. G. Appleton, A. J. Bailey, K. J. Barnham, J. R. Hall, *Inorg. Chem.* **1992**, *31*, 3077.

[38] A. M. Pizarro, V. P. Munk, C. Navarro-Ranninger, P. J. Sadler, *Angew. Chem. Int. Ed.* **2003**, *42*, 5339.

[39] A. M. Pizarro, *PhD Thesis* **2004**, Universidad Autónoma de Madrid, Spain.

[40] M. S. Davies, J. W. Cox, S. J. Berners-Price, W. Barklage, Y. Qu, N. Farrell, *Inorg. Chem.* **2000**, *39*, 1710.

[41] S. J. Barton, K. J. Barnham, A. Habtemariam, R. E. Sue, P. J. Sadler, *Inorg. Chim. Acta* **1998**, *273*, 8.

[42] S. J. Berners-Price, T. A. Frenkiel, U. Frey, J. D. Ranford, P. J. Sadler, *J. Chem. Soc. Chem. Commun.* **1992**, 789.

[43] G. Natile, M. Coluccia, *Coord. Chem. Rev.* **2001**, *216-217*, 383.

[44] M. Mikola, J. Arpalahti, *Inorg. Chem.* **1994**, *33*, 4439.

[45] V. Brabec, K. Neplechova, J. Kasparkova, N. Farrell, *J. Biol. Inorg. Chem.* **2000**, *5*, 364.

[46] J. Kasparkova, O. Novakova, V. Marini, Y. Najajreh, D. Gibson, J.-M. Perez, V. Brabec, *J. Biol. Chem.* **2003**, *278*, 47516.

Chapter 4

G-G Base-Pairing in Nucleobase Adducts of the Anticancer Drug *Cis*-[$PtCl_2(NH_3)$(2-picoline)] and its *Trans* Isomer

4.1 Abstract

Cis-[$PtCl_2(NH_3)$(2-picoline)](AMD473) is a sterically-hindered anticancer complex with a profile of chemical and biological activity that differs significantly from that of cisplatin. Adducts of AMD473 with neutral 9-ethylguanine (9-EtGH) and anionic (N1-deprotonated) 9-ethylguanine (9-EtG) as perchlorate and nitrate salts, and also a nitrate salt of the *trans* isomer (AMD443), have been prepared and their structures determined by X-ray crystallography: *cis*-[$Pt(NH_3)$(2-pic)(9-EtGH)$_2$]$(ClO_4)_2$ (**4**)·$2H_2O$·Me_2CO, *cis*-[$Pt(NH_3)$(2-pic)(9-EtGH)$_2$]$(NO_3)_2$ (**5**)·$2H_2O$, *cis*-[$Pt(NH_3)$(2-pic)(9-EtGH)(9-EtG)]NO_3 (**6**)·$3.5H_2O$, *trans*-[$Pt(NH_3)$(2-pic)(9-EtGH)(9-EtG)]NO_3 (**7**)·$8H_2O$. In all cases, platinum coordination is through N7 of neutral (**4**, **5**) and anionic (**6**, **7**) guanine. In each complex, the guanine bases are arranged in the head-to-tail conformation. In complex **4**, there is an infinite array of 6-molecule cycles, based on hydrogen bonding interactions. Pt^{II} coordinated at N7 acidifies the N1 proton of neutral 9-ethylguanine (pK_a = 9.57) to give pK_{a1} = 8.40 and pK_{a2} = 8.75 for complex **5**, and pK_{a1} = 7.77 and pK_{a2} = 9.00 for complex **7**. In complexes **6** and **7**, three intermolecular hydrogen bonds are formed between neutral and deprotonated guanine ligands involving O6, N1 and N2 sites. Unusually, both of the platinated guanine bases of complexes **6** and **7** participate in this triple G≡G hydrogen bonding. This is the first report of X-ray crystal structures of nucleobase adducts of the promising anticancer drug AMD473.

4.2 Introduction

Cisplatin, the world's best-selling anticancer drug, has been the subject of intense research over the last thirty-five years. The antitumour activity of cisplatin and various other anticancer platinum drugs is attributed to their ability to modify the structure of the DNA of cancer cells.[1] Cisplatin reacts with genomic DNA and yields a variety of mono-adducts and intra- and interstrand cross-links,[2] as well as protein-DNA cross-links.[1]

The most nucleophilic sites in duplex DNA are guanine (G) residues, especially those located adjacent to a second guanine residue. For Pt^{II} coordination, guanine N7 appears to be the preferred binding site. Therefore, it is not surprising that the major adduct of cisplatin with DNA is an intrastrand cross-link between the N7 atoms of adjacent guanine residues.[3] The coordinated guanine bases are orientated in a head-to-head (HH) conformation. However, the head-to-tail (HT) forms, characteristic of minor interstrand adducts, are thermodynamically favoured in all simple *cis*-$[PtA_2G_2]$ models (A = amine or half of a diamine), and the head-to-head form is relatively rare.[3, 4]

cis-$[PtCl_2(NH_3)$(2-picoline)] (AMD473) is a sterically-hindered anticancer complex with a profile of chemical and biological activity that differs significantly from that of cisplatin.[5] AMD473 has been administered to over 500 cancer patients in phase I and phase II clinical trials, in which it has demonstrated activity against a wide range of tumours and a manageable safety profile. AMD473 also has the potential to be administered as an oral formulation. The 2-methyl group hinders axial approach to Pt^{II} in AMD473, and as a result, hydrolysis occurs approximately four times more slowly than for cisplatin.[6] The introduction of steric bulk by the 2-

picoline ligand (Figure 4.1) in AMD473, may give rise to novel DNA platination reactions, such as differential binding to nucleobases and structures locked in a single conformation.

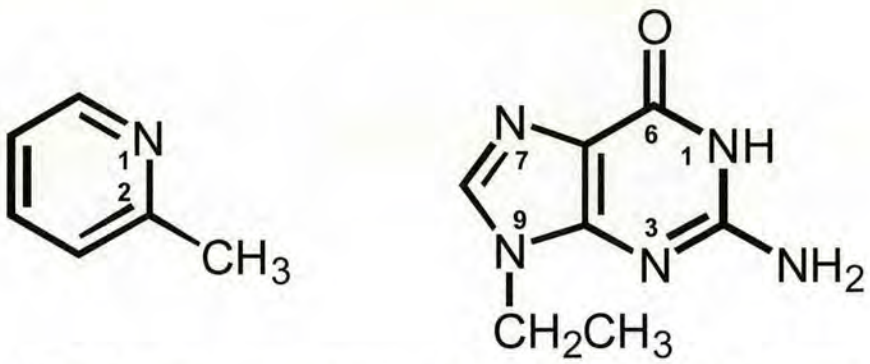

Figure 4.1 Schematic representation of 2-picoline and 9-ethylguanine (9-EtGH), including conventional numbering.

To gain further insight into stereochemical effects on the structure and dynamics of nucleobase adducts, adducts of AMD473 and its *trans* isomer, *trans*-$[PtCl_2(NH_3)(2\text{-pic})]$(AMD443), with 9-ethylguanine (9-EtGH) (Figure 4.1) have been studied in solution and in the solid state. The *trans* isomer also exhibits high cytotoxicity in a variety of cancer cell lines.[7]

4.3 Experimental

Preparations: 9-Ethylguanine was purchased from Sigma. *cis*-$[PtCl_2(NH_3)(2\text{-pic})]$ was kindly provided by AstraZeneca. The synthesis of *trans*-$[PtCl_2(NH_3)(2\text{-pic})]$ was based on previously published procedures.[8]

***cis*-$[Pt(NH_3)(2\text{-pic})(9\text{-EtGH})_2](ClO_4)_2$ (4)·$2H_2O$·Me_2CO:** *cis*-$[PtCl_2(NH_3)(2\text{-pic})]$ was reacted with 1.98 equiv of $AgClO_4$ (5 h, 323 K), followed by filtration of AgCl, and then addition of 2 mol equiv 9-EtGH (4 d, 323 K). Recrystallisation from acetone, and slow evaporation yielded **4** as colourless cubes.

***cis*-[Pt(NH$_3$)(2-pic)(9-EtGH)$_2$](NO$_3$)$_2$ (5)·2H$_2$O:** *cis*-[PtCl$_2$(NH$_3$)(2-pic)] was reacted with 1.96 mol equiv AgNO$_3$ (24 h, 323 K), followed by filtration of AgCl, and then addition of 2 mol equiv 9-EtGH (4-5 d, RT). Recrystallisation from hot water, and slow evaporation yielded **5** as colourless cubes from a solution at pH 3.55.

***cis*-[Pt(NH$_3$)(2-pic)(9-EtGH)(9-EtG)]NO$_3$ (6)·3.5H$_2$O:** *cis*-[PtCl$_2$(NH$_3$)(2-pic)] was reacted with 1.96 mol equiv AgNO$_3$ (24 h, 323 K), followed by filtration of AgCl, and then addition of 2 mol equiv 9-EtGH (24 h, 323 K). Recrystallisation from hot water, and slow evaporation yielded **6** as colourless cubes (at a measured pH of 7.98).

***trans*-[Pt(NH$_3$)(2-pic)(9-EtGH)(9-EtG)]NO$_3$ (7)·8H$_2$O:** *trans*-[PtCl$_2$(NH$_3$)(2-pic)] was reacted with 1.96 mol equiv AgNO$_3$ (24 h, RT), followed by filtration of AgCl, and then addition of 2 mol equiv 9-EtGH (4-5 d, 323 K). Colourless needles of **7** were obtained upon slow evaporation of an aqueous solution at pH 7.83.

NMR Spectroscopy: NMR spectra were recorded at 298 K, unless otherwise stated, on a Bruker DMX500 spectrometer (^{1}H 500.13 MHz), using 5 mm NMR tubes. Spectra were referenced to TSP via dioxane, δ 3.75. Water suppression was achieved by presaturation. Spectra were processed using XWINNMR (Version 3.5, Bruker UK Ltd).

Sample Preparation: NMR samples were prepared by taking aliquots of the aqueous solutions from the preparations of complexes **4** – **7**. All samples were prepared in 90% H$_2$O/10% D$_2$O unless otherwise stated.

pH Measurements: The pH values of solutions were determined using a Corning 145 pH meter equipped with a micro combination electrode, calibrated with Aldrich buffer solutions at pH 4, 7 and 10. No correction was made for deuterium isotope effects.

pK_a Values: These were determined by fitting the NMR pH titration curves (all 90% H_2O/10% D_2O) to the Henderson-Hasselbalch equation, assuming fast exchange on the NMR timescale of the protonated and deprotonated forms, using the program Kaleidagraph (Synergy Software, Reading, PA, USA).

Mass Spectrometry: Ion electrospray mass spectrometry was performed on a Platform II mass spectrometer (Micromass, Manchester, UK). The samples were infused at 8 μL/min and the ions were produced in an atmospheric pressure ionization (API)/ESI ion source. The source temperature was 383 K, and the drying gas flow rate was 300 L/h. A potential of 3.5 kV was applied to the probe tip, and cone voltage gradients of 20 – 40 V over 200 – 1000 Da were used. Data acquisition was performed on a Mass Lynx (V2.5) Windows NT PC data system. All samples were prepared in water.

X-ray Crystallography: Diffraction data for all crystals were collected with $Mo_{K\alpha}$ radiation on a Bruker Smart Apex CCD diffractometer equipped with an Oxford Cryosystems low-temperature device. Data for **6** were collected at 293 K, **5** and **7** were collected at 150 K, but those for **4** were collected at 240 K, as the sample appeared to undergo a phase change between this temperature and 220 K. All structures were solved by Dr. S Parsons using Patterson methods (DIRDIF)[9] and refined by full-matrix least squares against F^2 (SHELXTL).[10] H-atoms were

generally placed in calculated positions (see below); only full-weight atoms were refined with anisotropic displacement parameters. Crystal and refinement data are summarised in Table 4.1. Additional geometric calculations were accomplished with the program PLATON,[11] structures were visualised in SHELXTL-XP[10] and MERCURY.[12]

In structure **4**, the 9-Et groups are disordered. That attached to N91 is disordered over two positions in the ratio 70:30; the group attached to N92 was modelled similarly; however, the displacement parameters refined to large values, implying that the disorder is more extensive. Similarity restraints were applied to both 9-ethylguanine ligands. The anions and solvent of crystallisation were barely recognisable in difference maps, and were treated using the method of van der Sluis and Spek,[13] accounting for 150 e per formula unit. The formula, M_r, ρ *etc.* have all been calculated assuming that this complex contains $2ClO_4^-$, $2H_2O$ and one acetone molecule per formula unit.

Crystals of **5** were found to be non-merohedrally twinned through a two-fold rotation about [0 1 0]. This information was obtained using the program GEMINI.[14] Diffraction data from both domains were integrated simultaneously (SAINT version 7),[15] and all data were used for refinement. The twin law can also be expressed using the following matrix

$$\begin{pmatrix} -1 & 0 & 0 \\ -0.65 & 1 & -0.33 \\ 0 & 0 & -1 \end{pmatrix}.$$

The twinning has an affect on data with $2h + l = 3n$; it can be interpreted as a two-fold rotation about the *b*-axis of a metrically monoclinic super-cell with

dimensions a = 11.91, b = 66.75, c = 12.40 Å, β = 114.3°, obtained with the following transformation

$$\begin{pmatrix} -1 & 0 & 0 \\ 2 & -6 & 1 \\ 0 & 0 & 1 \end{pmatrix}$$ [16]

Coset decomposition of 2/*m* with respect to -1 implies that no further twinning needs to be considered.[17]

In **6**, the picoline ligand is disordered by a 180° rotation about the Pt-N bond. The occupancies of the alternative methyl positions were fixed at 0.75 and 0.25 after refinement. The two C-Me bonds were restrained to be of equal length. The molecules of water of crystallization based on O3W and O4W make unfavourable contacts with the minor disorder component, and the assumption was made that they have the same occupancy as the major component (0.75). The displacement parameter of O3W refined to a large value (0.14 $Å^2$), and it is possible that in reality its occupancy is less than 0.75; correlation between the occupancy and the displacement parameters means that it is difficult to draw the distinction from X-ray data alone. H-atoms were located on O1W, O2W and O4W in difference maps; after adjustment of the O-H distances and H-O-H angle to normal values, the entire molecules were treated as freely-rotating rigid groups. H-atoms have not been positioned on O3W.

The complexes in **6** are connected across -1 sites via N41-H41···N41A and N42-H42···N42A (N1-H···N1) hydrogen bonds. Thus, neither H41 nor H42 can be fully-occupied, as this would lead to the formation of a very close H···H contact across the inversion centres. Both of these sites were, therefore, assigned

occupancies of 0.5, which also ensures charge-balance. Similar comments apply to complex **7**.

The solvent and anion regions in the structure of **7** were treated in the same way as in **4**, amounting to 108.5 e per formula unit. The values of M_r, ρ etc. have been calculated on the assumption that these regions contain NO_3^- and $8H_2O$ molecules per formula unit.

Crystallographic data for the reported structures have been deposited with the Cambridge Crystallographic Data Centre: CCDC 264834 (**4**), 264835 (**5**), 264836 (**6**), and 264837 (**7**).

4.4 Results

X-ray Crystallography

Crystals containing *cis*-$[Pt(NH_3)(2\text{-pic})(9\text{-EtGH})_2]X_2$ (X = ClO_4, **4**·$2H_2O$·Me_2CO; X = NO_3, **5**·$2H_2O$) and *cis*- (**6**·$3.5H_2O$) or *trans*- (**7**·$8H_2O$) $[Pt(NH_3)(2\text{-pic})(9\text{-EtGH})(9\text{-EtG})]NO_3$ were obtained by reaction of the respective isomer of $[PtCl_2(NH_3)(2\text{-pic})]$ with slightly less than 2 mol equivalents of Ag^+, followed by reaction with 2 mol equivalents of 9-ethylguanine in water, and recrystallisation from acetone in the case of complex **4**, from water at pH 3.55 for complex **5**, and from water at pH 7.98 and 7.83 for complexes **6** and **7**, respectively. Crystallographic data and details of the refinement are listed in Table 4.1. Selected bond lengths and angles are given in Table 4.2, and the cations of **4** – **7** are shown in Figure 4.2. Hydrogen bond lengths and angles are given in Table 4.3. Rocking angles (Δ) and torsion angles (β) are listed in Table 4.4.

a)

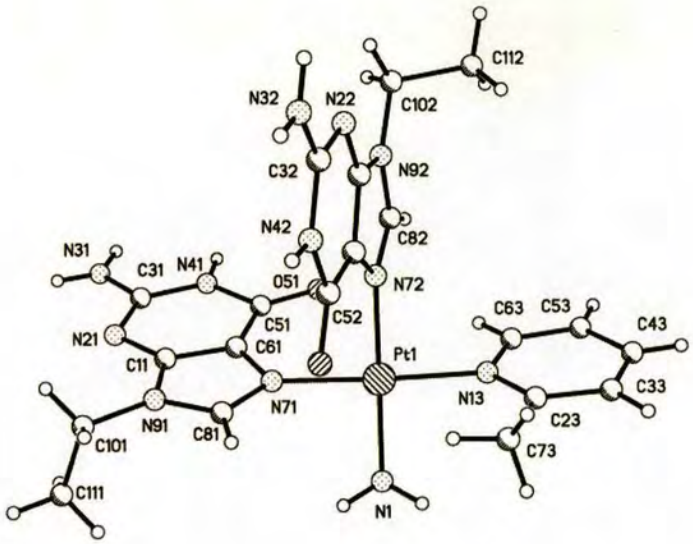
C112
N32
N22
C102
C32
N92
N42
C82
N31
C31
N41
O51
N72
C63
C53
C43
C51
C52
N21
C61
Pt1
C11
C33
N13
N71
C23
N91
C81
C101
C73
C111
N1

4

b)

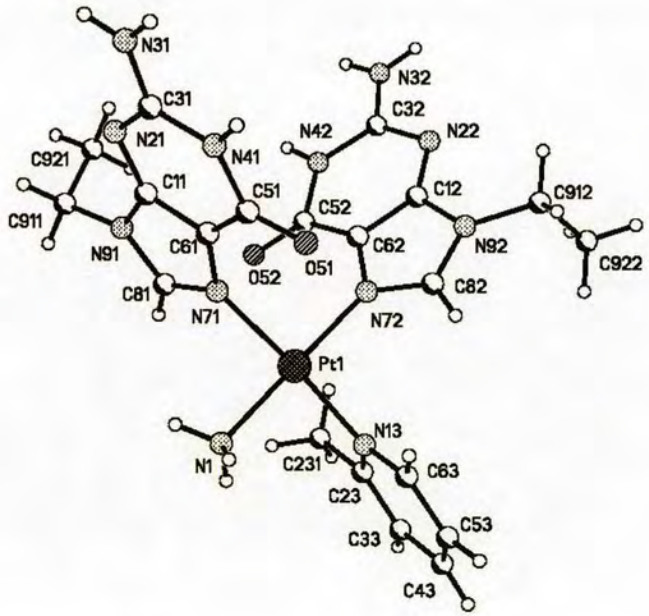
N31
N32
C31
C32
N21
N42
N22
N41
C921
C11
C51
C12
C912
C52
C911
C61
C62
N92
N91
O52
O51
C922
C81
C82
N71
N72
Pt1
N13
N1
C231
C63
C23
C53
C33
C43

5

c)

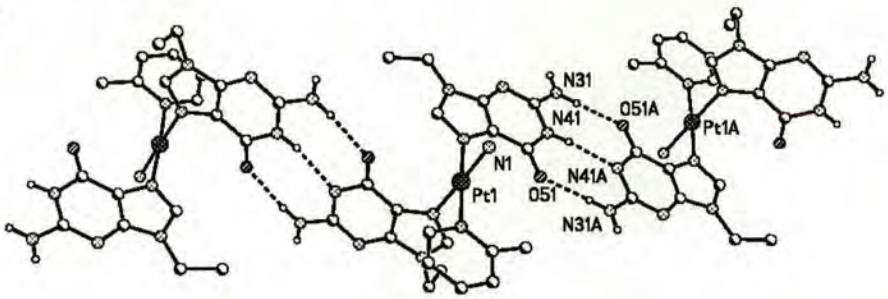

6

d)

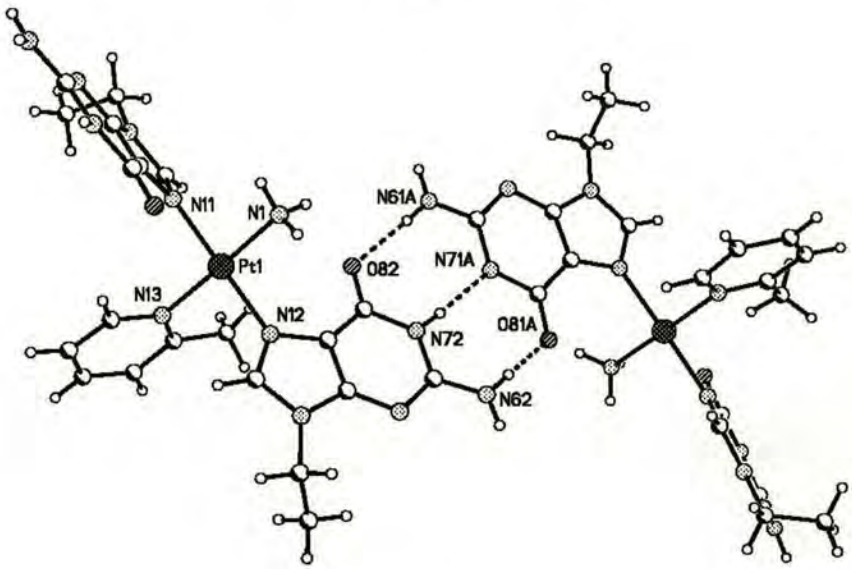

7

Figure 4.2 a) The cation *cis*-$[Pt(NH_3)(2\text{-pic})(9\text{-EtGH})_2]^{2+}$ in complex **4**. The planes of the 9-EtGH and 2-picoline rings are 70 - 80° relative to the Pt square-plane. The 9-EtGH bases are approximately perpendicular to one another. Intermolecular interactions are shown in Figure 4.3. b) The cation *cis*-$[Pt(NH_3)(2\text{-pic})(9\text{-EtGH})_2]^{2+}$ in complex **5**. The change in the anion compared to complex **4** has resulted in a significant decrease in the angle between the guanine base *cis* to 2-picoline and the Pt square-plane. The dihedral angle between the guanine bases is also reduced. There are additional H-bond interactions mediated by the anion. c) Intermolecular triple H-bonding in the structure of complex **6**, *cis*-$[Pt(NH_3)(2\text{-pic})(9\text{-EtGH})(9\text{-EtG})]^{+}$. The guanine bases are almost perpendicular to one another and each of the guanine bases and the 2-picoline are tilted by 70 - 80° relative to the platinum square plane. The cations form an infinite chain. d) Intermolecular triple H-bonding in the structure of

complex **7**, *trans*-$[Pt(NH_3)(2\text{-pic})(9\text{-EtGH})(9\text{-EtG})]^+$. Two molecules are shown, which form part of an infinite chain. The dihedral angle between the G bases is much smaller in this case, only 52°. The crystallographic numbering relates to the chemical numbering given in Figure 4.1, as follows: Complexes **4** and **5**: N71, N72 = N7. Complex **6**: N31 = $C2NH_2$; N41 = N1; O51 = O6. Complex **7**: N11, N12 = N7; O82 = O6; N71, N72 = N1; N61, N62 = $C2NH_2$.

Table 4.1 Crystallographic data for complexes **4** – **7**, in which **4** = *cis*-$[Pt(NH_3)(2\text{-pic})(9\text{-EtGH})_2](ClO_4)_2$, **5** = *cis*-$[Pt(NH_3)(2\text{-pic})(9\text{-EtGH})_2](NO_3)_2$, **6** = *cis*-$[Pt(NH_3)(2\text{-pic})(9\text{-EtGH})(9\text{-EtG})]NO_3$ and **7** = *trans*-$[Pt(NH_3)(2\text{-pic})(9\text{-EtGH})(9\text{-EtG})]NO_3$.

	4·$2H_2O$·Me_2CO	**5**·$2H_2O$	**6**·$3.5H_2O$	**7**·$8H_2O$
Empirical formula	$C_{23}H_{38}Cl_2N_{12}O_{13}Pt$	$C_{20}H_{32}N_{14}O_{10}Pt$	$C_{20}H_{34}N_{13}O_{8.5}Pt$	$C_{20}H_{43}N_{13}O_{13}Pt$
M_r	956.94	823.69	787.69	868.76
Crystal system	Triclinic	Triclinic	Triclinic	Monoclinic
Space group	$P\bar{1}$	$P\bar{1}$	$P\bar{1}$	$P2_1/n$
a (Å)	13.147(15)	11.9052(5)	8.8183(3)	16.0748(5)
b (Å)	14.056(16)	12.2098(4)	11.2332(4)	22.8397(8)
c (Å)	14.634(16)	12.4032(4)	15.7824(5)	17.5291(6)
α (°)	87.783(17)	72.813(2)	95.894(2)	90
β (°)	84.728(17)	65.613(2)	97.663(2)	97.891(2)
γ (°)	66.668(15)	67.423(2)	112.685(2)	90
V (Å^3)	2473(5)	1495.98(9)	1409.09(8)	6374.8(4)
Z	2	2	2	8
λ (Å)	0.71073	0.71073	0.71073	0.71073
T (K)	240(2)	150(2)	293(2)	150(2)
ρ_{calcd} (g cm^{-3})	1.285	1.829	1.857	1.810
μ_{calcd} (mm^{-1})	3.001	4.766	5.050	4.486
F (000)	952	816	782	3488
2θ range (°)	1.80 – 28.92	1.83 – 28.88	1.32 – 28.99	1.47 – 25.00
Refls. collected	20627	27532	13990	38056
Independent refl.	11352	12830	6655	11215
Reflns. (R_{int})	(0.0469)	(0.0489)	(0.0258)	(0.0654)
$R1$ [$F_0 > 4\sigma(F_0)$]	0.0477	0.0373	0.0353	0.0586
$wR2$ (all data)	0.1114	0.0929	0.0847	0.1424

In each complex, platinum coordination is through the N(7) sites of the two 9-ethylguanine ligands, which adopt the head-to-tail orientation. Platinum(II) has the usual square-planar geometry, and Pt – N bond lengths range from 1.999(6) Å to 2.047(8) Å, which is within the normal range for these types of complexes.

Table 4.2 Selected bond lengths (Å) and angles (°) for **4** – **7**, in which **4** = *cis*-$[Pt(NH_3)(2\text{-pic})(9\text{-EtGH})_2](ClO_4)_2$, **5** = *cis*-$[Pt(NH_3)(2\text{-pic})(9\text{-EtGH})_2](NO_3)_2$, **6** = *cis*-$[Pt(NH_3)(2\text{-pic})(9\text{-EtGH})(9\text{-EtG})]NO_3$ and **7** = *trans*-$[Pt(NH_3)(2\text{-pic})(9\text{-EtGH})(9\text{-EtG})]NO_3$.

Bond /Angle[a]	**4**	**5**	**6**	**7**[b]
Pt – N(1)	2.041(5)	2.023(4)	2.047(4)	2.034(7)
Pt – N(13)	2.018(5)	2.019(4)	2.022(4)	2.047(8)
Pt – N(71)	2.008(4)	2.015(4)	2.009(4)	1.999(6)
Pt – N(72)	2.018(5)	2.020(4)	2.017(4)	2.011(6)
N(13) – Pt – N(1)	90.99(19)	88.18(15)	90.03(16)	177.8(3)
N(72) – Pt – N(1)	179.05(15)	178.74(17)	178.53(15)	90.0(3)
N(71) – Pt – N(1)	90.11(18)	88.31(15)	89.26(16)	89.1(3)
N(72) – Pt – N(13)	89.37(18)	91.69(15)	89.94(15)	91.2(3)
N(71) – Pt – N(13)	175.18(16)	174.70(14)	177.53(14)	89.8(3)
N(71) – Pt – N(72)	89.60(17)	91.90(14)	90.83(15)	178.5(3)
PtN_4 / G1	73.62(19)	72.22(14)	86.00(15)	71.0(3)
PtN_4 / G2	71.24(19)	52.83(19)	70.78(17)	58.0(3)
G1 / G2	86.17(18)	71.25(14)	88.39(15)	51.9(3)

[a] Note that the crystallographic atomic numbering schemes (Figure 4.2) differ from the chemical numbering scheme used in the text.
[b] Numbering scheme in complex **7** differs from that of *cis* complexes but for comparison N11 = N71 and N12 = N72.

In complex **4**·$2H_2O$·Me_2CO, *cis*-$[Pt(NH_3)(2\text{-pic})(9\text{-EtGH})_2](ClO_4)_2$·$2H_2O$·$Me_2CO$, the *cis* 9-ethylguanine ligands are approximately perpendicular to one another (Figure 4.2a). The large dihedral angle of 86.17(18)°

between the guanine bases prevents any substantial intramolecular base–base interaction. The plane angles of the 9-ethylguanine ligands relative to the 2-picoline are 89.2(3)° and 6.0(3)°. There is high thermal motion and at temperatures lower than 240 K, the system appeared to undergo a phase change, but no data were collected at lower temperatures. The ethyl groups at the 9-position are disordered.

In addition, there are hydrogen bonds between NH_3 groups and the O6 of guanine (N – O 2.88 Å), as well as double hydrogen bonds between N3 positions and NH_2 groups (N – N 3.00, 3.03 Å) on neighbouring molecules. These features combine to create an infinite array of 6-molecule cycles, Figure 4.3.

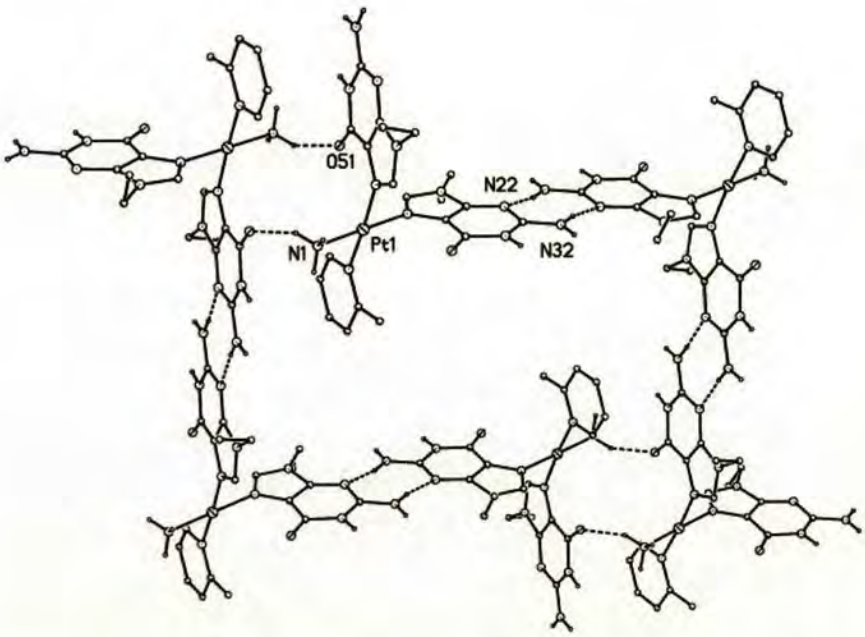

Figure 4.3 The six-molecule cyclic arrangement present in crystals of complex **4**. The intermolecular interactions involve alternating Pt – NH_3···O(6) H-bonding and double N(2)H_2···N3, N3···H_2N(2) H-bonding.

Table 4.3 Selected hydrogen bond lengths (Å) (with H··A < r(A) + 2.000) and angles (°) (<DHA > 110).

D – H	d(D – H)	d(H··A)	<DHA	d(D··A)	A
4:					
N1 – H1C	0.900	2.090	146.40	2.883	O51[a]
N31 – H31A	0.870	2.157	175.94	3.025	N21[b]
N32 – H32A	0.870	2.137	169.77	2.997	N22[c]
5:					
N32 – H32A	0.880	2.055	166.61	2.919	O51[a]
6:					
N31 – H31B	0.860	1.971	178.08	2.831	O51[d]
N41 – H41	0.860	2.078	172.81	2.934	N41[d]
N32 – H32B	0.860	1.999	168.37	2.847	O52[c]
N42 – H42	0.860	2.104	168.46	2.951	N42[c]
7:					
N61 – H61B	0.880	1.929	172.10	2.803	O82[e]
N62 – H62B	0.880	2.084	166.03	2.945	O81[f]
N72 – H72	0.880	2.059	177.00	2.938	N71[f]
N64 – H64B	0.880	1.965	170.69	2.837	O85[e]
N74 – H74	0.880	2.042	172.71	2.917	N75[e]
N65 – H65A	0.880	1.964	164.04	2.821	O84[f]

Equivalent positions: [a] -x, -y+1, -z+1, [b] -x, -y+2, -z+1, [c] -x+1, -y+1, -z, [d] -x+1, -y, -z+1, [e] x-1/2,-y+1/2, z-1/2, [f] x+1/2, -y+1/2, z+1/2.
Relationship between crystallographic and chemical numbering schemes:
Complex **4**: N1 = NH_3; N31, N32 = $C2NH_2$; N21, N22 = N3; O51 = O6
Complex **5**: N32 = $C2NH_2$; O51 = O6
Complex **6**: N31, N32 = $C2NH_2$; N41, N42 = N1; O51, O52 = O6
Complex **7**: N61, N62, N64, N65 = $C2NH_2$; N71, N72, N74, N75 = N1; O81, O82, O84, O85 = O6.

In complex **5**·$2H_2O$, *cis*-$[Pt(NH_3)(2\text{-pic})(9\text{-EtGH})_2](NO_3)_2 \cdot 2H_2O$, the dihedral angle between the *cis* 9-ethylguanine ligands is slightly smaller, 71.25(14)° (Figure 4.2b). The plane angles of the 9-ethylguanine ligands relative to 2-picoline are 76.5(2)° and 20.4(2)°. There is extensive hydrogen bonding between NH_3, N1, $C2NH_2$ and the NO_3 counterion, and O6, N3, and $C2NH_2$ are involved in H-bonding

with solvent water molecules. The only intermolecular H-bonding is between the $C2NH_2$ group and O6 (N – O 2.92 Å).

Table 4.4 Values for rocking angle Δ, which represents the difference between the two bond bending angles [C(5)-N(7)-Pt and C(8)-N(7)-Pt] and torsion angle β [C(8)-N(7)-Pt-NH_3(*cis*)], for complexes **4** – **7**.

	4	**5**	**6**	**7**
Rocking Angle Δ (°)	-7.68	4.35	-0.41	4.98
	-5.25	10.63	1.87	3.52
Torsion Angle β (°)	74.3	73.6	94	108.5[a]
				115.6[a]

[a] Average value.

In the cation of complex **6**·3.5H_2O, *cis*-[Pt(NH_3)(2-pic)(9-EtGH)(9-EtG)]NO_3·3.5H_2O, the 9-ethylguanine ligands are again almost perpendicular to one another, with a dihedral angle of 88.39(15)° (Figure 4.2c). The plane angles of the 9-ethylguanine ligands relative to 2-picoline are 88.9(2)° and 2.9(2)°. There is disorder about the Pt – N (pic) bond of 180° to give a distribution for the C2 and C6 positions of the 2-picoline ligand of 75% and 25%, respectively. There is intermolecular triple hydrogen bonding between the N1 of 9-EtG of one molecule and the N1H of 9-EtGH of an adjacent molecule (N – N 2.93 Å), which, together with $C2NH_2$ – O6 hydrogen bonds (N – O 2.83 Å), gives rise to a G – G^- base pair. The proton shared between the two N1 atoms of the 9-ethylguanine ligands appears to be disordered over two positions, a 1:1 mixture of N1H---N1A and N1---HN1A.

The *trans* 9-ethylguanine ligands in the cation of complex **7**·8H_2O, *trans*-[Pt(NH_3)(2-pic)(9-EtGH)(9-EtG)]NO_3·8H_2O, have a dihedral angle of 51.9(3)°, and the plane angles of the 9-ethylguanine ligands relative to the 2-picoline ligand are

85.5(5)° and 81.2(5)° (Figure 4.2d). This complex forms a triple hydrogen bond, similar to that in complex **6**, giving rise to a G – G^- base pair. The hydrogen bond lengths are 2.80 – 2.95 Å for NH_2 – O6 and 2.92 - 2.94 Å for N1(H) – N1. There are effectively two parallel chains formed through π – π stacking, which run in the same direction and interact with one another.

Solution Studies

Cis-$[Pt(NH_3)(2\text{-pic})(9\text{-EtGH})_2](ClO_4)_2$ (**4**)

The peak at m/z 763 in the positive-ion electrospray mass spectrum of complex **1** in water is assigned to the parent ion with an associated ClO_4^- counterion, $[Pt(NH_3)(2\text{-pic})(9\text{-EtGH})_2 \cdot ClO_4]^+$. The other peaks were assigned as follows: m/z = 584 $[Pt(NH_3)(2\text{-pic})(9\text{-EtGH}) \cdot ClO_4]^+$, m/z = 483 $[Pt(NH_3)(2\text{-pic})(9\text{-EtGH}) - H]^+$, m/z = 466 $[Pt(2\text{-pic})(9\text{-EtGH}) - H]^+$.

The ^1H NMR spectra of complex **4** in D_2O and acetone at 298 K are shown in Figure 4.4. Clearly, the solvent has a large effect on chemical shift; however, most noticeable is that the H8 signals for the 9-ethylguanine ligands are indistinguishable in aqueous solution, whereas in acetone, they are separated by 0.2 ppm. Therefore, the change in chemical shift of H8 in various acetone/H_2O mixtures was examined. The variation in chemical shift is plotted in Figure 4.5a. The spectra (Figure 4.5b) show the convergence of the two H8 signals as the molar fraction of water increases. The chemical shift of one of the H8 peaks (G1H8) is solvent dependent to a much greater extent than the other (G2H8).

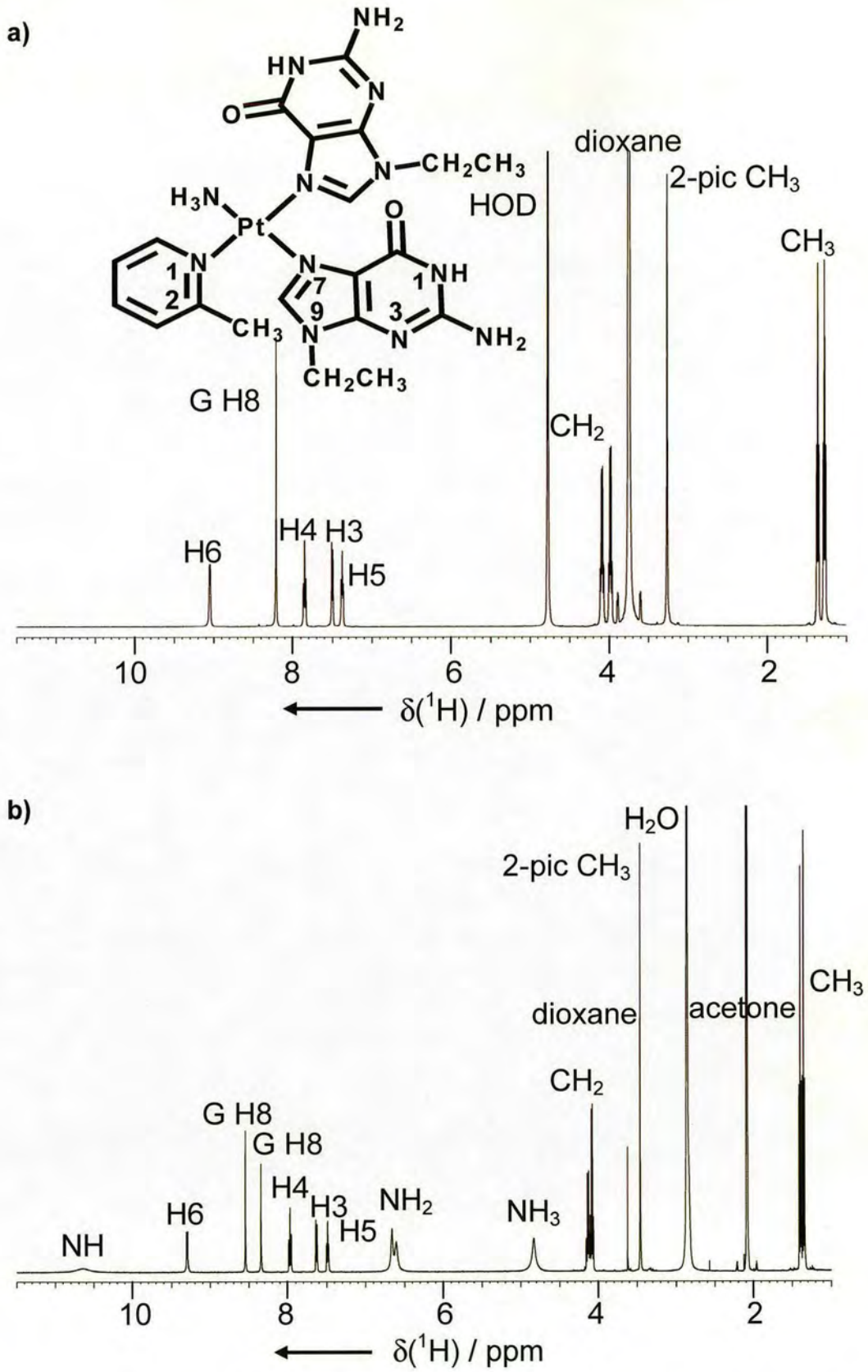

Figure 4.4 a) ^{1}H NMR spectrum of complex **4** in D_2O. b) ^{1}H NMR spectrum of complex **4** in d_6-acetone.

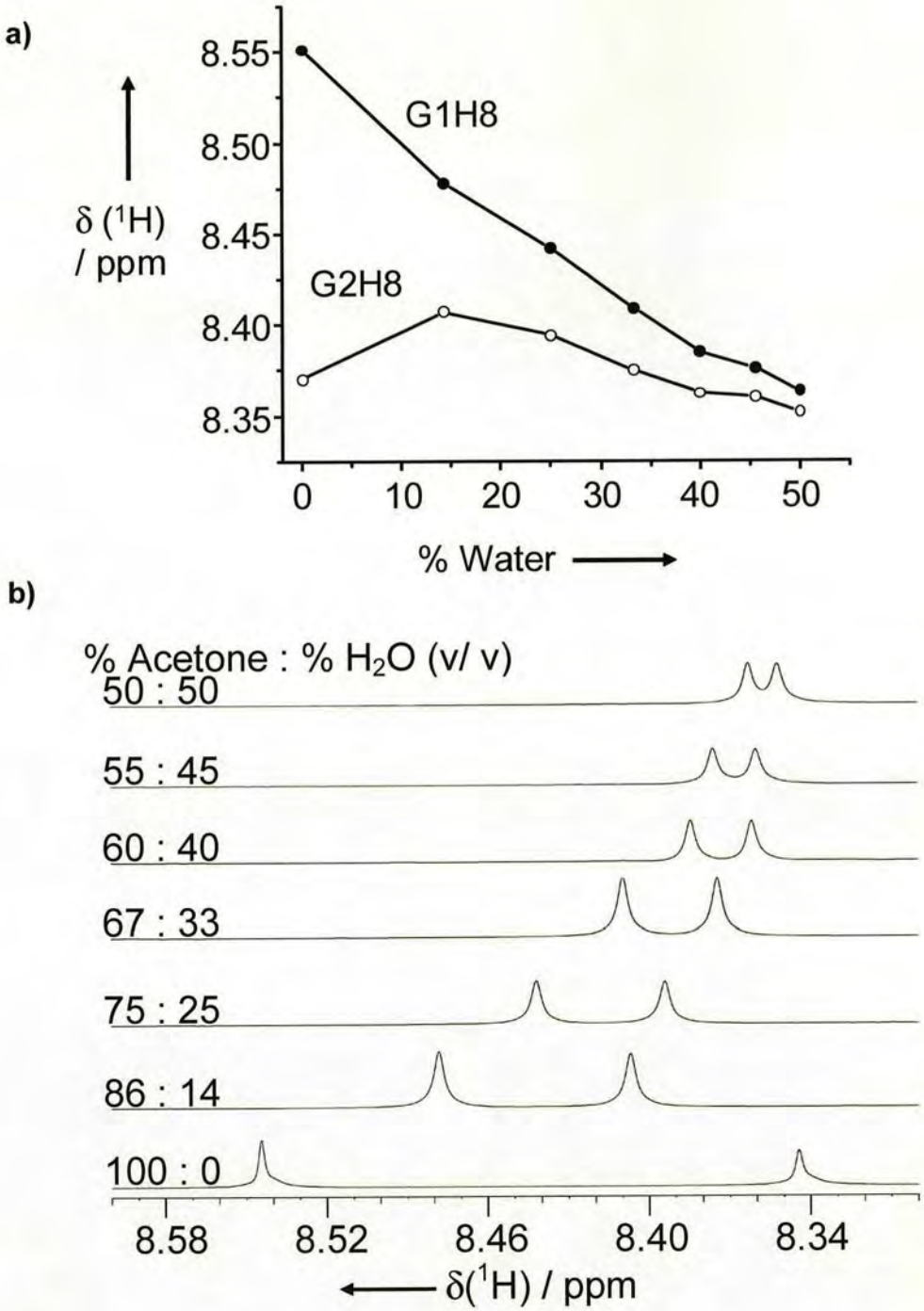

Figure 4.5 a) Plot of δ H8 for the two 9-EtGH ligands in complex **4** in d_6-acetone versus the % (v/v) of water, showing how the separation of the H8 signals decreases as the percentage of water increases. b) 9-Ethylguanine H8 region of the ^{1}H NMR spectra of complex **4** in acetone as a function of increasing water concentration.

The temperature dependence of the ^{1}H NMR spectrum of complex **4** in D_2O was further investigated between 278 K and 313 K (Figure 4.6). At low temperature, there are two individual H8 signals. Although the resonance for the H8 proton of one of the 9-ethylguanine ligands (G1H8) appears to be highly temperature dependent, the H8 peak for the other 9-ethylguanine (G2H8) is almost unaffected. This is clearly demonstrated by the plot of δ H8 shift versus temperature, shown in Figure 4.6a.

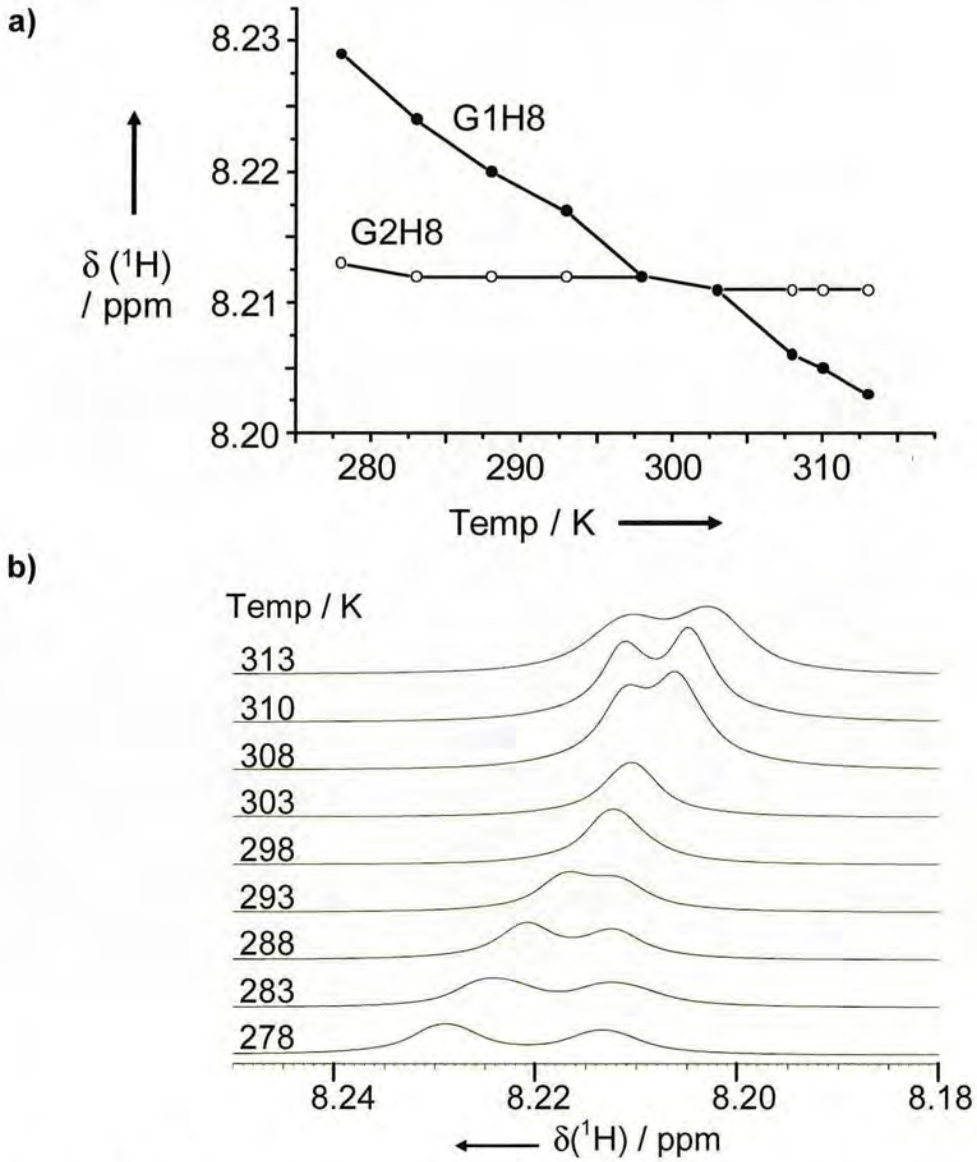

Figure 4.6 a) Plot of δ H8 versus temperature for complex **4** in D_2O. b) ^{1}H NMR spectra of complex **4** in D_2O showing the H8 region over the temperature range 278 K to 313 K.

A 2D ROESY spectrum of complex **4** in acetone (Figure 4.7) was recorded at 278 K to investigate the solution structure of this complex. Only one of the two H8 signals (G1H8) exhibits an NOE cross-peak to the 2-picoline methyl group. This H8 signal (G1H8) also exhibits an NOE cross-peak to the aromatic H6 proton of the 2-picoline ligand.

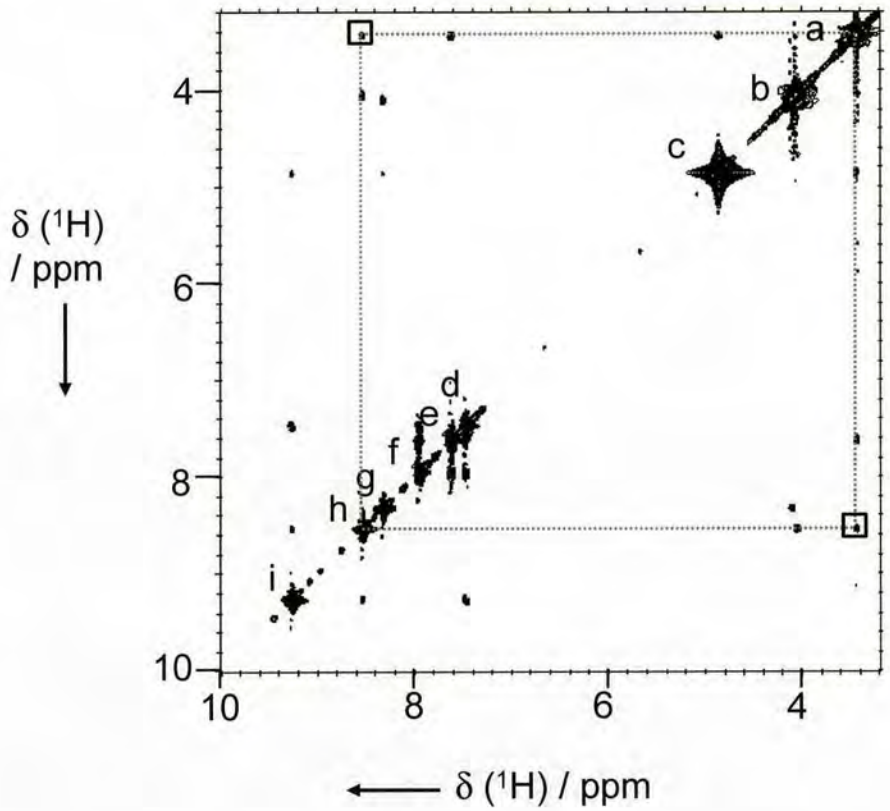

Figure 4.7 2D [^{1}H,^{1}H] ROESY NMR spectrum of complex **4** in d_6-acetone at 278 K. Assignments: a = 2-pic CH_3; b = Et CH_2; c = NH_3; d = H5 2-pic; e = H3 2-pic; f = H4 2-pic; g = H8 of 9-EtGH (G2); h = H8 of 9-EtGH (G1); i = H6 2-pic.

Trans-[Pt(NH_3)(2-pic)(9-EtGH)(9-EtG)]$NO_3 \cdot 8H_2O$ (**7**)

Positive-ion electrospray mass spectrometry showed peaks for the parent ion at m/z 662, assigned to [Pt(NH_3)(2-pic)(9-EtGH)$_2$ – H]$^+$, together with peaks

assignable to fragments: m/z = 645 $[Pt(2\text{-pic})(9\text{-EtGH})_2 - H]^+$, m/z = 466 $[Pt(2\text{-pic})(9\text{-EtGH}) - H]^+$.

The ^1H NMR spectrum of complex **7**, recorded in 90% H_2O/10% D_2O (Figure 4.8), contains only one set of peaks, corresponding to the two coordinated 9-ethylguanine ligands. The ^1H NMR chemical shifts of the peaks of complex **7** were not temperature dependent between 278 K and 318 K. A 2D NOESY spectrum revealed that there is an NOE cross-peak for the H8 signal of the 9-ethylguanine ligands and the 2-picoline CH_3 group.

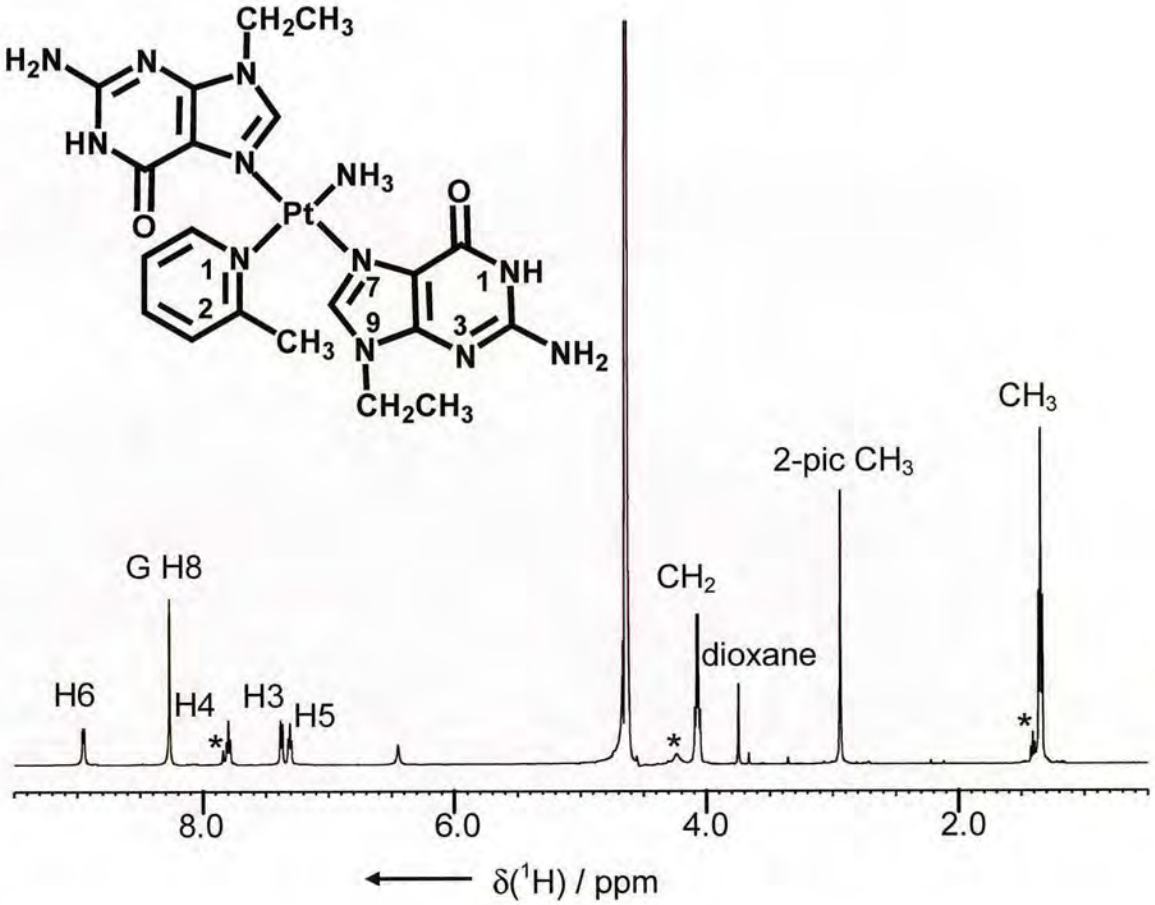

Figure 4.8 ^1H NMR spectrum of complex **7** in 90% H_2O/10% D_2O. The complex was prepared in situ by mixing *trans*-$[Pt(NH_3)(2\text{-pic})(OH_2)_2](NO_3)_2$ with a slight excess of 9-EtGH and hence small peaks for 9-EtGH are also present, labelled *.

In the pH range from 2 – 12, the pH-dependent ^{1}H NMR chemical shift measurements for complex **5** in 90% H_2O/10% D_2O show two acid-base equilibria, corresponding to the deprotonation of the two inequivalent N1H sites of the 9-ethylguanine ligands (Figure 4.9a). The pK_a values are 8.40 and 8.75. Complex **7** also has two acid-base equilibria (Figure 4.9b), with pK_a values of 7.77 and 9.00. The pK_a values for free 9-ethylguanine under the same conditions were determined to be 3.22 (N7) and 9.94 (N1H). These values are compared with those of cisplatin adducts in Table 4.5.

Table 4.5 Comparison of pK_a values for N1H of 9-EtGH in the complexes studied here (**5** and **7**), and for related adducts.

Species	pK_a N1(H)	Reference
9-ethylguanine	9.57	[18]
cis-$[Pt(NH_3)(2\text{-pic})(9\text{-EtGH})_2]^{2+}$	8.40, 8.75	Present work
trans-$[Pt(NH_3)(2\text{-pic})(9\text{-EtGH})_2]^{2+}$	7.77, 9.00	Present work
cis-$[Pt(NH_3)_2(9\text{-EtGH})_2]^{2+}$	7.76, 8.36	[18]
cis-$[Pt(NH_3)_2(9\text{-EtGH})_2]^{2+}$	8.01, 8.66	[19]
trans-$[Pt(NH_3)_2(9\text{-EtGH})_2]^{2+}$	7.90, 8.54	[19]

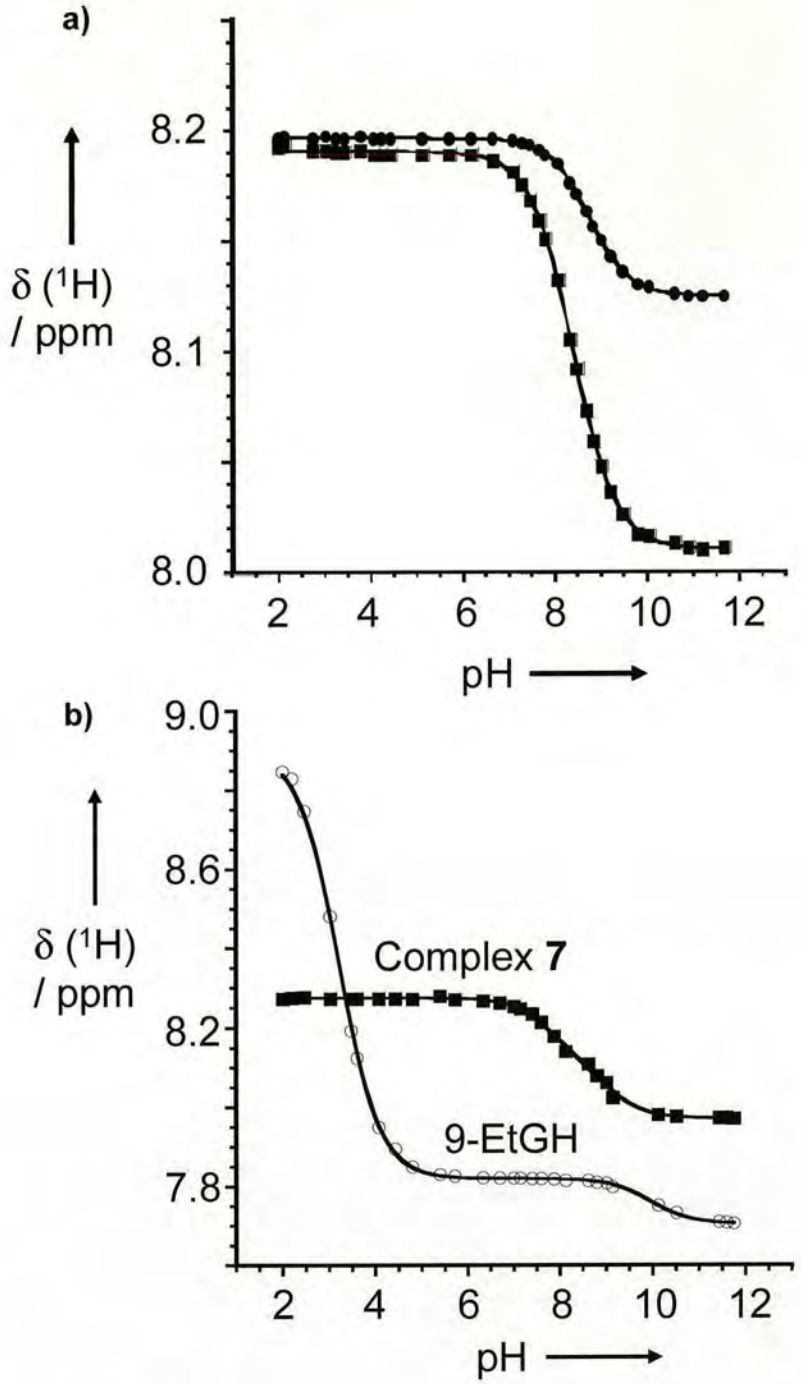

Figure 4.9 Dependence of the H8 chemical shifts of a) complex **5** and b) complex **7** and free 9-ethylguanine on pH. Note that there are two distinguishable H8 peaks for complex **5**, but unambiguous assignments cannot be made. The solution of **7** also contained a small amount of free 9-ethylguanine. The curves are computer fits to the Henderson-Hasselbalch equation, and give the pK_a values listed in Table 4.5.

4.5 Discussion

In the past, structural investigations of platinum-nucleobase complexes concentrated almost exclusively on cisplatin compounds,[20-35] and consequently, relatively few structural studies of nucleobase complexes of *trans* Pt^{II} compounds have been reported. Details of many of these *trans* complexes are summarised in a review by Lippert.[36] Here, bisnucleobase adducts of the sterically-hindered anticancer compound *cis*-[$PtCl_2(NH_3)$(2-pic)] (AMD473) and its *trans* isomer AMD443 have been studied. Three crystal structures of AMD473 adducts and one of an AMD443 adduct containing the model nucleobase 9-ethylguanine have been determined (**4** – **7**). These are the first X-ray structures of nucleobase adducts of {$Pt(NH_3)$(2-pic)} anticancer complexes.

Coordination at the N7 position of guanine was confirmed in each case, as was a head-to-tail orientation of the bases. The head-to-tail forms are characteristic of the minor interstrand adducts formed by cisplatin with DNA, and are thermodynamically favored in all simple *cis*-[PtA_2G_2] models (A = amine or half of a diamine, G = guanine derivative).[3] However, there are few examples of the head-to-head conformation, which is the more realistic model for a Pt-DNA complex.[20-22]

The main difference between complexes **4** and **5** is the anion; perchlorate and nitrate, respectively. Complex **4** exhibits a rare case of negative rocking angles (-7.68°, -5.25°; i.e. C(8)-N(7)-Pt angles > C(5)-N(7)-Pt angles). For complex **5**, the rocking angles are positive, as observed typically in structures of related complexes.[37] In complex **5**, the nitrate anion acts as a spacer between molecules and dominates the H-bond interactions. Consequently, there is only one type of intermolecular H-bond, between $C2NH_2$ and O6, and hence complex **5** is unable to

form the type of cycle described for **4**. Other structural differences may be simply a consequence of crystal packing. Complexes **5** and **6** differ in the charge on the complex and in the number of counterions and water molecules in the unit cell. A further and most intriguing difference is that in complex **5**, the guanine base in the head orientation with respect to the methyl group of 2-picoline is *trans* to the 2-picoline ligand, whereas in complex **6**, the analogous guanine base is *cis* to the 2-picoline ligand. This indicates that both head and tail orientations of 9-ethylguanine relative to the *cis* 2-picoline ligand are possible, although intermolecular interactions may favour only one of these orientations. It is expected that complexes **4**, **5** and **6** adopt the same structure in solution (at the same pH).

Complex **7** is a rare example of a *trans* bis(nucleobase) Pt^{II} complex that has a large dihedral angle of 51.9(3)° between the two bases. Another example is *trans*-$[Pt(MeNH_2)_2(1\text{-}MeC)_2](PF_6)_2$, with a dihedral angle of 56(1)°.[38] In most other bisnucleobase complexes of *trans*-$[(am)_2Pt]$, the bases are reasonably coplanar.[38-42] This large dihedral angle may result from the steric hindrance imposed by the bulky 2-picoline ligand.

Complexes **6** and **7** have the most interesting structural features. Both exhibit intermolecular triple hydrogen bonding involving NH_2, NH and O6, which give rise to a G – G^- base pair. There are various reports of PtG^- - G and PtG^- - GPt hydrogen bonding caused by deprotonation at the N1 position of Pt^{II}-bound guanine.[32-35, 38, 39, 43, 44] Five X-ray structures for such complexes have been reported. Three of these are monoguanine complexes: *cis*-$[Pt(NH_3)_2(9\text{-}EtGH)(1\text{-}MeC)][Pt(NH_3)_2(9\text{-}EtG)(1\text{-}MeC)](ClO_4)_3$,[33] *trans*-$[\{Pt(NH_3)_2(tmade)(9\text{-}EtGH)\}\cdot\{Pt(NH_3)_2(tmade)(9\text{-}EtG)\}](ClO_4)_2\cdot NO_3\cdot 1.6H_2O$ (where tmade = $N^{6'},N^{6'},N^{9}$-trimethyladenine),[38] {*trans*,

trans-$[(NH_3)_2Pt(1\text{-}MeU)(9\text{-}EtA)Pt(NH_2CH_3)_2(9\text{-}EtGH_{0.5})](ClO_4)_{2.5}\cdot 1.25H_2O\}_2$.[43] The other two, *cis*-$[Pt(NH_3)_2(9\text{-}EtG)_2]\cdot 9\text{-}EtGH\cdot 7H_2O$[32] and $[\{Pt(NH_3)(9\text{-}MeGH)_2(9\text{-}MeG)\}\{Pt(NH_3)(9\text{-}MeGH)_3\}\{1\text{-}MeC\}_4](ClO_4)_3\cdot 4H_2O$,[44] contain two coordinated guanine residues, but only one of these is involved in triple H-bonding. In complexes **6** and **7**, both platinated guanines are involved in G≡G triple hydrogen bonding. As a result, complexes **6** and **7** form infinite chains, but complex **7** does so in a more zigzag manner. This appears to be the first report of structures in which both platinated guanines participate in G≡G triple hydrogen bonding. The triple H-bond lengths for complexes **6** and **7** range from 2.80 – 2.95 Å for NH_2 – O6 and 2.92 – 2.95 Å for N1(H) – N1; these values are comparable with 2.83(1) Å and 2.90(1) Å, respectively, in *trans*-$[\{Pt(NH_3)_2(tmade)(9\text{-}EtGH)\}\{Pt(NH_3)_2(tmade)(9\text{-}EtG)\}]^{3+}$.[38]

For the cation in complex **4**, *cis*-$[Pt(NH_3)(2\text{-}pic)(9\text{-}EtGH)_2]^{2+}$, there are four different stereoisomers (2 x HT and 2 x HH). Because the 2-methyl group can be on the upper or lower side of the platinum plane, four geometrical head-to-tail isomers are possible. Only two of these will be distinguishable, however, by NMR, and therefore, four H8 signals should be observed. In reality, only two H8 peaks are observed. An explanation for this is either fast interconversion of head-to-tail conformations on the NMR timescale, or the molecule is locked into a single configuration at this temperature. The 2D ROESY spectrum of complex **4** at 278 K clearly shows an NOE cross-peak for only one of the two H8 signals of 9-ethylguanine (G1H8) and the methyl group of the 2-picoline ligand (Figure 4.7), suggesting a head-to-tail orientation of the guanine bases. If the solution structure was locked into the same configuration as that observed by X-ray crystallography for the solid state, the only observable NOE contact between the methyl group of the 2-

picoline ligand and an H8 proton would correspond to the 9-ethylguanine ligand *trans* to 2-picoline. Interestingly, G1H8 exhibits a greater solvent and temperature dependence than the second H8 peak, G2H8 (Figure 4.5 and Figure 4.6). It can be argued that the 9-ethylguanine *cis* to the 2-picoline exhibits the more marked temperature and solvent dependence, especially if there is rapid rotation about the Pt – N bonds. Rapid interconversion of head-to-tail conformers is common in Pt(II) diamine complexes.[45, 46] Rapid rotation should give rise to H8···CH_3 NOEs for both coordinated guanine bases, whereas only one ROESY cross-peak is detected. This suggests that the two H8 peaks observed contain four overlapping H8 signals. The major contribution to the observed NOE is probably from the 9-ethylguanine ligand *cis* to 2-picoline, in view of its intensity (medium compared to strong for the H6/H5 of 2-pic), and for which the H8···CH_3 distance is much shorter (ca. 3 Å versus 4.9 Å for a trans 9-ethylguanine; NOE $\propto r^{-6}$). However, it is difficult to interpret NOEs quantitatively in a dynamic system. Moreover, the NOE cross-peak between the G1H8 peak and the aromatic H6 peak of the 2-picoline ligand further substantiates the argument that G1H8 corresponds to the 9-ethylguanine ligand *cis* to 2-picoline.

For *trans*-$[Pt(NH_3)(2\text{-pic})(9\text{-EtGH})_2]^{2+}$ from **7**, there are also four different stereoisomers (2 x HT and 2 x HH; Figure 4.10). The two HT isomers (Figure 4.10a) are enantiomers. Therefore, only one HT configuration will be observed by NMR. As the two 9-ethylguanine ligands are in slightly different environments, we expect to observe two sets of peaks, however, experimentally, only one set of peaks is observed. This could be due to fast rotation about the Pt–2-pic bond, or to fast rotation of the guanine bases. Although Reedijk and co-workers[47] reported slow rotation about the Pt-2-pic bonds at room temperature in *cis*-$[Pt(2\text{-pic})_2(Puo)_2]^{2+}$ (Puo

= guanosine or 9-methylhypoxanthine), they confirmed that rotation of these 6-oxopurines is fast on the NMR timescale from -30 to +90 °C.

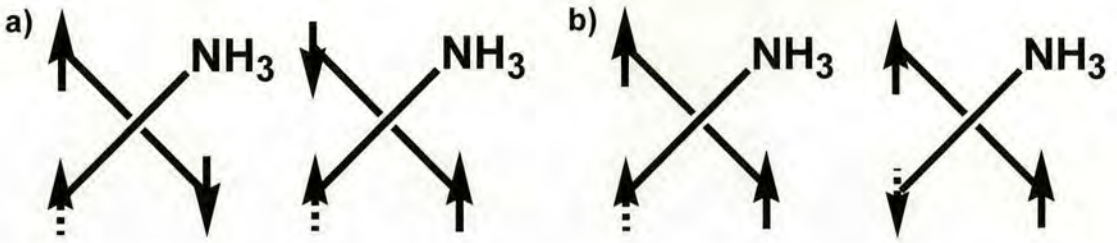

Figure 4.10 a) Head-to-tail enantiomers of *trans*-$[Pt(NH_3)(2\text{-pic})(9\text{-EtGH})_2]^{2+}$. b) Head-to-head isomers of *trans*-$[Pt(NH_3)(2\text{-pic})(9\text{-EtGH})_2]^{2+}$. Solid arrows represent the orientation of the 9-ethylguanine ligands, and dotted arrows represent that of the 2-picoline methyl group with respect to the platinum square plane.

The pK_a values of 8.40 and 8.75 for complex **5**, and 7.77 and 9.00 for complex **7**, which are assignable to N1H deprotonation of coordinated 9-ethylguanine, are 0.6 – 1.8 units lower than that for free 9-ethylguanine (Table 4.5). This observed acidification is a consequence of the inductive effect of Pt at the N7 position of guanine, and lies within the range observed for similar amine complexes (Table 4.5).

The guanine-guanine pairing pattern observed in complexes **6** and **7** represents a model for a nucleobase mispair. There is probably little chance of formation of such a guanine pair in DNA, as it is necessary to have independently metallated guanines in close proximity. However, with RNA and its enormous structural diversity, such possibilities are more likely.

4.6 Conclusions

In this study of bisnucleobase adducts of the sterically-hindered anticancer drug AMD473 and its *trans* isomer AMD443, three AMD473 adducts and an AMD443 adduct containing 9-ethylguanine have been synthesised and characterised. Each of the complexes has a head-to-tail arrangement of the guanine bases in contrast to the head-to-head arrangement preferred in DNA. Platination at the N7 position was confirmed in each case. Interesting triple hydrogen bonding was revealed in the structures of both the *cis* and *trans* 9-ethylguanine adducts, giving rise to G-G$^-$ base pairs for both coordinated guanine bases. The pK_a value of N1H of 9-ethylguanine was lowered significantly by N7 coordination to Pt^{II}, most notably for the *trans* complex (**7**) relative to free 9-ethylguanine.

4.7 References

[1] E. R. Jamieson, S. J. Lippard, *Chem. Rev.* **1999**, *99*, 2467.

[2] A. M. J. Fichtinger-Schepman, J. L. van der Veer, J. H. J. den Hartog, P. H. M. Lohman, J. Reedijk, *Biochemistry* **1985**, *24*, 707.

[3] S. O. Ano, F. P. Intini, G. Natile, L. G. Marzilli, *J. Am. Chem. Soc.* **1997**, *119*, 8570.

[4] J. S. Saad, T. Scarcia, K. Shinozuka, G. Natile, L. G. Marzilli, *Inorg. Chem.* **2002**, *41*, 546.

[5] J. Holford, F. Raynaud, B. A. Murrer, K. Grimaldi, J. A. Hartley, M. Abrams, L. R. Kelland, *Anti-Cancer Drug Design* **1998**, *13*, 1.

[6] Y. Chen, Z. Guo, S. Parsons, P. J. Sadler, *Chem. Eur. J.* **1998**, *4*, 672.

[7] K. Harrap, *ICR Report*, Unpublished Results, AnorMED Inc., **1992**.

[8] G. B. Kauffman, D. O. Cowan, *Inorg. Synth.* **1963**, *7*, 239.

[9] P. T. Beurskens, G. Beurskens, W. P. Bosman, R. de Gelder, S. Garcia-Granda, R. O. Gould, R. Israel, J. M. M. Smits, The DIRDIF96 Program System, Technical Report of the Crystallography Laboratory, University of Nijmegem, Nijmegen (The Netherlands), **1996**.

[10] G. M. Sheldrick, SHELXTL, University of Göttingen, Göttingen (Germany), **2001**.

[11] A. L. Spek, PLATON, A Multipurpose Crystallographic Tool, Utrecht University, Utrecht (The Netherlands), **2004**.

[12] I. J. Bruno, J. C. Cole, P. R. Edgington, M. Kessler, C. F. Macrae, P. McCabe, J. Pearson, R. Taylor, *Acta Crystallogr. Sect. B* **2002**, *58*, 389.

[13] P. van der Sluis, A. L. Spek, *Acta Crystallogr. Sect. A* **1990**, *46*, 194.

[14] R. A. Sparks, GEMINI, Bruker AXS, Madison, Wisconsin (USA), **1999**.

[15] Bruker AXS, SAINT Version 7, Madison, Wisconsin (USA), **2003**.

[16] Y. L. Page, *J. Appl. Crystallogr.* **1982**, *15*, 255.

[17] H. D. Flack, *Acta Crystallogr. Sect. A* **1987**, *A43*, 564.

[18] R. Griesser, G. Kampf, L. E. Kapinos, S. Komeda, B. Lippert, J. Reedijk, H. Sigel, *Inorg. Chem.* **2003**, *42*, 32.

[19] B. Song, J. Zhao, R. Griesser, C. Meiser, H. Sigel, B. Lippert, *Chem. Eur. J.* **1999**, *5*, 2374.

[20] B. Lippert, G. Raudaschl, C. J. L. Lock, P. Pilon, *Inorg. Chim. Acta* **1984**, *93*, 43.

[21] H. Schöllhorn, G. Raudaschl-Sieber, G. Müller, U. Thewalt, B. Lippert, *J. Am. Chem. Soc.* **1985**, *107*, 5932.

[22] S. E. Sherman, D. Gibson, A. H.-J. Wang, S. J. Lippard, *J. Am. Chem. Soc.* **1988**, *110*, 7368.

[23] G. Frommer, H. Schöllhorn, U. Thewalt, B. Lippert, *Inorg. Chem.* **1990**, *29*, 1417.

[24] G. Schröder, J. Kozelka, M. Sabat, M.-H. Fouchet, R. Beyerle-Pfnür, B. Lippert, *Inorg. Chem.* **1996**, *35*, 1647.

[25] R. E. Cramer, P. L. Dahlstrom, M. J. T. Seu, T. Norton, M. Kashiwagi, *Inorg. Chem.* **1980**, *19*, 148.

[26] R. W. Gellert, R. Bau, *J. Am. Chem. Soc.* **1975**, *97*, 7379.

[27] S. Grabner, J. Plavec, N. Bukovec, D. D. Leo, R. Cini, G. Natile, *J. Chem. Soc. Dalton. Trans.* **1998**, 1447.

[28] R. Cini, S. Grabner, N. Bukovec, L. Cerasino, G. Natile, *Eur. J. Inorg. Chem.* **2000**, 1601.

[29] R. K. O. Sigel, E. Freisinger, B. Lippert, *J. Biol. Inorg. Chem.* **2000**, *5*, 287.

[30] F. Schwarz, B. Lippert, H. Schöllhorn, U. Thewalt, *Inorg. Chim. Acta* **1990**, *176*, 113.

[31] R. Beyerle-Pfnür, B. Brown, R. Faggiani, B. Lippert, C. J. L. Lock, *Inorg. Chem.* **1985**, *24*, 4001.

[32] G. Schröder, B. Lippert, M. Sabat, C. J. L. Lock, R. Faggiani, B. Song, H. Sigel, *J. Chem. Soc. Dalton. Trans.* **1995**, 3767.

[33] R. Faggiani, B. Lippert, C. J. L. Lock, R. A. Speranzini, *Inorg. Chem.* **1982**, *21*, 3216.

[34] G. Schröder, M. Sabat, I. Baxter, J. Kozelka, B. Lippert, *Inorg. Chem.* **1997**, *36*, 490.

[35] B. Lippert, *J. Am. Chem. Soc.* **1981**, *103*, 5691.

[36] B. Lippert, *Met. Ions Biol. Syst.* **1996**, *33*, 105.

[37] S. Yao, J. P. Plastaras, L. G. Marzilli, *Inorg. Chem.* **1994**, *33*, 6061.

[38] C. Meiser, E. Freisinger, B. Lippert, *J. Chem. Soc. Dalton. Trans.* **1998**, 2059.

[39] A. Schreiber, M. S. Lüth, A. Erxleben, E. C. Fusch, B. Lippert, *J. Am. Chem. Soc.* **1996**, *118*, 4124.

[40] O. Krizanovic, M. Sabat, R. Beyerle-Pfnür, B. Lippert, *J. Am. Chem. Soc.* **1993**, *115*, 5538.

[41] I. Dieter-Wurm, M. Sabat, B. Lippert, *J. Am. Chem. Soc.* **1992**, *114*, 357.

[42] E. Freisinger, I. B. Rother, M. S. Lüth, B. Lippert, *Proc. Natl. Acad. Sci. USA* **2003**, *100*, 3748.

[43] R. K. O. Sigel, S. M. Thompson, E. Freisinger, F. Glahé, B. Lippert, *Chem. Eur. J.* **2001**, *7*, 1968.

[44] E. Freisinger, S. Meier, B. Lippert, *J. Chem. Soc. Dalton. Trans.* **2000**, 3274.

[45] H. C. Wong, K. Shinozuka, G. Natile, L. G. Marzilli, *Inorg. Chim. Acta* **2000**, *297*, 36.

[46] N. Margiotta, P. Papadia, F. P. Fanizzi, G. Natile, *Eur. J. Inorg. Chem.* **2003**, 1136.

[47] A. T. M. Marcelis, J. L. van der Veer, J. C. M. Zwetsloot, J. Reedijk, *Inorg. Chim. Acta* **1983**, *78*, 195.

Chapter 5

Interactions of Guanine Nucleosides with Sterically-Hindered Platinum Picoline Anticancer Complexes

5.1 Abstract

Adducts of the promising anticancer drug *cis*-[$PtCl_2(NH_3)$(2-pic)] (AMD473) and its *trans* isomer, which is also cytotoxic in a variety of cancer cell lines, with guanosine (Guo) and 2'-deoxyguanosine (2'-dGuo) have been prepared and characterised in solution by 1D ^1H, 2D [^1H,^1H] NMR spectroscopy and ESI mass spectrometry. Pt^{II} coordination at the N7 position is confirmed in all cases, increasing the acidity of the N1H sites of neutral guanosine and 2'-deoxyguanosine. Interestingly, there is a slightly larger effect on the pK_a of N1H in the *trans* complex compared to the *cis* complex, lowering the pK_a values by about 1.4 log units and 0.8-1.2 log units, respectively, as compared to the free nucleoside. Based on the NOEs, the complexes *cis*-$[Pt(NH_3)$(2-pic)$(Guo)_2]^{2+}$, *cis*-$[Pt(NH_3)$(2-pic)$(2'\text{-}dGuo)_2]^{2+}$ and *trans*-$[Pt(NH_3)$(2-pic)$(2'\text{-}dGuo)_2]^{2+}$ are assigned as head-to-tail conformations. A chromatographic study of AMD473 with guanosine and substituted guanosine bases confirmed the preference for N7 platination and revealed that the rates of reaction followed the order Guo > 1-MeGuo > 7-MeGuo, implying that substituents at the N1 position of guanosine may cause some steric retardation. Reactions between aquated ^{15}N-labelled AMD473 and guanosine (1:2) at 298 K have been studied in aqueous solution at millimolar concentrations using 2D [^1H,^{15}N] HSQC NMR spectroscopy. The reaction proceeds through two mono(guanosine) intermediate species to yield the dominant product *cis*-$[Pt(NH_3)$(2-pic)$(Guo)_2]^{2+}$. Initial guanosine substitution *trans* to 2-picoline is faster than substitution *cis* to 2-picoline due to steric hindrance, but the rates for the second guanosine substitution appear similar.

5.2 Introduction

Cisplatin is one of the most successful antitumour drugs developed in recent years and many studies of the molecular mechanism of antitumour effect of platinum drugs have revealed that the antitumour activity stems from the interaction of these compounds with intracellular DNA.[1] The complex cisplatin and related Pt^{II} analogues cross-link adjacent purine bases (two Gs or one A and one G) of a DNA strand that are capable of inhibiting replication and transcription.[1-3]

The major site of attack by Pt am(m)ine anticancer complexes is N7 of guanine, which is readily accessible in the major groove of duplex DNA and is the strongest electron donor of the four bases.[4-7] Complexes containing Pt – N1 binding have been prepared previously[8] but under physiological conditions N1 of guanine in duplex DNA is involved in Watson-Crick base-pairing. This position is therefore not available for metal binding. The nature of the non-leaving groups of platinum anticancer complexes, i.e. the amine ligands, plays an important, but not completely defined role in the anticancer activity of the drug. The requirement that at least one H be attached to each amine for significant anticancer activity[9, 10] has led to the speculation that this NH group forms a hydrogen-bond to the O6 of guanine[10, 11] or a phosphate oxygen.[6, 12-17] In DNA, these platinum compounds cross-link adjacent purine residues[1-3] in a 'head-to-head' conformation in which both the H8 atoms are on the same side of the platinum coordination plane.[7, 14, 16, 18-21] When the two nucleot(s)ide moieties are not linked by a phosphodiester group, the purines can have orientations in which the H8s are on opposite sides of the platinum coordination plane, designated 'head-to-tail'. Normally only head-to-tail complexes are detected in solution and in most solid state crystallographic studies.[1, 22-26] The head-to-head

atropisomers are difficult to isolate and have been found in only a few crystal structures of *cis*-$[Pt(NH_3)_2(9\text{-EtGH})_2]X_2$.[27, 28]

The X-ray structure determination of *cis*-$[Pt(NH_3)_2\{d(pGpG)\}]$ by Sherman et al in 1985[21] provided the first detailed picture of the effects of cisplatin binding to a dinucleotide segment of DNA. The structure (four independent molecules in the asymmetric unit) revealed essential features predicted by the 9-EtGH model compounds (e.g. large dihedral angles between G planes of 76-87°, destacking of guanines, only minor deviations of platinum from G planes), but in addition showed that the guanines are in the normal (for B-DNA) anti conformation, with the 5'-sugars in C3'-endo (C2'-exo) and the 3'-sugars in the C2'-endo (and C1'-exo) puckering, as predicted by NMR spectroscopy.[19] Another, potentially significant feature of these structures are the H-bonding interactions between a NH_3 group and a 5'-phosphate oxygen.[2, 21]

The characterisation of DNA adducts of transplatin is not as detailed and complete as that of cisplatin adducts. As a consequence of the inherent difference in geometry, cisplatin and transplatin form different adducts.[29-31] Specifically, transplatin cannot form the 1,2-intrastrand cross-links, which represent by far the most abundant adducts of cisplatin.[3] On the other hand, the *trans* isomer displays a greater variation in nucleobase donor sites.[31]

Apart from stereochemical considerations the question concerning changes in electronic structure, as well as in acid-base and hydrogen-bonding properties of guanine as a consequence of metal binding appears to be of considerable significance for both *cis* and *trans* isomers.

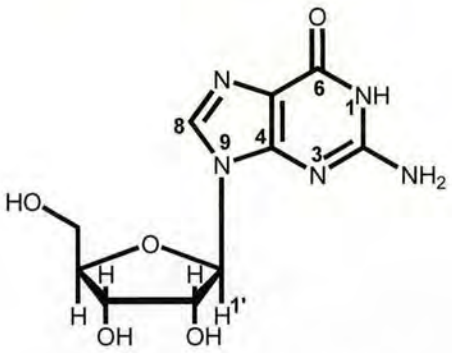

Guanosine (Guo)

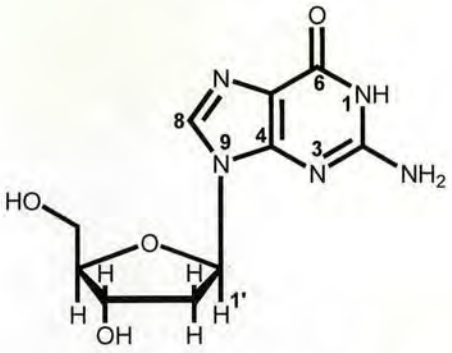

2'-deoxyguanosine (2'-dGuo)

In this work, the reactions of the platinum anticancer complex, *cis*-[$PtCl_2(NH_3)$(2-pic)] (AMD473), and various guanosine derivatives have been investigated primarily by HPLC followed by a combination of ESI mass spectrometry and 1D ^1H and 2D [^1H,^{15}N] HSQC NMR spectroscopy to identify the principal reaction products. A kinetic study of the reaction of aquated ^{15}N-AMD473 and guanosine has been performed by 2D [^1H,^{15}N] HSQC NMR spectroscopy. Finally, a selection of bis(guanosine) adducts of AMD473 and its *trans* isomer, which is also cytotoxic in a variety of cancer cell lines, has been prepared and characterised.

5.3 Experimental

Materials: 1-methylguanosine was purchased from ICN Biomedicals, 7-methylguanosine and guanosine were purchased from Sigma and 2'-deoxyguanosine was purchased from Acros. *cis*-[$PtCl_2(NH_3)$(2-pic)] was kindly provided by AstraZeneca. *cis*-[$PtCl_2(^{15}NH_3)$(2-pic)] was synthesised based on a previously published procedure,[32] employing *cis*-[$PtCl_2(^{15}NH_3)_2$] as the starting material. The synthesis of *trans*-[$PtCl_2(NH_3)$(2-pic)] was based on previously published procedures[33] and is described in Chapter 3.

HPLC: Analytical separations were carried out on a Gilson HPLC station with a 306 pump system, 234 auto-injector and series 1100 Hewlett Packard diode array detector, using a Nucleosil C_{18} reversed-phase column (250 x 4.6 mm, Hichrom).

The time courses of reactions between *cis*-$[PtCl_2(NH_3)(2\text{-pic})]$ (2 mM, 400 μL) and guanosine, 1-methylguanosine, and 7-methylguanosine (2 mM, 400 μL) at 1:1 molar ratios were carried out at 310 K and followed chromatographically by injections of aliquots of the mixture onto the HPLC column at various time intervals after mixing, with detection at 220 nm. All samples were prepared in an aqueous solution of 0.02 M $NaClO_4$, pH 5.5. A gradient elution method was employed using a water/acetonitrile mixture, with 0.1 % TFA.

The samples for semipreparative separation contained 4 mM *cis*-$[PtCl_2(^{15}NH_3)(2\text{-pic})]$ and 4 mM guanosine or 1-methylguanosine. The fractions collected were frozen in liquid nitrogen and lyophilized using a Modulyo Edwards freeze-drier.

Kinetic NMR Experiment: *cis*-$[PtCl_2(^{15}NH_3)(2\text{-pic})]$ (3 mM) was firstly reacted with 1.96 mol equiv $AgNO_3$ (24 h, 323 K), and filtered to remove AgCl. The reaction of the aquated species with guanosine was conducted at a 1:2 molar ratio. Samples contained 0.1 M $NaClO_4$ to maintain a constant ionic strength. The pH value at the beginning of the experiment was 6.46.

$[Pt(NH_3)(2\text{-pic})(G)_2](NO_3)_2$: Adducts were prepared by reaction of *cis*-$[PtCl_2(NH_3)(2\text{-pic})]$ or *trans*-$[PtCl_2(NH_3)(2\text{-pic})]$ with 1.96 mol equiv $AgNO_3$ (24 h, 323 K), filtration of AgCl, and then addition of 2 mol equiv of guanosine or 2'-deoxyguanosine and left to react for 24 h at 323 K.

NMR Spectroscopy: NMR spectra were recorded at 298 K, unless otherwise stated, on a Bruker DMX500 spectrometer (^{1}H 500.13 MHz), using 5 mm NMR tubes. Spectra were referenced to TSP via dioxane, δ 3.75. Water suppression was achieved by presaturation. Spectra were processed using XWINNMR (Version 3.5, Bruker UK Ltd).

pH Measurements: The pH values of solutions were determined using a Corning 145 pH meter equipped with a micro combination electrode, calibrated with Aldrich buffer solutions at pH 4, 7 and 10. No correction was made for deuterium isotope effects.

pK_a Values: These were determined by fitting the NMR pH titration curves (all 90% H_2O/10% D_2O) to the Henderson-Hasselbalch equation, with the assumption of fast exchange on the NMR timescale of protonated and deprotonated forms, using the program Kaleidagraph (Synergy Software, Reading, PA, USA).

Mass Spectrometry: Ion electrospray mass spectrometry was performed on a Platform II mass spectrometer (Micromass, Manchester, UK). The samples were infused at 8 μL/min and the ions produced in an atmospheric pressure ionization (API)/ESI ion source. The source temperature was 383 K, and the drying gas flow rate was 300 L/h. A potential of 3.5 kV was applied to the probe tip, and cone voltage gradients of 20 – 45 V over 200 – 1000 Da were used. Data acquisition was performed on a Mass Lynx (V2.5) Windows NT PC data system. All samples were prepared in water.

5.4 Results

1. HPLC Reactions of *cis*-[$PtCl_2(NH_3)$(2-pic)] with Guanosine Derivatives

The hydrolysis of *cis*-[$PtCl_2(NH_3)$(2-pic)] at 310 K was firstly monitored by HPLC (Appendix 1). Initially, only one peak was detected at 16.8 min, assigned to the dichloro species. Two major species were detected after 1 h with elution times of 11.3 and 19.1 min. A number of smaller peaks were detected also during the time course with elution times of 9.9, 11.3, 15.4, 22.2 and 31.5 min. This allowed ready identification of any hydrolysis products formed during reactions with nucleobases.

Reactions between *cis*-[$PtCl_2(NH_3)$(2-pic)] (2 mM) and guanosine or 1-methylguanosine or 7-methylguanosine (1:1 molar ratio, pH 5.5, 310 K) were investigated by HPLC time course experiments. HPLC chromatograms for these reactions are shown in Figure 5.1.

For the reaction of *cis*-[$PtCl_2(NH_3)$(2-pic)] with guanosine, initially only two peaks are observed corresponding to *cis*-[$PtCl_2(NH_3)$(2-pic)] with an elution time of ca. 15.4 min and guanosine ca. 19.3 min. As the reaction progresses, these peaks decrease in intensity and small peaks for intermediates and products emerged. The peaks at 10.4 and 18.5 min appear to be intermediate species from hydrolysis and they initially increase in intensity and then decrease slightly as the main product peaks at the far end of the chromatogram (26.8 min, **F1** and 29.3 min, **F2**) become more prominent (Figure 5.1).

In the reaction of 1-methylguanosine and *cis*-[$PtCl_2(NH_3)$(2-pic)], the 1-methylguanosine peak is at 20.0 min and it appears that there is a small intermediate species formed, likely due to hydrolysis, which elutes immediately before 1-methylguanosine. At around 2 h of reaction two new peaks appear towards the end of

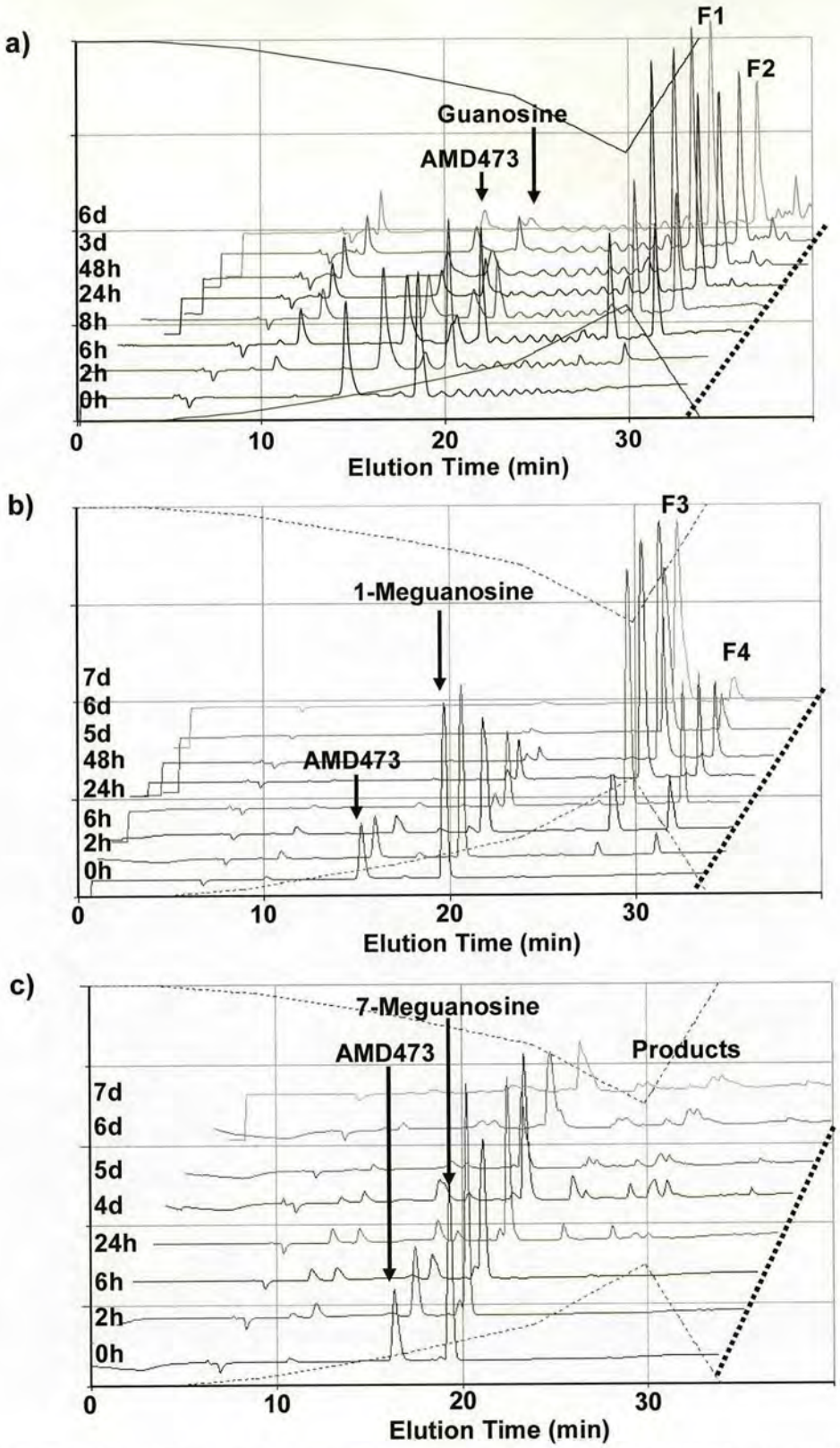

Figure 5.1 Chromatograms of reactions of AMD473 with a) guanosine, b) 1-Meguanosine and c) 7-Meguanosine (1:1) in 0.02 M $NaClO_4$ at 310 K, pH 5.5 (the sloping lines at the top and bottom represent the gradient of aqueous and organic eluents, respectively).

the chromatogram. The peak at ca. 27.0 min (**F3**) becomes the dominant product and that at 30.1 min (**F4**) behaves as an intermediate (Figure 5.1).

For the reaction of 7-methylguanosine and *cis*-$[PtCl_2(NH_3)(2\text{-pic})]$, the 7-methylguanosine peak eluted just before 20 min. There are two small hydrolysis peaks between 10 and 12 min and several small product peaks appear at the far end of the chromatogram. Interestingly, this reaction is much slower than that of 1-methylguanosine as the product peaks are only evident after 24 hours whereas for 1-methylguanosine there are product peaks after only 2 hours (Figure 5.1).

To obtain further structural information, *cis*-$[PtCl_2(^{15}NH_3)(2\text{-pic})]$ was reacted with guanosine and 1-methylguanosine and the fractions eluting at 26.8 (**F1**) and 29.3 min (**F2**) for the guanosine reaction and those at 27.0 (**F3**) and 30.1 min (**F4**) for the 1-methylguanosine reaction from the 48 h reaction mixtures were collected by HPLC separation and analysed by direct infusion ESI-MS and a combination of 1D ^1H and 2D [^1H,^{15}N] HSQC NMR spectroscopy.

ESI-MS Identification of Adducts

For the reaction of *cis*-$[PtCl_2(^{15}NH_3)(2\text{-pic})]$ and guanosine, the mass spectrum at a cone voltage of 45 eV for the fraction **F1** is shown in Figure 5.2. There are a large number of fragment peaks but the majority of these can be easily assigned. The parent ion at m/z 871.4 corresponds to the bis(guanosine) adduct, $[Pt(^{15}NH_3)(2\text{-pic})(Guo)_2\text{-H}]^+$. The other major peaks are assigned as follows: m/z 625.3 – $[PtCl(^{15}NH_3)(2\text{-pic})(Guo)]^+$, m/z 588.3 – $[Pt(^{15}NH_3)(2\text{-pic})(Guo)\text{-H}]^+$, m/z 532.1 – $[PtCl(^{15}NH_3)(Guo)]^+$, m/z 514.1 – $[PtCl_2(^{15}NH_3)(2\text{-pic})]TFA{\cdot}Na^+$, m/z 496.2 – $[PtCl_2(2\text{-pic})]TFA{\cdot}Na^+$, m/z 456.3 – $[Pt(^{15}NH_3)(2\text{-pic})(Guanine)\text{-H}]^+$, m/z 438.1 – $[Pt(2\text{-pic})(Guanine)\text{-H}]^+$, m/z 399.1 – $[PtCl_2(^{15}NH_3)(2\text{-pic})]Na^+$.

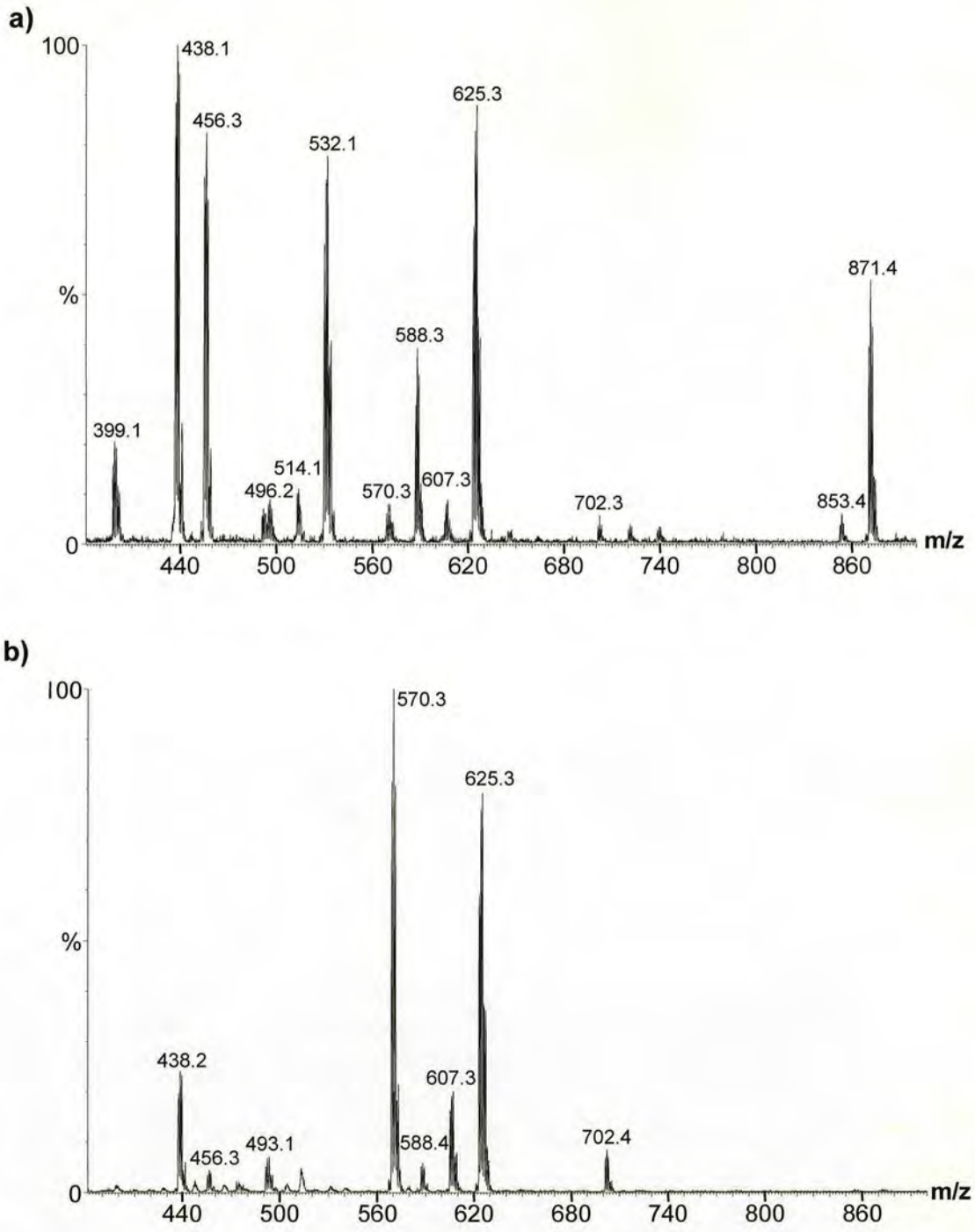

Figure 5.2 ESI mass spectra at a cone voltage of 45 eV for a) fraction **F1** and b) fraction **F2** from the reaction of ^{15}N-AMD473 and guanosine, see Figure 5.1.

The mass spectrum at 45 eV for the fraction **F2** is shown in Figure 5.2. The parent ion at m/z 702.4 corresponds to $[Pt(^{15}NH_3)(2\text{-pic})(Guo)\text{-}H]^+ \cdot TFA$. The other

major peaks are assigned as follows: m/z 625.3 – $[PtCl(^{15}NH_3)(2\text{-pic})(Guo)]^+$, m/z 607.3 – $[PtCl(2\text{-pic})(Guo)]^+$, m/z 588.4 – $[Pt(^{15}NH_3)(2\text{-pic})(Guo)\text{-}H]^+$, m/z 570.3 – $[Pt(2\text{-pic})(Guo)\text{-}H]^+$, m/z 493.1 – $[PtCl(^{15}NH_3)(2\text{-pic})(Guanine)]^+$, m/z 456.3 – $[Pt(^{15}NH_3)(2\text{-pic})(Guanine)\text{-}H]^+$, m/z 438.2 – $[Pt(2\text{-pic})(Guanine)\text{-}H]^+$.

For the reaction of *cis*-$[PtCl_2(^{15}NH_3)(2\text{-pic})]$ and 1-methylguanosine, the mass spectra at 45 eV for the fractions **F3** and **F4** are shown in Appendix 2. Likewise, there are a large number of fragment peaks but assignments are similar to those of fractions **F1** and **F2**. The parent ion for fraction **F3** at m/z 899.5 corresponds to the bis(guanosine) adduct, $[Pt(^{15}NH_3)(2\text{-pic})(1\text{-MeGuo})_2\text{-}H]^+$. The other major peaks are assigned as follows: m/z 871.4 – $[Pt(^{15}NH_3)(2\text{-pic})(Guo)_2\text{-}H]^+$, m/z 716.3 – $[Pt(^{15}NH_3)(2\text{-pic})(1\text{-MeGuo})_2\text{-}H]^+\cdot TFA$, m/z 702.3 – $[Pt(^{15}NH_3)(2\text{-pic})(Guo)\text{-}H]^+\cdot TFA$, m/z 639.3 – $[PtCl(^{15}NH_3)(2\text{-pic})(1\text{-MeGuo})]^+$, m/z 625.3 – $[PtCl(^{15}NH_3)(2\text{-pic})(Guo)]^+$, m/z 588.3 – $[Pt(^{15}NH_3)(2\text{-pic})(Guo)\text{-}H]^+$, m/z 546.3 – $[PtCl(^{15}NH_3)(1\text{-MeGuo})]^+$, m/z 532.1 – $[PtCl(^{15}NH_3)(Guo)]^+$, m/z 514.2 – $[PtCl_2(^{15}NH_3)(2\text{-pic})]TFA\cdot Na^+$, m/z 496.2 – $[PtCl_2(2\text{-pic})]TFA\cdot Na^+$, m/z 470.3 – $[Pt(^{15}NH_3)(2\text{-pic})(1\text{-MeGuanine})\text{-}H]^+$, m/z 452.3 – $[Pt(2\text{-pic})(1\text{-MeGuanine})\text{-}H]^+$, m/z 438.1 – $[Pt(2\text{-pic})(Guanine)\text{-}H]^+$, m/z 399.1 – $[PtCl_2(^{15}NH_3)(2\text{-pic})]Na^+$.

The mass spectrum for the fraction **F4** has a parent ion at m/z 716.3, corresponding to $[Pt(^{15}NH_3)(2\text{-pic})(1\text{-MeGuo})\text{-}H]^+\cdot TFA$. The other major peaks are assigned as follows: m/z 639.3 – $[PtCl(^{15}NH_3)(2\text{-pic})(1\text{-MeGuo})]^+$, m/z 621.3 – $[Pt(2\text{-pic})(1\text{-MeGuo})Cl]^+$, m/z 584.3 – $[Pt(2\text{-pic})(1\text{-MeGuo})\text{-}H]^+$, m/z 452.3 – $[Pt(2\text{-pic})(1\text{-MeGuanine})\text{-}H]^+$.

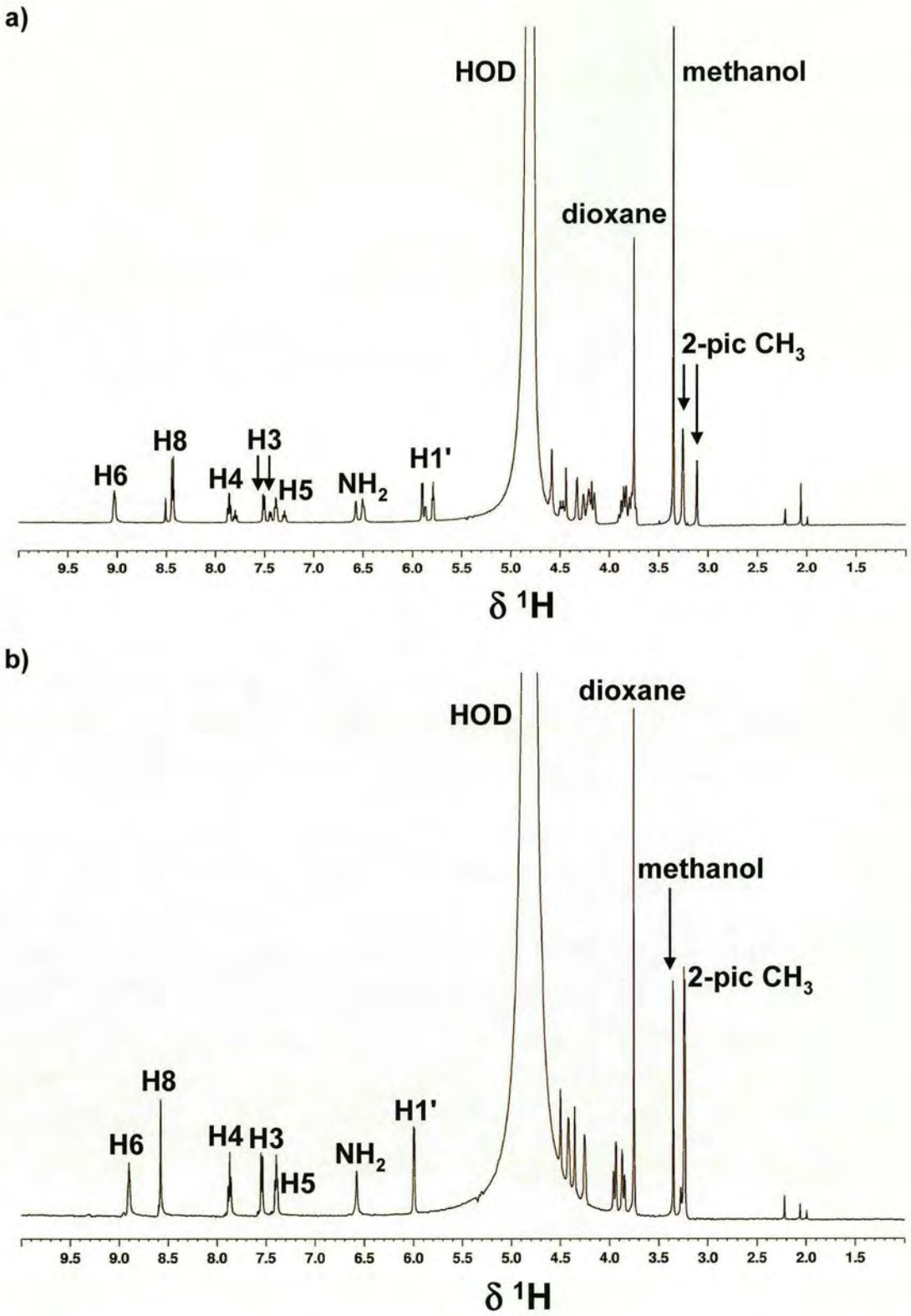

Figure 5.3 ^{1}H NMR spectra in H_2O/D_2O at 298 K of a) fraction **F1** and b) fraction **F2**, from the reaction of ^{15}N-AMD473 and guanosine, see Figure 5.1.

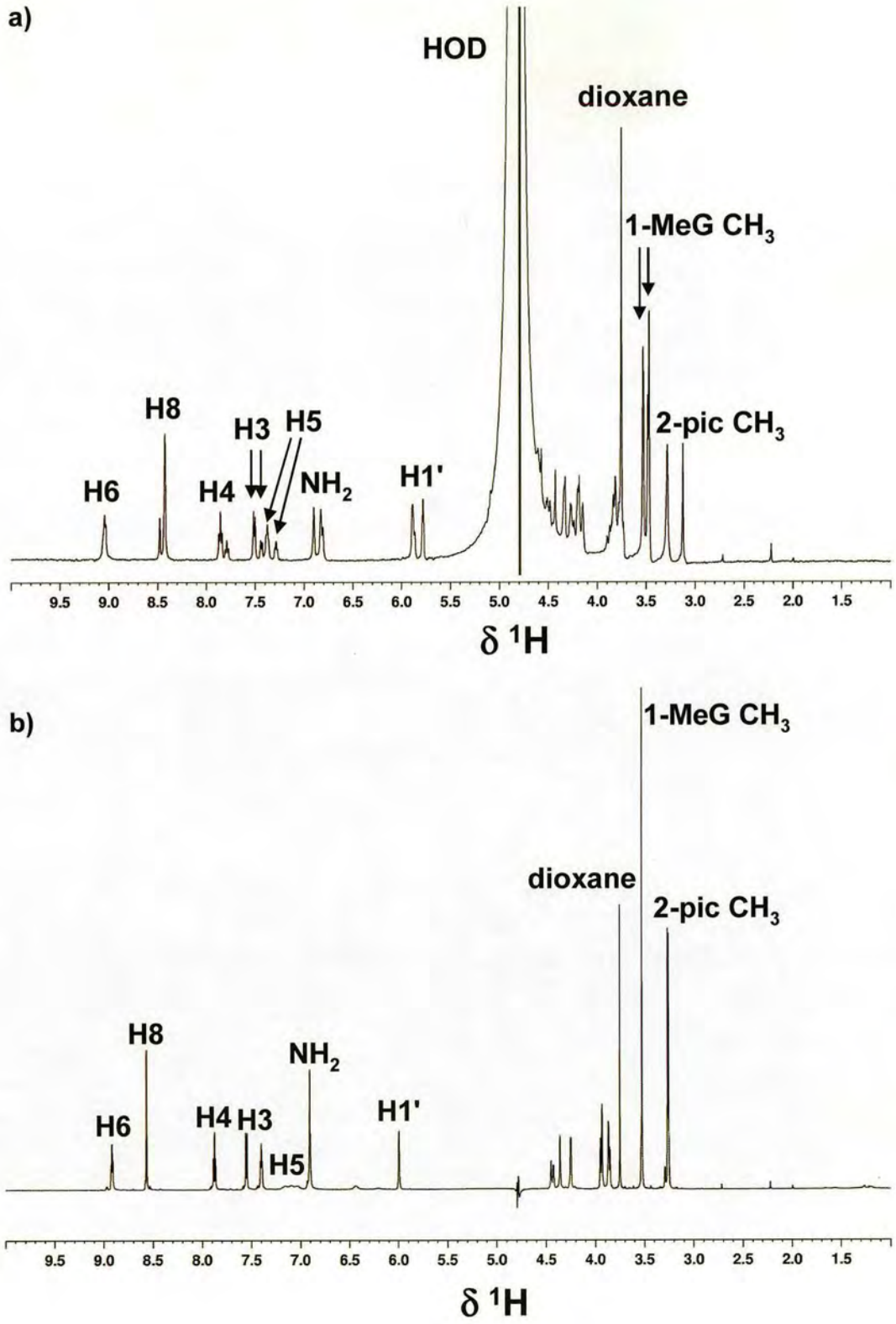

Figure 5.4 ^{1}H NMR spectra in H_2O/D_2O at 298 K of a) fraction **F3** and b) fraction **F4**, from the reaction of ^{15}N-AMD473 and 1-Meguanosine, see Figure 5.1.

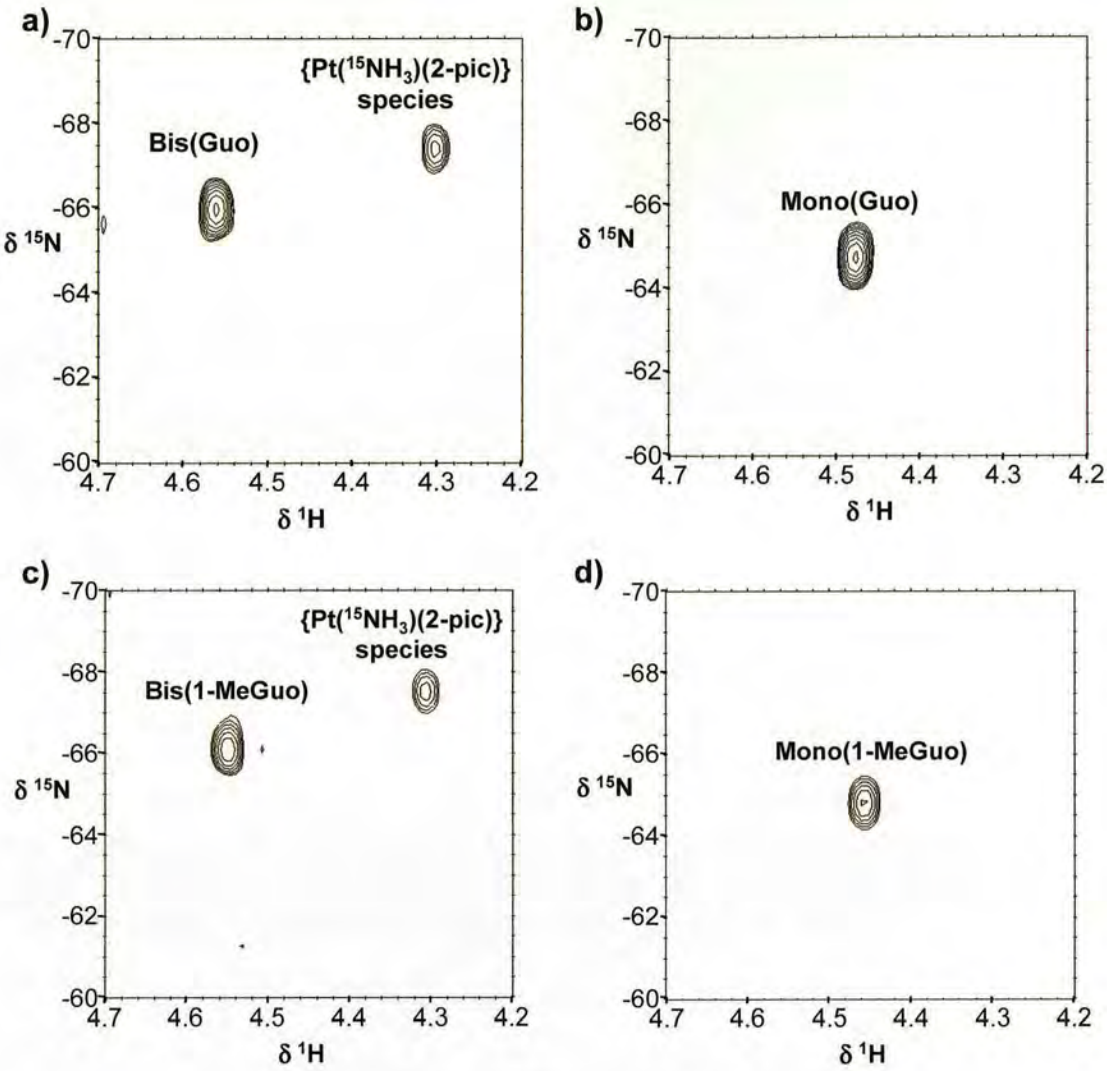

Figure 5.5 2D [^{1}H,^{15}N] HSQC NMR spectra in H_2O/D_2O at 298 K of a) fraction **F1** and b) fraction **F2** from the reaction of ^{15}N-AMD473 and guanosine, and c) fraction **F3** and d) fraction **F4** from the reaction of ^{15}N-AMD473 and 1-Meguanosine.

NMR Characterisation

The ^{1}H NMR chemical shift data for fractions **F1-F4** are summarised in Table 5.1. ^{1}H NMR spectra for fractions **F1** and **F2** are given in Figure 5.3 and those for **F3** and **F4** in Figure 5.4. The ^{1}H NMR spectra for fractions **F1** and **F3** for the reaction of *cis*-[$PtCl_2$($^{15}NH_3$)(2-pic)] with guanosine and 1-methylguanosine, respectively, are very similar. Likewise, fractions **F2** and **F4** appear almost identical.

There are clearly two species present in fractions **F1** and **F3**, as indicated from two sets of aromatic picoline peaks in a ratio of approximately 3:1. Integration of the spectra implies that the major species is the bis(nucleobase) Pt adduct, along with an additional AMD473 species, likely to be a mono(nucleobase) adduct.

Table 5.1 ^{1}H NMR chemical shifts for fractions **F1** – **F4** (see Figure 5.1).

Fraction	δ ^{1}H[a]	
	H8	H1'
F1	8.42 (s)	5.79 (t)
	8.44 (s)	5.90 (d)
	8.50 (s)[b]	5.87[b]
F2	8.57 (s)	5.99 (d)
F3	8.42 (s)	5.78 (t)
	8.48 (s)[b]	5.90 (t)
		5.87[b]
F4	8.56 (s)	5.94 (d)
	8.58 (s)	

[a] Note that multiplicities given in parenthesis are as they appear but as discussed in the text may be composed of overlapping signals. [b] Minor species.

[^{1}H,^{15}N] 2D HSQC NMR spectra for fractions **F1**, **F2** and **F3**, **F4** are shown in Figure 5.5. For fraction **F1** there are two peaks at 4.30, -67.47 ppm and 4.56, -66.03 ppm, the latter corresponding to the bis(guanosine) adduct. The **F3** fraction has a peak with chemical shifts of 4.55, -66.14 ppm, assigned as the bis(1-Meguanosine) adduct, and a second peak with chemical shifts of 4.30, -67.59 ppm, which are almost identical to those of fraction **F1**. Similarly, a peak at 4.48, -64.75 ppm is

observed for fraction **F2** whilst that of fraction **F4** is at 4.46, -64.85 ppm. These peaks are assigned as mono(guanosine) adducts.

2. Time Course of *cis*-[Pt($^{15}NH_3$)(2-pic)(OH_2)$_2$](NO_3)$_2$ with guanosine (1:2)

$^{15}NH_3$-labelled *cis*-[$PtCl_2$($^{15}NH_3$)(2-pic)], from which the chloride ligands were previously removed with $AgNO_3$ (forming the diaqua adduct), was reacted with 2 mol equiv guanosine in an aqueous solution containing 0.1 M $NaClO_4$ and monitored by [^{1}H,^{15}N] 2D HSQC NMR spectroscopy for 20 h at 298 K. Figure 5.6 shows the HSQC spectra at the beginning and end of the reaction. Initially, there are eight cross-peaks present, five of which can be attributed to hydrolysis species (labeled *). The principal hydrolysis peak **a**, at 4.70, -83.81 ppm, has a ^{15}N chemical

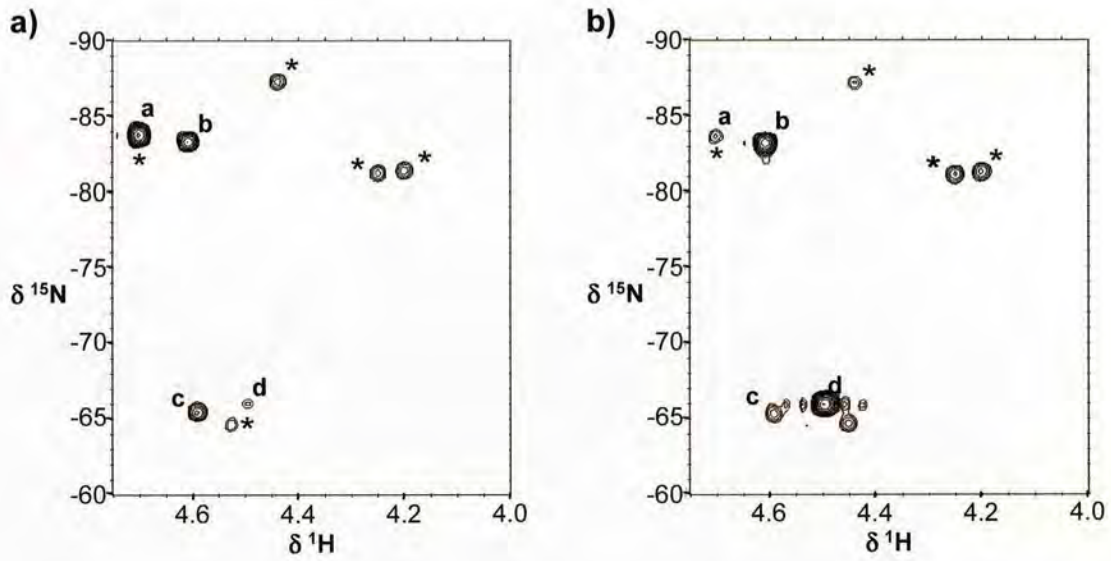

Figure 5.6 2D [^{1}H,^{15}N] HSQC NMR spectra for the reaction of aquated ^{15}N-AMD473 and guanosine (1:2) at 298 K a) 0.33 h and b) 19.94 h after the start of the reaction. Assignments: **a**, *cis*-[Pt($^{15}NH_3$)(2-pic)(OH_2)$_2$]$^{2+}$; **b**, *cis*-[Pt($^{15}NH_3$)(2-pic)(OH_2)(Guo)]$^{2+}$ with OH_2 *trans* to $^{15}NH_3$; **c**, *cis*-[Pt($^{15}NH_3$)(2-pic)(OH_2)(Guo)]$^{2+}$ with guanosine *trans* to $^{15}NH_3$; **d**, *cis*-[Pt($^{15}NH_3$)(2-pic)(Guo)$_2$]$^{2+}$; * hydrolysis products.

shift indicative of ammine *trans* to oxygen and is attributed to *cis*-$[Pt(^{15}NH_3)(2\text{-pic})(OH_2)_2]^{2+}$. Peak **a** gradually decreases in intensity as the peaks **b** (4.60, -83.37 ppm) and **c** (4.59, -65.50 ppm) both increase for a time and then gradually decrease, implying they are assignable to intermediate species. Peaks **b** and **c** are likely to be *cis*-$[Pt(^{15}NH_3)(2\text{-pic})(OH_2)(Guo)]^{2+}$ adducts with H_2O *trans* to $^{15}NH_3$ and 2-pic, respectively. Peak **d** at 4.49, -66.09 ppm, which is very weak in the initial spectrum, becomes the dominant product over time and is assigned as the *cis*-$[Pt(^{15}NH_3)(2\text{-pic})(Guo)_2]^{2+}$ adduct. A simplified time-dependence of the concentrations of the main species detected during the reaction is shown in Figure 5.7. The proposed reaction pathway is shown in Scheme 5.1 and a fit of the data was attempted using the program SCIENTIST (Version 2.01, MicroMath Inc.). However, it was not possible to attain a satisfactory fit of the data with this scheme and therefore no rate constants were determined.

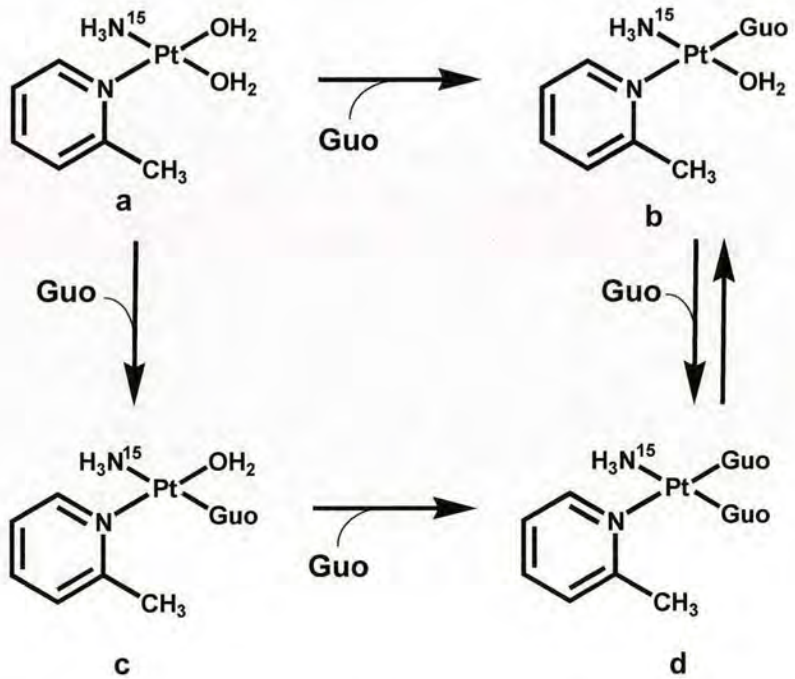

Scheme 5.1 Proposed pathway for reaction of *cis*-$[Pt(^{15}NH_3)(2\text{-pic})(OH_2)_2]^{2+}$ with guanosine (1:2). Charges have been omitted for clarity.

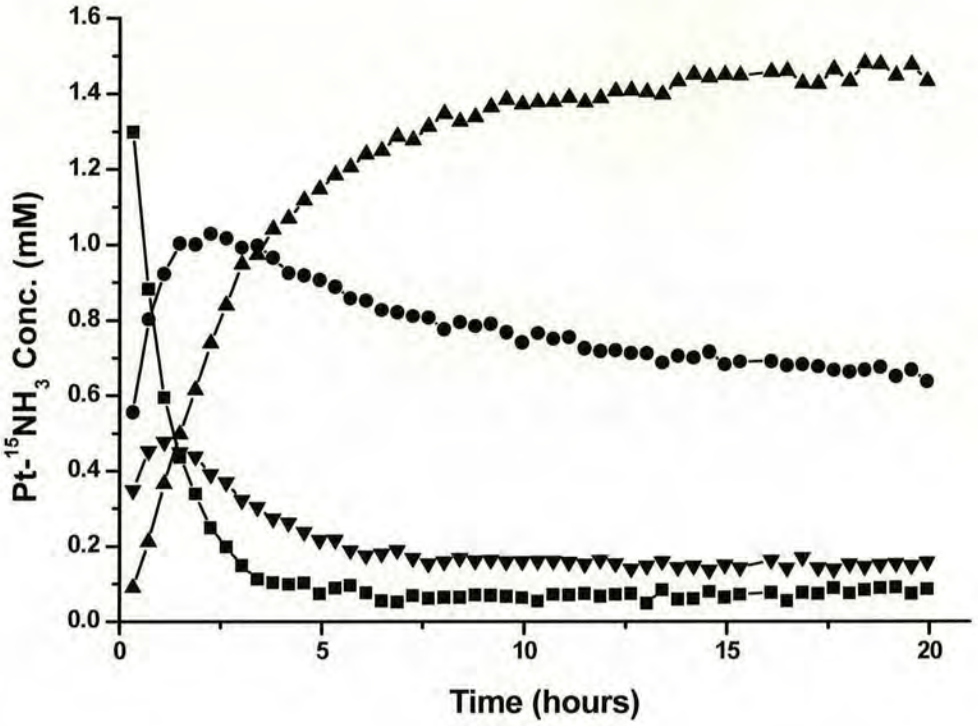

Figure 5.7 Concentration versus time profile for the reaction of *cis*-[Pt($^{15}NH_3$)(2-pic)$(OH_2)_2$]$(NO_3)_2$ and guanosine (1:2) at 298 K. Concentration values were calculated from the integration of the 2D cross-peaks in the [^{1}H,^{15}N] spectra. (■) **a**, *cis*-[Pt($^{15}NH_3$)(2-pic)$(OH_2)_2]^{2+}$; (●) **b**, *cis*-[Pt($^{15}NH_3$)(2-pic)(OH_2)(Guo)$]^{2+}$ with OH_2 *trans* to $^{15}NH_3$; (▼) **c**, *cis*-[Pt($^{15}NH_3$)(2-pic)(OH_2)(Guo)$]^{2+}$ with guanosine *trans* to $^{15}NH_3$; (▲) **d**, *cis*-[Pt($^{15}NH_3$)(2-pic)$(Guo)_2]^{2+}$.

3. Guanosine Adducts of *cis*- and *trans*-[$PtCl_2(NH_3)$(2-pic)]

Adducts of both *cis*- and *trans*-[$PtCl_2(NH_3)$(2-pic)] with guanosine (Guo) and 2'-deoxyguanosine (2'-dGuo) were prepared and characterised in solution by ESI mass spectrometry and both 1D ^{1}H and 2D NMR spectroscopy.

cis-[$Pt(NH_3)$(2-pic)$(Guo)_2](NO_3)_2$

The parent ion at m/z 870.6 in the positive ion electrospray mass spectrum in water, is assigned to [$Pt(NH_3)$(2-pic)$(Guo)_2$-H]$^+$. The other peaks were assigned as follows: m/z 738.4 – [$Pt(NH_3)$(2-pic)(Guo)(Guanine)-H]$^+$, m/z 606.4 – [$Pt(NH_3)$(2-pic)$(Guanine)_2$ - H]$^+$, m/z 588.4 – [$Pt(NH_3)$(2-pic)(Guo) - H]$^+$, m/z 455.3 –

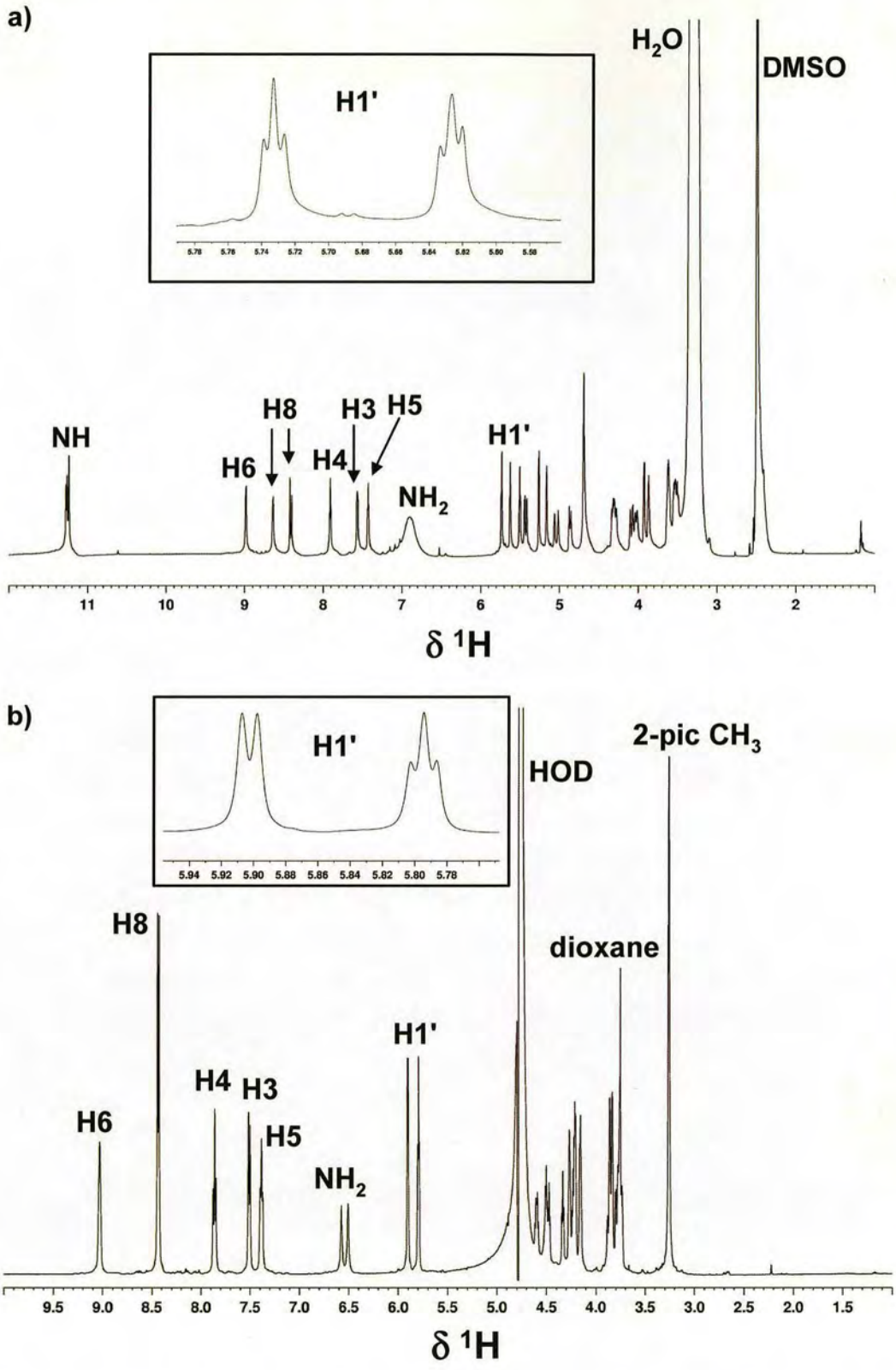

Figure 5.8 ^{1}H NMR spectra of *cis*-$[Pt(NH_3)(2\text{-pic})(Guo)_2](NO_3)_2$ at 298 K in a) d_6-DMSO and b) H_2O/D_2O.

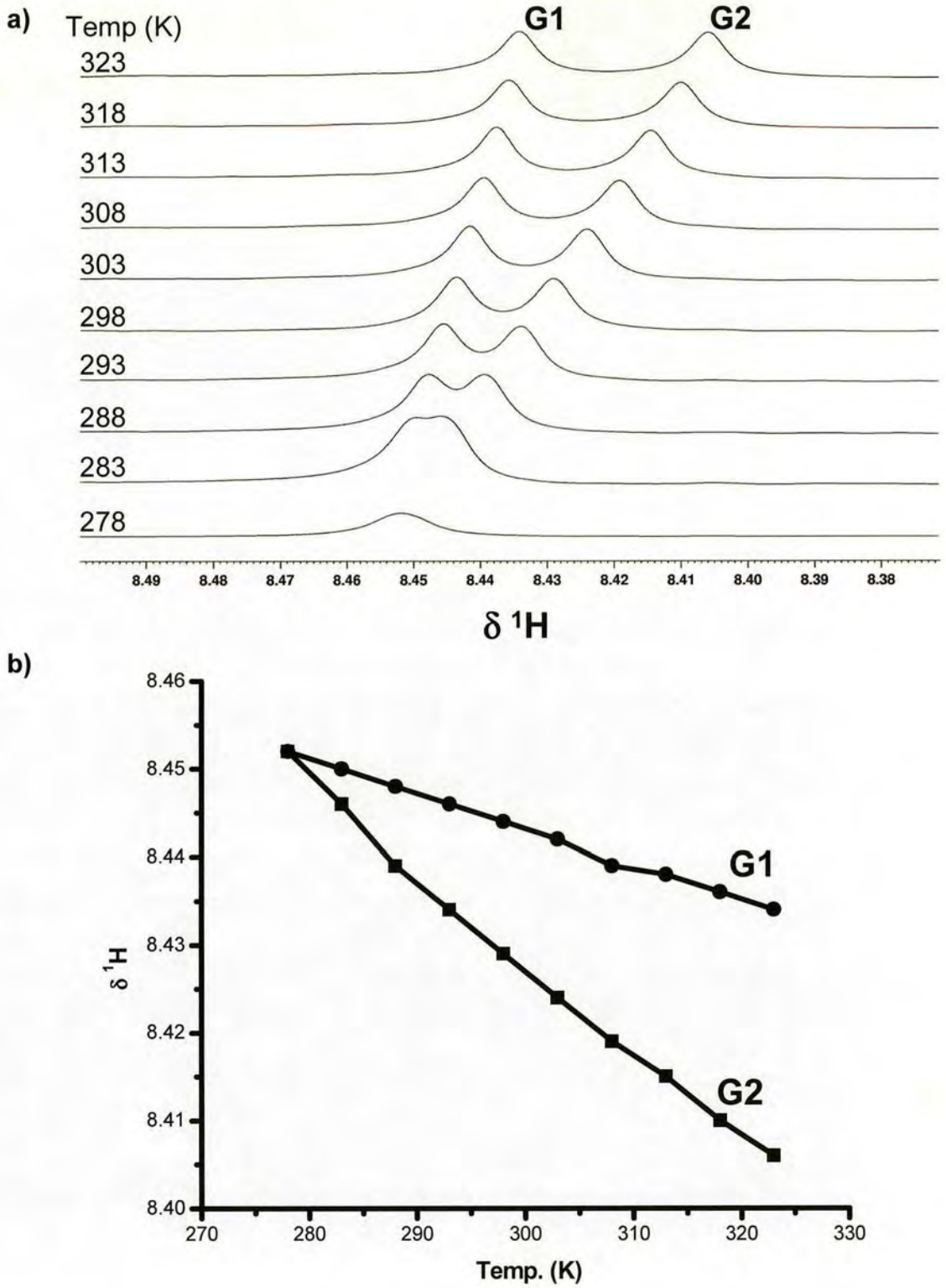

Figure 5.9 a) ^{1}H NMR spectra showing the temperature dependence of the H8 signals and b) plot of δ H8 versus temperature of *cis*-$[Pt(NH_3)(2\text{-pic})(Guo)_2](NO_3)_2$ in H_2O/D_2O.

$[Pt(NH_3)(2\text{-pic})(Guanine) - H]^+$, m/z 438.2 – $[Pt(2\text{-pic})(Guanine) - H]^+$.

The ^1H NMR spectra of *cis*-$[Pt(NH_3)(2\text{-pic})(Guo)_2](NO_3)_2$ in H_2O/D_2O and DMSO at 298 K are shown in Figure 5.8. A selection of peaks is listed in Table 5.2. Clearly the solvent has a large effect on chemical shift, but most noticeable is that the H8 signals for the guanosine ligands only give rise to two H8 peaks in H_2O/D_2O, whereas in DMSO four H8 peaks are distinguishable. Moreover, in H_2O/D_2O the H1' sugar protons appear to give rise to a doublet and triplet, which is most unexpected as two doublets would be expected. In DMSO two triplets are observed. Therefore, a further ^1H spectrum in H_2O/D_2O was recorded at a different frequency and it was found that the "coupling constants" at 500 MHz are 4.5 and 4 Hz whilst at 800 MHz the "coupling constants" are 4.8 and 5.6 Hz. This implies that in fact there are two sets of overlapping doublets.

The temperature dependence of the ^1H NMR spectrum was investigated between 278 K and 323 K (Figure 5.9). At low temperature there is only one broad H8 signal which is gradually resolved into two and the separation of the signals increases with increasing temperature. This is clearly demonstrated by the plot of δ H8 shift versus temperature shown in Figure 5.9.

A 2D NOESY spectrum in H_2O/D_2O was recorded at 298 K in order to investigate the solution structure of the complex (Figure 5.10). However, only one H8 signal for the two H8 protons can be distinguished and this exhibits an NOE cross-peak to the 2-picoline methyl group. An NOE cross-peak between the aromatic H6 proton of the 2-picoline ligand and the H8 peak is also observed.

In the pH range from 2 – 12, the pH-dependent ^1H NMR chemical shift measurements of the H8 peaks in 90% H_2O/10% D_2O show two acid-base equilibria

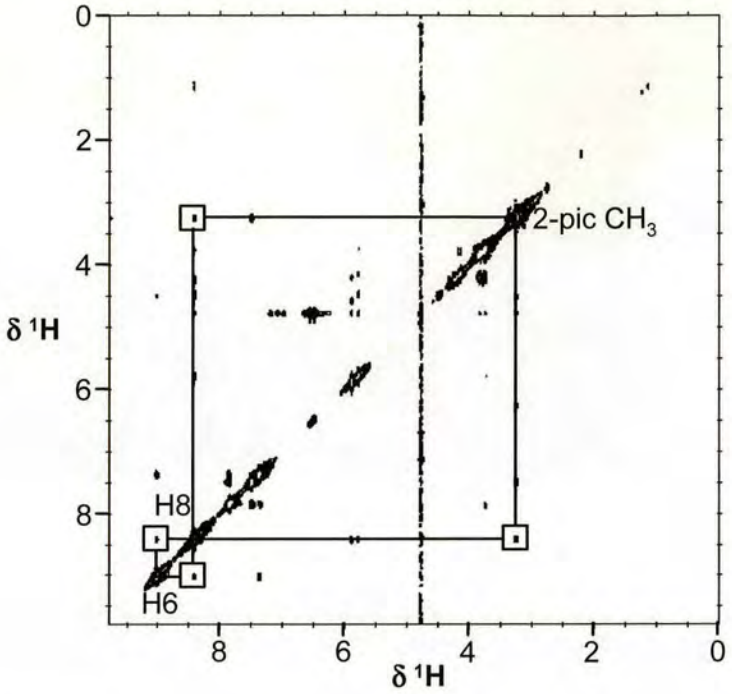

Figure 5.10 2D [^{1}H,^{1}H] NOESY NMR spectrum of *cis*-[Pt(NH_3)(2-pic)($Guo)_2$]($NO_3)_2$ at 298 K in H_2O/D_2O.

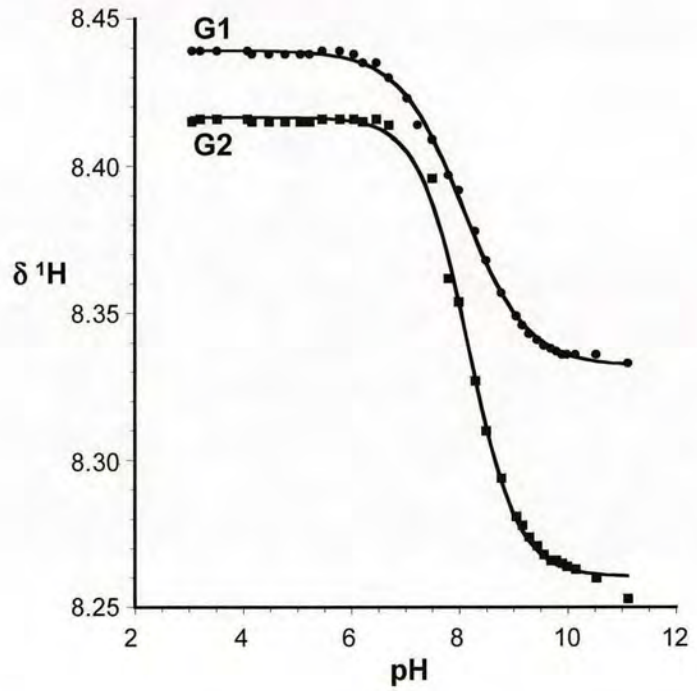

Figure 5.11 pH dependence of the H8 chemical shifts of *cis*-[Pt(NH_3)(2-pic)($Guo)_2$]($NO_3)_2$. The curves represent computer fits to the Henderson-Hasselbalch equation, and give the pK_a values listed in Table 5.3.

corresponding to the deprotonation of the two inequivalent N1H sites of the guanosine ligands (Figure 5.11). The pK_a values of 8.07 and 8.17 were determined from computer fits to the Henderson-Hasselbalch equation.

***cis*-[Pt(NH$_3$)(2-pic)(2'-dGuo)$_2$](NO$_3$)$_2$**

The parent ion at m/z 838.5 in the positive ion electrospray mass spectrum in water, is assigned to $[Pt(NH_3)(2\text{-pic})(2'\text{-dGuo})_2\text{-H}]^+$. The other peaks were assigned as follows: m/z 722.3 – $[Pt(NH_3)(2\text{-pic})(2'\text{-dGuo})(\text{Guanine})\text{-H}]^+$, m/z 606.2 – $[Pt(NH_3)(2\text{-pic})(\text{Guanine})_2 - H]^+$, m/z 454.9 – $[Pt(NH_3)(2\text{-pic})(\text{Guanine}) - H]^+$, m/z 437.9 – $[Pt(2\text{-pic})(\text{Guanine}) - H]^+$.

The ^{1}H NMR spectrum of *cis*-[Pt(NH$_3$)(2-pic)(2'-dGuo)$_2$](NO$_3$)$_2$ in H_2O/D_2O is shown in Appendix 3. A selection of peaks is listed in Table 5.2. In this case, there are four very close but distinguishable H8 signals and two symmetrical triplets for the H1' sugar protons.

The temperature dependence of the ^{1}H NMR spectrum was investigated between 278 K and 323 K (Figure 5.12). At low temperature there are four H8 signals. With increasing temperature two of these signals gradually merge into one, as exemplified by the plot of δ H8 shift versus temperature shown in Figure 5.12.

A 2D ROESY spectrum in H_2O/D_2O was recorded at 298 K (Appendix 4) in order to investigate the solution structure of the complex. The H8 signals at 8.36 and 8.38 ppm are indistinguishable in the 2D spectrum, but it appears that only these H8 peaks have an NOE cross-peak to the 2-picoline methyl group, ruling out the likelihood of a head-to-head configuration. This complex also exhibits an NOE cross-peak between the afore-mentioned H8 signals and the aromatic H6 proton of the 2-picoline ligand.

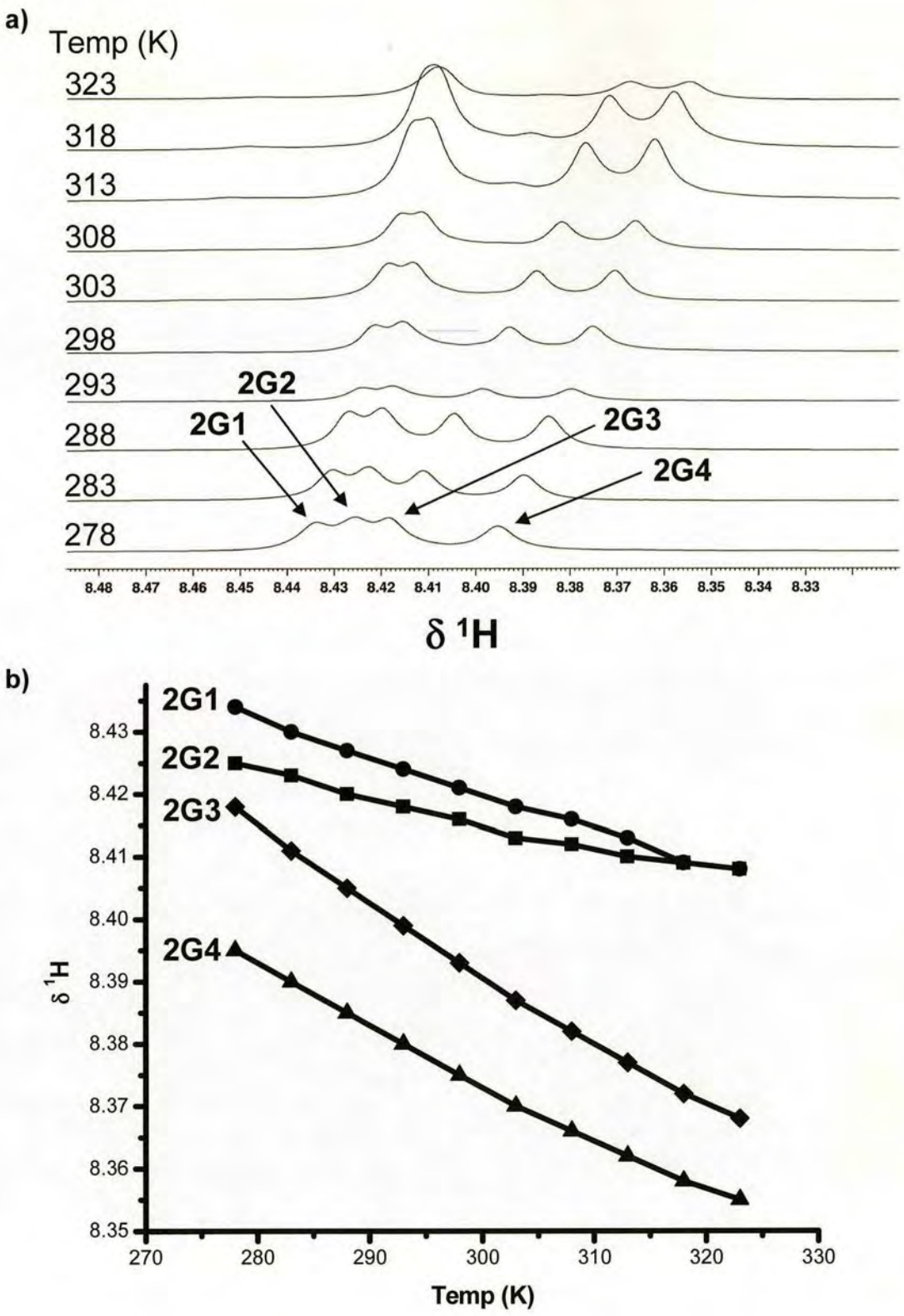

Figure 5.12 a) ^{1}H NMR spectra showing the temperature dependence of the H8 signals and b) plot of δ H8 versus temperature of *cis*-[Pt(NH_3)(2-pic)(2'-dGuo)$_2$](NO_3)$_2$ in H_2O/D_2O.

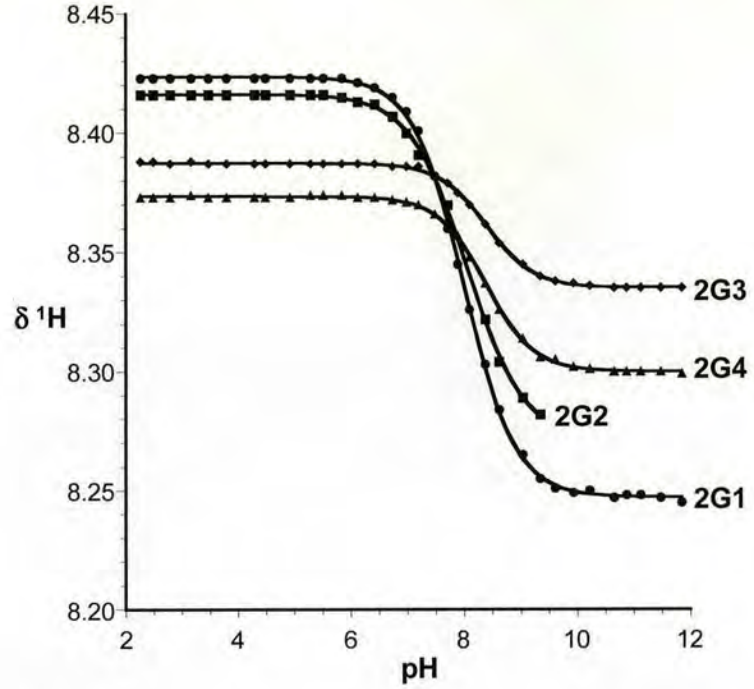

Figure 5.13 pH dependence of the H8 chemical shifts of *cis*-$[Pt(NH_3)(2\text{-pic})(2'\text{-dGuo})_2](NO_3)_2$. The curves represent computer fits to the Henderson-Hasselbalch equation, and give the pK_a values listed in Table 5.3.

In the pH range from 2 – 12, the pH-dependent ^1H NMR chemical shift measurements of the H8 peaks in 90% H_2O/10% D_2O show four acid-base equilibria corresponding to the deprotonation of inequivalent N1H sites of the guanosine ligands (Figure 5.13). The pK_a values determined from computer fits are 8.00, 8.05, 8.38 and 8.40.

***trans*-$[Pt(NH_3)(2\text{-pic})(Guo)_2](NO_3)_2$**

The parent ion at m/z 870.5 in the positive ion electrospray mass spectrum in water, is assigned to $[Pt(NH_3)(2\text{-pic})(Guo)_2\text{-H}]^+$. The other peaks were assigned as follows: m/z 738.4 – $[Pt(NH_3)(2\text{-pic})(Guo)(Guanine)\text{-H}]^+$, m/z 606.2 – $[Pt(NH_3)(2\text{-pic})(Guanine)_2 - H]^+$, m/z 588.2 – $[Pt(NH_3)(2\text{-pic})(Guo) - H]^+$, m/z 437.9 – $[Pt(2\text{-pic})(Guanine) - H]^+$.

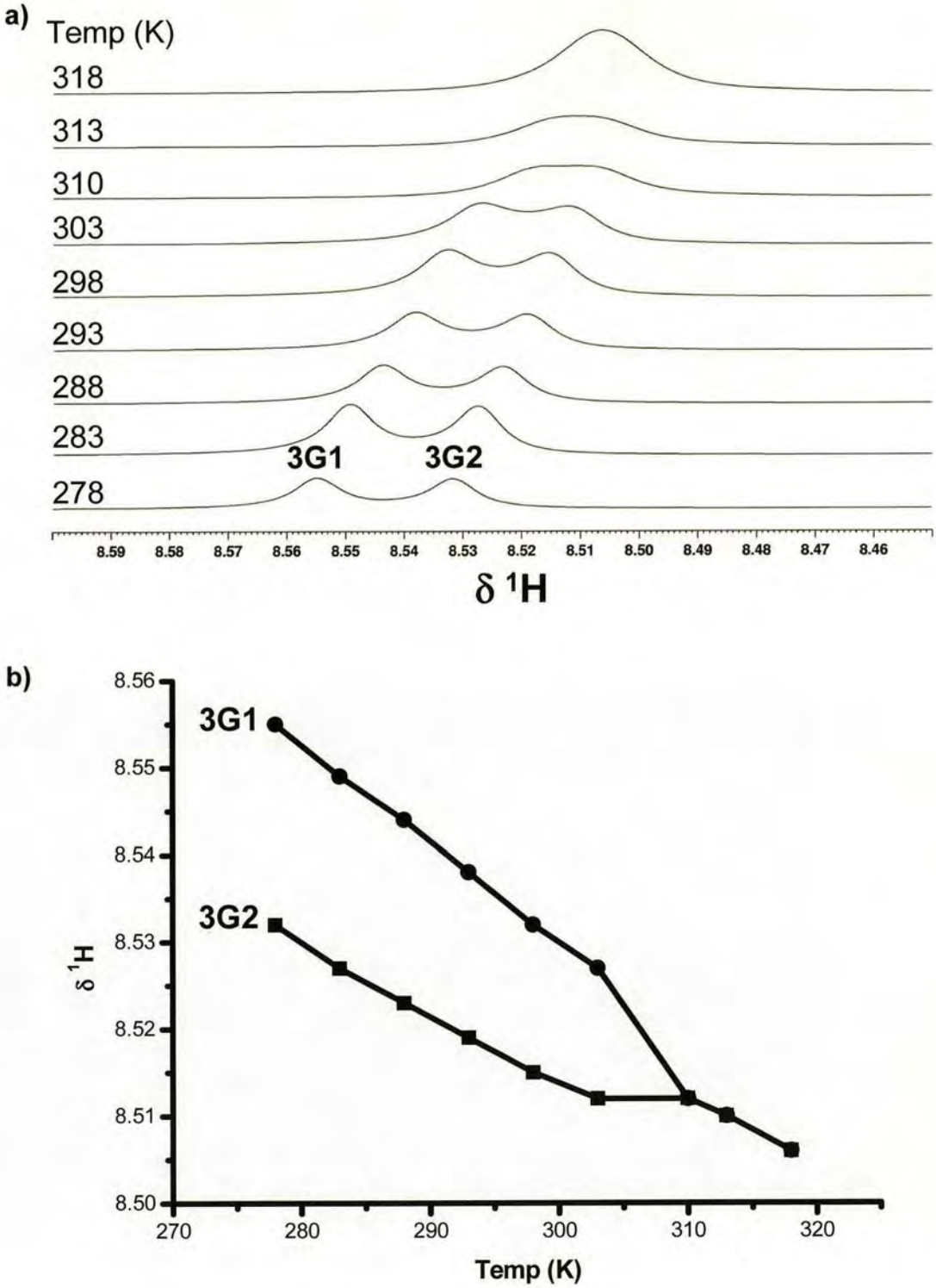

Figure 5.14 a) ^{1}H NMR spectra showing the temperature dependence of the H8 signals and b) plot of δ H8 versus temperature of *trans*-[Pt(NH_3)(2-pic)($Guo)_2$]($NO_3)_2$ in H_2O/D_2O.

The ^{1}H NMR spectrum of *trans*-[Pt(NH_3)(2-pic)($Guo)_2$]($NO_3)_2$ in H_2O/D_2O is shown in Appendix 5. A selection of peaks is listed in Table 5.2. Again, only two H8 peaks are observed and interestingly, there is only one doublet corresponding to the H1' sugar protons.

The temperature dependence of the ^{1}H NMR spectrum was investigated between 278 K and 318 K (Figure 5.14). At low temperature there are two H8 signals which merge into one broad signal around 310 K. This is clearly demonstrated by the plot of δ H8 shift versus temperature shown in Figure 5.14.

A 2D NOESY spectrum in H_2O/D_2O was recorded at 298 K in order to investigate the solution structure of the complex. However, only one H8 signal for the two H8 protons can be distinguished and this exhibits an NOE cross-peak to the 2-picoline methyl group. Unfortunately, this does not elucidate any particular solution structure.

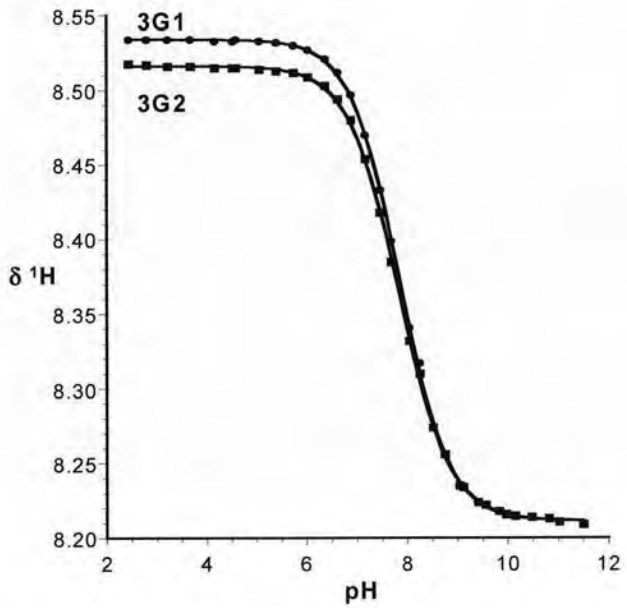

Figure 5.15 pH dependence of the H8 chemical shifts of *trans*-[Pt(NH_3)(2-pic)($Guo)_2$]($NO_3)_2$. The curves represent computer fits to the Henderson-Hasselbalch equation, and give the pK_a values listed in Table 5.3.

In the pH range from 2 – 12, the pH-dependent ^{1}H NMR chemical shift measurements of the H8 peaks in 90% H_2O/10% D_2O show two acid-base equilibria corresponding to the deprotonation of the two inequivalent N1H sites of the guanosine ligands (Figure 5.15). The associated pK_a values are 7.84 and 7.85.

***trans*-[Pt(NH$_3$)(2-pic)(2'-dGuo)$_2$](NO$_3$)$_2$**

The parent ion at m/z 838.6 in the positive ion electrospray mass spectrum in water, is assigned to $[Pt(NH_3)(2\text{-pic})(2'\text{-dGuo})_2\text{-H}]^+$. The other peaks were assigned as follows: m/z 722.4 – $[Pt(NH_3)(2\text{-pic})(2'\text{-dGuo})(\text{Guanine})\text{-H}]^+$, m/z 606.2 – $[Pt(NH_3)(2\text{-pic})(\text{Guanine})_2 - \text{H}]^+$, m/z 589.0 – $[Pt(2\text{-pic})(\text{Guanine})_2 - \text{H}]^+$, m/z 438.0 – $[Pt(2\text{-pic})(\text{Guanine}) - \text{H}]^+$.

The ^{1}H NMR spectrum of *trans*-$[Pt(NH_3)(2\text{-pic})(2'\text{-dGuo})_2](NO_3)_2$ in H_2O/D_2O is shown in Appendix 6. A selection of peaks is listed in Table 5.2. Two H8 signals for platinated 2'-deoxyguanosine are observed and unexpectedly, only a single triplet is observed for the H1' sugar protons.

The temperature dependence of the ^{1}H NMR spectrum was investigated between 278 K and 318 K (Figure 5.16) and is almost identical to that of *trans*-$[Pt(NH_3)(2\text{-pic})(\text{Guo})_2](NO_3)_2$, as there are two H8 signals at low temperature which merge into one broad signal around 310 K. A plot of δ H8 shift versus temperature is shown in Figure 5.16.

A 2D ROESY spectrum in H_2O/D_2O recorded at 298 K revealed that the H8 signals are again indistinguishable in the 2D spectrum (Figure 5.17) and have a cross-peak to the 2-picoline methyl group. As in the case of *cis*-$[Pt(NH_3)(2\text{-pic})(\text{Guo})_2](NO_3)_2$ and *cis*-$[Pt(NH_3)(2\text{-pic})(2'\text{-dGuo})_2](NO_3)_2$, there is an NOE cross-

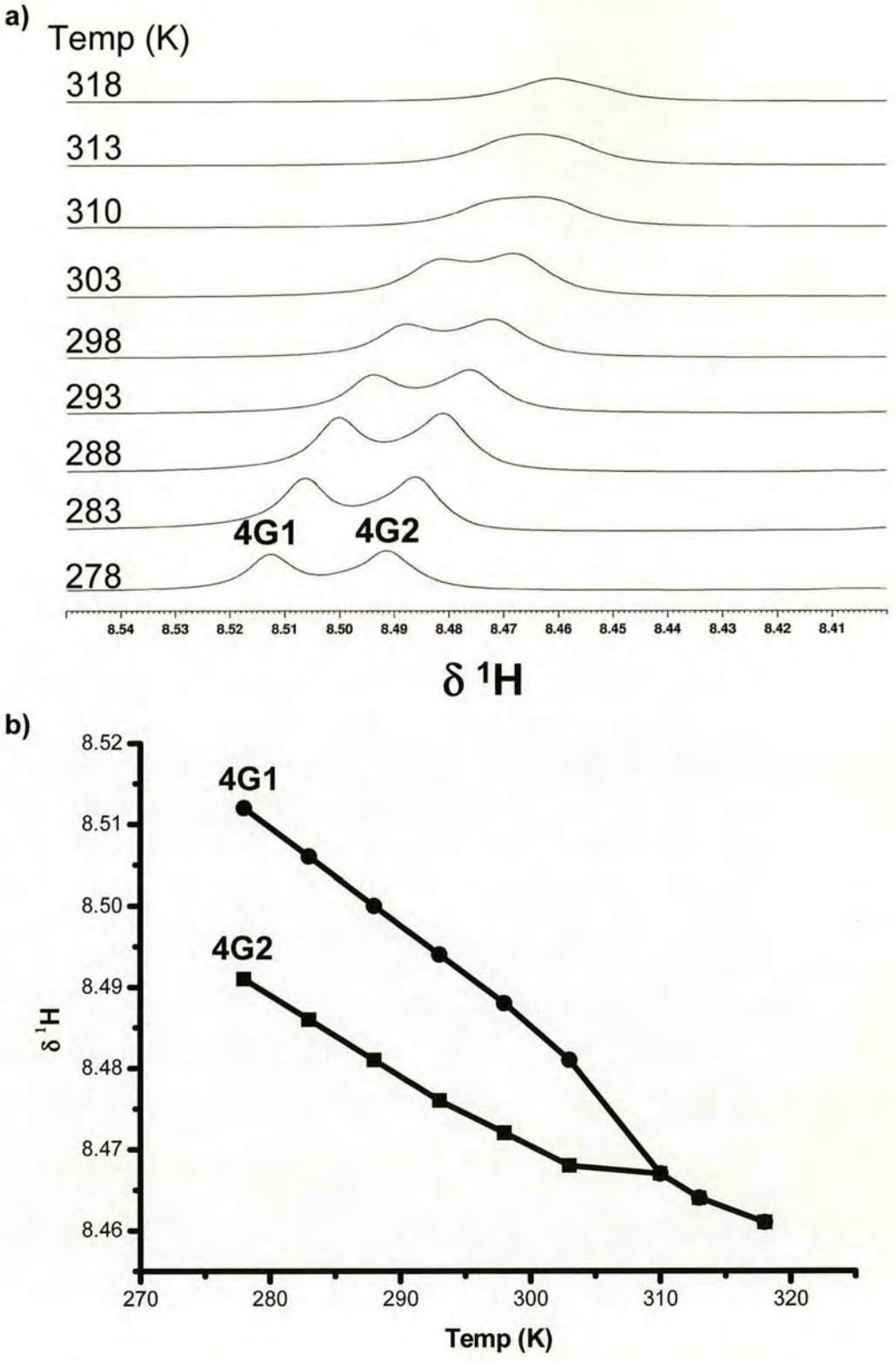

Figure 5.16 a) ^{1}H NMR spectra showing the temperature dependence of the H8 signals and b) plot of δ H8 versus temperature of *trans*-[Pt(NH_3)(2-pic)(2'-dGuo)$_2$](NO_3)$_2$ in H_2O/D_2O.

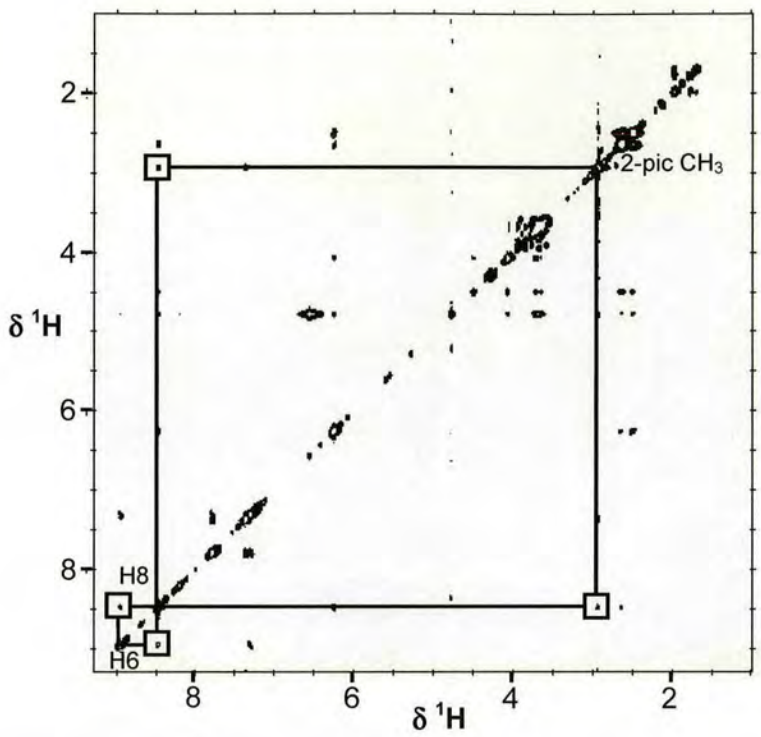

Figure 5.17 2D [^{1}H,^{1}H] ROESY NMR spectrum of *trans*-[Pt(^{15}NH$_3$)(2-pic)(2'-dGuo)$_2$](NO$_3$)$_2$ at 298 K in H$_2$O/D$_2$O.

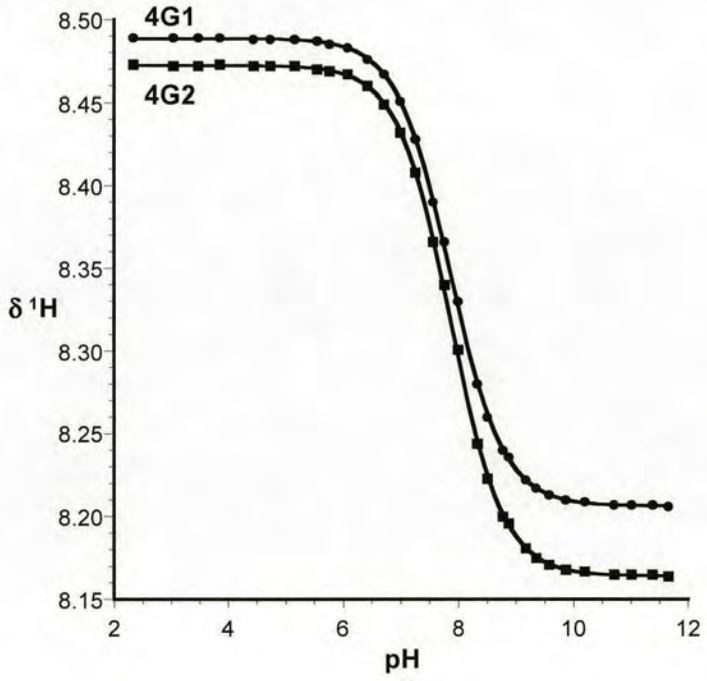

Figure 5.18 pH dependence of the H8 chemical shifts of *trans*-[Pt(NH$_3$)(2-pic)(2'-dGuo)$_2$](NO$_3$)$_2$. The curves represent computer fits to the Henderson-Hasselbalch equation, and give the pK$_a$ values listed in Table 5.3.

peak between the 2'-deoxyguanosine H8 signals and the aromatic H6 proton of the 2-picoline ligand.

In the pH range from 2 – 12, the pH-dependent ^{1}H NMR chemical shift measurements of the H8 peaks in 90% H_2O/10% D_2O show two acid-base equilibria corresponding to the deprotonation of inequivalent N1H sites of the guanosine ligands (Figure 5.18). The associated pK_a values are 7.86 and 7.87.

Table 5.2 ^{1}H NMR chemical shifts for the complexes *cis*-[Pt(NH_3)(2-pic)(Guo)$_2$](NO_3)$_2$, *cis*-[Pt(NH_3)(2-pic)(2'-dGuo)$_2$](NO_3)$_2$, *trans*-[Pt(NH_3)(2-pic)(Guo)$_2$](NO_3)$_2$ and *trans*-[Pt(NH_3)(2-pic)(2'-dGuo)$_2$](NO_3)$_2$.

Complex	δ ^{1}H	
	H8	H1'
cis-[Pt(NH_3)(2-pic)(Guo)$_2$](NO_3)$_2$	8.43 (s)	5.79 (t)
	8.44 (s)	5.90 (d)
cis-[Pt(NH_3)(2-pic)(2'-dGuo)$_2$](NO_3)$_2$	8.36 (s)	6.16 (t)
	8.38 (s)	6.27 (t)
	8.41 (s)	
	8.41 (s)	
trans-[Pt(NH_3)(2-pic)(Guo)$_2$](NO_3)$_2$	8.52 (s)	5.89 (d)
	8.54 (s)	
trans-[Pt(NH_3)(2-pic)(2'-dGuo)$_2$](NO_3)$_2$	8.48 (s)	6.26 (t)
	8.49 (s)	

5.5 Discussion

Nucleobase complexes of platinum anticancer drugs have been extensively studied because they provide a basis from which to interpret reactions with DNA.

1. HPLC Reactions of *cis*-[$PtCl_2(NH_3)$(2-pic)] with Guanosine Derivatives

In order to both simplify and contrast the binding behaviour of *cis*-[$PtCl_2(NH_3)$(2-pic)] with nucleobases, guanosine and N1- and N7-methylated guanosines were employed as model compounds. Reverse phase chromatographic analysis using a water/acetonitrile gradient elution method revealed the formation of a significant intermediate (elution time 29-30 min) and a predominant reaction product (~27 min) for *cis*-[$PtCl_2(NH_3)$(2-pic)] reactions with guanosine and 1-methylguanosine. Reaction of *cis*-[$PtCl_2(NH_3)$(2-pic)] with 7-methylguanosine was extremely slow and gave rise to very few reaction products, which are assumed to be N1-bound complexes. This is in agreement with a previous report that revealed 1-methylguanosine reacts with $[Pt(dien)(H_2O)]^{2+}$ ten times more readily than 7-methylguanosine.[34]

ESI-MS allowed identification of the isolated HPLC fractions **F1-F4** (Figure 5.1). Fractions **F1** and **F3** both contained a parent ion corresponding to the bis(guanosine) and bis(1-methylguanosine) adducts, respectively. For fractions **F2** and **F4**, only mono(guanosine/1-methylguanosine) adducts were detected. In the present study, trifluoroacetate (TFA) was used as an ion-pairing reagent because of its volatility and the results show that with 0.1% TFA present and a suitable acetonitrile gradient, adducts of *cis*-[$PtCl_2(NH_3)$(2-pic)] with guanosine derivatives in aqueous solution can be easily separated. However, the subsequent ESI-MS assays indicate formation of various TFA adducts.

The ^{1}H NMR spectra of fractions **F1** and **F3** (Figures 5.3 and 5.4) unambiguously show the presence of platinated nucleobase in a 2:1 ratio of nucleobase to {Pt($^{15}NH_3$)(2-pic)}, confirming that the dominant product is the bis(nucleobase) adduct. Nevertheless, both the 1D ^{1}H and [^{1}H,^{15}N] 2D NMR spectra reveal the presence of an additional {Pt($^{15}NH_3$)(2-pic)} species, having ^{15}N chemical shifts of -67.47 and -67.59 ppm for fractions **F1** and **F3**, respectively, which are consistent with that expected for an ammine ligand *trans* to chloride or nitrogen. It seems likely that this species is a mono(nucleobase) adduct, probably with the nucleobase *cis* to the 2-picoline ligand, which coincidentally elutes at the same time as the bis(nucleobase) adducts. This hypothesis is supported by the ESI-MS data in which peaks for [PtCl($^{15}NH_3$)(2-pic)(Guo)]$^{+}$ and [PtCl($^{15}NH_3$)(2-pic)(1-MeGuo)]$^{+}$ were obtained.

The ^{15}N chemical shifts of the cross-peaks for the bis(nucleobase) adducts verify that the ammine ligand is likely *trans* to nitrogen. The chemical shifts of the bis(nucleobase) adducts from **F1** and **F3** are in good agreement with the presence of *cis*-[Pt($^{15}NH_3$)(2-pic)(Guo)$_2$]$^{2+}$, as formed in the kinetic reaction in section 2. Integration of the 2D cross-peaks in the [^{1}H,^{15}N] HSQC spectra of fractions **F1** and **F3** (Figure 5.5) indicates there is a 3:1 ratio of the bis(nucleobase) adduct to the mono(nucleobase) adduct.

From a combination of ^{1}H and [^{1}H,^{15}N] NMR spectra, fractions **F2** and **F4** are compatible with a single platinated mono(nucleobase) species. The ^{15}N chemical shifts again imply that the ammine is *trans* to chloride or nitrogen. Therefore, taking into account previously determined hydrolysis data for *cis*-[PtCl$_2$($^{15}NH_3$)(2-pic)] which reports faster hydrolysis *trans* to the 2-picoline ligand due to steric

hindrance,[35] along with the ^{15}N chemical shifts and ESI-MS data, it seems likely that fractions **F2** and **F4** both contain *cis*-[PtCl($^{15}NH_3$)(2-pic)(nucleobase)]$^+$, with the nucleobase *trans* to the 2-picoline ligand.

2. Time Course of *cis*-[Pt($^{15}NH_3$)(2-pic)$(OH_2)_2$]$(NO_3)_2$ with guanosine (1:2)

Since the reaction of *cis*-[$PtCl_2$($^{15}NH_3$)(2-pic)] with guanosine was slow when studied by NMR (67% reaction in 19 h), *cis*-[$PtCl_2$($^{15}NH_3$)(2-pic)] was firstly reacted with 1.96 equiv $AgNO_3$ to give mainly *cis*-[Pt($^{15}NH_3$)(2-pic)$(OH_2)_2$]$(NO_3)_2$, and some other minor hydrolysis products, and then reacted with guanosine (1:2). The principal hydrolysis peak **a** at 4.70, -83.81 ppm (Figure 5.6) is believed to be due to *cis*-[Pt($^{15}NH_3$)(2-pic)$(OH_2)_2$]$^{2+}$. The hydrolysis peaks in the upper region of the spectra, i.e. less than -80 ppm for ^{15}N, are likely to be *cis*-[Pt($^{15}NH_3$)(2-pic)(OH/OH_2)(Cl/OH/OH_2)] species, whilst the hydrolysis peak at 4.52, -64.68 ppm is probably *cis*-[PtCl($^{15}NH_3$)(2-pic)(OH_2/OH)] with the chloride ligand *trans* to the ammine. Only the hydrolysis peak **a** undergoes a significant change in concentration during the time course of the reaction and for simplicity, the other hydrolysis species were omitted from the kinetic profile. From the ^{15}N chemical shift data and reaction profiles, peaks **b-d** can be tentatively assigned as indicated in Scheme 5.1. It is noteworthy that the initial rate of formation of **b**, *cis*-[Pt($^{15}NH_3$)(2-pic)(OH_2)(Guo)]$^+$ with the guanosine *trans* to the 2-picoline ligand, is faster than that of **c**, *cis*-[Pt($^{15}NH_3$)(2-pic)(OH_2)(Guo)]$^+$ with the guanosine *cis* to the 2-picoline ligand. This may be expected as there is less steric hindrance for formation of **b** relative to **c**. However, the rates of the second guanosine substitution appear similar for **b** and **c**, which is quite unexpected.

3. Guanosine Adducts of *cis*- and *trans*-[$PtCl_2(NH_3)$(2-pic)]

The combination of ESI mass spectrometry, 1D ^1H and 2D [^1H,^1H] NMR spectroscopy unambiguously identify the platinum complexes as bis(nucleobase) adducts. Platination at the N7 position was confirmed in each case by the absence of a N7 protonation below pH 6 in the pH titrations (Figures 5.11, 5.13, 5.15, 5.18). Coordination of electrophilic Pt^{II} to the ring atoms of the nucleobases withdraws electron density from the ring. As a result, the heteroatom of neutral nucleobases capable of deprotonation becomes more acidic and those capable to accept a proton become more basic. For example, the N(1)H proton of 9-substituted 6-oxopurines is acidified by 1.2 – 2 log units upon platination of the N(7) site, depending predominantly on the charge of the platinum compounds.[36-38] The pK_a values for *cis*-[$Pt(NH_3)$(2-pic)$(Guo)_2$]$^{2+}$ (8.07, 8.17), *cis*-[$Pt(NH_3)$(2-pic)$(2'\text{-dGuo})_2$]$^{2+}$ (8.00, 8.05, 8.38, 8.48), *trans*-[$Pt(NH_3)$(2-pic)$(Guo)_2$]$^{2+}$ (7.84, 7.85) and *trans*-[$Pt(NH_3)$(2-pic)$(2'\text{-dGuo})_2$]$^{2+}$ (7.86, 7.87) are in agreement with literature values[39] (Table 5.3). It is noteworthy that the pK_a values for both *trans* adducts are lower than those of the *cis*. This was also found to be the case for *cis*- and *trans*-[$Pt(NH_3)_2$(9-EtGH)$_2$]$^{2+}$ but surprisingly, replacement of the coordinated ammonia by methylamine reverses the situation.[39]

For *cis*-[$Pt(NH_3)$(2-pic)$(Guo)_2$]$^{2+}$, only one broad H8 peak is present at low temperature (Figure 5.9). This can be attributed to both coincidental overlap of H8 and restricted rotation of guanosine, where a specific configuration is favoured. As discussed in Chapter 4, one of the H8 peaks (G2) is more affected by temperature than the other and it is probable that G2 corresponds to the guanosine *cis* to the 2-picoline ligand.

Table 5.3 Comparison of pK_a values for N1H of 9-EtGH, Guo and 2'-dGuo in the complexes studied here and in cisplatin adducts.

Species	pK_a N1(H)	Reference
9-EtGH	9.57	[39]
$H(Guo)^+$	9.22	[39]
$H(2'\text{-dGuo})^+$	9.24	[39]
cis-$[Pt(NH_3)_2(9\text{-EtGH})_2]^{2+}$	8.01, 8.66	[39]
trans-$[Pt(NH_3)_2(9\text{-EtGH})_2]^{2+}$	7.90, 8.54	[39]
cis-$[Pt(NH_3)_2(2'\text{-dGuo})Cl]^+$	7.84	[39]
trans-$[Pt(NH_3)_2(2'\text{-dGuo})Cl]^+$	8.24	[39]
cis-$[Pt(NH_3)(2\text{-pic})(Guo)_2]^{2+}$	8.07, 8.17	Present work
cis-$[Pt(NH_3)(2\text{-pic})(2'\text{-dGuo})_2]^{2+}$	8.00, 8.05, 8.38, 8.40	Present work
trans-$[Pt(NH_3)(2\text{-pic})(Guo)_2]^{2+}$	7.84, 7.85	Present work
trans-$[Pt(NH_3)(2\text{-pic})(2'\text{-dGuo})_2]^{2+}$	7.86, 7.87	Present work

In the case of *cis*-$[Pt(NH_3)(2\text{-pic})(2'\text{-dGuo})_2]^{2+}$, four H8 peaks are present even at low temperature, two of which coalesce around 320 K (Figure 5.12). Similarly, it seems that two of the four peaks (2G3 and 2G4) experience a greater temperature dependence and these are likely to be the guanosine bases *cis* to the 2-picoline ligand in two different configurations.

The *trans* adducts exhibit a very similar temperature dependence to one another, characterised by the coalescence of two H8 peaks around 310 K (Figures 5.14 and 5.16). This can be attributed to slow rotation of the guanosine bases at low temperature.

For *cis*-$[Pt(NH_3)(2\text{-pic})(2'\text{-dGuo})_2]^{2+}$, further credence for the assignment of the two upfield H8 peaks (2G3 and 2G4) to guanosine bases *cis* to the 2-picoline ligand is given from the 2D ROESY spectrum (Appendix 4) as there is an NOE cross-peak between the two upfield H8 peaks and the aromatic H6 proton of the 2-picoline ligand. An NOE cross-peak of this strength is only likely if the guanosine is *cis* relative to the 2-picoline ligand.

For *cis*-$[Pt(NH_3)(2\text{-pic})(Guo)_2]^{2+}$, it is believed that the unexpected doublet and triplet obtained for the H1' protons (Figure 5.8) are due to two sets of overlapping doublets. Unusually, the nonequivalence of the guanosine ligands is not reflected in the H8 but in the H1' protons. This may be indicative of some particular stereoselective interaction of the ribose ring or of some particular sugar conformation originating from extensive hydrogen bonding. The situation is inversed for the *trans* isomer where two H8 signals and only one H1' doublet are observed (Appendix 5). It seems likely that this H1' doublet must be similarly overlapped. Platinum coordination to nucleobases and in particular, nucleotides, is known to induce a change in the sugar-ring conformation from S-type (C2'-*endo*) to N-type (C3'-*endo*), which changes the H1' – H2' coupling constant.[14, 40] For the *cis*- and *trans*-$[Pt(NH_3)(2\text{-pic})(Guo)_2]^{2+}$ adducts, the H1' – H2' coupling constants were not measurable due to coincidental overlap of signals. The values of $J_{1'\text{-}2'}$ for the *cis*- and *trans*-$[Pt(NH_3)(2\text{-pic})(2'\text{-dGuo})_2]^{2+}$ adducts (ca. 6-6.5 Hz) are consistent with predominantly S-type configuration.[14]

It has been proposed that, in solution, rotation about the Pt – N7 bond is crucial in forming the DNA lesion between adjacent purines. Restricted rotation about the Pt – N7 bonds can potentially lead to three different bis(nucleobase)

stereoisomers for square-planar complexes having two *cis* ligands with C_2 local symmetry: two head-to-tail (HT) and one head-to-head (HH) species, with the H8s of the guanosine bases on the opposite side or on the same side of the Pt coordination plane, respectively. The asymmetry of the ribose sugar influences the number of signals that can be observed in the NMR spectrum. Thus, the HT enantiomers become diastereoisomers and should be distinguishable by NMR. Each HT isomer is C_2-symmetrical and has one H8 signal. Therefore, four H8 signals in total are expected for the three stereoisomers. If the *cis*-PtA_2 moiety lacks local C_2 symmetry (eg. two different As or an unsymmetrical chelate), four different stereoisomers (two HT and two HH) are possible. However, it has been found that the HT forms are thermodynamically favoured in most simple *cis*-$[PtA_2G_2]$ models.[41] Each H8 is non-equivalent for both HT stereoisomers, giving a total of four H8 signals for the HT stereoisomers. For *cis*-$[PtCl_2(NH_3)(2\text{-pic})]$, the 2-methyl group can be on the upper or lower side of the platinum plane for each HT stereoisomer, so theoretically eight H8 signals should be observed for the two HT isomers, together with four methyl signals when there is slow rotation on the NMR timescale about both Pt – N7 guanosine and Pt – N picoline bonds. In the *cis*-$[Pt(NH_3)(2\text{-pic})(Guo)_2]^{2+}$ adduct, only two H8 signals and one methyl signal were observed, suggesting rotation about both Pt – N7 guanosine and Pt – N picoline bonds is fast on the NMR timescale. However, for the *cis*-$[Pt(NH_3)(2\text{-pic})(2'\text{-dGuo})_2]^{2+}$ adduct, four H8 signals and two methyl signals were observed. This suggests that rotation of 2'-deoxyguanosine about the Pt – N7 bond is fast on the NMR timescale but slow about the Pt – N bond for 2-picoline.

For *cis*-$[Pt(NH_3)(2\text{-pic})(Guo)_2]^{2+}$ and *cis*-$[Pt(NH_3)(2\text{-pic})(2'\text{-dGuo})_2]^{2+}$ an NOE is observed between 2-picoline H6 and guanosine H8, which corresponds to the guanosine *cis* to 2-picoline and in a tail orientation relative to the methyl group of 2-picoline. Thus, the NOE observed for the methyl group of 2-picoline to guanosine H8 may arise as a consequence of a guanosine positioned *trans* to 2-picoline in a head orientation relative to the methyl group of 2-picoline. Therefore, it seems likely that both *cis*-$[Pt(NH_3)(2\text{-pic})(Guo)_2]^{2+}$ and *cis*-$[Pt(NH_3)(2\text{-pic})(2'\text{-dGuo})_2]^{2+}$ adopt head-to-tail orientations.

For the *trans* complexes there are four different stereoisomers (2 x HT and 2 x HH). Because of the chiral ribose of the guanosine bases, the HT enantiomers again become diastereoisomers. Therefore, four H8 signals should be observed for the two HT isomers. In each of the *trans* adducts, only two H8 signals are observed implying that either there is fast rotation about the guanosine bases and/or the Pt – 2-picoline bond or alternatively, that one configuration is particularly favoured. The NOEs observed for *trans*-$[Pt(NH_3)(2\text{-pic})(2'\text{-dGuo})_2]^{2+}$ from the H8 signal to 2-pic H6 and the 2-pic methyl group suggest a heat-to-tail orientation of the guanosine bases.

5.6 Conclusions

The subject of the conformational and dynamic properties of nucleobase complexes is of considerable fundamental chemical interest. A greater understanding of these phenomena may help to explain the high selectivity of platinum compounds towards guanine bases.

This work has provided an insightful comparison of the binding of guanosine to *cis*-$[PtCl_2(NH_3)(2\text{-pic})]$ (AMD473), a promising anticancer drug, and its *trans*

isomer. N7 platination was confirmed in all cases and a variety of Pt bis(guanosine) adducts were identified and characterised. Coordination of Pt^{II} to the guanosine N7 site lowers the basicity of the N1H site by about 0.8-1.2 log units and about 1.4 log units for the *cis* and *trans* isomers, respectively, as compared to the free nucleoside. Based on the NOEs, the complexes *cis*-$[Pt(NH_3)(2\text{-pic})(Guo)_2]^{2+}$, *cis*-$[Pt(NH_3)(2\text{-pic})(2'\text{-dGuo})_2]^{2+}$ and *trans*-$[Pt(NH_3)(2\text{-pic})(2'\text{-dGuo})_2]^{2+}$ are assigned as head-to-tail conformations. The reaction of *cis*-$[Pt(^{15}NH_3)(2\text{-pic})(OH_2)_2]^{2+}$ with guanosine (1:2), was followed by $[^1H,^{15}N]$ HSQC spectroscopy and proceeded through two mono(guanosine) intermediate species to yield the dominant product *cis*-$[Pt(NH_3)(2\text{-pic})(Guo)_2]^{2+}$. Interestingly, the initial rate of formation of the intermediate *cis*-$[Pt(^{15}NH_3)(2\text{-pic})(OH_2)(Guo)]^{+}$ was faster for guanosine substitution in the *trans* position than in the *cis* position to 2-picoline due to steric hindrance, though the rates of the second guanosine substitution appear similar for both intermediates. In a separate study, the preference for N7 binding was demonstrated by a chromatographic analysis of *cis*-$[PtCl_2(NH_3)(2\text{-pic})]$ and substituted guanosine bases, which also confirmed the rate of reactions followed the order Guo > 1-MeGuo > 7-MeGuo.

5.7 References

[1] S. Grabner, J. Plavec, N. Bukovec, D. D. Leo, R. Cini, G. Natile, *J. Chem. Soc. Dalton. Trans.* **1998**, 1447.

[2] S. E. Sherman, S. J. Lippard, *Chem. Rev.* **1987**, *87*, 1153.

[3] A. Eastman, *Biochemistry* **1986**, *25*, 3912.

[4] I. Saito, M. Takayama, H. Sugiyama, K. Nakatani, *J. Am. Chem. Soc.* **1995**, *117*, 6406.

[5] A. M. J. Fichtinger-Schepman, J. L. v. d. Veer, J. H. J. d. Hartog, P. H. M. Lohman, J. Reedijk, *Biochemistry* **1985**, *24*, 707.

[6] S. J. Berners-Price, U. Frey, J. D. Ranford, P. J. Sadler, *J. Am. Chem. Soc.* **1993**, *115*, 8649.

[7] M. J. Bloemink, J. Reedijk, *Met. Ions Biol. Syst.* **1996**, *32*, 641.

[8] G. Frommer, I. Mutikainen, F. J. Pesch, E. C. Hillgeris, H. Preut, B. Lippert, *Inorg. Chem.* **1992**, *31*, 2429.

[9] J. Reedijk, A. M. J. Fichtinger-Schepman, A. T. v. Oosterom, P. v. d. Putte, *Structure and Bonding* **1987**, *67*, 53.

[10] Y. Xu, G. Natile, F. P. Intini, L. G. Marzilli, *J. Am. Chem. Soc.* **1990**, *112*, 8177.

[11] T. W. Hambley, *Inorg. Chem.* **1988**, *27*, 1073.

[12] M. J. Bloemink, R. J. Heeterbrij, K. Inagaki, Y. Kidani, J. Reedijk, *Inorg. Chem.* **1992**, *31*, 4656.

[13] S. J. Berners-Price, T. A. Frenkiel, J. D. Ranford, P. J. Sadler, *J. Chem. Soc. Dalton. Trans.* **1992**, 2137.

[14] C. S. Fouts, L. G. Marzilli, R. A. Byrd, M. F. Summere, G. Zon, K. Shinozuka, *Inorg. Chem.* **1988**, *27*, 366.

[15] J. Kozelka, G. A. Petsko, S. J. Lippard, *J. Am. Chem. Soc.* **1985**, *107*, 4079.

[16] S. E. Sherman, D. Gibson, A. H.-J. Wang, S. J. Lippard, *J. Am. Chem. Soc.* **1988**, *110*, 7368.

[17] J. Reedijk, *Inorg. Chim. Acta* **1992**, *198-200*, 873.

[18] G. Admiraal, J. L. v. d. Veer, R. A. G. d. Graaff, J. H. J. d. Hartog, J. Reedijk, *J. Am. Chem. Soc.* **1987**, *109*, 592.

[19] J. H. J. d. Hartog, C. Altona, J.-C. Chottard, J.-P. Girault, J.-Y. Lallemand, F. A. A. A. M. d. Leeuw, J. Reedijk, *Nucleic Acids Res.* **1982**, *10*, 4715.

[20] J. P. Caradonna, S. J. Lippard, *Inorg. Chem.* **1988**, *27*, 1454.

[21] S. E. Sherman, D. Gibson, A. H.-J. Wang, S. J. Lippard, *Science* **1985**, *230*, 412.

[22] M. D. Reily, L. G. Marzilli, *J. Am. Chem. Soc.* **1986**, *108*, 6785.

[23] R. K. O. Sigel, E. Freisinger, B. Lippert, *J. Biol. Inorg. Chem.* **2000**, *5*, 287.

[24] J. D. Orbell, M. R. Taylor, S. L. Birch, S. E. Lawton, L. M. Vilkins, L. J. Keefe, *Inorg. Chim. Acta* **1988**, *152*, 125.

[25] G. Schroder, B. Lippert, M. Sabat, C. J. L. Lock, R. Faggiani, B. Song, H. Sigel, *J. Chem. Soc. Dalton. Trans.* **1995**, *23*, 3767.

[26] R. E. Cramer, P. L. Dahlstrom, M. J. T. Seu, T. Norton, M. Kashiwagi, *Inorg. Chem.* **1980**, *19*, 148.

[27] B. Lippert, G. Raudaschl, C. J. L. Lock, P. Pilon, *Inorg. Chim. Acta* **1984**, *93*, 43.

[28] H. Schollhorn, G. Raudaschl-Sieber, G. Muller, U. Thewalt, B. Lippert, *J. Am. Chem. Soc.* **1985**, *107*, 5932.

[29] A. Eastman, M. A. Barry, *Biochemistry* **1987**, *26*, 3303.

[30] A. Eastman, M. M. Jennerwein, D. L. Nagel, *Chem.-Biol. Interactions* **1988**, *67*, 71.

[31] B. Lippert, *Met. Ions Biol. Syst.* **1996**, *33*, 105.

[32] M. J. Abrams, C. M. Giandomenico, J. F. Vollano, D. A. Schwartz, *Inorg. Chim. Acta* **1987**, *131*, 3.

[33] G. B. Kauffman, D. O. Cowan, *Inorg. Synth.* **1963**, *7*, 239.

[34] M. Ritala, J. Arpalahti, *Inorg. Chem.* **1991**, *30*, 2826.

[35] Y. Chen, Z. Guo, S. Parsons, P. J. Sadler, *Chem. Eur. J.* **1998**, *4*, 672.

[36] B. Lippert, *Prog. Inorg. Chem.* **1989**, *37*, 1.

[37] M. Mikola, P. Oksman, J. Arpalahti, *J. Chem. Soc. Dalton. Trans.* **1996**, 3101.

[38] J. Arpalahti, *Inorg. Chem.* **1990**, *29*, 4598.

[39] B. Song, J. Zhao, R. Griesser, C. Meiser, H. Sigel, B. Lippert, *Chem. Eur. J.* **1999**, *5*, 2374.

[40] K. Okamoto, V. Behnam, M. T. P. Viet, M. Polissiou, J.-Y. Gauthier, S. Hanessian, T. Theophanides, *Inorg. Chim. Acta* **1986**, *123*, L3.

[41] S. O. Ano, F. P. Intini, G. Natile, L. G. Marzilli, *J. Am. Chem. Soc.* **1997**, *119*, 8570.

Chapter 6

Interactions of the Anticancer Complex *Trans*-[$PtCl_2(NH_3)$(2-picoline)] with DNA

6.1 Abstract

Kinetic studies of the reaction of the anticancer complex *trans*-[$PtCl_2(NH_3)$(2-picoline)] (AMD443) with the self-complementary 12-mer DNA duplex, d(TATGGTACCATA)$_2$, using 1D ^1H and 2D [^1H,^{15}N] HSQC NMR spectroscopy at 298 K are reported, and compared to reactions of cisplatin and transplatin. Aquation of AMD443 is revealed to be the rate-limiting step in the formation of monofunctional DNA adducts. Models for monofunctional adducts indicate no particular stereoselective preference for G4 or G5.

6.2 Introduction

Coordination of Pt^{II} to nucleic acid constituents and DNA has been the subject of numerous studies over the past two decades.[1-6] Great attention has been paid to the binding properties of Pt^{II} compounds with *cis* geometry, in particular, because of the biological activity of cisplatin and related compounds. By contrast, far less is known of the clinically ineffective transplatin and corresponding *trans* derivatives.[7] However, detailed knowledge of the binding behaviour of transplatin and its structural analogues is of importance in understanding the factors which affect the biological activity of Pt^{II} species.

There is convincing evidence that the cytotoxicity of cisplatin is due to the bifunctional platination of DNA.[8] In the major adduct, cisplatin forms 1,2-cross-links between adjacent purines in d(GpG) or d(ApG) sequences.[9] These lesions result in a roll of 26-50° between the guanine bases involved in the cross-link and a global bend of the helix axis towards the major groove.[10-13] Also, the cisplatin cross-link unwinds the duplex and induces a widening and flattening of the minor groove

in the vicinity of platination sites. These features result in the recognition of DNA by high mobility group protein (HMG), leading to blocking of gene transcription.[8]

Both *cis*- and *trans*-platin preferentially bind to GN7 and yield monofuctional adducts in the first platination step. However, unlike cisplatin, transplatin cannot form (N7, N7) intrastrand cross-links with adjacent purines due to geometrical constraints. On the other hand, transplatin has been shown to form 1,3-intrastrand adducts with d(GNG)[14] and d(ANG)[15] sequences (N = any nucleotide). The trinucleotides d(GpTpG)[16] and d(GpCpG)[17] have been used as models for studying 1,3-chelation. Gel electrophoresis has shown that the *trans*-[$Pt(NH_3)_2$(d(GTG)-GN7, GN7)] cross-link bends the DNA double helix 26° and unwinds it by 45°.[18] An 18° kink of the helix axis was observed for a 1,3-adduct of *trans*-$Pt(NH_3)_2$[CCTCG*AG*TCTCC] and its complementary strand using NMR techniques.[14]

In addition to geometric differences between *cis*- and *trans*-platin adducts, kinetic factors may be responsible for differences in antitumour activity. It is believed that the hydrolysis to form monoaqua species prior to binding to DNA is the rate-determining step.[19] Due to the *trans* effect, Cl>N>O, the non-active transplatin reacts faster than cisplatin in the first step of aquation and binding. This is probably the reason why transplatin is more reactive towards peptides in the extracellular medium, preventing the platinum complex from reaching the target DNA.

As transplatin is kinetically more reactive than cisplatin,[20] it was proposed that the antitumour activity of *trans* compounds could be increased by using sterically bulky ligands to reduce the rate of replacement of chloro ligands.[21] Natile and Coluccia recently reviewed the progress of *trans* platinum anticancer agents.[13]

Three kinds of bulky ligands were described: (1) aliphatic amines, (2) pyridine-like ligands, and (3) iminoether ligands. The compound *trans*-[$PtCl_2$(amine)(isopropylamine)], for example, where the steric hindrance is enhanced by substitution of aliphatic amines for NH_3 in transplatin, demonstrates higher cytotoxic activity than cisplatin.[22]

Pyridine-like ligands greatly enhance the cytotoxicity of *trans*-Pt^{II} complexes. Generally, the cytotoxicity of the *trans* complexes, *trans*-[$PtCl_2$(L)(L')] [L = L' = pyridine or thiazole, or L = quinoline, L' = R'R''SO], are approximately one order of magnitude greater than transplatin, and they are at least not lower than their *cis* isomers. A significant feature of such *trans* complexes is that they are not cross-resistant to cisplatin in either L1210 leukaemia or human ovarian tumour cells.[23] Similarly, the iminoethers have been shown to be more active as *trans* isomers than as *cis* isomers.[24-26]

The *trans* isomer (AMD443) of the promising anticancer drug *cis*-[$PtCl_2(NH_3)$(2-picoline)] (AMD473), which is currently in phase II clinical trials, exhibits a similar profile of cytotoxicity, and is indeed more cytotoxic than AMD473 in a variety of cell lines.[27, 28] The bulky methyl group of the picoline ligand in AMD473 inhibits attack at the platinum and slows the rate of aquation.[29] The steric hindrance imposed by the methyl group is less in the *trans* complex than in the *cis* isomer (Chapter 3), but it is expected that it will still have a significant influence on the aquation and binding behaviour of AMD443.

It is of interest to examine how the picoline ligand in the *trans* platinum(II) complex, AMD443, affects the DNA-binding profile. In this study, the reaction of a self-complementary 12-mer DNA duplex, $d(TATGGTACCATA)_2$, with $^{15}NH_3$

labelled *trans*-[$PtCl_2(^{15}NH_3)$(2-pic)] was monitored by 1D ^1H and 2D [^1H,^{15}N] HSQC spectroscopy. The structures of the monofunctional adducts of B-form DNA were also investigated by molecular modelling. The results are discussed in relation to similar studies performed on relevant complexes.

6.3 Experimental

Materials: 2-picoline was purchased from Aldrich. The 12-mer oligonucleotide, d(TATGGTACCATA), was prepared as a sodium salt by the Oligonucleotide Synthesis Service at Cancer Research UK. *Trans*-[$PtCl_2(^{15}NH_3)$(2-pic)] was prepared by the procedure described in Chapter 3.

The concentration of the 12-mer single strand was determined by UV according to its ε value at 260 nm (ε = 112.3 x 10^3 $M^{-1}cm^{-1}$). The synthetic self-complementary oligonucleotide was annealed by firstly dissolving in 1 mL of high purity water, then denatured by heating at 368 K for 5 min. The oligonucleotide was then slowly renatured by stepwise cooling. The DNA was incubated at 338 K for 10 min, 310 K for 30 min, 338 K for 10 min, 310 K for 4 h and then slowly cooled to room temperature. The annealed oligonucleotide was stored at 253 K.

NMR Spectroscopy: NMR spectra were recorded at 298 K, unless otherwise stated, on a Bruker DMX500 spectrometer (^1H 500.13 MHz) or Bruker AVA600 (^1H 599.81 MHz) using 5 mm NMR tubes. All samples were prepared in 90% H_2O/10% D_2O and contained 0.02 M $NaClO_4$ to maintain a constant ionic strength. Spectra were referenced to TSP via dioxane, δ 3.75. Water suppression was achieved by presaturation. Spectra were processed using XWINNMR (Version 3.5, Bruker UK Ltd).

pH Measurements: The pH values of solutions were determined using a Corning 145 pH meter equipped with a micro combination electrode, calibrated with Aldrich buffer solutions at pH 4, 7 and 10. No correction was made for deuterium isotope effects.

Molecular Modelling: Molecular modelling was carried out by Dr. Vivienne Munk using SYBYL version 6.9 (Tripos Inc.). Models were energy-minimised using the Tripos force field. Models were considered energy-minimised when a constant energy was achieved.

6.4 Results

The reaction of *trans*-[$PtCl_2(^{15}NH_3)$(2-picoline)] with the 12-mer DNA duplex at an approximately 1:1 molar ratio (0.8 mM, pH 7.3, 0.02 M $NaClO_4$, 90% H_2O/10% D_2O, 298 K) was followed by 1D ^1H and 2D [^1H,^{15}N] HSQC NMR spectroscopy for a period of ca. 25 h. Figure 6.1 shows the HSQC spectra at various time intervals throughout the reaction.

Initially, two cross-peaks are observed. The most intense peak **a**, at 3.80, -69.44 ppm, corresponds to *trans*-[$PtCl_2(^{15}NH_3)$(2-picoline)]. Based on the chemical shifts, peak **b** at 3.80, -67.51 ppm is assignable to the monochloro monoaqua species, confirmed by NMR pH titration in Chapter 3. The intensity of the peak for the dichloro species decreases with time and the monochloro monoaqua species behaves as an intermediate, with the intensity increasing for the first three hours and then gradually decreasing. After ca. 1.6 h, two new but very weak peaks appear at 4.18, -65.30 ppm and 4.32, -65.29 ppm, peaks **c** and **d**, respectively. Peak **c** may be a monochloro monoguanine adduct, assigned on the basis of its reaction profile. Its

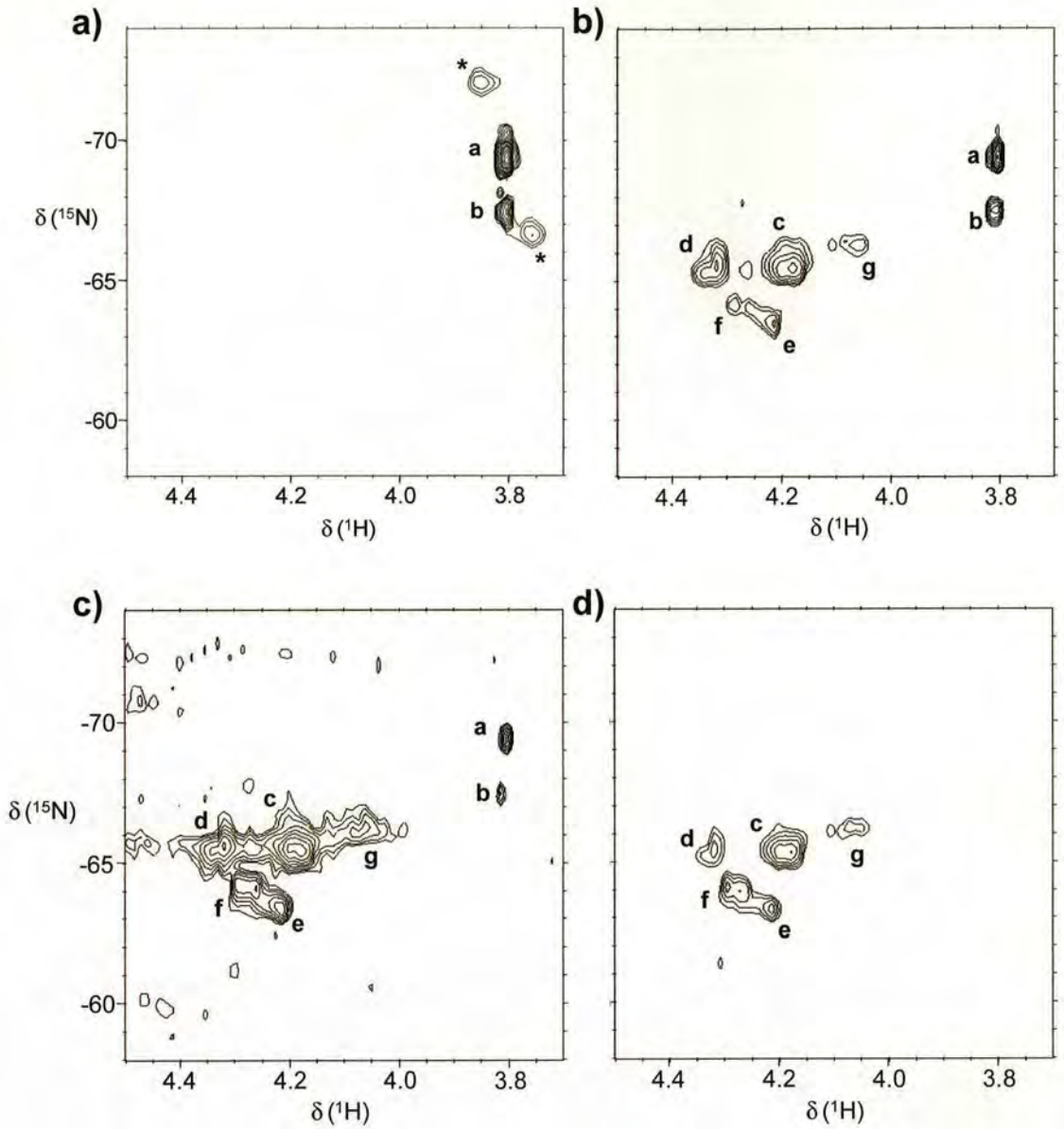

Figure 6.1 [^{1}H,^{15}N] HSQC NMR spectra (298 K) of a 1:1 solution of *trans*-[$PtCl_2(^{15}NH_3)$(2-pic)] and 12-mer DNA duplex a) 0.51 h, b) 8.25 h, c) 16.12 h and d) 25.12 h after the start of the reaction. Peak assignments: **a** = *trans*-[$PtCl_2(^{15}NH_3)$(2-pic)], **b** = *trans*-[$PtCl(OH_2)(^{15}NH_3)$(2-pic)]$^{+}$, **c** = monochloro monoguanine adduct, **d** = monochloro monoguanine adduct, **e**, **f** and **g** are unassigned, * = ^{195}Pt satellites.

intensity increases steadily and then appears to reach equilibrium after ca. 10.5 h. Peak **c** represents the major reaction product, corresponding to ca. 40 % of the total Pt – $^{15}NH_3$ species. Peak **d** increases in intensity initially, levels off around 10 h and then starts to decrease slightly after ca. 15 h, indicating it may be an intermediate species. It seems likely that peak **d** corresponds to a monochloro monoguanine adduct also, as there are two guanines (G_4 and G_5) available for binding. A fifth peak (**e**) is observed after 2.2 h at 4.21, -63.44 ppm. The intensity of this peak also increases with time but even after ca. 25 h of reaction, only accounts for ca. 11.5 % of the total Pt – $^{15}NH_3$ species present. The cross-peaks experience significant broadening over time. At ca. 7.1 h two further peaks are observed at 4.28, -64.33 ppm and 4.05, -66.28 ppm, **f** and **g**, respectively. Both increase in intensity over time although the intensity of peak **g** seems to decrease slightly towards the end of the reaction. It is difficult to assign the peaks unambiguously, but peak **f** appears to increase in intensity at the expense of peak **d** (particularly evident ca. 20 h) and may therefore be assignable to a bisadduct, such as a GC or GA interstrand cross-link.

A time-dependence of the concentrations of the main species detected during the reaction is shown in Figure 6.2. Due to the complexity of the reaction and the presence of unassigned peaks no attempt was made to fit the data to obtain rate constants. Half-lives for peaks **a** and **c** were derived from the computer fits of the concentration versus time profiles using the program Microcal Origin 7.5 (Appendix 7), and are listed in Table 6.1.

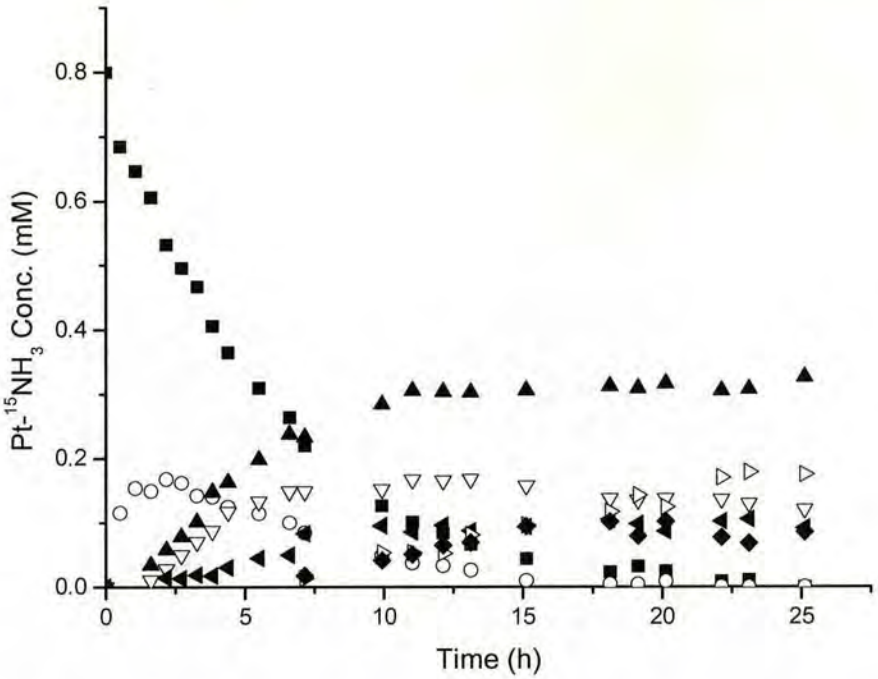

Figure 6.2 Kinetic profile for the reaction of *trans*-[$PtCl_2(^{15}NH_3)$(2-pic)] and 12-mer duplex DNA d(TATGGTACCATA)$_2$ at 298 K as determined by integration of the 2D cross-peaks shown in Figure 6.1. Assignments: (■) **a** = *trans*-[$PtCl_2(^{15}NH_3)$(2-pic)], (○) **b** = *trans*-[$PtCl(OH_2)(^{15}NH_3)$(2-pic)]$^+$, (▲) **c** = monochloro monoguanine adduct, (▽) **d** = monochloro monoguanine adduct, (◀) **e**, (▷) **f** and (◆) **g** are unassigned.

Table 6.1 Chemical shifts and half-lives for peaks **a** – **g** in the reaction of *trans*-[$PtCl_2(^{15}NH_3)$(2-pic)] with the self-complementary 12-mer DNA duplex d(TATGGTACCATA)$_2$ at 298 K (see Figure 6.1).

Peak	δ ^{1}H, ^{15}N	Assignments	Half-life (h)
a	3.80, 69.44	Dichloro	4.02
b	3.80, -67.51	Monoaqua monochloro	-
c	4.18, -65.30	Monochloro monoguanine	3.82
d	4.32, -65.29	Monochloro monoguanine	-
e	4.21, -63.44	-	-
f	4.28, -64.33	-	-
g	4.05, -66.28	-	-

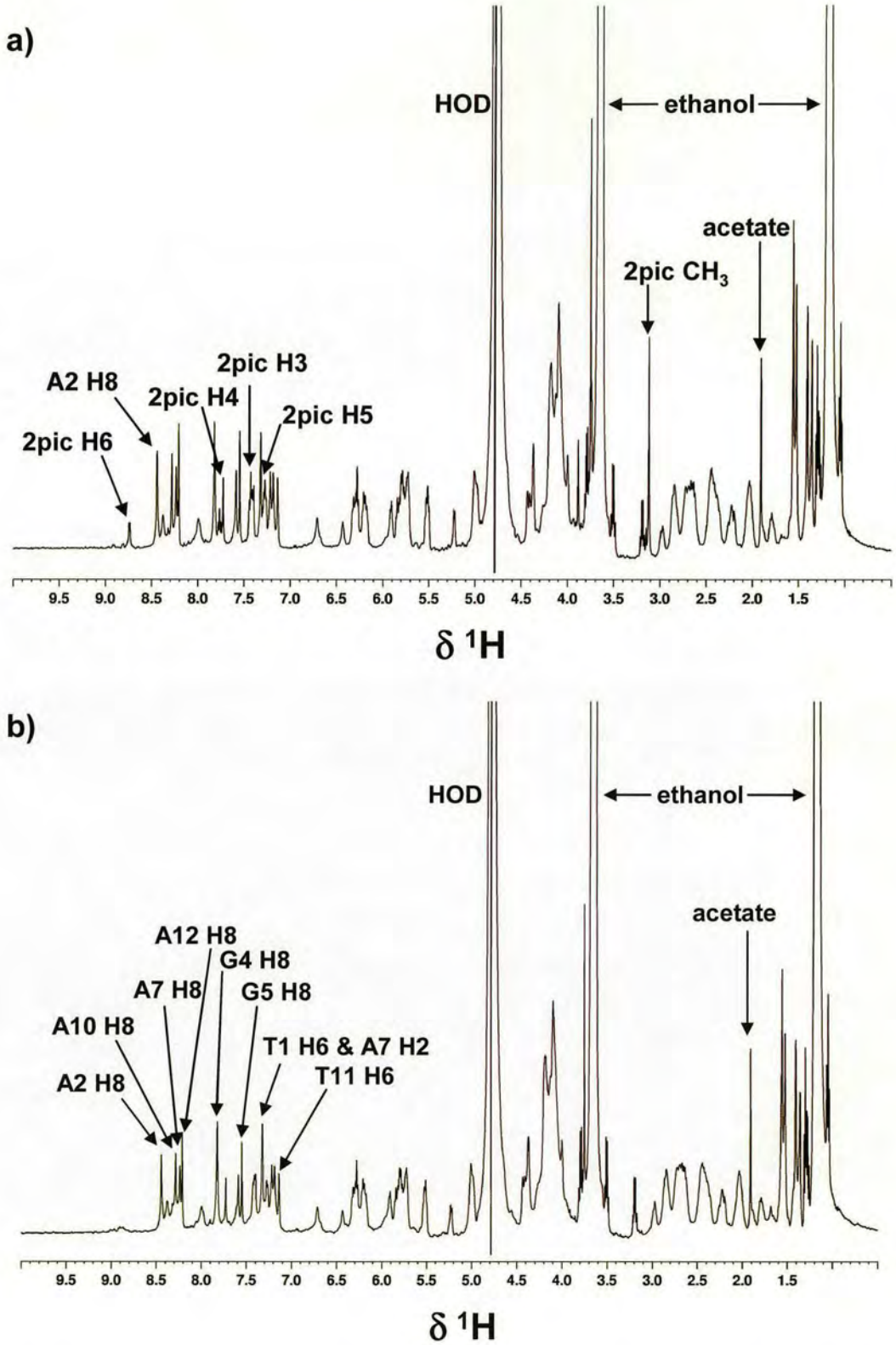

Figure 6.3 ^{1}H NMR spectra (298 K) of *trans*-[$PtCl_2(^{15}NH_3)$(2-pic)] with 12-mer DNA duplex at a) 0.2 h and b) 20.4 h after the start of the reaction.

The ^{1}H NMR spectra of the reaction are most intriguing. In the first ^{1}H spectrum recorded 0.2 h after the start of the reaction (Figure 6.3), the aromatic proton signals and methyl signal of the 2-picoline ligand of *trans*-[$PtCl_2(NH_3)$(2-pic)] are clearly visible: 8.74 ppm (d), H6; 7.76 ppm (t), H4; 7.43 ppm (d), H3; 7.29 ppm (t); 3.12 ppm (s), CH_3. However, these signals decrease in intensity over time and are no longer visible after ca. 10.2 h. It is noteworthy that a plot of the intensity of the H6 aromatic peak of the 2-picoline ligand correlates approximately with the decrease in intensity in the 2D [^{1}H,^{15}N] HSQC spectra of the dichloro species AMD443 (Figure 6.4).

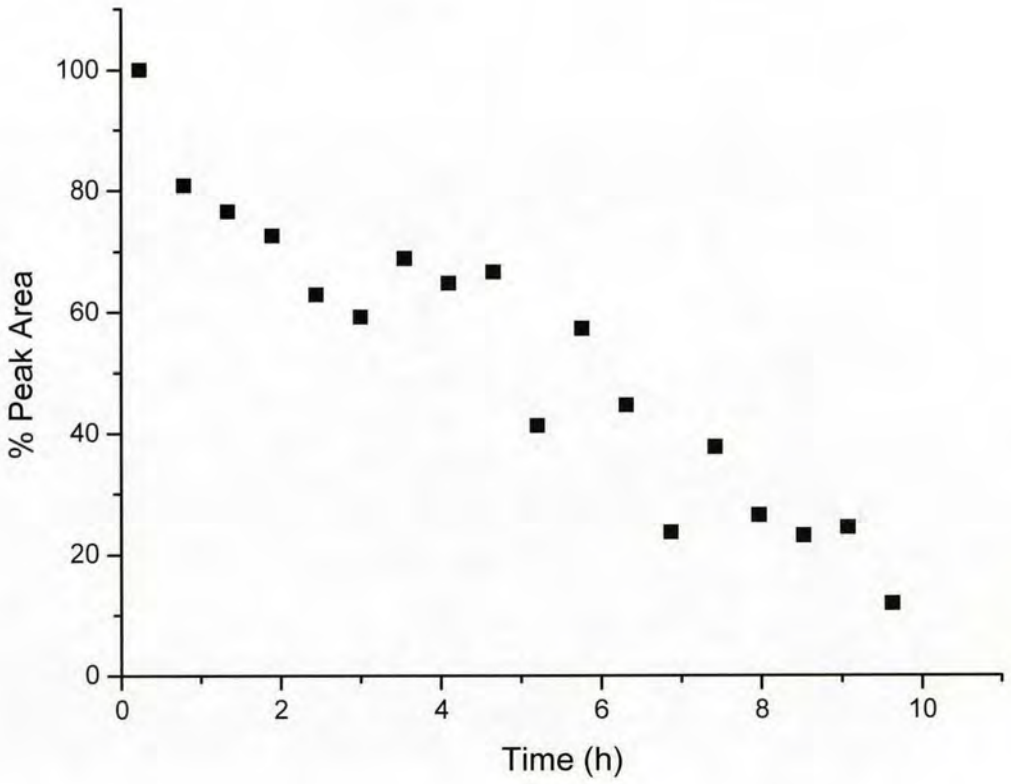

Figure 6.4 Plot of intensity of aromatic H6 ^{1}H NMR resonance of 2-picoline ligand versus time during the reaction of *trans*-[$PtCl_2(^{15}NH_3)$(2-pic)] and 12-mer duplex DNA at 298 K.

There are few observable changes in the ^{1}H NMR spectrum of the 12-mer duplex DNA during the reaction but there appears to be a slight upfield shift of 0.01 ppm for the signal around 7.54 ppm, assigned as the G5(H8) signal. Also, there are some very small signals visible at ca. 8.81, 8.90 and 8.92 ppm, which may be due to the H6 proton of bound AMD443. A 2D [^{1}H,^{1}H] NOESY spectrum of the free 12-mer duplex (284 K) is shown in Figure 6.5 and this can be compared with the 2D [^{1}H,^{1}H] NOESY spectrum (298 K) recorded after completion of the reaction, Figure 6.6. The ^{1}H NMR peaks for the duplex were partially assigned based on previous work by Sletten.[30] The hydrogen-bonding in the imino region (12-14 ppm) seemed to remain unperturbed upon platination. Interestingly, there are less cross-peaks at higher temperature implying an increased fluxionality of the platinated duplex.

Eight molecular models of the monofunctional G adducts of the 12-mer duplex were built by docking $\{PtCl(NH_3)(2\text{-pic})\}^+$ onto the G_4 or G_5 of the G_4G_5 site, and are shown in Figure 6.7. The models differed as follows: the 2-methyl group orientated towards the 3'-end of the DNA (Methyl-Down) with the 2-picoline orientated either away from the G_4 bound H8 (**a**) or towards the G_4 bound H8 (**b**); the 2-methyl group orientated towards the 5'-end of the DNA (Methyl-Up) with the 2-picoline orientated either away from the G_4 bound H8 (**c**) or towards the G_4 bound H8 (**d**); Methyl-Down with 2-picoline orientated either away from the G_5 bound H8 (**e**) or towards the G_5 bound H8 (**f**); Methyl-Up with 2-picoline orientated either away from the G_5 bound H8 (**g**) or towards the G_5 bound H8 (**h**). There is only a small variation in the relative energies of the models (2033 – 2049 kcalmol^{-1}). However, it is noteworthy that models **b**, **d**, **f** and **h**, which all have two ammine

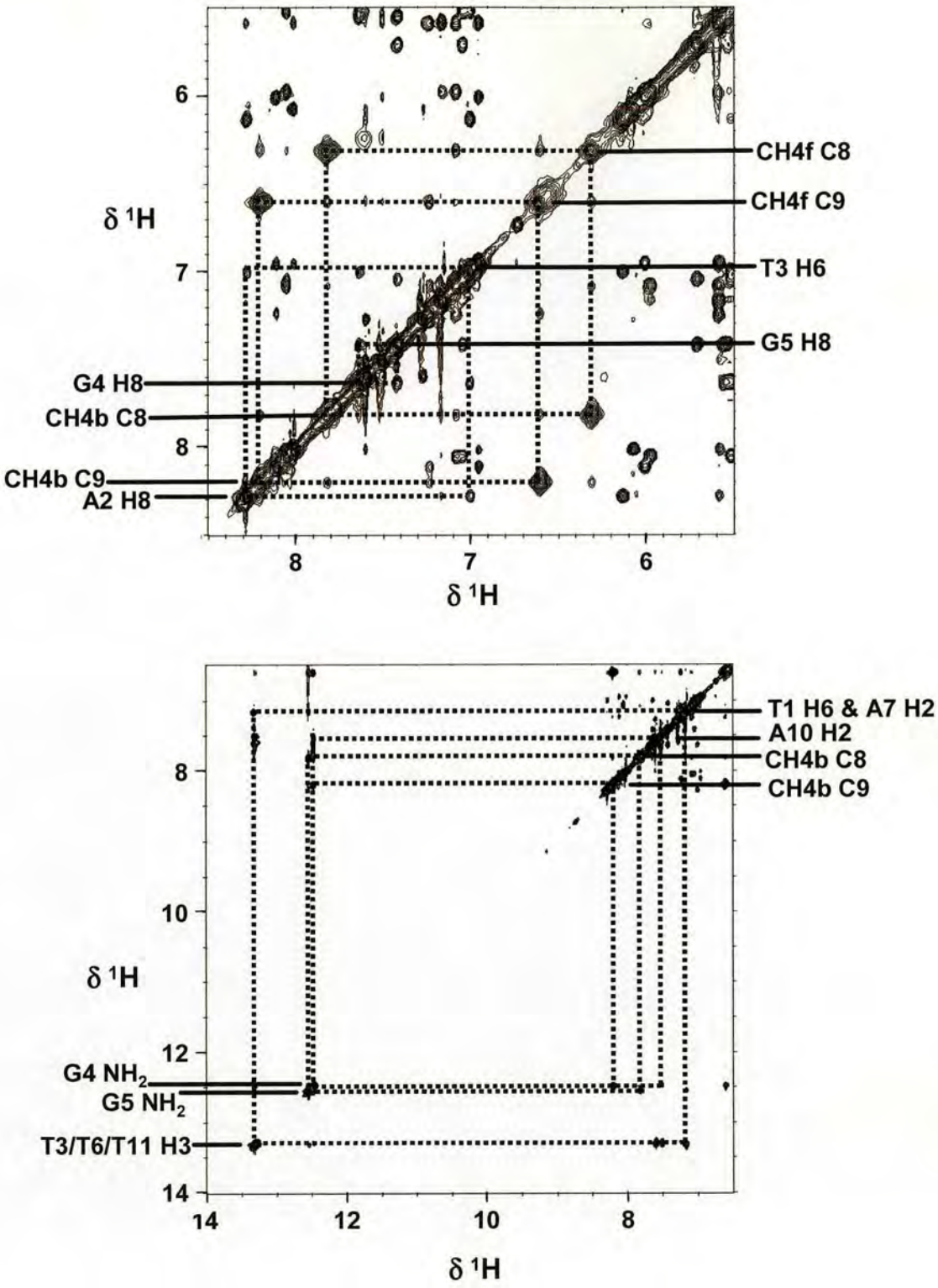

Figure 6.5 2D [^{1}H,^{1}H] NOESY NMR spectrum (mixing time 250 ms) of 12-mer duplex DNA d(TATGGTACCATA)$_2$ in 0.02 M $NaClO_4$ at 284 K. CH4b is the cytosine amino proton involved in H-bonding in the CG base pair, CH4f is the non-H-bonded amino proton.

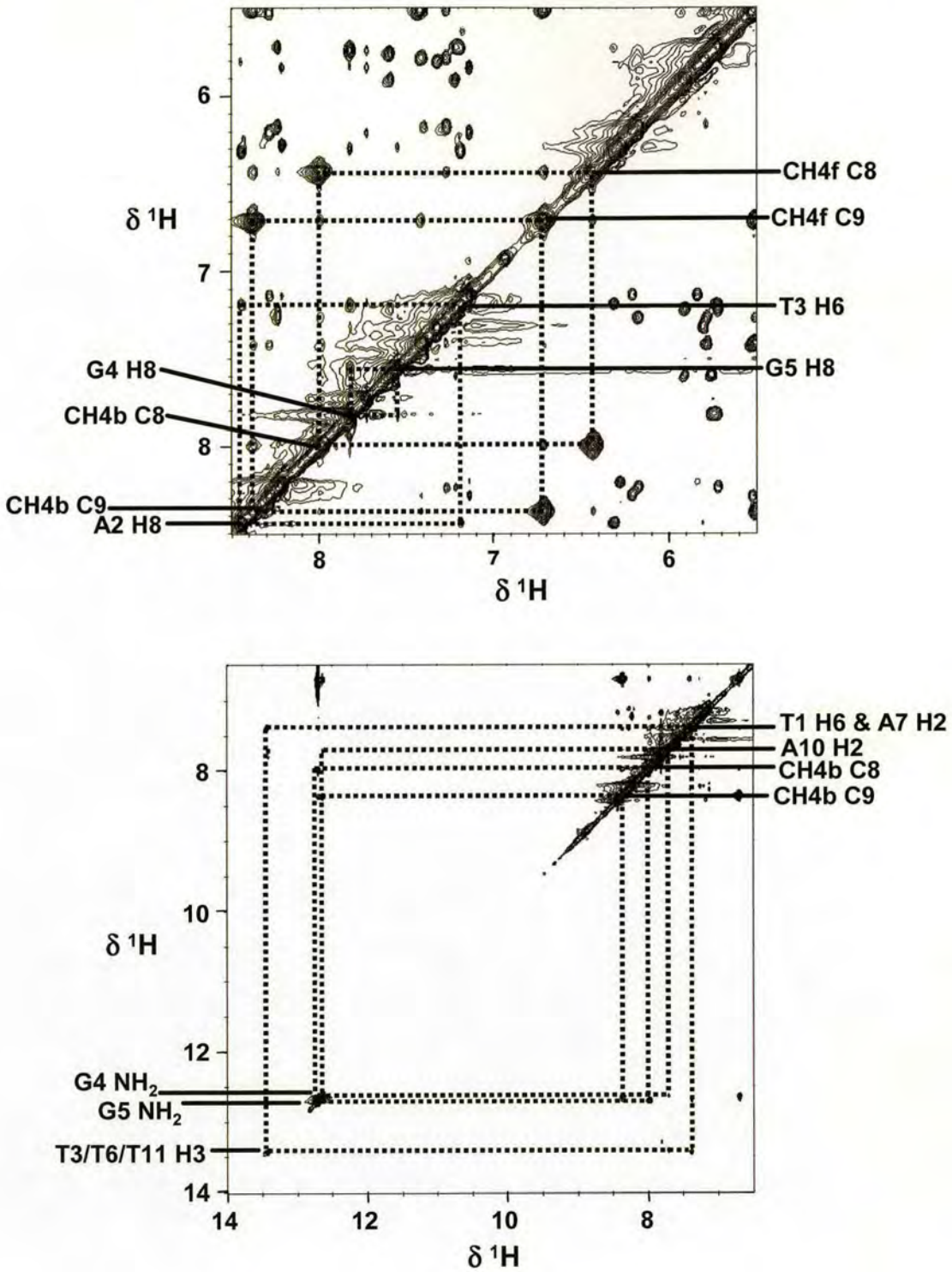

Figure 6.6 2D [^{1}H,^{1}H] NOESY NMR spectrum (mixing time 250 ms) of *trans*-[$PtCl_2(^{15}NH_3)$(2-pic)] and 12-mer duplex DNA in 0.02 M $NaClO_4$ at 298 K. CH4b is the cytosine amino proton involved in H-bonding in the CG base pair, CH4f is the non-H-bonded amino proton.

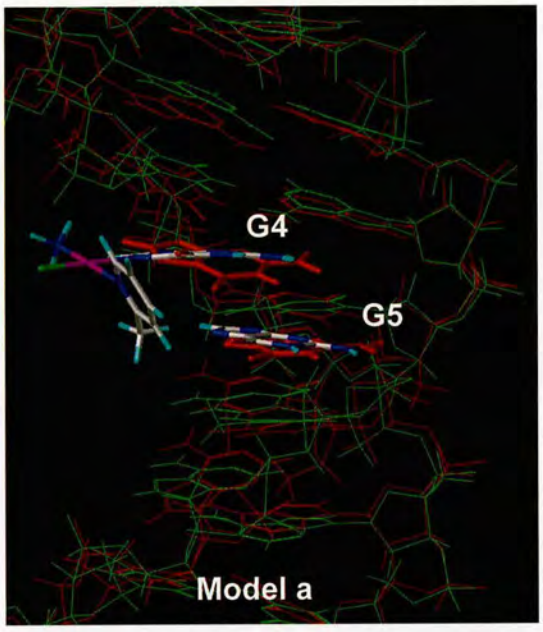
G4
G5
Model a

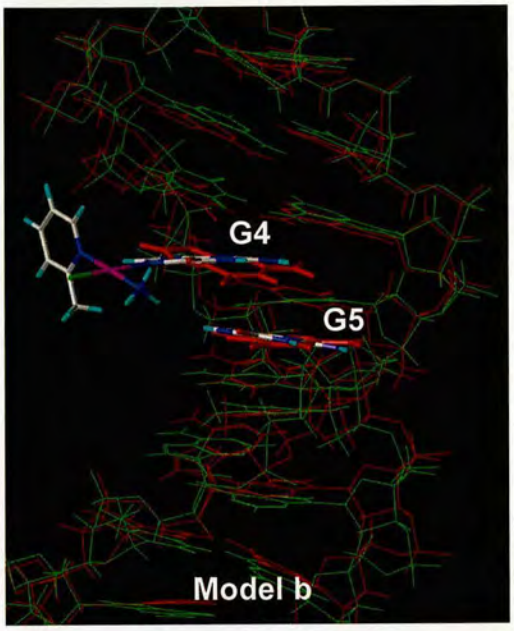
G4
G5
Model b

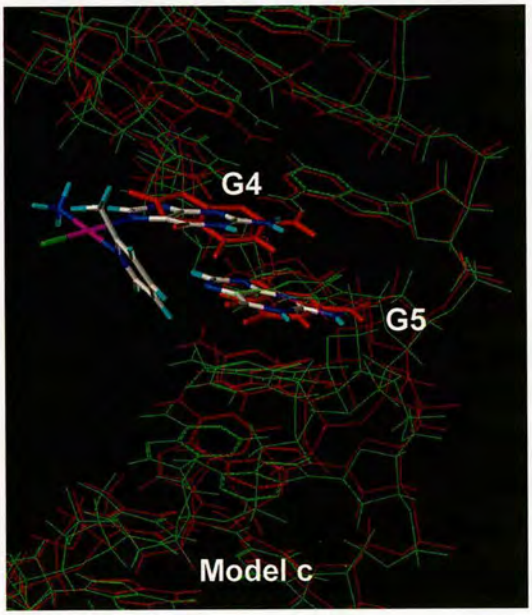
G4
G5
Model c

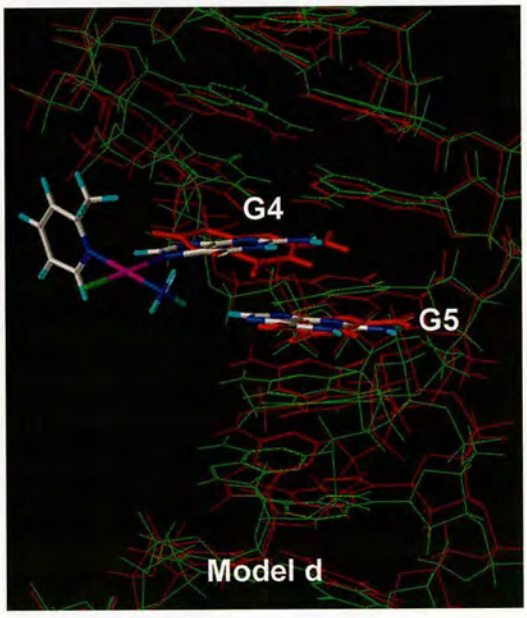
G4
G5
Model d

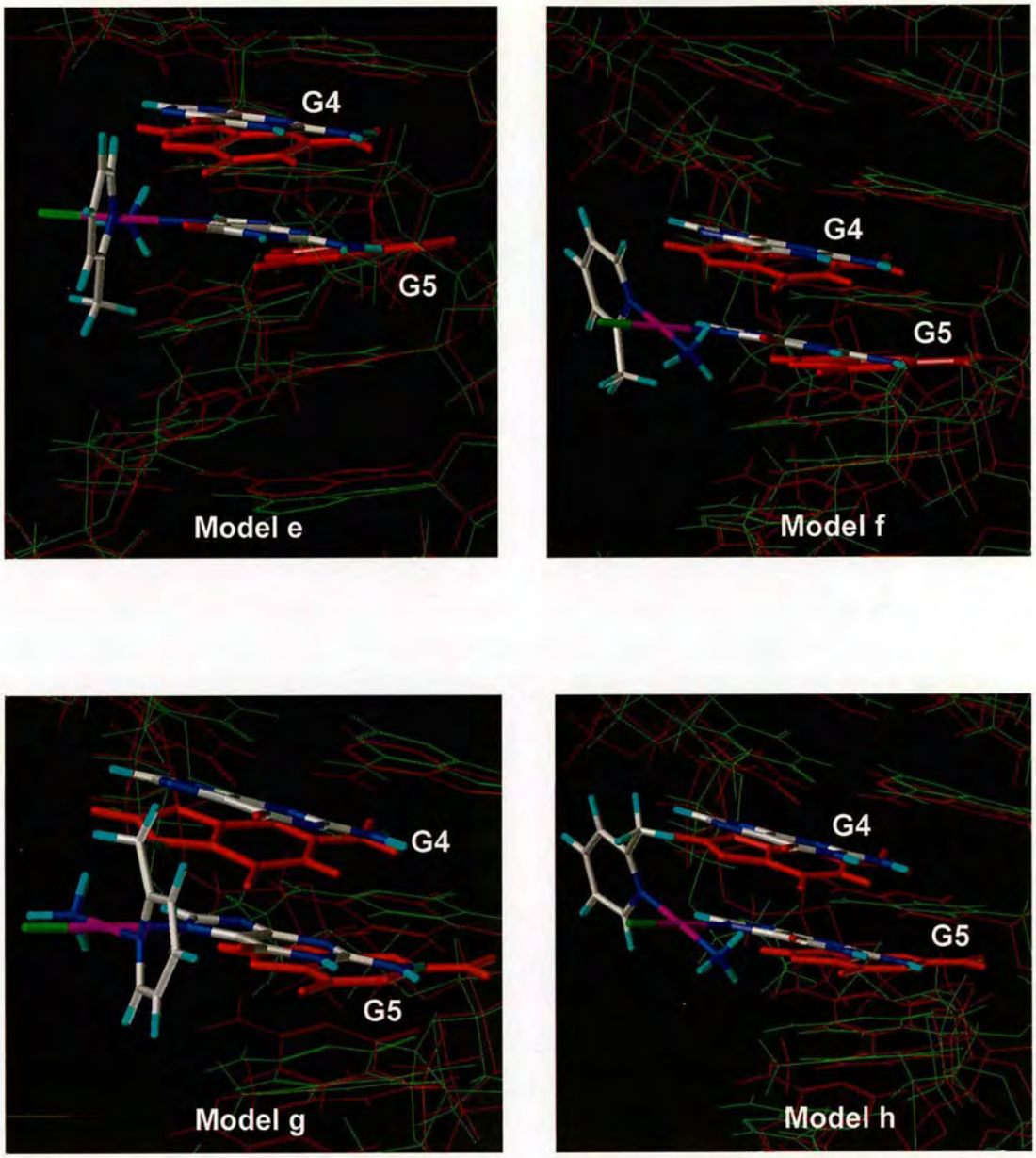

Figure 6.7 Molecular models of the G* adduct of the 12-mer duplex DNA, where G* represents binding with *trans*-{PtCl(2-pic)(NH_3)}$^+$. Unplatinated DNA – red, platinated DNA – green and atom colours are used for G bases of platinated DNA and *trans*-{PtCl(2-pic)(NH_3)}$^+$.

hydrogen bonds to the coordinated guanine O6 (distances = 1.79 – 2.34 Å), have the lowest energies. Hydrogen bonds are also observed in models **a** and **c** between a proton of the ammine group and the phosphate backbone (distances = 2.15 – 2.22 Å). No major steric clashes are observed for any of the models and it appears that only a slight movement of the guanine bases and nearest bases is sufficient to accommodate the platination.

6.5 Discussion

The differences in antitumour activity between *cis*-and *trans*- Pt(II) species have been attributed to three principal factors: 1) the structural perturbation of DNA induced by platination, 2) the kinetics of adduct formation, and 3) the sequence selectivity of binding to DNA. Therefore, in this work the interaction of *trans*-[$PtCl_2(^{15}NH_3)$(2pic)] with duplex DNA has been investigated.

[$^1H,^{15}N$] HSQC NMR has proven to be a powerful method for studying DNA platination reactions by cisplatin and its analogues.[31-35] Unfortunately, this technique yields less information for *trans* complexes (as the ^{15}N shifts are strongly influenced by the *trans* ligand which remains unchanged for *trans* complexes), but has nevertheless provided a useful insight into the reaction profile. Initially, only two cross-peaks, **a** and **b**, were present in the [$^1H,^{15}N$] NMR spectrum (Figure 6.1), which were unambiguously assigned as *trans*-[$PtCl_2(^{15}NH_3)$(2pic)] and *trans*-[$PtCl(OH_2)(^{15}NH_3)$(2pic)]$^+$, respectively, based on a previous NMR pH titration described in Chapter 3. Three more cross-peaks, **c**, **d** and **e**, are visible ca. 2 h after the start of the reaction. Peaks **c** and **d** were assigned as monochloro monoguanine adducts of G_4 and G_5, based on their reaction profiles. Although unconfirmed, peak **f** may be tentatively assigned as a bifunctional adduct, possibly a GC or GA

interstrand cross-link. Although the GC interstrand cross-link is favoured by transplatin,[36] molecular modelling indicates that the GG interstrand cross-link is sterically more compatible for *trans* complexes containing planar ligands, such as *trans*-[$PtCl_2(NH_3)$(quinoline)] and *trans*-[$PtCl_2(py)_2$].[3] No assignment has been made for cross-peaks **e** and **g** but they may be due to any of a variety of species including adenine and cytosine adducts or possibly a ApTpG intrastrand adduct for example. A further possibility is a monoguanine monoaqua adduct. The [^1H,^{15}N] cross-peaks experienced significant broadening during the reaction which may be a consequence of tumbling due to the high molecular weights of the species formed.

The rate-limiting step in the binding of cisplatin to DNA has long been considered to be aquation of the first chloro ligand.[19] The present study shows that this is also true for *trans*-[$PtCl_2(NH_3)$(2pic)] as the monochloro monoaqua species (peak **b**) is formed prior to any binding to DNA and hence, aquation is the rate-limiting step in formation of the monofunctional adduct.

The lack of change of the DNA proton signals in the ^1H spectra remains unexplained and is worthy of further investigation. An H8 downfield shift of 0.3-0.6 ppm would be expected upon platination[30] and the shifted signal may be overlapped with other signals such as A2H8. However, no additional cross-peak was observed in the 2D NOESY spectrum. The gradual decrease in intensity and subsequent loss of proton signals for the 2-picoline ligand suggests that the complex is binding to DNA and the signals for bound complex are broad. [^1H,^{15}N] NMR also suggests binding of AMD443 in several sites.

Experimentally determined rate constants for reactions of transplatin with double-stranded DNA are in the range for Cl^- hydrolysis, k being between 5.4×10^{-5}

s^{-1} ($t_{1/2}$ = 3.6 h)[37] and 9.6 x 10^{-5} s^{-1} ($t_{1/2}$ = 2.0 h)[38] at 310 K. However, these values do not differ significantly from those of cisplatin, k = 10.2 x 10^{-5} s^{-1} ($t_{1/2}$ = 1.9 h).[38] In this work, a half-life of 3.8 h at 298 K (Table 6.1) has been determined for formation of one of the monoguanine adducts. This half-life is significantly slower than hydrolysis of the first chloride ($t_{1/2}$ = 1.8 h, calculated based on values determined in Chapter 3) and this may be a consequence of the steric hindrance of the 2-picoline ligand. However, it has been reported that the presence of DNA can slow the aquation of cisplatin[39] leading to a slower rate of monofunctional adduct formation also, assuming the reaction proceeds through the monoaquated species. Reported half-lives for closure of monofunctional to bifunctional adducts at 310 K vary between 3.1 h[38] and 24 h[40] to 30 h[41] for transplatin. Possibly these discrepancies are due to differences in methods applied, ^{195}Pt NMR spectroscopy[38] and monoadduct trapping by nucleophiles.[40, 41] In contrast, closure of the cisplatin monoadducts to the cross-links occurs somewhat faster, with k = 9.2 x 10^{-5} s^{-1} to 4.5-5 x 10^{-5} s^{-1} at 310 K, corresponding to $t_{1/2}$ = 2.1 h[38] and ca. 4 h,[42] respectively.

Molecular modelling of the various guanine-bound monofunctional adducts revealed that there is no particular energetic preference for any of the isomers. This is perhaps not very surprising given the fact that the monofunctional adducts have a greater degree of freedom. It is likely that a bifunctional adduct would be much more stereoselective, as reported in the case of *cis*-[$PtCl_2(NH_3)$(2-pic)] which was found to form a highly selective GG intrastrand bischelate with a 14-mer DNA duplex.[35]

6.6 Conclusions

A major rationale for these studies is the desire to compare the DNA-binding profile of a new *trans*-Pt(II) anticancer complex with that of cisplatin and transplatin. In particular, studies of both kinetics and structure may lead to an understanding of how distinct DNA-drug binding profiles may lead to improved antitumour activity.

Labelling of the new *trans* anticancer complex *trans*-[$PtCl_2(^{15}NH_3)$(2-pic)] has allowed an insight to be gained into the kinetics and mechanisms of its reactions with a DNA duplex. [^1H,^{15}N] HSQC spectra clearly showed that *trans*-[$PtCl_2(^{15}NH_3)$(2-pic)] is consumed in the reaction with the 12-mer duplex to produce an intermediate monoaqua adduct and a further five species, two of which have been assigned as monoguanine adducts in the G_4 and G_5 positions and a further species has been postulated to be a GC or GA interstrand cross-link. The ^1H NMR spectra were more difficult to interpret as there were few changes in the DNA signals. However, it was clear that platination did not cause major perturbations of the duplex structure. The apparent loss of signals for the 2-picoline ligand in *trans*-[$PtCl_2(^{15}NH_3)$(2-pic)] is a further indication of binding to DNA as the new signals were broadened, indicative of formation of a higher molecular weight species. Models of the monofunctional guanine adducts revealed no isomer was particularly favourable. Further investigations of DNA interactions with *trans*-[$PtCl_2(NH_3)$(2-pic)] are warranted to unravel the origin of antitumour activity of platinum complexes with leaving ligands in the *trans* conformation.

6.7 References

[1] B. Lippert, *Prog. Inorg. Chem.* **1989**, *37*, 1.

[2] J. Arpalahti, *Met. Ions Biol. Syst.* **1996**, *32*, 379.

[3] N. Farrell, *Met. Ions Biol. Syst.* **1996**, *32*, 603.

[4] M. J. Bloemink, J. Reedijk, *Met. Ions Biol. Syst.* **1996**, *32*, 641.

[5] T. W. Hambley, *J. Chem. Soc. Dalton. Trans.* **2001**, 2711.

[6] J. Reedijk, *Proc. Natl. Acad. Sci. USA* **2003**, *100*, 3611.

[7] B. Lippert, *Met. Ions Biol. Syst.* **1996**, *33*, 105.

[8] D. B. Zamble, S. J. Lippard, in *Cisplatin*, Verlag Helvetica Chimica Acta, Zürich, **1999**, pp. 73.

[9] J. Reedijk, A. M. J. Fichtinger-Schepman, A. T. v. Oosterom, P. v. d. Putte, *Structure and Bonding* **1987**, *67*, 53.

[10] P. M. Takahara, C. A. Frederick, S. J. Lippard, *J. Am. Chem. Soc.* **1996**, *118*, 12309.

[11] D. Yang, S. S. G. E. v. Boom, J. Reedijk, J. H. v. Boom, A. H.-J. Wang, *Biochemistry* **1995**, *34*, 12912.

[12] A. Gelasco, S. J. Lippard, *Biochemistry* **1998**, *37*, 9230.

[13] G. Natile, M. Coluccia, *Coord. Chem. Rev.* **2001**, *216-217*, 383.

[14] C. A. Lepre, L. Chassot, C. E. Costello, S. J. Lippard, *Biochemistry* **1990**, *29*, 811.

[15] C. A. Lepre, K. G. Strothkamp, S. J. Lippard, *Biochemistry* **1987**, *26*, 5651.

[16] J. L. v. d. Veer, G. J. Ligtvoet, H. v. d. Elst, J. Reedijk, *J. Am. Chem. Soc.* **1986**, *108*, 3860.

[17] D. Gibson, S. J. Lippard, *Inorg. Chem.* **1987**, *26*, 2275.

[18] J. M. Malinge, M. Leng, in *Cisplatin*, Verlag Helvetica Chimica Acta, Zürich, **1999**, pp. 159.

[19] N. P. Johnson, J. D. Hoeschele, R. O. Rahn, *Chem. Biol. Interact.* **1980**, *30*, 151.

[20] E. Wong, C. M. Giandomenico, *Chem. Rev.* **1999**, *99*, 2451.

[21] N. Farrell, T. T. B. Ha, J.-P. Souchard, F. L. Wimmer, S. Cros, N. P. Johnson, *J. Med. Chem.* **1989**, *32*, 2240.

[22] E. I. Montero, S. Diaz, A. M. González-Vadillo, J. M. Pérez, C. Alonso, C. Navarro-Ranninger, *J. Med. Chem.* **1999**, *42*, 4264.

[23] N. Farrell, L. R. Kelland, J. D. Roberts, M. V. Beusichem, *Cancer Res.* **1992**, *52*, 5065.

[24] M. Coluccia, A. Boccarelli, M. A. Mariggio, N. Cardellicchio, P. Caputo, F. P. Intini, G. Natile, *Chem. Biol. Interact.* **1995**, *98*, 251.

[25] M. Coluccia, A. Nassi, F. Loseto, A. Boccarelli, M. A. Mariggio, D. Giordano, F. P. Intini, P. A. Caputo, G. Natile, *J. Med. Chem.* **1993**, *36*, 510.

[26] L. R. Kelland, C. F. J. Barnard, I. G. Evans, B. A. Murrer, B. R. C. Theobald, S. B. Wyer, P. M. Goddard, M. Jones, M. Valenti, A. Bryant, P. M. Rogers, K. R. Harrap, *J. Med. Chem.* **1995**, *38*, 3016.

[27] J. Holford, F. Raynaud, B. A. Murrer, K. Grimaldi, J. A. Hartley, M. Abrams, L. R. Kelland, *Anti-Cancer Drug Design* **1998**, *13*, 1.

[28] K. Harrap, *Unpublished Results*, AnorMED Inc., **1992**.

[29] Y. Chen, Z. Guo, S. Parsons, P. J. Sadler, *Chem. Eur. J.* **1998**, *4*, 672.

[30] J. Vinje, J. A. Parkinson, P. J. Sadler, T. Brown, E. Sletten, *Chem. Eur. J.* **2003**, *9*, 1620.

[31] K. J. Barnham, S. J. Berners-Price, T. A. Frenkiel, U. Frey, P. J. Sadler, *Angew. Chem. Int. Ed. Engl.* **1995**, *34*, 1874.

[32] S. J. Berners-Price, K. J. Barnham, U. Frey, P. J. Sadler, *Chem. Eur. J.* **1996**, *2*, 12831291.

[33] M. S. Davies, S. J. Berners-Price, T. W. Hambley, *J. Am. Chem. Soc.* **1998**, *120*, 11380.

[34] P. d. S. Murdoch, Z. Guo, J. A. Parkinson, P. J. Sadler, *J. Biol. Inorg. Chem.* **1999**, *4*, 32.

[35] Y. Chen, J. A. Parkinson, Z. Guo, T. Brown, P. J. Sadler, *Angew. Chem. Int. Ed.* **1999**, *38*, 2060.

[36] V. Brabec, M. Leng, *Proc. Natl. Acad. Sci. USA* **1993**, *90*, 5345.

[37] H. M. Ushay, T. D. Tullius, S. J. Lippard, *Biochemistry* **1981**, *20*, 3744.

[38] D. P. Bancroft, C. A. Lepre, S. J. Lippard, *J. Am. Chem. Soc.* **1990**, *112*, 6860.

[39] M. S. Davies, S. J. Berners-Price, T. W. Hambley, *Inorg. Chem.* **2000**, *39*, 5603.

[40] A. Eastman, M. A. Barry, *Biochemistry* **1987**, *26*, 3303.

[41] J.-L. Butour, N. P. Johnson, *Biochemistry* **1986**, *25*, 4534.

[42] J.-M. Malinge, M. Leng, *Nucleic Acids Res.* **1988**, *16*, 7663.

Chapter 7

Reactions of Sterically-Hindered Platinum Anticancer Complexes with Sulfur-Containing Biomolecules

7.1 Abstract

The kinetics and mechanism of the reaction of the ^{15}N-labelled anticancer compound *trans*-[$PtCl_2(^{15}NH_3)$(2-picoline)] (AMD443) with guanosine 5'-monophosphate (5'-GMP) and the tripeptide glutathione (GSH) have been investigated by 2D [^1H,^{15}N] HSQC NMR spectroscopy. For the reaction of *trans*-[$PtCl_2(^{15}NH_3)$(2-picoline)] with 5'-GMP, the products were readily identified by their cross-peaks in the 2D NMR spectra. The integrated peak intensities versus time were used to obtain rate constants by a non-linear optimization procedure. The formation of the monochloro GMP adduct takes place via a bimolecular process involving the monochloro monoaqua species and the entering nucleotide; the concentration of this adduct reaches a maximum value after about 10 hours at 298 K. Subsequently, monoaqua GMP and bifunctional GMP adducts are formed in successive steps. Competitive reactions of *trans*-[$PtCl_2(^{15}NH_3)$(2-picoline)] with GSH and 5'-GMP show a clear preference for GSH adduct formation. The reactions of *cis*- and *trans*-[$PtCl_2(^{15}NH_3)$(2-picoline)] with ^{15}N-labelled L-methionine have also been studied using [^1H,^{15}N] 2D NMR spectroscopy. The steric effect of 2-picoline reduces the reactivity of *cis*-[$PtCl_2(^{15}NH_3)$(2-picoline)] towards L-methionine and the hydrolysis reaction predominates. *Trans*-[$PtCl_2(^{15}NH_3)$(2-picoline)] was very reactive in the presence of L-methionine and intriguingly lost ammonia at low pH suggesting the possibility of *S*, *N* methionine chelation.

7.2 Introduction

It is now widely accepted that the antitumour activity of platinum anticancer drugs is due to the platination of DNA, most commonly the guanine bases.[1, 2]

However, reactions with other molecules in biological fluids are likely to affect the efficiency with which platinum compounds reach that target, as well as being involved in drug toxicity. The interaction of platinum with the sulfur nucleophilic centres of certain biomolecules is believed to play important roles in the metabolism of cisplatin or of its analogues.[3-6] Examples include platinum binding to the sulfhydryl group of kidney proteins, the likely origin of the renal toxicity of cisplatin;[7-9] interaction with intracellular glutathione, which leads to inactivation of the drug and cell resistance;[10, 11] the proposed use of extracellular glutathione, as protection of cisplatin toxicity,[12] use of sulfur nucleophiles (such as dithiocarbamates) as rescue agents in the case of acute toxicity;[13] also Pt binding to thiols in DNA polymerase-α is probably connected with the mechanism of cytotoxicity.[14-16] It has also been proposed that Pt-methionine complexes formed *in vivo* may provide a route for DNA platination[17, 18] and/or a way to dispose of platinum, since these kinds of complexes have been found in the urine of patients treated with cisplatin,[19] and in those of animals treated with carboplatin.[20]

Methionine (L-MetH) is an important amino acid which is involved in the metabolism of platinum drugs. The complex [Pt(L-Met-*S*,*N*)$_2$] which has been isolated from the urine of patients treated with cisplatin, exists in aqueous solution as a mixture of *cis* and *trans* isomers which undergo interconversion,[21] but these are unreactive species which can be considered to be a detoxified form of platinum. However, Deegan et al. have reported that *in vivo*, cisplatin incubated with methionine has reduced nephrotoxicity while the cytotoxicity against cancer cells is maintained.[22] Methionine and its derivatives can form stable ring-opened complexes with carboplatin and its analogues.[20] Since carboplatin, [Pt(cbdca-*O*,*O*')$(NH_3)_2$]

(cbdca = 1,1-dicarboxycyclobutane), itself reacts with nucleobases very slowly, it is conceivable that a methionine-containing peptide or protein may play an important role in transport or activation of carboplatin and in the transfer of Pt onto DNA. S-bound methionine can be displaced by N7 of the DNA base guanine.[18, 23]

Methionine is able to coordinate to Pt^{II} in a very versatile manner in aqueous solution. A simple system of L-methionine and $K_2[PtCl_4]$ in molar ratio 2:1 generates over ten Pt species.[24] Thioether sulfur, amino nitrogen and carboxylate oxygen[25] are all capable of binding to Pt^{II}. The favoured binding site is sulfur, and S,N-chelation is a common binding mode. In methionine-containing peptides, coordination of the amide N is also possible.[26, 27]

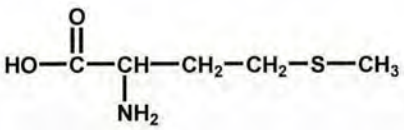

Methionine

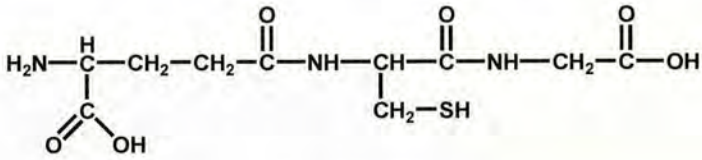

Glutathione

Glutathione (GSH), a cysteine-containing tripeptide (γ-L-Glu-L-Cys-Gly), is the predominant intracellular thiol with concentrations typically ranging from 0.5-10 mM.[11] It has a variety of physiologically important functions such as metabolism, catalysis, transport and the protection of cells against reactive oxygen species, peroxidase, and xenobiotics.[28] The cytotoxicity of cisplatin has been shown to be enhanced by depletion of cellular GSH in some tumour cells. GSH is over-expressed in cisplatin-resistant cells and the Pt-GS adducts can be pumped out of cells through a novel ATP dependent GS-X pump.[29, 30] At physiological pH, Pt^{II} complexes usually show a kinetic preference for the thiols cysteine and glutathione over 5'-GMP, even in the presence of excess nucleotide.[15] Reactions of cisplatin and

transplatin with glutathione in intact human red blood cells have been investigated.[31] Transplatin was found to react more rapidly, suggesting that in the case of cisplatin higher percentages of the drug dose may reach the cell nucleus, before inactivation with GSH takes place.

The promising anticancer drug *cis*-[$PtCl_2(NH_3)$(2-picoline)] (AMD473) appears to circumvent thiol-mediated resistance mechanisms whilst still maintaining the ability to form cytotoxic lesions with DNA.[32, 33] The 2-picoline ligand is almost perpendicular to the Pt square-plane such that the 2-methyl group lies directly over the square-plane and precludes access of incoming thiols. A recent study of the reactions of AMD473 with 5'-GMP and GSH reported both mono- and bis-GMP adducts were formed during competitive reactions.[34] The *trans* isomer of AMD473, *trans*-[$PtCl_2(NH_3)$(2-picoline)] (AMD443), is also cytotoxic in a variety of cancer cell-lines,[35] and it is therefore of interest to investigate and contrast the reactions of AMD473 and AMD443 with biologically-relevant thiols. In this work, the kinetics of interaction of AMD443 with 5'-GMP, and in the presence of GSH, have been investigated with the use of both 1D ^1H and 2D [^1H,^{15}N] HSQC NMR spectroscopy. Also, the reactions of AMD473 and AMD443 with L-methionine have been studied using 2D [^1H,^{15}N] HSQC NMR spectroscopy.

7.3 Experimental

Chemicals and preparations of complexes: 2-Picoline, glutathione and 5'-guanosine monophosphate were purchased from Aldrich and ^{15}N-L-methionine from ICN Biomedicals. *cis*-[$PtCl_2(^{15}NH_3)$(2-pic)] was synthesised based on a previously published procedure,[36] employing *cis*-[$PtCl_2(^{15}NH_3)_2$] as the starting material. The synthesis of *trans*-[$PtCl_2(^{15}NH_3)$(2-pic)] is described in Chapter 3.

pH Measurements: The pH values of solutions were determined using a Corning 145 pH meter equipped with a micro combination electrode, calibrated with Aldrich buffer solutions at pH 4, 7 and 10. The pH was adjusted with dilute solutions of $HClO_4$ and NaOH. No correction was made for deuterium isotope effects.

NMR Spectroscopy: NMR spectra were recorded at 298 K on Bruker DMX500 (^1H 500.13 MHz) or Bruker AVA600 (^1H 599.81 MHz) spectrometers using 5 mm NMR tubes. All samples were prepared in 90% H_2O/10% D_2O and contained 0.1 M $NaClO_4$ to maintain a constant ionic strength. Spectra were referenced to TSP via dioxane for ^1H (δ 3.75), and 1 M $^{15}NH_4Cl$ in 1.5 M HCl for ^{15}N (external). Water suppression was achieved by presaturation. 2D [^1H,^{15}N] HSQC NMR spectra were optimized for ^1J(N,H) = 72 Hz. Spectra were processed using XWINNMR (Version 3.5, Bruker UK Ltd).

Kinetic Measurements: For kinetic analysis of NMR spectra, peak volumes were measured and the relative concentrations of each species were calculated at each time point. The appropriate differential equations were integrated numerically, and the rate constants were determined with the assistance of Dr. Junyong Zhang (University of Western Australia) by a non-linear optimization procedure using the program SCIENTIST (version 2.01, MicroMath Inc.).

For the reaction of ^{15}N-AMD443 with 5'-GMP (shown in Scheme 7.1), and assuming that at time t the concentrations of species a, b, c, d, e, Cl^- and 5'-GMP are A, B, C, D, E, CL and L, respectively, the corresponding reaction rates are:

$$A' = -k_1 \cdot A + k_2 \cdot B \cdot CL$$

$$B' = k_1 \cdot A - k_2 \cdot B \cdot CL - k_3 \cdot B \cdot L$$

$C' = k_3 \cdot B \cdot L - k_4 \cdot C$

$D' = k_4 \cdot C - k_5 \cdot D \cdot L$

$E' = k_5 \cdot D \cdot L$

$CL' = k_1 \cdot A - k_2 \cdot B \cdot CL + k_4 \cdot C$

$L' = -k_3 \cdot B \cdot L - k_5 \cdot D \cdot L$

The above model equations were used in least squares fitting of the NMR data (the change of concentration of each species with time), with a set of initial parameters chosen to perform the simulations.

7.4 Results

Reaction of *trans*-[$PtCl_2(^{15}NH_3)$(2-pic)] and 5'-GMP

Both 1D ^1H and 2D [^1H,^{15}N] HSQC NMR spectroscopy were used to monitor the reactions between *trans*-[$PtCl_2(^{15}NH_3)$(2-pic)] (3 mM) and 5'-GMP in a 1:2 ratio at 298 K and pH 6.4. Figure 7.1 shows the aromatic region of a selection of 1D ^1H spectra recorded at different time intervals after the start of the reaction. The H8 peak of free 5'-GMP gradually diminishes in intensity while three new H8 peaks emerge. The mono-adduct, represented by the new peaks **c** and **d**, is gradually converted to the bis-adduct represented by peak **e**.

Three cross-peaks were present in the initial 2D [^1H,^{15}N] HSQC NMR spectrum. Spectra recorded 0.6 h and 24.3 h after the start of the reaction are shown in Figure 7.2. The ^1H-^{15}N cross-peaks representing the different species are all well separated and easily integrated. The most intense peak, **a**, at 3.81, -69.39 ppm is *trans*-[$PtCl_2(^{15}NH_3)$(2-pic)]. Peak **a** gradually decreases in intensity and is no longer detectable ca. 24 h after the start of the reaction. Peak **b** at 3.83, -67.47 ppm is known to be the monoaqua monochloro species, as determined previously by NMR pH

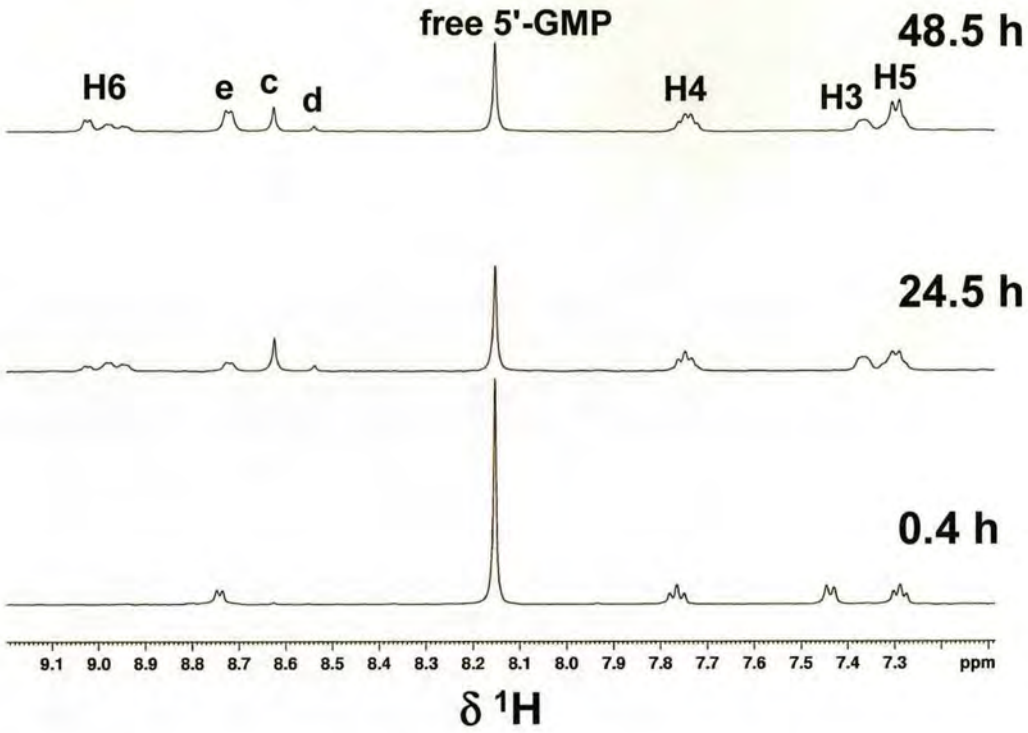

Figure 7.1 Aromatic region of 1D ^{1}H NMR spectra in H_2O/D_2O for the reaction between *trans*-[$PtCl_2(^{15}NH_3)$(2-pic)] and 5'-GMP (1:2) at selected reaction times (298 K). Peaks **c**, **d** and **e** are assigned to the H8 peaks of *trans*-[$PtCl(^{15}NH_3)$(2-pic)(5'-GMP)]$^{+}$, *trans*-[$Pt(H_2O)(^{15}NH_3)$(2-pic)(5'-GMP)]$^{2+}$ and *trans*-[$Pt(^{15}NH_3)$(2-pic)(5'-$GMP)_2$]$^{2+}$, respectively. **H3-H6** correspond to the aromatic protons of the 2-picoline ligand.

titration (Chapter 3). Peak **b** behaves as an intermediate as its intensity increases initially and then decreases steadily until ca. 15 h when it is no longer detectable. The least intense peak **c** is assigned as the monochloro mono(5'-GMP) adduct on the basis of its reaction profile. Peak **c** increases in intensity for the first 10 h of the reaction and then its intensity steadily decreases as that of peak **e** increases. Peak **d** at 4.10, -64.46 ppm begins to emerge ca. 3 h after the start of the reaction and is assigned as the monoaqua mono(5'-GMP) adduct. Peak **d** increases in intensity initially but levels off ca. 12 h after the start of the reaction. Peak **e** at 4.41, -63.87

ppm is observable ca. 6 h after the start of the reaction and is assigned as the bis(5'-GMP) adduct. This assignment was made on the basis of the reaction profile and from a previous ^{1}H and [^{1}H,^{15}N] NMR characterisation of *trans*-[$Pt(NH_3)(2\text{-pic})(5'\text{-GMP})_2$]$(NO_3)_2$. Peak **e** gradually increases in intensity throughout the reaction.

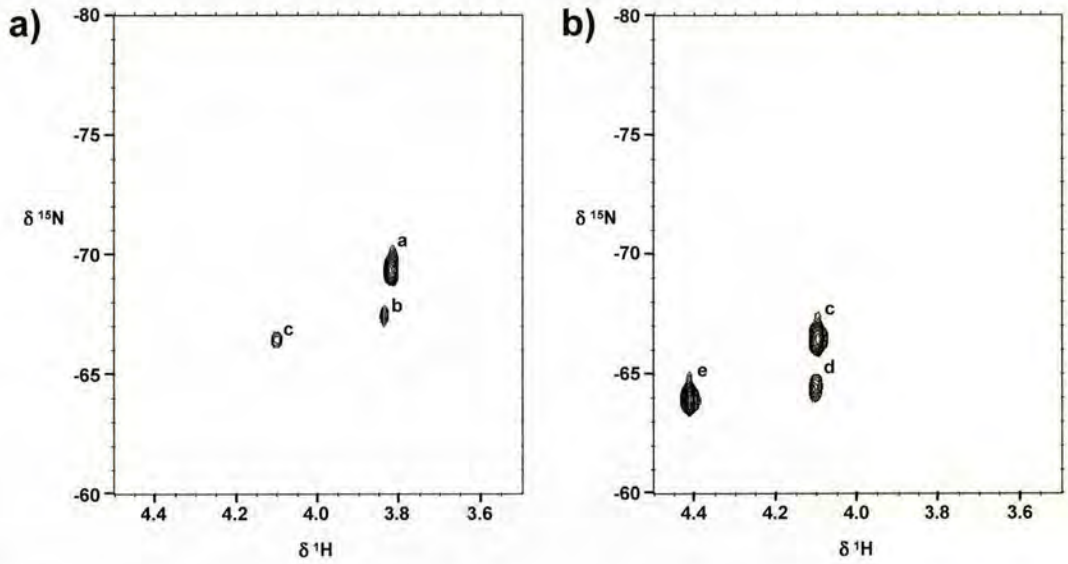

Figure 7.2 2D [^{1}H,^{15}N] HSQC spectra for the reaction between *trans*-[$PtCl_2(^{15}NH_3)$(2-pic)] and 5'-GMP (298 K) a) 0.6 h and b) 24.3 h after the start of the reaction. Peak assignments: **a** = *trans*-[$PtCl_2(^{15}NH_3)$(2-pic)], **b** = *trans*-[$PtCl(H_2O)(^{15}NH_3)$(2-pic)]$^{+}$, **c** = *trans*-[$PtCl(^{15}NH_3)$(2-pic)(5'-GMP)]$^{+}$, **d** = *trans*-[$Pt(H_2O)(^{15}NH_3)$(2-pic)(5'-GMP)]$^{2+}$ and **e** = *trans*-[$Pt(^{15}NH_3)$(2-pic)$(5'\text{-GMP})_2$]$^{2+}$.

A kinetic fit to the reaction profile in Scheme 7.1 is shown in Figure 7.3 and the rate constants for each step are listed in Table 7.1. The data are consistent with initial hydrolysis of the chloride ligand followed by 5'-GMP substitution in two steps to give the final bis(5'-GMP) product.

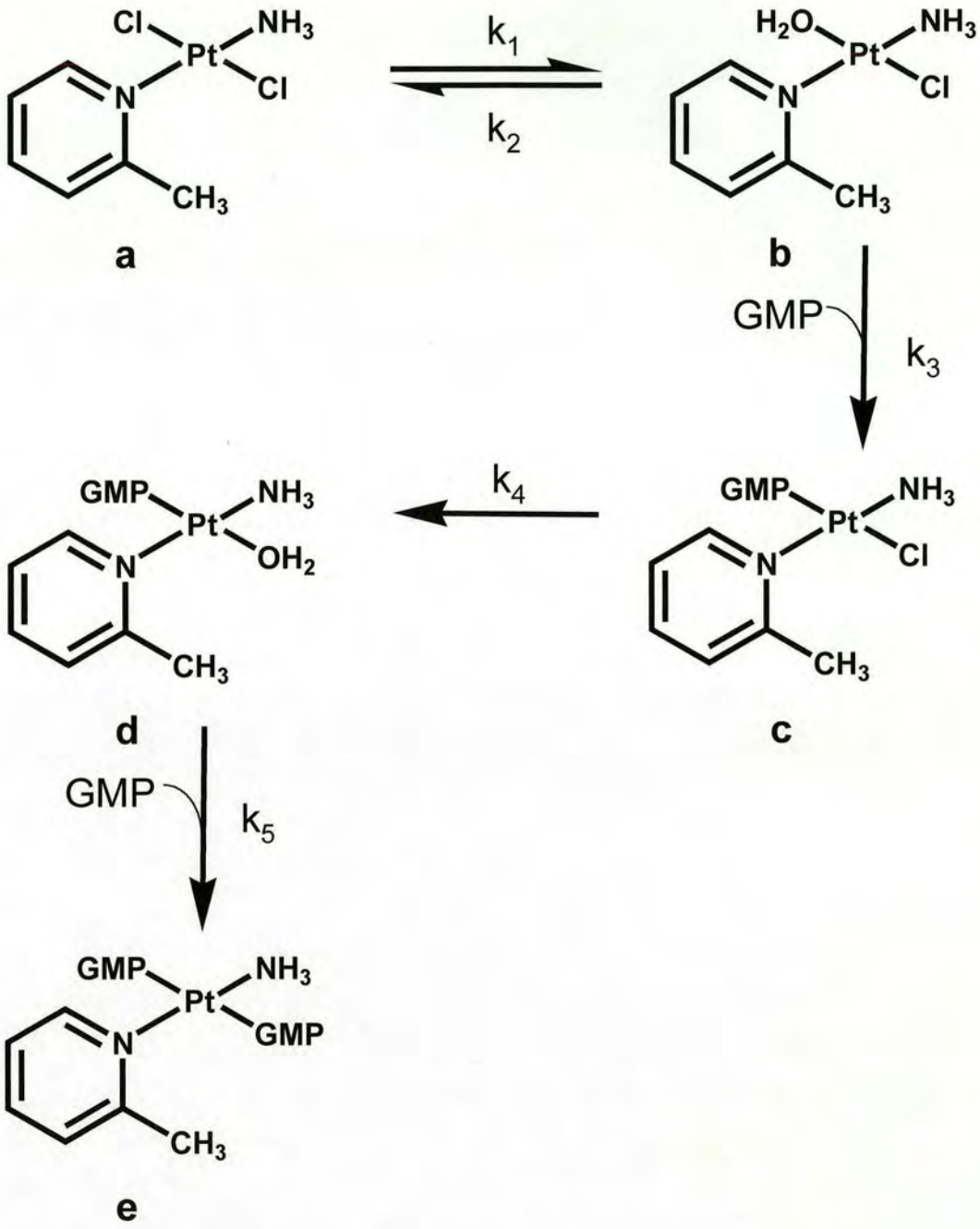

Scheme 7.1 Pathway for the reaction between *trans*-[$PtCl_2(^{15}NH_3)$(2-pic)] and 5'-GMP. The corresponding rate constants are listed in Table 7.1. Charges on complexes are omitted.

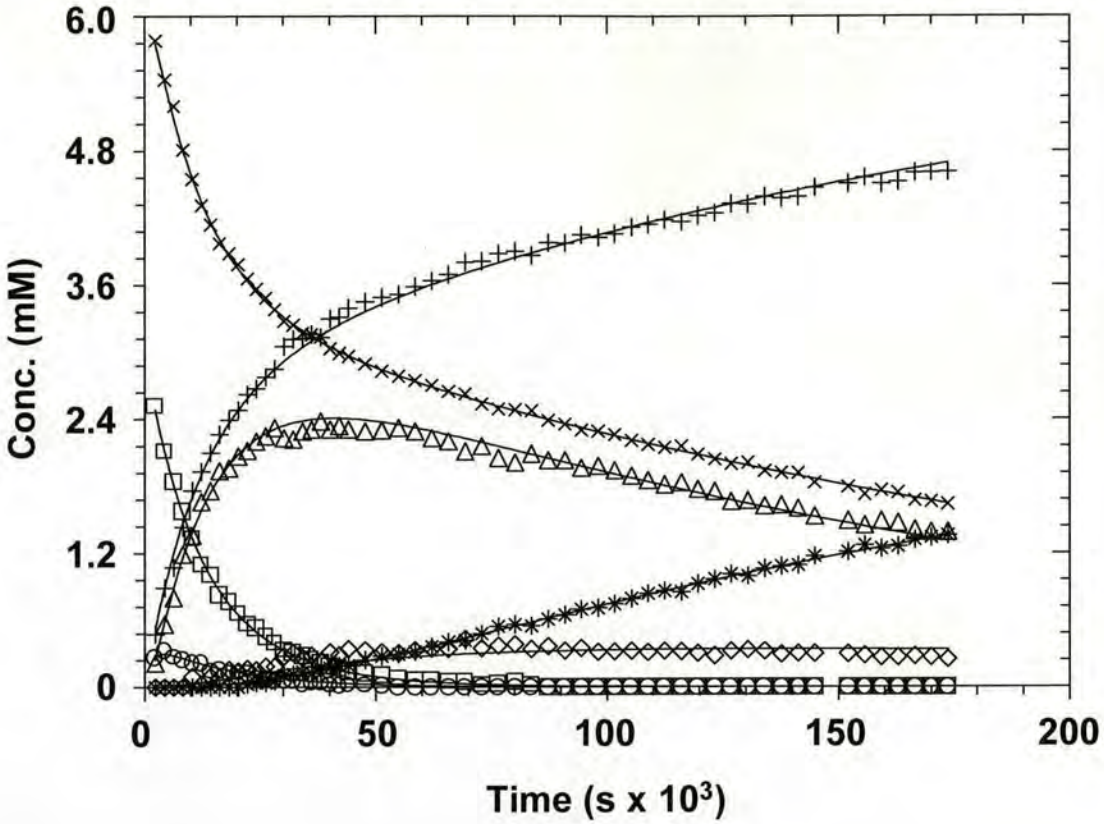

Figure 7.3 Computer best fits based on the rate constants in Table 7.1 and experimental NMR points for the time course of the reaction between *trans*-[$PtCl_2(^{15}NH_3)$(2-pic)] and 5'-GMP (298 K). Symbols represent calculated data for 5'-GMP (x) and Cl^- (+), and experimental data based on integration of 2D cross-peaks for a = *trans*-[$PtCl_2(^{15}NH_3)$(2-pic)] (□), b = *trans*-[$PtCl(H_2O)(^{15}NH_3)$(2-pic)]$^+$ (○), c = *trans*-[$PtCl(^{15}NH_3)$(2-pic)(5'-GMP)]$^+$ (△), d = *trans*-[$Pt(H_2O)(^{15}NH_3)$(2-pic)(5'-GMP)]$^{2+}$ (◇), e = *trans*-[$Pt(^{15}NH_3)$(2-pic)$(5'\text{-GMP})_2$]$^{2+}$ (∗).

Table 7.1 Rate constants for the reaction of *trans*-[$PtCl_2(^{15}NH_3)$(2-pic)] with 5'-GMP at 298 K (0.1 M $NaClO_4$), see Scheme 7.1.

Step	Rate Constant
k_1 (s^{-1})	8.25×10^{-5}
k_2 ($M^{-1}s^{-1}$)	2.46×10^{-2}
k_3 ($M^{-1}s^{-1}$)	1.05×10^{-1}
k_4 (s^{-1})	5.28×10^{-6}
k_5 ($M^{-1}s^{-1}$)	1.28×10^{-2}

Reaction of *trans*-[$PtCl_2(^{15}NH_3)$(2-pic)] with GSH

The reaction of *trans*-[$PtCl_2(^{15}NH_3)$(2-pic)] (3 mM) with GSH (1:2, pH 7.1) at 298 K was followed by 2D [^1H,^{15}N] HSQC NMR spectroscopy. In the initial [^1H,^{15}N] HSQC spectrum recorded ca. 0.6 h after the start of the reaction there are six cross-peaks present (Figure 7.4). The intense peak **2a**, at 3.82, -69.36 ppm, is *trans*-[$PtCl_2(^{15}NH_3)$(2-pic)] and its intensity decreases steadily until ca. 9 h when it becomes undetectable. Peak **2b** at 3.66, -68.24 ppm is unassigned but increases in intensity slightly throughout the reaction, though even at the end of the reaction it accounts for only ca. 6 % of the total Pt – $^{15}NH_3$ species. Peak **2c** at 3.87, -64.65 ppm increases in intensity for ca. 35 h and then experiences a sudden decrease in intensity, coincident with a similarly sharp increase in intensity of peak **2d**. Peak **2d** at 3.90, -64.29 ppm increases in intensity to become the major reaction product, accounting for ca. 38 % of the total Pt – $^{15}NH_3$ species at the end of the reaction. It seems plausible that peak **2d** may correspond to *trans*-[$Pt(^{15}NH_3)$(2-pic)$(GS)_2$]. Peak **2e** at 3.94, -64.31 ppm increases in intensity initially and then appears to level off ca. 20 h after the start of the reaction. Peak **2f** at 3.99, -65.05 ppm behaves as a typical intermediate such as *trans*-[$PtCl(^{15}NH_3)$(2-pic)(GS)], with its intensity increasing for the first 6 h of reaction and then decreasing steadily. Peak **2g** at 4.36, -59.28 ppm appears ca. 5 h after the start of the reaction and its intensity initially increases until ca. 10 h and then decreases slightly. After 5 h of reaction, peaks **2h** (4.45, -60.11 ppm) and **2i** (4.47, -58.89) also appear. Peak **2h** behaves as an intermediate and is consumed within 20 h of the reaction whilst peak **2i** seems to maintain a very low and almost constant intensity. The unassigned peaks are presumably all GSH adducts.

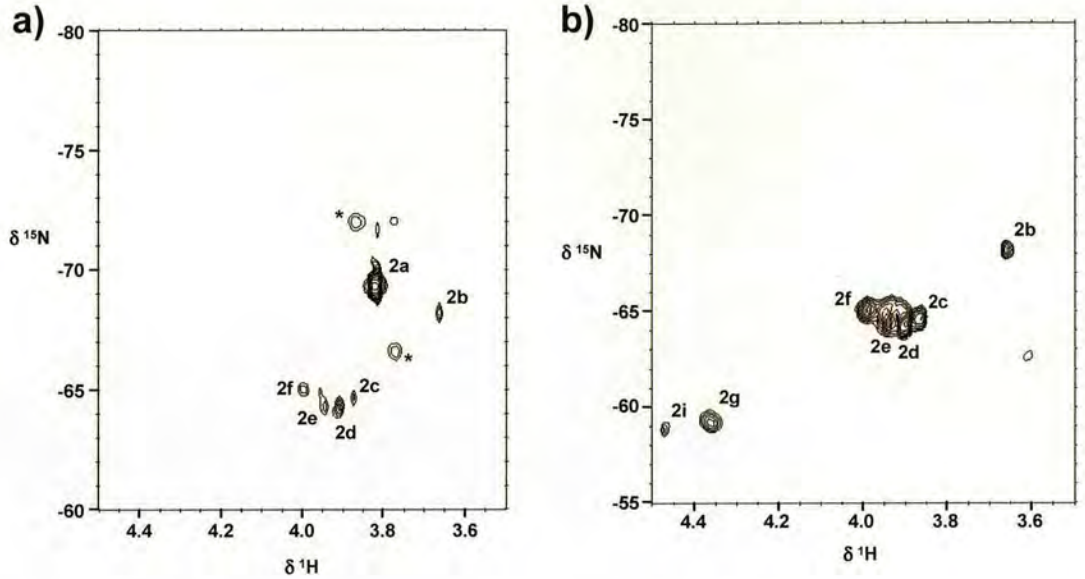

Figure 7.4 2D [^{1}H,^{15}N] HSQC spectra for the reaction between *trans*-[$PtCl_2(^{15}NH_3)$(2-pic)] and GSH (298 K) a) 0.6 h, and b) 24.2 h after the start of the reaction. **2a** = *trans*-[$PtCl_2(^{15}NH_3)$(2-pic)], * = ^{195}Pt satellites.

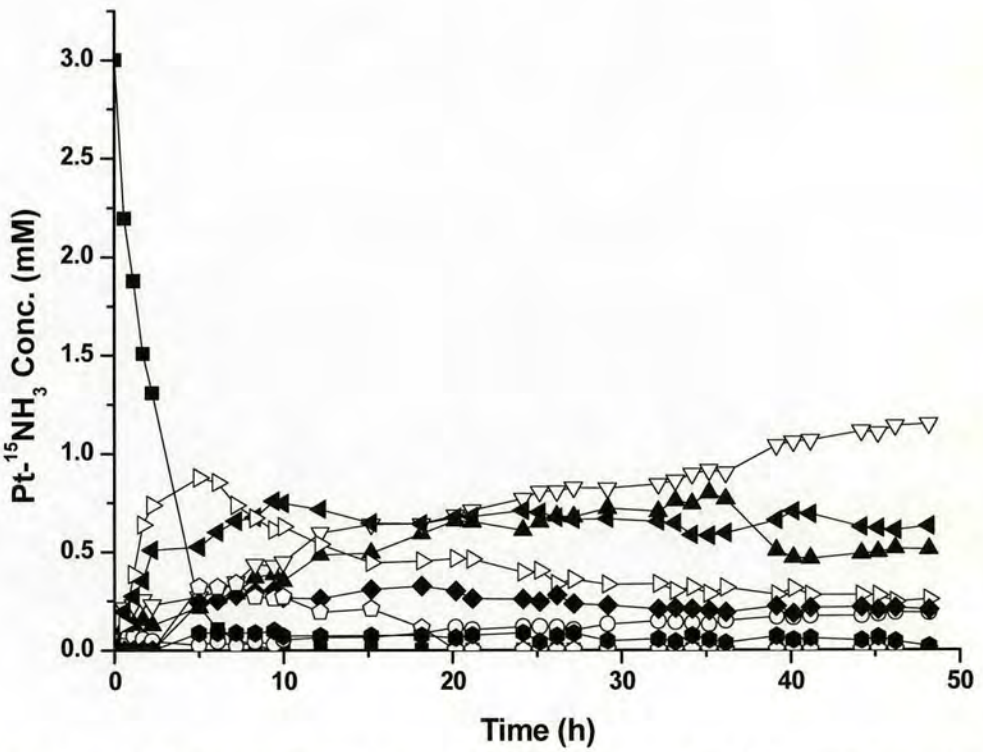

Figure 7.5 Concentration versus time profile for the reaction of *trans*-[$PtCl_2(^{15}NH_3)$(2-pic)] and GSH at 298 K. (■) peak **2a**, (○) peak **2b**, (▲) peak **2c**, (▽) peak **2d**, (◀) peak **2e**, (▷) peak **2f**, (◆) peak **2g**, (⬠) peak **2h**, (⬢) peak **2i** (see Figure 7.4).

Intriguingly, no cross-peak corresponding to the monoaqua monochloro species was observed, implying that the reactions may proceed directly with the dichloro species or that any monoaqua monochloro species is being consumed as soon as it is produced.

The concentration versus time profiles for the major species in the reaction are shown in Figure 7.5.

Reaction of *trans*-[$PtCl_2(^{15}NH_3)$(2-pic)] with GSH and 5'-GMP

The reaction of *trans*-[$PtCl_2(^{15}NH_3)$(2-pic)] (2 mm) with GSH in the presence of 5'-GMP (1:2:2) was followed by 2D [^1H,^{15}N] HSQC NMR spectroscopy at 298 K, pH 7.0. Spectra recorded after 0.6 h and 24.2 h of reaction are shown in Figure 7.6.

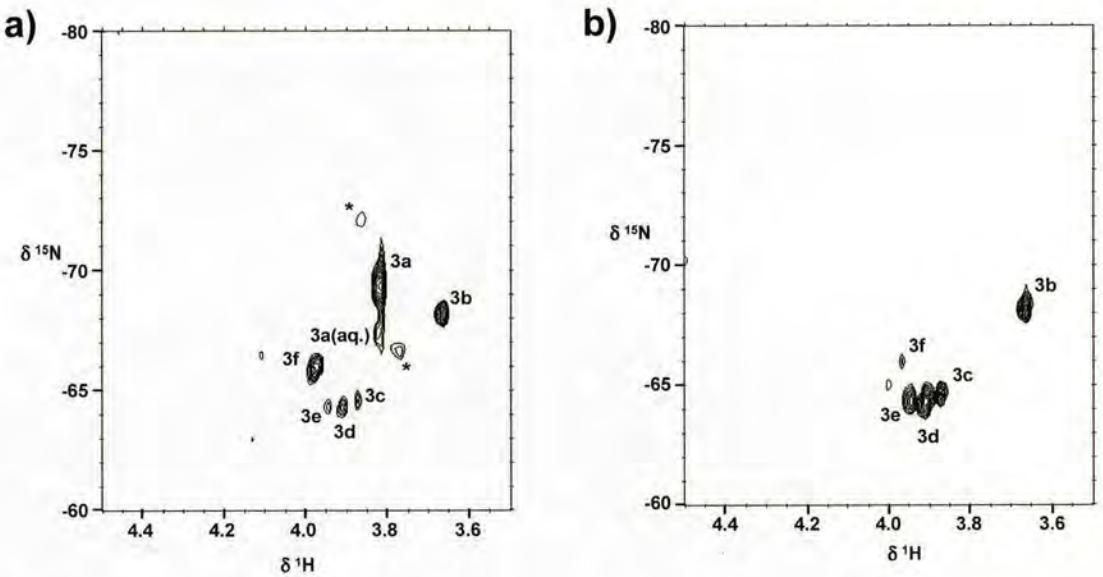

Figure 7.6 2D [^1H,^{15}N] HSQC spectra for the reaction between *trans*-[$PtCl_2(^{15}NH_3)$(2-pic)] and 5'-GMP and GSH (298 K) a) 0.6 h, and b) 24.2 h after the start of the reaction. **3a** = *trans*-[$PtCl_2(^{15}NH_3)$(2-pic)], **3a(aq.)** = *trans*-[$PtCl(OH_2)(^{15}NH_3)$(2-pic)]$^+$, * = ^{195}Pt satellites.

In the initial spectrum the most intense peak **3a**, at 3.81, -69.36 ppm, corresponds to *trans*-[$PtCl_2(^{15}NH_3)$(2-pic)] and its intensity decreases to zero within

5 h of the start of the reaction. A further six cross-peaks are present initially. Peak **3a(aq.)** at 3.82, -67.46 ppm is attributable to *trans*-[$PtCl(OH_2)(^{15}NH_3)$(2-pic)]$^+$. This peak is very weak and is no longer observable after only 2 h. Peak **3b** at 3.66, -68.25 ppm is the same as peak **2b** from the reaction of *trans*-[$PtCl_2(^{15}NH_3)$(2-pic)] and GSH. Its intensity increases throughout the reaction but in this case peak **3b** accounts for ca. 35 % of the total Pt – $^{15}NH_3$ species at the end of the reaction compared to ca. 6 % in the *trans*-[$PtCl_2(^{15}NH_3)$(2-pic)] and GSH reaction. Likewise, peaks **3c** (3.87, -64.59 ppm), **3d** (3.90, -64.31 ppm), **3e** (3.94, -64.35 ppm) and **3f** (3.97, -65.92 ppm) correspond to peaks **2c**, **2d**, **2e** and **2f**, respectively, from the reaction of *trans*-[$PtCl_2(^{15}NH_3)$(2-pic)] with GSH. The reaction profiles are also comparable, with peak **3d** as the major reaction product, assumed to be *trans*-[$Pt(^{15}NH_3)$(2-pic)$(GS)_2$], accounting for ca. 39 % of the total Pt – $^{15}NH_3$ species at the end of the reaction and peaks **3c** and **3e** increasing initially and then leveling off. It is noteworthy however, that in this reaction peak **3f**, tentatively assigned as *trans*-[$PtCl(^{15}NH_3)$(2-pic)(GS)], is entirely consumed ca. 36 h after the start of the reaction whereas in the reaction of *trans*-[$PtCl_2(^{15}NH_3)$(2-pic)] with GSH, peak **2f** accounts for ca. 9 % of the total Pt – $^{15}NH_3$ species at the end of the reaction. After ca. 2 h a peak at 3.99, -65.07 ppm, peak **3g**, appears. This peak behaves as an intermediate, increasing in intensity until ca. 5 h then decreasing gradually to zero at ca. 35 h. A very weak peak **3h** at 4.09, -66.70 ppm is also observed after ca. 2h. This peak resembles peak **c**, the monochloro mono(5'-GMP) adduct, from the reaction of *trans*-[$PtCl_2(^{15}NH_3)$(2-pic)] and 5'-GMP. Its intensity increases slightly until ca. 5 h when it begins to decrease and disappears ca. 35 h after the start of the reaction. At its maximum intensity, peak **3h** accounts for only ca. 6 % of the total Pt – $^{15}NH_3$ species.

The concentration versus time profiles for the major species in the reaction are shown in Figure 7.7.

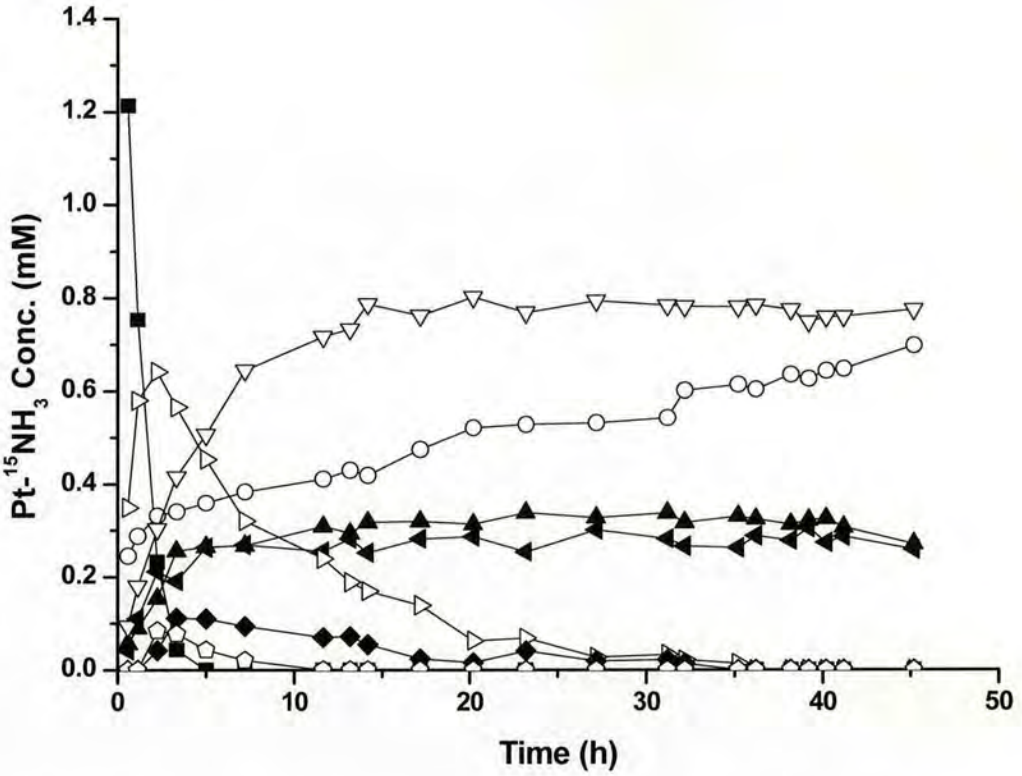

Figure 7.7 Concentration versus time profile for the reaction of *trans*-[$PtCl_2(^{15}NH_3)$(2-pic)] and 5'-GMP and GSH at 298 K. (■) peak **3a**, (○) peak **3b**, (▲) peak **3c**, (▽) peak **3d**, (◀) peak **3e**, (▷) peak **3f**, (◆) peak **3g**, (⬠) peak **3h** (see Figure 7.6).

Reaction of *cis*-[$PtCl_2(^{15}NH_3)$(2-pic)] and ^{15}N-L-MetH

The reaction of *cis*-[$PtCl_2(^{15}NH_3)$(2-pic)] (5 mM) and ^{15}N-L-MetH in a 1:1 molar ratio at pH 6.2 and 298 K was followed by 2D [^{1}H,^{15}N] NMR spectroscopy for a period of 24 h. In the initial [^{1}H,^{15}N] spectrum, recorded 0.5 h after the start of the reaction (Figure 7.8), there are three cross-peaks present. Peak **4a** at 4.20, -66.89 ppm is the most intense peak and corresponds to *cis*-[$PtCl_2(^{15}NH_3)$(2-pic)]. This peak exponentially decreases in intensity and appears to reach an equilibrium ca. 23 h after the start of the reaction. Peak **4b** at 4.54, -61.68 ppm is consistent with

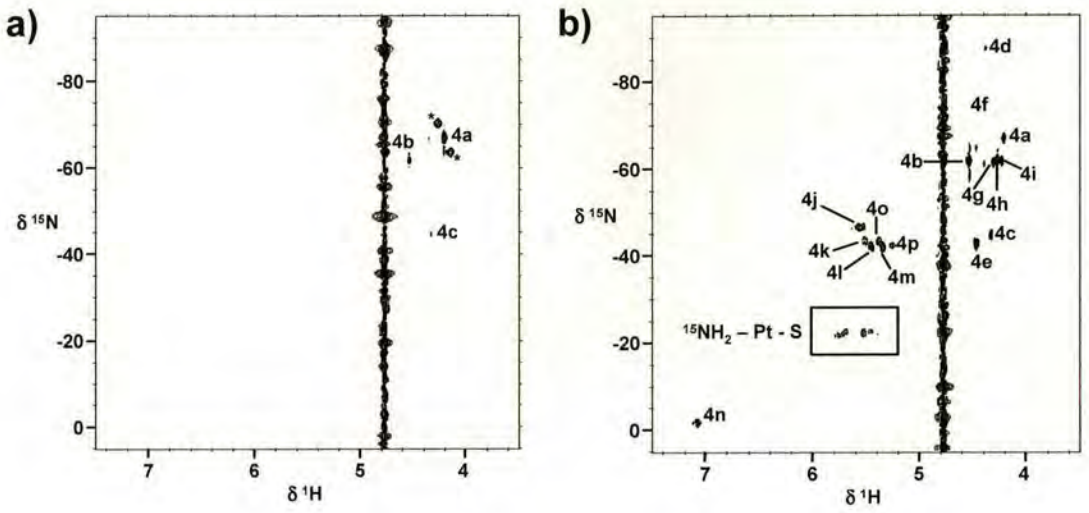

Figure 7.8 2D [^{1}H,^{15}N] HSQC spectra for the reaction between *cis*-[$PtCl_2(^{15}NH_3)$(2-pic)] and ^{15}N-L-MetH (298 K, pH 6.2) a) 0.5 h, and b) 24.2 h after the start of the reaction. **4a** = *cis*-[$PtCl_2(^{15}NH_3)$(2-pic)], **4b** = *cis*-[$PtCl(OH_2)(^{15}NH_3)$(2-pic)]$^{+}$, **4d** = *cis*-[$PtCl(OH_2)(^{15}NH_3)$(2-pic)]$^{+}$, **4n** = NH_4^{+}, * = ^{195}Pt satellites.

assignment to *cis*-[$PtCl(OH_2)(^{15}NH_3)$(2-pic)]$^{+}$, with a ^{15}N shift diagnostic of ^{15}N *trans* to N or Cl, i.e. the water ligand is *trans* to the 2-picoline. This peak gradually increases in intensity but seems to reach a maximum intensity ca. 10 h after the start of the reaction and then decreases slightly in intensity. This peak is the major reaction product and accounts for ca. 25 % of the Pt-^{15}N species at the end of the reaction. The third peak, **4c**, at 4.33, -44.77 ppm is initially relatively weak in intensity and is unassigned, but its intensity gradually increases throughout the reaction and it is also a significant product. After 1.6 h of reaction, a weak cross-peak **4d** at 4.35, -87.11 ppm is observable, assigned as *cis*-[$PtCl(OH_2)(^{15}NH_3)$(2-pic)]$^{+}$, with the water ligand *trans* to $^{15}NH_3$ as the ^{15}N shift here is diagnostic of ^{15}N *trans* to O. The intensity of this peak remains very low throughout the course of the reaction. Peak **4h** (4.27, -61.91 ppm), which appears after ca. 3.3 h of reaction, increases in intensity to become one of the significant products. Also notable is the appearance of

an ammonium peak (peak **4n**) at 7.08, -1.54 ppm ca. 6.2 h after the start of the reaction, which can be seen in Figure 7.8.

There are many different species formed in this reaction but their cross-peak intensities remain very low. A list of cross-peaks is given in Table 7.2. Due to the complicated nature of the reaction the concentration versus time profile includes only the major species involved in the reaction, Figure 7.9.

Table 7.2 Proton and ^{15}N chemical shifts for the reaction of *cis*-[$PtCl_2(^{15}NH_3)$(2-pic)] and ^{15}N-L-MetH at pH 6.2, 298 K. Spectra are shown in Figure 7.8.

Peak	δ (^{1}H)	δ (^{15}N) (*trans* to)
4a	4.20	-66.89 (Cl, N)
4b	4.54	-61.68 (Cl, N)
4c	4.33	-44.77 (S)
4d	4.35	-87.11 (O)
4e	4.46	-42.42 (S)
4f	4.44	-64.70 (Cl, N)
4g	4.30	-61.20 (Cl, N)
4h	4.27	-61.91 (Cl, N)
4i	4.22	-61.26 (Cl, N)
4j	5.55	-46.16 (O)
4k	5.46	-43.00 (O)
4l	5.41	-41.78 (O)
4m	5.30	-41.72 (O)
4n	7.08	-1.54
4o	5.34	-42.98 (O)
4p	5.21	-42.03 (O)

The 2D NMR spectrum of the solution was recorded after 7 d at 298 K and the cross-peaks were unchanged. The pH was then raised to 8.8, and the time dependence of the resultant [^{1}H,^{15}N] 2D NMR spectra investigated for a period of 24 h. However, only the first spectrum recorded after 0.5 h (Figure 7.10) yielded

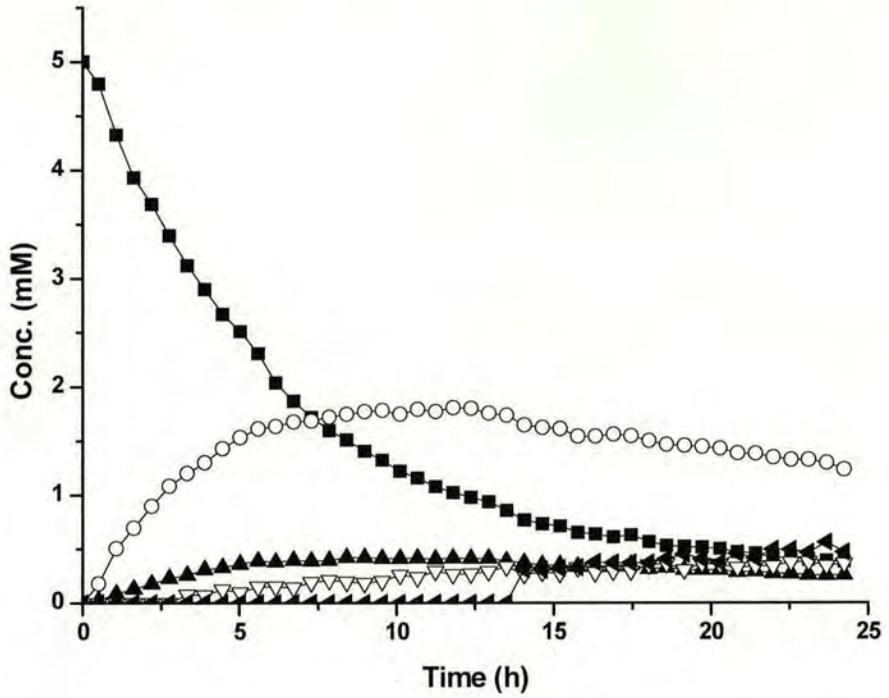

Figure 7.9 Concentration versus time profile for the reaction of *cis*-[$PtCl_2(^{15}NH_3)$(2-pic)] and ^{15}N-L-MetH at 298 K, pH 6.2. (■) peak **4a**, (○) peak **4b**, (▲) peak **4c**, (▽) peak **4h**, (◀) $^{15}NH_2$-Pt-S species, (see Figure 7.8).

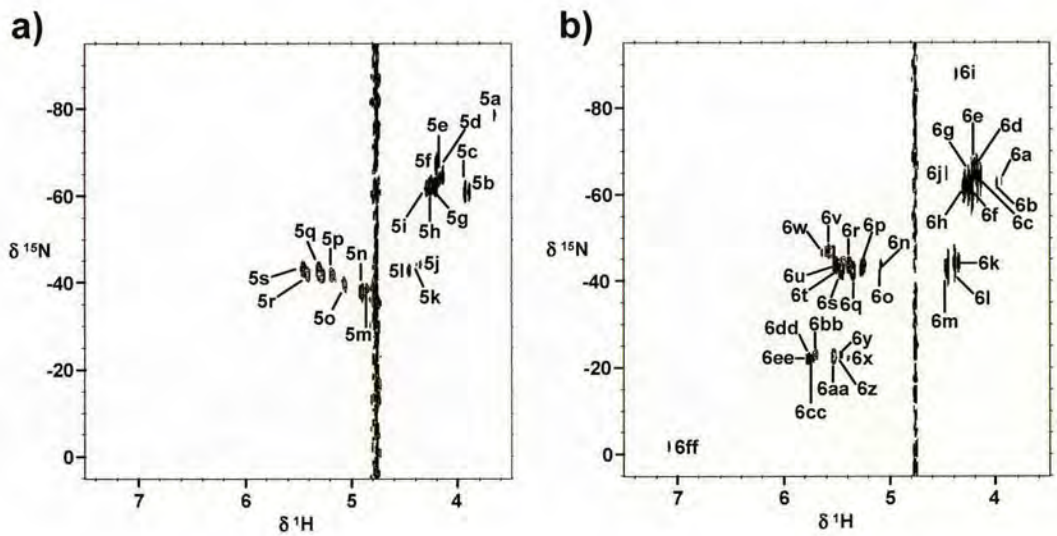

Figure 7.10 2D [^{1}H,^{15}N] HSQC spectra for the reaction between *cis*-[$PtCl_2(^{15}NH_3)$(2-pic)] and ^{15}N-L-MetH (298 K) a) pH 8.8, 0.5 h and b) pH 3.3, 0.7 h after the start of the reaction. Peaks are listed in Tables 7.3 and 7.4.

significant changes and there appeared to be no time dependence of the cross-peaks thereafter. The cross-peaks are listed in Table 7.3.

Table 7.3 Proton and ^{15}N chemical shifts for the reaction of *cis*-[$PtCl_2(^{15}NH_3)$(2-pic)] and ^{15}N-L-MetH at pH 8.8, 298 K, see Figure 7.10.

Peak	δ (^{1}H)	δ (^{15}N) (*trans* to)
5a	3.66	-78.59 (O)
5b	3.89	-60.94 (Cl, N)
5c	3.93	-60.81 (Cl, N)
5d	4.14	-64.65 (Cl, N)
5e	4.17	-63.98 (Cl, N)
5f	4.20	-67.25 (Cl, N)
5g	4.21	-62.10 (Cl, N)
5h	4.26	-62.22 (Cl, N)
5i	4.29	-61.68 (Cl, N)
5j	4.35	-44.15 (S)
5k	4.39	-44.27 (S)
5l	4.46	-42.75 (S)
5m	4.90	-37.91 (Cl, N / O)
5n	4.92	-37.91 (Cl, N / O)
5o	5.06	-39.82 (Cl, N / O)
5p	5.18	-41.81 (O)
5q	5.29	-42.41 (O)
5r	5.41	-42.05 (O)
5s	5.45	-43.17 (O)

The pH of the above solution was then lowered to 3.3 and the time dependence was again followed by [^{1}H,^{15}N] 2D NMR spectroscopy for 24 h at 298 K. Similarly, only the first spectrum, recorded 0.7 h after the change of pH, showed any change in the cross-peaks, Figure 7.10. These peaks are listed in Table 7.4.

Table 7.4 Proton and ^{15}N chemical shifts for the reaction of *cis*-[$PtCl_2(^{15}NH_3)$(2-pic)] and ^{15}N-L-MetH at pH 3.3, 298 K, see Figure 7.10.

Peak	δ (^{1}H)	δ (^{15}N) (*trans* to)
6a	3.95	-63.02 (Cl, N)
6b	3.99	-62.65 (Cl, N)
6c	4.15	-64.11 (Cl, N)
6d	4.18	-63.93 (Cl, N)
6e	4.20	-66.90 (Cl, N)
6f	4.22	-62.04 (Cl, N)
6g	4.27	-62.23 (Cl, N)
6h	4.30	-61.60 (Cl, N)
6i	4.37	-87.85 (O)
6j	4.46	-64.91 (Cl, N)
6k	4.35	-44.26 (S)
6l	4.39	-44.29 (S)
6m	4.46	-42.96 (S)
6n	5.07	-43.68 (O)
6o	5.08	-43.92 (O)
6p	5.25	-43.16 (O)
6q	5.34	-42.31 (O)
6r	5.39	-43.64 (O)
6s	5.45	-42.99 (O)
6t	5.50	-43.59 (O)
6u	5.52	-43.64 (O)
6v	5.57	-46.83 (O)
6w	5.64	-46.50 (O)
6x	5.39	-22.15 (S / Cl, N)
6y	5.45	-22.91 (S / Cl, N)
6z	5.46	-22.91 (S / Cl, N)
6aa	5.23	-22.58 (S / Cl, N)
6bb	5.70	-22.82 (S / Cl, N)
6cc	5.74	-22.00 (S / Cl, N)
6dd	5.76	-22.21 (S / Cl, N)
6ee	5.78	-22.04 (S / Cl, N)
6ff	7.08	-1.96

Reaction of *trans*-[$PtCl_2(^{15}NH_3)$(2-pic)] and ^{15}N-L-MetH

The reaction of *trans*-[$PtCl_2(^{15}NH_3)$(2-pic)] (5 mM) and ^{15}N-L-MetH in a 1:1 molar ratio at pH 6.3 and 298 K was followed by [^{1}H,^{15}N] 2D NMR spectroscopy for a period of ca. 24 h. Spectra recorded after 0.6 h and 24.3 h are shown in Figure 7.11.

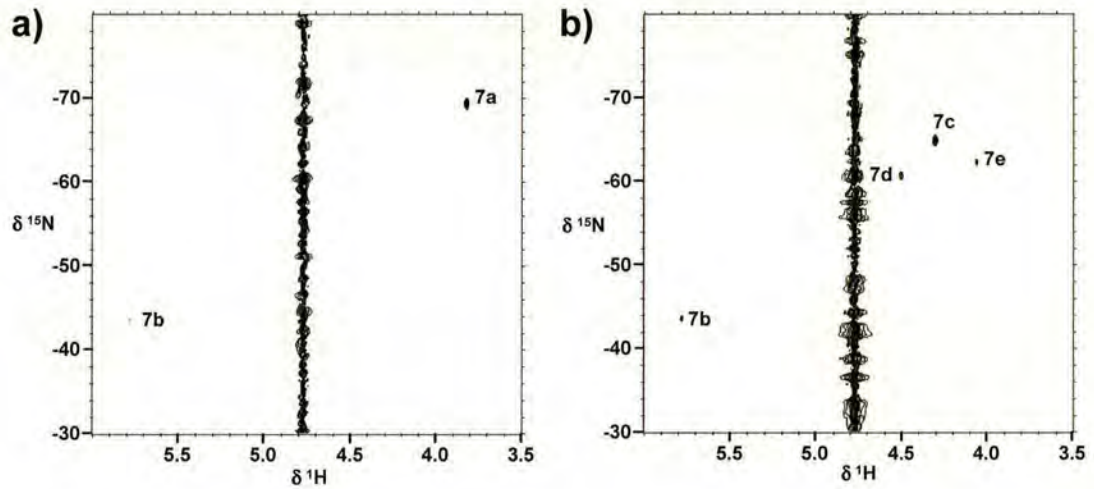

Figure 7.11 2D [^{1}H,^{15}N] HSQC spectra for the reaction between *trans*-[$PtCl_2(^{15}NH_3)$(2-pic)] and ^{15}N-L-MetH (298 K, pH 6.3) a) 0.6 h, and b) 24.3 h after the start of the reaction. **7a** = *trans*-[$PtCl_2(^{15}NH_3)$(2-pic)].

After 0.6 h of reaction only one new cross-peak at 5.78, -43.56 ppm (peak **7b**) was present in the spectrum in addition to cross-peak **7a** (3.82, -69.41 ppm) of the starting complex, *trans*-[$PtCl_2(^{15}NH_3)$(2-pic)]. Peak **7a** decreased in intensity with time and was no longer observable ca. 8 h after the start of the reaction. Peak **7b** initially increased in intensity with time and then ca. 13 h after the start of the reaction, started to decrease slightly in intensity. A third cross-peak, peak **7c** (4.30, -64.78 ppm), appears ca. 1.2 h after the start of the reaction. Due to its shifts, it seems unlikely that this peak is due to hydrolysis products but no definitive assignment can be made. The intensity of this peak increases rapidly for the first 10 h of reaction and then decreases slightly. After 14.9 h of reaction a fourth cross-peak at 4.50, -60.61

ppm, peak **7d** is observed. This peak then increases very slighty in intensity and is the second most intense peak at the end of the reaction. A further cross-peak is observed ca. 15.5 h after the start of the reaction at 4.06, -62.33 ppm (peak **7e**). This peak increases slightly in intensity for the duration of the reaction but remains the least intense peak. The concentration versus time profile is shown in Figure 7.12.

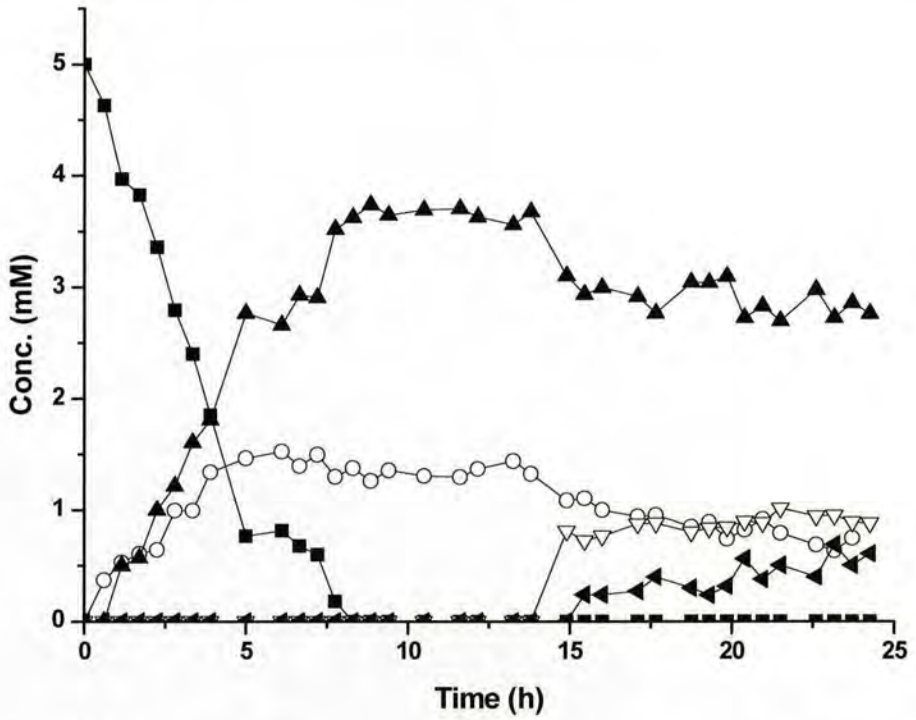

Figure 7.12 Concentration versus time profile for the reaction of *trans*-$[PtCl_2(^{15}NH_3)(2\text{-pic})]$ and ^{15}N-L-MetH at 298 K, pH 6.3. (■) peak **7a**, (○) peak **7b**, (▲) peak **7c**, (▽) peak **7d**, (◀) peak **7e**, (see Figure 7.11).

After one week, the pH of the above solution was raised from 3.4 to 8.5, and the time dependence of the resultant [^{1}H,^{15}N] 2D NMR spectra was investigated for a period of 14 h. In the first spectrum (Figure 7.13), recorded 0.5 h after the pH adjustment, a very intense peak at 4.23, -62.94 ppm (peak **8a**) was present together with a rather weak peak at 4.15, -63.00 ppm (peak **8b**). A further two broad cross-peaks at 5.58, -18.56 ppm and 5.47, -17.54 ppm, peaks **8c** and **8d**, respectively, were

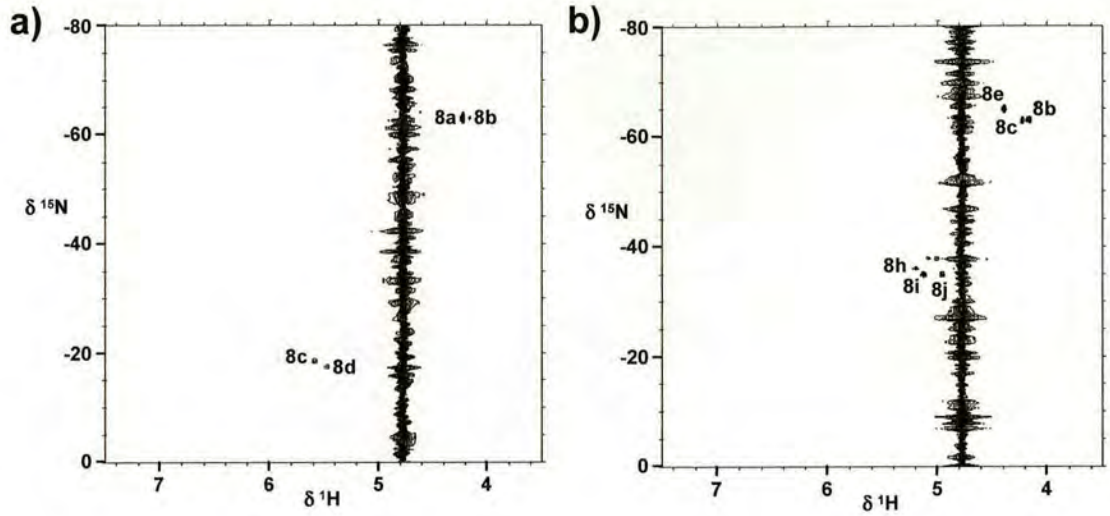

Figure 7.13 2D [^{1}H,^{15}N] HSQC spectra for the reaction between *trans*-[$PtCl_2(^{15}NH_3)$(2-pic)] and ^{15}N-L-MetH (298 K, pH 8.5) a) 0.5 h, and b) 13.1 h after the start of the reaction.

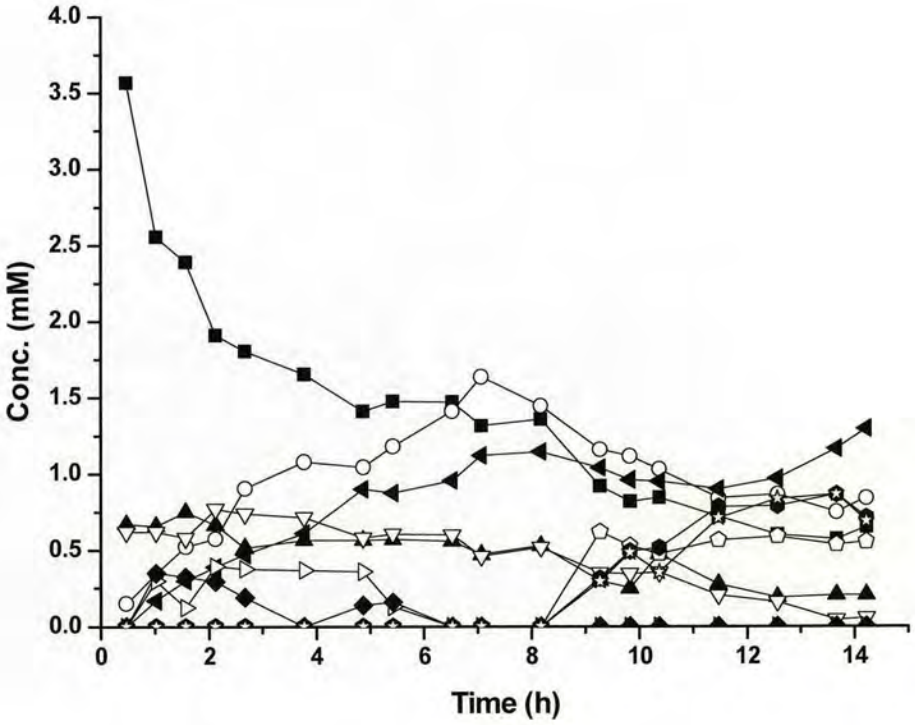

Figure 7.14 Concentration versus time profile for the reaction of *trans*-[$PtCl_2(^{15}NH_3)$(2-pic)] and ^{15}N-L-MetH at 298 K, pH 8.5. (■) peak **8a**, (○) peak **8b**, (▲) peak **8c**, (▽) peak **8d**, (◀) peak **8e**, (▷) peak **8f**, (◆) peak **8g**, (⬠) peak **8h**, (●) peak **8i**, (☆) peak **8j** (see Figure 7.13).

also observed. Peak **8a** decreases in intensity with time whilst peak **8b** increases for the first 7 h and then decreases in intensity. The intensities of both peaks **8c** and **8d** are almost unchanged until ca. 8 h of reaction when they start to decrease slightly. Peak **8e** at 4.39, -64.98 ppm is observable after 1 h of reaction. This peak increases in intensity to become the main reaction product. Two very weak cross-peaks, peak **8f** at 5.30, -17.57 ppm and peak **8g** at 5.19, -18.50 ppm, are also observed at 1 h but they are no longer detectable ca. 6 h after the start of the reaction. After ca. 9 h of reaction three further cross-peaks are observable at 5.20, -36.10 ppm, 5.12, -34.99 ppm and 4.95, -35.14 ppm corresponding to peaks **8h**, **8i** and **8j**, respectively. The intensity of peak **8h** remains relatively constant whilst the intensities of peaks **8i** and **8j** increase. The concentration versus time profile is shown in Figure 7.14.

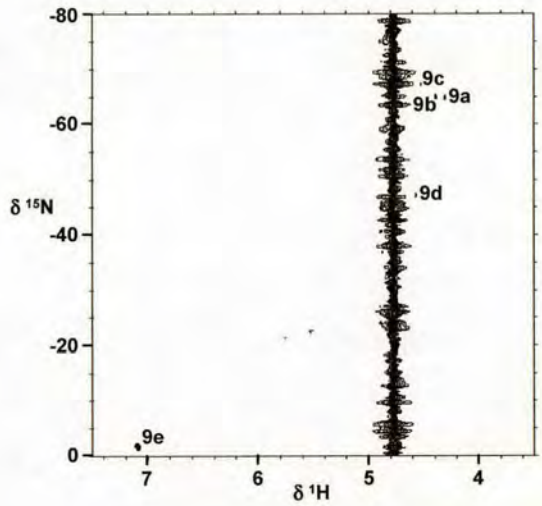

Figure 7.15 2D [^{1}H,^{15}N] HSQC spectrum for the reaction between *trans*-[$PtCl_2(^{15}NH_3)$(2-pic)] and ^{15}N-L-MetH (298 K, pH 3.5) 0.5 h after the start of the reaction. **9e** = $^{15}NH_4^+$.

When the pH of the above solution was lowered to 3.5, there were five clear cross-peaks present in the initial spectrum (Figure 7.15) at 4.30, -64.82 ppm, 4.39, -64.94 ppm, 4.52, -67.23 ppm, 4.57, -47.32 ppm, including an ammonium peak at 7.09, -

1.69 ppm, peaks **9a-9e** respectively. There were also some very broad signals between 5.4 to 5.8 and -20 to -25 ppm, attributable to $^{15}NH_2$-Pt-S species. The progress of the reaction was monitored for 24 h but no changes were observed.

7.5 Discussion

Cis-[$PtCl_2(NH_3)$(2-picoline)] (AMD473) is an exciting new anticancer drug which has a different spectrum of biological activity compared to cisplatin and is active against cisplatin-resistant cell lines and xenographs.[33] Its *trans* isomer, *trans*-[$PtCl_2(NH_3)$(2-picoline)] (AMD443), is also cytotoxic in a variety of cancer cell lines and similarly overcomes cisplatin resistance.[35] Cisplatin is renowned for its severe side-effects, some of which may arise from its interactions with sulfur-containing molecules, for example the dose-limiting nephrotoxicity may be due to the coordination of Pt^{II} to the thiol residues of enzymes in the kidneys.[5] In contrast, *cis*-[$PtCl_2(NH_3)$(2-pic)] exhibits reduced nephrotoxicity.[37] In order to shed light on the chemical reactivity of *trans*-[$PtCl_2(NH_3)$(2-picoline)] and to elucidate the potential roles of both steric hindrance and *trans* geometry, kinetic studies of reactions of *trans*-[$PtCl_2(^{15}NH_3)$(2-pic)] with 5'-GMP and GSH have been made and compared to reported results for its *cis* isomer and related compounds. Also, the reactions of ^{15}N-labelled L-MetH with *cis*-[$PtCl_2(^{15}NH_3)$(2-pic)] and *trans*-[$PtCl_2(^{15}NH_3)$(2-pic)] at a variety of pH values have been investigated.

Reactions with 5'-GMP

The concentration versus time profile for the reaction of *trans*-[$PtCl_2(^{15}NH_3)$(2-pic)] with 5'-GMP fitted well to the reaction mechanism shown in Scheme 7.1, confirming that it is two-step and two-stage: initial hydrolysis followed by 5'-GMP substitution to give the 1:1 Pt-5'-GMP adduct, and then further hydrolysis

and 5'-GMP substitution to give the final product, the bis(5'-GMP) complex. The rate of the first step is similar to that determined previously for hydrolysis of *trans*-$[PtCl_2(^{15}NH_3)(2\text{-pic})]$ (Chapter 3). Compared to the rate constant for the second stage of binding of 5'-GMP to *cis*-$[Pt(NH_3)_2(5'\text{-GMP})(H_2O)]^{2+}$ (298 K, 0.24 $M^{-1}s^{-1}$),[38] that of *trans*-$[PtCl_2(NH_3)(2\text{-pic})]$ is an order of magnitude smaller. Also, for comparison, rate constants for *trans*-$[PtCl_2(NH_3)(2\text{-pic})]$ and related compounds are listed in Table 7.5.[34, 39, 40] As expected, *trans*-$[PtCl_2(NH_3)(2\text{-pic})]$ tends to react faster than its *cis* isomer, except for the second hydrolysis step.[34] This suggests that NH_3 has a higher *trans* effect than N7 of GMP. Sletten et al. have also reported that the second chloride ligand in *trans*-EE monofunctional adducts is not easily displaced.[39] Despite the slower hydrolysis of the first chloride in *trans*-$[PtCl_2(NH_3)(2\text{-pic})]$, the rate of monofunctional binding with GMP is comparable in magnitude to those of *trans*-$[PtCl_2\{E\text{-HN=C(OMe)Me}\}_2]$ (*trans*-EE)[39] and *trans*-$[PtCl_2(NH_3)(c\text{-}C_6H_{11}NH_2)]$.[40] The rate of formation of the bis-adduct is also comparable with *trans*-$[PtCl_2(NH_3)(c\text{-}C_6H_{11}NH_2)]$, though that of *trans*-EE is particularly slow.

Table 7.5 Rate constants for the reactions of *trans*-$[PtCl_2(NH_3)(2\text{-pic})]$ (AMD443), *cis*-$[PtCl_2(NH_3)(2\text{-pic})]$ (AMD473), *trans*-$[PtCl_2(NH_3)(c\text{-}C_6H_{11}NH_2)]$ and *trans*-$[PtCl_2\{E\text{-HN=C(OMe)Me}\}_2]$ (*trans*-EE) with GMP.

	AMD443[a] (298 K)	AMD473[b] (296 K)	*trans*-EE[c] (298 K)	*trans*-$C_6H_{11}NH_2$[d] complex (310 K)
k_1	8.25×10^{-5} s^{-1}	6.87, 5.87×10^{-6} s^{-1}	1.95×10^{-4} s^{-1}	1.89×10^{-4} s^{-1}
k_2	0.03 $M^{-1}s^{-1}$	-	0.08 $M^{-1}s^{-1}$	-
k_3	0.11 $M^{-1}s^{-1}$	7.97, 6.67×10^{-3} $M^{-1}s^{-1}$	0.27 $M^{-1}s^{-1}$	0.19 $M^{-1}s^{-1}$
k_4	5.28×10^{-6} s^{-1}	8.53, 2.77×10^{-5} s^{-1}	1.31×10^{-5} $M^{-1}s^{-1}$	2.91×10^{-5} s^{-1}
k_5	0.01 $M^{-1}s^{-1}$	4.2, 0.59×10^{-2} $M^{-1}s^{-1}$	9.96×10^{-3} $M^{-1}s^{-1}$	0.043 $M^{-1}s^{-1}$

[a] This work. [b] Ref.34. There are two rate constants for each step depending on whether substitution occurs *cis* or *trans* to the 2-picoline ligand. [c] Ref. 39. [d] Ref. 40.

Reactions with GSH

The reactions of cisplatin and related platinum compounds with S-containing nucleophiles usually occur via direct substitution without prior aquation,[5] as observed for methionine, GSH and metallothionein.[41-43] The present work confirms that GSH mainly reacts directly with *trans*-$[PtCl_2(NH_3)(2\text{-pic})]$. On the contrary, the reaction of *cis*-$[PtCl_2(NH_3)(2\text{-pic})]$ with GSH was found to proceed via hydrolysis.[34] In light of the current results, it seems likely that this is due to the steric hindrance of *cis*-$[PtCl_2(NH_3)(2\text{-pic})]$[44] whereby binding of GSH is slowed down and hydrolysis is fast enough to compete with direct substitution.

The major product from reaction of cysteine derivatives with *cis*-diam(m)inoplatinum(II) complexes is thought to be the bridged dimer $[(am)_2Pt(\mu_2\text{-}SR)_2Pt(am)_2]$, where am is am(m)ine or one half of a diamine.[45, 46] These bridged complexes are unlikely to be reactive towards DNA bases, although the ammine complexes can slowly release ammonia. Investigations of the reaction of cisplatin with GSH[13, 45, 47] indicate that initially intermediate species such as *cis*-$[PtCl(NH_3)_2(GS)]$ and $[Pt_2(NH_3)_4(GS)_2]$ can indeed be formed. These unstable products lose NH_3 upon standing, eventually forming polymeric $[Pt(GS)_2]_n$ with coordination exclusively via the S atom, but with several different Pt – S and Pt – S – Pt environments.

The reaction of transplatin with two equivalents of GSH[47] results in the bis-substituted complex *trans*-$[Pt(NH_3)_2(SG)_2]$ in which glutathione is coordinated exclusively via the S atom. *Trans*-$[PtCl(NH_3)_2(SG)]$ was found in the first step and reacted either with GSH to form *trans*-$[Pt(NH_3)_2(SG)_2]$, or with *trans*-$[PtCl_2(NH_3)_2]$ to give the S-bridged complex *trans*-$[\{(NH_3)_2PtCl\}_2SG]^+$. This reacted with GSH

regenerating *trans*-[PtCl(NH_3)$_2$(SG)]. On this basis, peaks **d** and **f** (Figure 7.4) may therefore be tentatively assigned as *trans*-[Pt($^{15}NH_3$)(2-pic)(SG)$_2$] and *trans*-[PtCl($^{15}NH_3$)(2-pic)(SG)], respectively.

No rate constants were determined for the reaction of *trans*-[PtCl$_2$($^{15}NH_3$)(2-pic)] with GSH due to its complicated nature, but the time-dependent plot (Figure 7.5) showed that *trans*-[PtCl$_2$($^{15}NH_3$)(2-pic)] was quickly consumed to produce several different GSH adducts.

Competitive binding of GSH and 5'GMP

At neutral pH, GMP cannot usually compete with thiols for binding to Pt^{II} when both ligands are present at equal concentrations.[15] Likewise, for the reaction of *trans*-[PtCl$_2$($^{15}NH_3$)(2-pic)] with GSH and 5'GMP, the majority of products were almost identical to those observed in the absence of nucleotide. However, a weak peak (peak **h**, 4.09, -66.70 ppm) possibly attributable to the monochloro mono(5'-GMP) adduct was surprisingly observed. This adduct is normally formed via prior aquation. The corresponding cross-peak for *trans*-[PtCl(OH_2)($^{15}NH_3$)(2-pic)]$^+$ was identified at 3.82, -67.46 ppm, peak **3a(aq.)**, but its intensity is very low and the peak is no longer observable after 2 hours. The presence of this peak is unexpected in this reaction when no such peak was observed in the reaction of *trans*-[PtCl$_2$($^{15}NH_3$)(2-pic)] with GSH. It is possible that this may have arisen because *trans*-[PtCl$_2$($^{15}NH_3$)(2-pic)] underwent aquation even before addition of the other reactants. Reedijk et al have previously reported that despite [Pt(dien)Cl]$^+$ reacting more quickly with GSH and GS-Me in the presence of 5'-GMP, only binding of 5'-GMP was observed in a competition experiment of [Pt(dien)(H_2O)]$^+$ with 5'-GMP and GS-Me.[41]

Reactions of L-MetH with *cis*- and *trans*-[$PtCl_2(NH_3)$(2-pic)]

The NMR data show that at pH 6.2, initial binding of L-MetH to *cis*-[$PtCl_2(^{15}NH_3)$(2-pic)] is likely to take place via Cl^- displacement by S which has a high affinity for Pt^{II}. However, there are also hydrolysis adducts present, as reported for the reaction of GSH with *cis*-[$PtCl_2(^{15}NH_3)$(2-pic)].[34] The monoaqua adduct, *cis*-[$PtCl(OH_2)(^{15}NH_3)$(2-pic)]$^+$, with the water ligand *trans* to the 2-picoline, is by far the major reaction product. This result is perhaps not very surprising as *cis*-[$PtCl_2(NH_3)$(2-pic)] was specifically designed to reduce drug inactivation by intracellular thiols by introducing steric bulk (2-methyl group of picoline) round the platinum atom, which restricts the access of thiols to the reactive centre of the molecule.[33] Conversely, cisplatin is well known to react rapidly with sulfur containing amino acids such as methionine, and these reactions are reported to increase the nephrotoxicity of cisplatin.[48] The presence of an ammonium peak observed after ca. 6 h of the initial reaction (pH 6.2) and in the low pH reaction suggests the possibility of complexation by S,N-chelated L-methionine. Ammonia release has been reported for reactions of cisplatin and methionine with formation of ring-closed complexes such as [$Pt(NH_3)$(Met-*S*)(Met-*S*,*N*)] and [Pt(Met-*S*,*N*)$_2$].[5, 49] The Pt-S bond formed with methionine weakens the Pt-NH_3 bond in cisplatin due to the *trans* influence.

In contrast, *trans*-[$PtCl_2(^{15}NH_3)$(2-pic)] is very reactive in the presence of L-MetH at pH 6.3. No peaks for hydrolysis adducts of *trans*-[$PtCl_2(^{15}NH_3)$(2-pic)] were observed, indicating that binding to L-MetH is also likely to occur via direct substitution, though this may be followed by subsequent hydrolysis. There are four cross-peaks present at the end of the reaction but it has not been possible to

unambiguously assign these peaks. However, it seems plausible that *trans*-[PtCl($^{15}NH_3$)(2-pic)(L-Met-*S*)], *trans*-[Pt(OH_2)($^{15}NH_3$)(2-pic)(L-Met-*N*)]$^+$, and *trans*-[Pt($^{15}NH_3$)(2-pic)(L-Met-*S*)$_2$] may be formed. A bis complex is also formed on reaction of methionine with transplatin, i.e. [*trans*-Pt(NH_3)$_2$(Met-*S*)$_2$].[5] On raising the pH to 8.5, several new time-dependent peaks were observed, but due to the complexity of the reaction, no further analysis was attempted. Intriguingly, when the pH was lowered to 3.5, a cross-peak corresponding to free NH_4^+ (7.09, 1.69 ppm) was observed. For *trans*-[$PtCl_2$($^{15}NH_3$)(2-pic)] such ammonia release cannot be rationalised by a *trans* influence, and the formation of a S,N-methionine chelate appears to be involved which is unprecedented.

7.6 Conclusions

Labelling of the new anticancer complex *trans*-[$PtCl_2$($^{15}NH_3$)(2-pic)] has allowed detailed insight to be gained into the kinetics and mechanisms of its reaction with 5'-GMP and glutathione. *Trans*-[$PtCl_2$($^{15}NH_3$)(2-pic)] was very reactive in the presence of glutathione and in a competitive reaction with 5'-GMP and glutathione, a clear preference was established for GSH adduct formation. Thus, there is a contrasting behaviour of the *cis*- and *trans*-[$PtCl_2$($^{15}NH_3$)(2-pic)] isomers towards glutathione. The reactivity of *cis*-[$PtCl_2$($^{15}NH_3$)(2-pic)] with L-methionine was greatly reduced compared to cisplatin, in agreement with previous reports that the steric hindrance of the 2-picoline ligand precludes access to the Pt centre and is therefore less susceptible to reaction with incoming thiols. However, this was not the case for the reaction of *trans*-[$PtCl_2$($^{15}NH_3$)(2-pic)] with L-methionine, which appeared to proceed via direct substitution, entirely consuming *trans*-[$PtCl_2$($^{15}NH_3$)(2-pic)] within 8 h of reaction.

7.7 References

[1] W. I. Sundquist, S. J. Lippard, *Coord. Chem. Rev.* **1990**, *100*, 293.

[2] J. Reedijk, *Inorg. Chim. Acta* **1992**, *198-200*, 873.

[3] N. Farrell, *Transition Metal Complexes as Drugs and Chemotherapeutic Agents*, Kluwer, Dordrecht, The Netherlands, **1989**.

[4] Z. Guo, P. J. Sadler, *Adv. Inorg. Chem.* **2000**, *49*, 183.

[5] E. L. M. Lempers, J. Reedijk, *Adv. Inorg. Chem.* **1991**, *37*, 175.

[6] J. Reedijk, *Chem. Commun.* **1996**, 801.

[7] R. F. Borch, M. E. Pleasants, *Proc. Natl. Acad. Sci. USA* **1979**, *76*, 6611.

[8] S. V. Pizzo, M. W. Swaim, P. A. Roche, S. L. Gonias, *J. Inorg. Biochem.* **1988**, *33*, 67.

[9] J. Bongers, J. U. Bell, D. E. Richardson, *J. Inorg. Biochem.* **1988**, *34*, 55.

[10] S. L. Bruhn, T. H. Jeffrey, S. J. Lippard, *Prog. Inorg. Chem.* **1990**, *38*, 477.

[11] A. Eastman, M. A. Barry, *Biochemistry* **1987**, *26*, 3303.

[12] M. Tedeschi, A. D. Cesare, S. Oriana, P. Perego, A. Silva, P. Venturino, F. Zunino, *Cancer Treatment Reviews* **1991**, *18*, 253.

[13] P. C. Dedon, R. F. Borch, *Biochem. Pharmacol.* **1987**, *36*, 1955.

[14] R. N. Bose, D. Li, M. Kennedy, S. Basu, *J. Chem. Soc. Chem. Commun.* **1995**, 1731.

[15] R. N. Bose, S. Moghaddas, E. L. Weaver, E. H. Cox, *Inorg. Chem.* **1995**, *34*, 5878.

[16] T. J. Kelley, S. Moghaddas, R. Bose, S. Basu, *Cancer Biochemistry Biophysics* **1993**, *13*, 135.

[17] S. S. G. E. v. Boom, J. Reedijk, *J. Chem. Soc. Chem. Commun.* **1993**, 1397.

[18] K. J. Barnham, M. I. Djuran, P. d. S. Murdoch, P. J. Sadler, *J. Chem. Soc. Chem. Commun.* **1994**, 721.

[19] C. M. Riley, L. A. Sternson, A. J. Repta, S. A. Slyter, *Anal. Biochem.* **1983**, *130*, 203.

[20] K. J. Barnham, U. Frey, P. d. S. Murdoch, J. D. Ranford, P. J. Sadler, *J. Am. Chem. Soc.* **1994**, *116*, 11175.

[21] P. d. S. Murdoch, J. D. Ranford, P. J. Sadler, S. J. Berners-Price, *Inorg. Chem.* **1993**, *32*, 2249.

[22] P. M. Deegan, I. S. Pratt, M. P. Ryan, *Toxicology* **1994**, *89*, 1.

[23] J.-M. Teuben, S. S. G. E. v. Boom, J. Reedijk, *J. Chem. Soc. Dalton Trans.* **1997**, 3979.

[24] R. E. Norman, J. D. Ranford, P. J. Sadler, *Inorg. Chem.* **1992**, *31*, 877.

[25] T. G. Appleton, J. W. Connor, J. R. Hall, *Inorg. Chem.* **1988**, *27*, 130.

[26] Z. Guo, T. W. Hambley, P. d. S. Murdoch, P. J. Sadler, U. Frey, *J. Chem. Soc. Dalton. Trans.* **1997**, 469.

[27] A. F. M. Siebert, W. S. Sheldrick, *J. Chem. Soc. Dalton Trans.* **1997**, 385.

[28] A. Meister, *Pharmacol. Ther.* **1991**, *51*, 155.

[29] T. Ishikawa, F. Ali-Osman, *J. Biol. Chem.* **1993**, *268*, 20116.

[30] T. Ishikawa, C. D. Wright, H. Ishizuka, *J. Biol. Chem.* **1994**, *269*, 29085.

[31] S. J. Berners-Price, P. W. Kuckel, *J. Inorg. Biochem.* **1990**, *38*, 327.

[32] J. Holford, S. Y. Sharp, B. A. Murrer, M. Abrams, L. R. Kelland, *Br. J. Cancer* **1998**, *77*, 366.

[33] J. Holford, F. Raynaud, B. A. Murrer, K. Grimaldi, J. A. Hartley, M. Abrams, L. R. Kelland, *Anti-Cancer Drug Design* **1998**, *13*, 1.

[34] Y. Chen, Z. Guo, J. A. Parkinson, P. J. Sadler, *J. Chem. Soc. Dalton Trans.* **1998**, 3577.

[35] K. Harrap, *Unpublished Results*, AnorMED Inc., **1992**.

[36] M. J. Abrams, C. M. Giandomenico, J. F. Vollano, D. A. Schwartz, *Inorg. Chim. Acta* **1987**, *131*, 3.

[37] F. I. Raynaud, F. E. Boxall, P. M. Goddard, M. Valenti, M. Jones, B. A. Murrer, M. Abrams, L. R. Kelland, *Clin. Cancer Res.* **1997**, *3*, 2063.

[38] S. Eapen, M. Green, I. M. Ismail, *J. Inorg. Biochem.* **1985**, *24*, 233.

[39] Y. Liu, F. P. Intini, G. Natile, E. Sletten, *J. Chem. Soc. Dalton. Trans.* **2002**, 3489.

[40] S. J. Barton, K. J. Barnham, U. Frey, A. Habtermariam, R. E. Sue, P. J. Sadler, *Aust. J. Chem.* **1999**, *52*, 173.

[41] M. I. Djuran, E. L. M. Lempers, J. Reedijk, *Inorg. Chem.* **1991**, *30*, 2648.

[42] B. J. Corden, *Inorg. Chim. Acta* **1987**, *137*, 125.

[43] K. J. Barnham, M. I. Djuran, P. d. S. Murdoch, J. D. Ranford, P. J. Sadler, *Inorg. Chem.* **1996**, *35*, 1065.

[44] Y. Chen, Z. Guo, S. Parsons, P. J. Sadler, *Chem. Eur. J.* **1998**, *4*, 672.

[45] T. G. Appleton, J. W. Connor, J. R. Hall, P. D. Prenzler, *Inorg. Chem.* **1989**, *28*, 2030.

[46] T. G. Appleton, *Coord. Chem. Rev.* **1997**, *166*, 313.

[47] S. J. Berners-Price, P. W. Kuchel, *J. Inorg. Biochem.* **1990**, *38*, 305.

[48] Z. Stefánka, S. Hann, G. Koellensperger, G. Stingeder, *J. Anal. At. Spectrom.* **2004**, *19*, 894.

[49] R. E. Norman, P. J. Sadler, *Inorg. Chem.* **1988**, *27*, 3583.

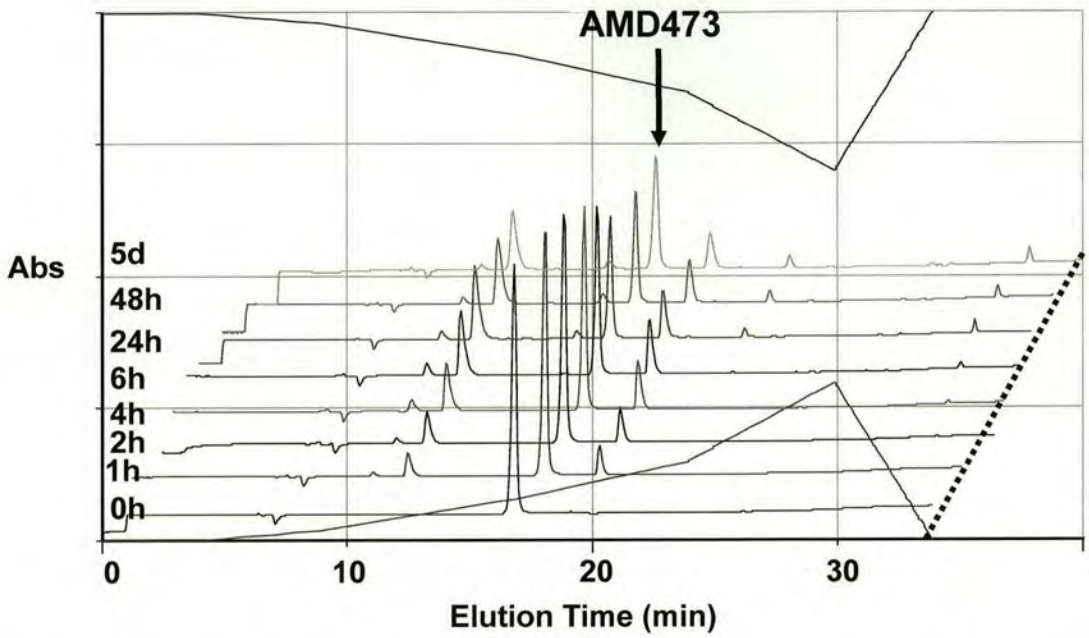

Appendix 1 Chromatogram for hydrolysis of AMD473 in 0.02 M $NaClO_4$, pH 5.5, 310 K, λ = 220 nm (the sloping lines at the top and bottom represent the gradient of aqueous and organic eluents, respectively).

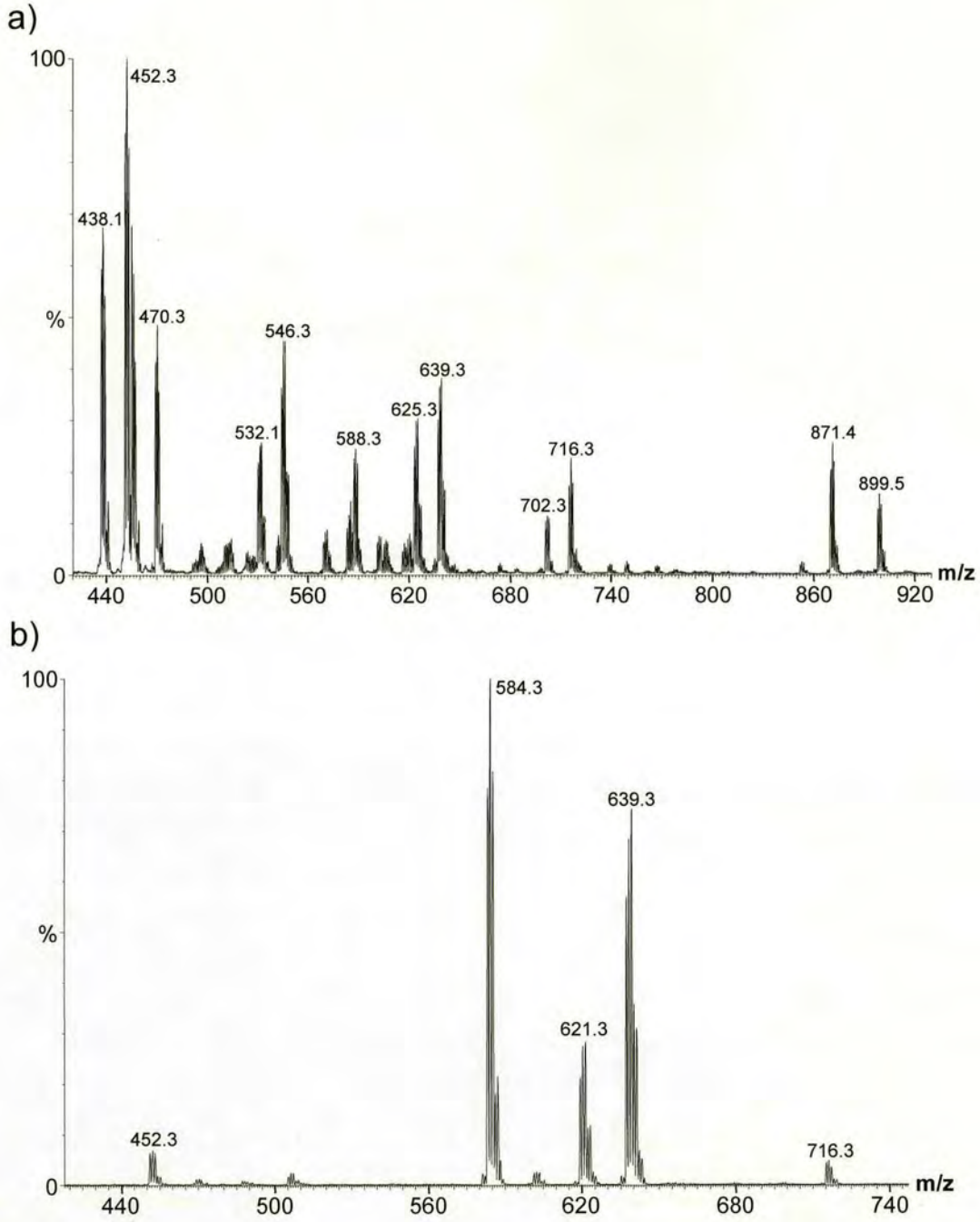

Appendix 2 ESI mass spectra at a cone voltage of 45 eV for a) fraction **F3** and b) fraction **F4**, from the reaction of ^{15}N-AMD473 and 1-Meguanosine, see Figure 5.1.

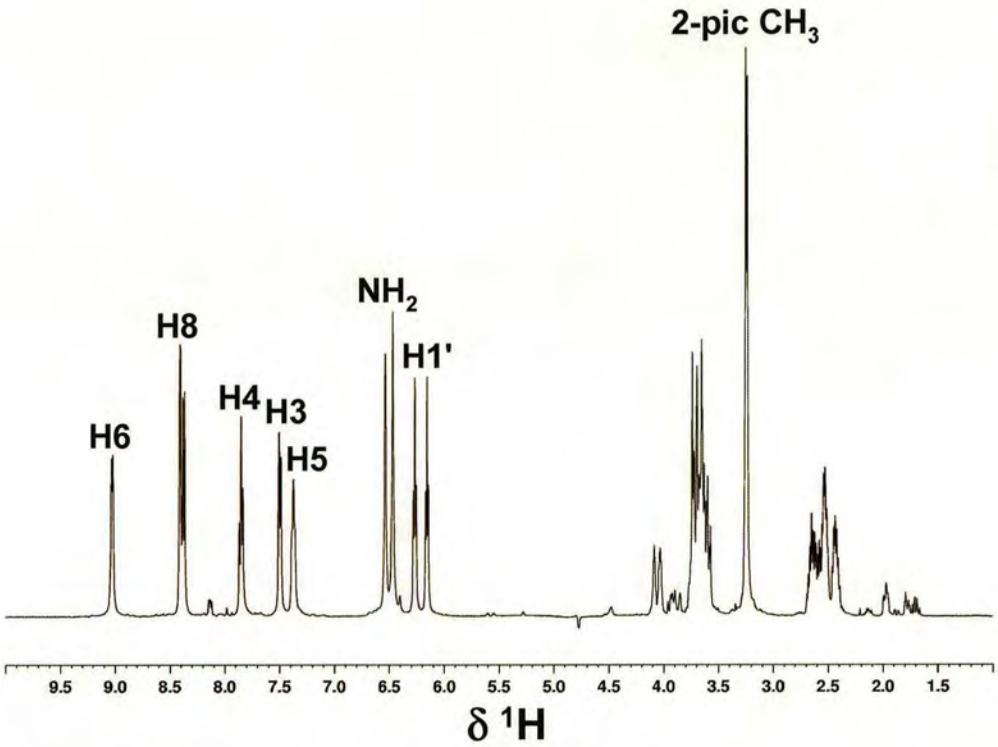

Appendix 3 ^{1}H NMR spectrum of *cis*-[Pt(NH_3)(2-pic)(2'-dGuo)$_2$](NO_3)$_2$ in H_2O/D_2O at 298 K (peaks H3-H6 are aromatic proton signals of picoline ligand).

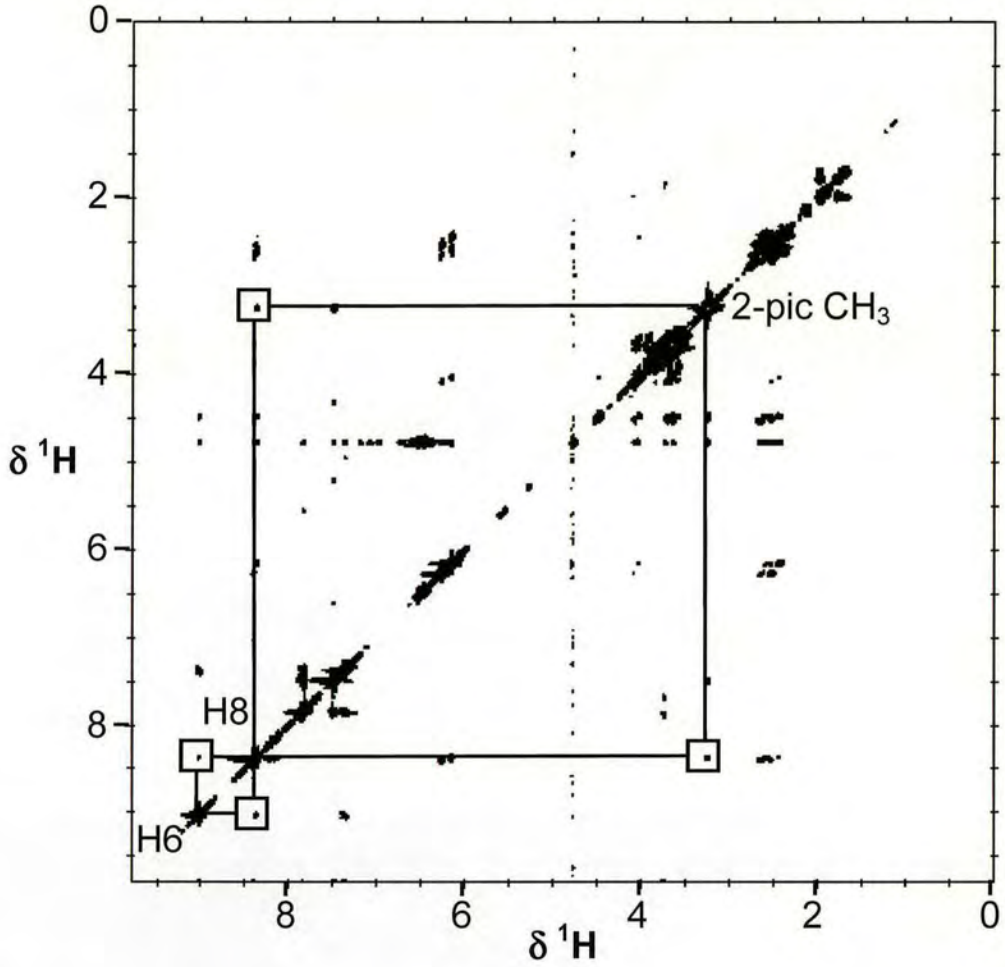

Appendix 4 [^{1}H,^{1}H] ROESY NMR spectrum of *cis*-[Pt(NH_3)(2-pic)(2'-dGuo)$_2$](NO_3)$_2$ in H_2O/D_2O (H6 corresponds to aromatic signal of picoline ligand).

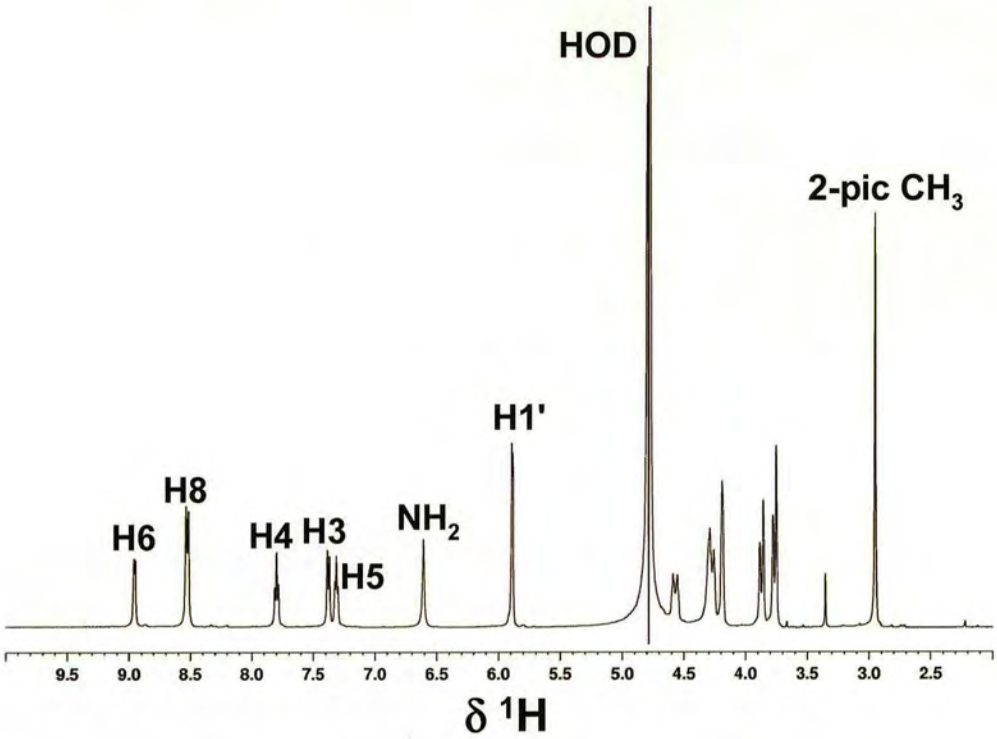

Appendix 5 ^{1}H NMR spectrum of *trans*-[Pt(NH_3)(2-pic)($Guo)_2$]($NO_3)_2$ in H_2O/D_2O at 298 K (peaks H3-H6 are aromatic proton signals of picoline ligand).

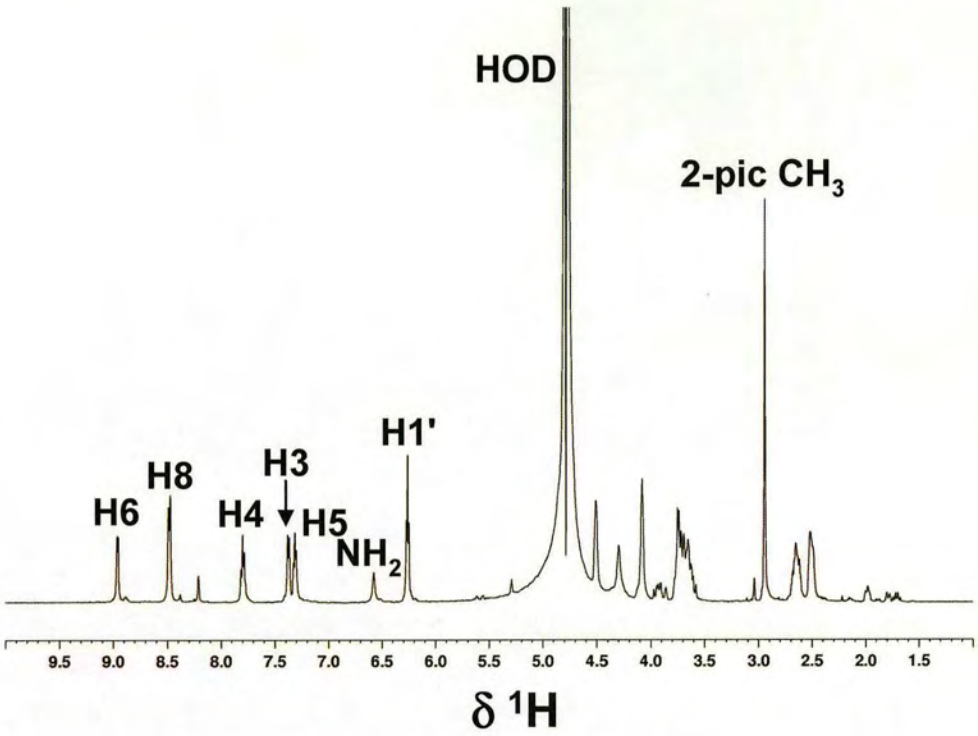

Appendix 6 ^{1}H NMR spectrum of *trans*-$[Pt(NH_3)(2\text{-pic})(2'\text{-dGuo})_2](NO_3)_2$ in H_2O/D_2O at 298 K (peaks H3-H6 are aromatic proton signals of picoline ligand).

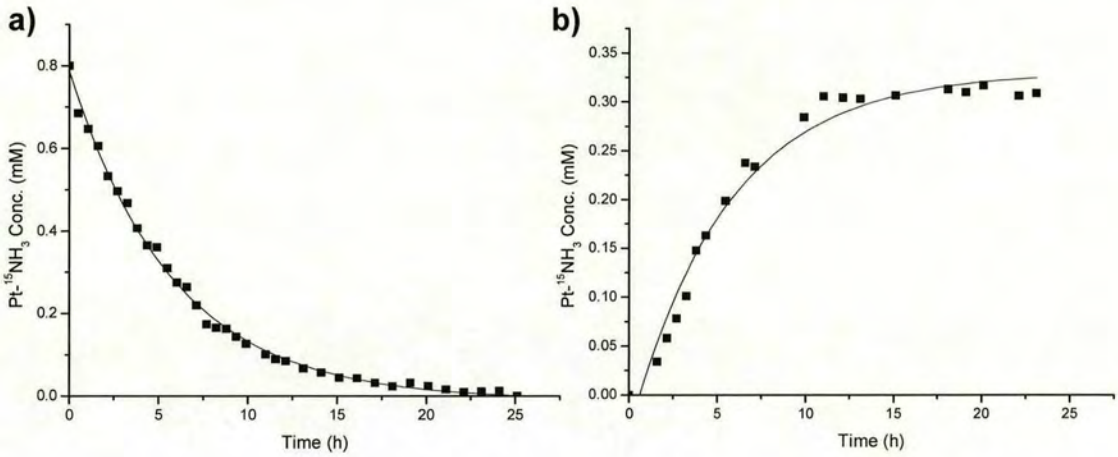

Appendix 7 Pseudo-first order computer fits of the concentration versus time profiles for the reaction of *trans*-[$PtCl_2(^{15}NH_3)$(2-pic)] and 12-mer duplex DNA, d(TATGGTACCATA)$_2$, at 298 K, as determined by integration of the 2D cross-peaks shown in Figure 6.1, a) peak **a** and b) peak **c**.

Courses Attended

1) Transferable skills courses: UNIX I, poster making, writing skills, and introduction to HTML.

2) Undergraduate Bioinorganic Chemistry lecture course, Professor Chapman, 2002.

3) Undergraduate Medicinal Inorganic Chemistry lecture course, Professor Sadler, 2002.

4) Undergraduate X-ray Diffraction lecture course, Dr. Parsons, 2002.

5) Postgraduate NMR Spectroscopy lecture course, 2003.

6) Weekly Inorganic Section Seminars during the terms 2001-2004.

Conferences Attended

1) 8th International Conference on the Chemistry of the Platinum Group Metals, University of Southampton, UK, July 2002.

2) 36th USIC conference, University of Edinburgh, UK, September 2002.

3) European COST programme D20 meeting, Brno, Czech Republic, November 2002 (oral presentation).

4) 37th USIC conference, University of Strathclyde, UK, September 2003.

5) 9th International Symposium on Platinum Coordination Compounds in Cancer Chemotherapy, New York, USA, October 2003 (poster presentation).

6) European COST programme D20 meeting, Bari, Italy, February 2004 (oral presentation).

7) 6th International Meeting on Recognition Studies in Nucleic Acids, University of Sheffield, UK, April 2004 (poster presentation).

Publications

1) G-G Base-Pairing in Nucleobase Adducts of the Anticancer Drug *cis*-$[PtCl_2(NH_3)(2\text{-picoline})]$ and Its *trans* Isomer.

Geraldine McGowan, Simon Parsons, and Peter J. Sadler

Chem. Eur. J. 2005, *11*, 4396-4404.

2) The contrasting chemistry of *cis* and *trans* Pt^{II} diamine anticancer compounds: hydrolysis studies of picoline complexes.

Geraldine McGowan, Simon Parsons, and Peter J. Sadler

Inorg. Chem. 2005, *44*, 7459-7467.